

Doctoral theses at NTNU, 2021:134

Sveinung Ørjan Nesheim

Competitive timber floors

Optimisation of hollow section timber floor elements for adaptable buildings

ISBN 978-82-326-6481-8 (printed ver.)
ISBN 978-82-326-5399-7 (electronic ver.)
ISSN 1503-8181 (printed ver.)
ISSN 2703-8084 (electronic ver.)

Doctoral theses at NTNU, 2021:134

NTNU
Norwegian University of
Science and Technology
Thesis for the degree of
Philosophiae Doctor
Faculty of Engineering
Department of Structural Engineering

Sveinung Ørjan Nesheim

Competitive timber floors

Optimisation of hollow section timber floor elements for adaptable buildings

Thesis for the degree of Philosophiae Doctor

Trondheim, April 2021

Norwegian University of Science and Technology

Faculty of Engineering

Department of Structural Engineering



Norwegian University of
Science and Technology

NTNU

Norwegian University of Science and Technology

Thesis for the degree of Philosophiae Doctor

Faculty of Engineering
Department of Structural Engineering

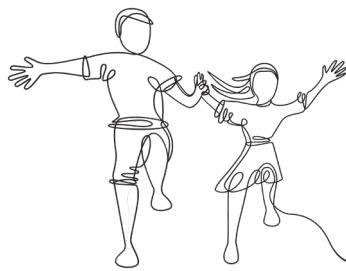
© Sveinung Ørjan Nesheim

ISBN 978-82-326-6481-8 (printed ver.)
ISBN 978-82-326-5399-7 (electronic ver.)
ISSN 1503-8181 (printed ver.)
ISSN 2703-8084 (electronic ver.)

Doctoral theses at NTNU, 2021:134



Printed by Skipnes Kommunikasjon AS



F

or Nils Frimann and Ebba Vive

Now let's go tickle dragons!

Det er håpløst og vi gir oss ikke

– Jan Erik Vold, “Nyttårsdiktet”, 1969
(occasionally recited by Professor Malo during advisory sessions)

Contents

Preface	IX
Acknowledgments	X
Summary	XII
List of publications	XVII
PART I: Synopsis	1
1 Introduction.....	3
1.1 New role for the built environment	3
1.1.1 The environmental and political backdrop.....	3
1.1.2 Timber as a viable building resource for the future	4
1.1.3 Prosperous market potential.....	5
1.1.4 A new generation of timber buildings.....	7
1.1.5 Rough terrain still ahead	7
1.2 The Woodsol project	8
1.2.1 WP2 Production and assembly.....	10
1.2.2 WP3 Moment resisting frames.....	10
1.2.3 WP4 Flooring systems	10
1.2.4 WP5 Acoustics.....	11
1.2.5 WP6 Prototypes.....	11
1.2.6 WP7 Dissemination.....	11
1.3 Timber flooring systems in adaptable buildings.....	11
1.3.1 Floor layout and available floor element solutions	11
1.3.2 The structural role of the flooring system	15
1.4 Competitiveness of long-span timber floor elements	15
1.4.1 Material appropriateness	15
1.4.2 Approaching serviceability consent for structural response	18
1.4.3 Determination of floor element response	22
1.4.4 Pursuing competitiveness.....	24
1.4.5 Increased competitiveness through optimisation	24
1.4.6 Environmental challenges	27
2 Research approach	28
2.1 Background	28
2.1.1 Mid-term research approach findings	30
2.1.2 Matured research approach	31
2.2 Ethical issues.....	32
2.3 Research objective and questions.....	33

3	Research method.....	35
3.1	Methods at a glance.....	35
3.2	Information retrieval.....	36
3.2.1	Databases.....	36
3.2.2	Search inquiry key words.....	37
3.2.3	Interpretation and sorting of literature.....	39
3.2.4	Materials database.....	39
3.3	Numerical methods.....	40
3.3.1	Numerical representation of the flooring system.....	40
3.3.2	Optimisation of the floor element based on FEA.....	45
3.3.3	Determination of human induced vibration.....	46
3.3.4	Shear flow analysis.....	48
3.4	Analytical methods.....	48
3.4.1	Floor serviceability.....	48
3.4.2	Experimental Modal Analysis.....	55
3.4.3	Power Spectral Density.....	55
3.4.4	Accounting of consumed resources during manufacture.....	56
3.5	Experimental methods.....	57
3.5.1	Experimental Modal Analysis (EMA).....	57
3.5.2	Deflection tests.....	60
3.5.3	Cyclic load.....	61
3.6	Systems analysis.....	61
3.7	Real-life approach.....	64
3.8	Optimisation.....	64
3.8.1	Method.....	64
3.8.2	Theory.....	66
3.8.3	Results and implications.....	67
4	Research.....	69
4.1	Objectives and findings.....	69
4.1.1	Paper I.....	69
4.1.2	Paper II.....	70
4.1.3	Paper III.....	70
4.1.4	Paper IV.....	71
4.1.5	Paper V.....	72
4.1.6	Paper VI.....	73
4.2	Answers to research questions.....	74
4.3	Further work.....	78
5	Reproducibility and information access.....	81
6	References.....	82

PART II: Dissemination	97
1 Peer-reviewed articles	99
1.1 Paper I.....	100
1.2 Paper II.....	140
1.3 Paper III.....	175
1.4 Paper IV.....	206
2 Conference proceedings papers.....	249
2.1 Paper V.....	250
2.2 Paper VI.....	271
3 Presentations and appearances	290
3.1 Presentations.....	291
3.2 appearances	292
PART III: Appendix	293
Annex A. Codes and drafts.....	295
Annex A.I Material database code.....	296
Annex A.II PSACHS development information	301
Annex A.III PSACHS input file format	302
Annex A.IV Script for PSD of individual walking load.....	306
Annex A.V Technical drawings of thin field web floor element	308
Annex B. Philosophic exercises	314
Annex B.I Skrik I – Slit i ukjent terreng.....	315
Annex B.II Skrik II – Strinakkjen og jordormen	316

Preface

The present doctoral thesis has been submitted to the Norwegian University of Science and Technology (NTNU) in Trondheim (Norway) for the degree of *Philosophiae Doctor*. The work has been carried out at the Timber Structures Research Group at NTNU's Department of Structural Engineering, with Professor Kjell Arne Malo at NTNU as advisor, and Senior Research Scientist Nathalie Labonnote at SINTEF as co-advisor.

The work is part of the Woodsol research project funded by the Research Council of Norway. It is an article-based thesis containing four journal, and two conference, articles. The thesis is divided into three parts. Part 1 presents a synopsis of the work, Part 2 contains publications, presentations and appearances, and Part 3 comprises the appendices. All the journal articles were submitted to international peer-reviewed journals, and the conference articles to the relevant conference proceedings publications.

The undersigned was the sole author of Papers I, III, V and VI, and was the main author of Paper IV, in which aspects of the theory and theory implementation were carried out in cooperation with the Tampere University in Finland. The undersigned was the second author of Paper II. The undersigned declares herewith that this thesis and appended papers have been written by him and that the work presented here is the result of original research that has not previously been submitted for a degree at this university or any other institution.

The undersigned was admitted to the doctoral programme in August 2016 and the thesis submitted in January 2021. The position included one year as a teaching assistant at the Department of Structural Engineering at NTNU. The doctoral period coincided with the arrival of two wonderful and adventurous children, and study at times accompanied by baby babble and sleep deprivation. The doctorate was completed in accordance with its agreed duration, inclusive of parental leave, and during the final year under the stress imposed by highly restrictive Covid-19 infection control measures. The challenges have all helped to lend a sense of perspective, brightness and solidarity.



Sveinung Ørjan Nesheim

Trondheim, 21st January 2021

Acknowledgments

I take this opportunity to extend my sincere gratitude to my advisor, Professor Kjell Arne Malo, who heads the Timber Structures Research Group at the Norwegian University of Science and Technology (NTNU). Our talks have been illuminating and have always enhanced my perspectives and the relevance of the topic under discussion. I also wish to extend my deepest gratitude to my co-advisor, Senior Research Scientist Nathalie Labonnote at SINTEF, for her constant support and encouragement, and for her accurate and swift responses to my enquiries. I thank both advisors for their thoughts and comments, and for their comprehensive and meticulous evaluations of my manuscripts, which considerably enhanced the quality of my work. I would also like to express my appreciation to the Research Council of Norway, which has funded the Woodsol project and my doctoral position.

I am particularly grateful for the assistance and cooperation provided by Assistant Professor Kristo Mela in relation to the work on optimisation. He and his colleagues at the Faculty of Built Environment at the Tampere University in Finland welcomed me most generously and with the best attention to academic common benefits during my two weeks stay at Tampere University. My collaboration with Assistant Professor Mela was highly rewarding and resulted in co-authoring a paper together.

I owe a very important debt to the former SINTEF Byggforsk (now SINTEF Community) in Oslo and Trondheim for assisting in my work on timber constructions. I extend my gratitude to my colleagues at *Høgskoleringen* for all the opportunities given, and for granting me leave to carry out my doctorate studies. I would also like to thank my excellent colleagues at *Vinderen*, some with roots at the Norwegian Building Research Institute (NBI), for teaching me so much about sound and practical building constructions. The ground floor coffee breaks held the most interesting discussions and reports which still offer silent guidance. I also benefited from welcoming acquaintances made at the Norwegian University of Life Sciences (NMBU) and the Norwegian Institute of Wood Technology (*Treteknisk*).

Experimental testing has made up a considerable part of this project, and I am very grateful to the laboratory staff at the Department of Structural Engineering at NTNU, not least to technicians Bjørn Strickert Schjølberg, Terje Petersen and Steinar Seehuus, and the laboratory manager Odd Kristian Nerdahl, who helped me to prepare my experiments. I also extend my gratitude to Asle Skauge and Kenneth Sundli at IT support for their generous assistance, the Head of Department, and all the welcoming administrative staff.

I would like to express my appreciation of my fellow doctoral students Aivars Vilguts and Simone Conta, who were involved in the design of the mock-up frame assembly. I am grateful to have shared an office with Aivars, and greatly enjoyed

Competitive timber floors – Acknowledgments

our wide-ranging discussions. We have both benefited from the guidance we offered each other. I would also like to extend my gratitude to current and former members of the Timber Structures Research Group, not least to Kolbein Bell for his time and attentiveness to my questions.

I take the opportunity to acknowledge and extend my gratitude to Åge Holmestad at the company Moelven Limtre AS for our valuable discussions and his accommodating attitude. I also acknowledge the members of the Woodsol project group for our interesting discussions and the information they provided. I extend my warm appreciation to Ebbe Smith at PLM Technology for his guidance and help in realising the iSight workshop and the optimisation approach in iSight.

I acknowledge also Leif Joar Lassesen at Charlottenlund Upper Secondary School (CVGS) for his positive and supportive attitude and problem-solving mindset during the erection and testing of the structural scale model. I am also grateful to Moelven Limtre AS for providing the glulam and LVL required for the experimental programme. My thanks also to Peter Engström-Øren at SFS intec AS and to Eugenio Facchini at Rothoblaas for providing fasteners for the scale model.

I wish also to express my appreciation and extend my gratitude to Kathinka Leikanger Friquin at SINTEF Community for our discussions and her advice in the field of fire resistance. I thank Christofer Skaar at SINTEF Community for valuable discussions concerning the environmental performance of building materials, and Torfinn Ottesen at SINTEF Ocean for guidance on FFT filtering.

I also acknowledge the efforts of the Assessment Committee, consisting of 1st opponent Professor Anders Qvale Nyrud at NMBU, 2nd opponent Senior advisor Tomi Toratti at the Federation of Finnish woodworking industries, and the administrator Associate professor Haris Stamatopoulos at NTNU.

I could not have completed my doctoral thesis without the support and understanding of my loving family. I extend my heartfelt appreciation to Gry aka Bobo for being so cheerful and solution-oriented, to brave Nils Frimann for being so patient, understanding and positive, and to Ebba Vive for her constant smiles and perfect timing. I wish to express my sincere gratitude to my dear parents for their support and encouragement, to my grandparents, who have exerted such a great influence on me, and to my beloved sister whom I am sailing with. My thanks also goes to my parents-in-law for their support and help during this period. I am deeply grateful to Kippis and Pedal and my remarkable friends for their inspiration in matters of aesthetics and materiality and architecture, theatre and culture, music and arts, fine tools and crafts, and for hauling me into meaningful nonsense and daring ventures. The insight and awareness has provided me with a sublime understanding of the essential and Vitruvian balance between poetry and construction, now more than ever relevant for reputable engineering.

Summary

The greater utilisation of timber in the building sector has the potential to contribute to reductions in greenhouse gas emissions, which represent a major and universal challenge to the sector as a whole. Global population growth and urbanization are placing increasing demands on a need for multi-storey, space-efficient, sustainable and adaptable buildings. The Woodsol research project was established to develop commercial structural solutions for urban buildings and was financed by the Research Council of Norway (RCN). The work performed in this doctoral programme is linked to Work Package 4 (WP4) of the Woodsol project.

The objective of WP4 was to explore a comprehensive design for long-span floor elements for utilisation in moment-resisting frames, possibly by enhancing the properties of Timber-Concrete Composites (TCCs). The scope and objective of the present work was influenced by findings from correlated work packages, most notably WP2, which addressed topics related to production and assembly. WP2 examined properties related to storey height, span, grid and the size of structural elements, and exposed conditions and specifications needed for floor elements to meet architectural expectations. It also addressed the space required for technical installation, as well as flexibility specifications that provide opportunities for expected adaptations. The efforts and achievements of the work packages addressing moment-resisting connectors and acoustics also influenced formulation of the objectives and scope of the present work.

Research matured and was appropriately adapted during the first two years of the doctoral project. Focus was gradually transferred from numerical studies of the behaviour of composite materials and the interface and effect of moment-resisting end constraints, to the broader aspects of developing timber floor elements for commercial and adaptable buildings. This shift was motivated by results derived from correlated work packages, and strongly influenced by findings made as part of literature reviews.

TCCs have been the object of much research attention. Published articles addressing the topic have rendered guidelines for TCCs, but related solutions are strongly associated with increased carbon emissions, a factor which detracted from the primary competitive benefit offered by timber-based floor elements. For this reason, TCCs were disregarded as the project progressed and its scope refined.

This work has shown that the design of floor elements as an inherent structural component of moment-resisting frames is achievable. A moment-resisting connector that transfers rotational stiffness between a column and a floor element introduces loads to connected members through an arrangement of threaded rods. The structural interface between the rods and the edge joists of the floor element is flexible and

practical. While the global building system is critically influenced by the rotational stiffness of the frames, the design of the floor element is less affected. Moment resisting end restraints yield a positive ratio of span to depth for the floor element, but other less studied factors are likely to exert a greater influence in determining increased competitiveness.

Research into suitable serviceability criteria for timber floors has been carried out for more than 30 years. Consent has advanced in recent years, but uncertainty of the outcome made research linked to current methods for vibration serviceability less attractive. The uncertainty encouraged a focus on issues not directly related to serviceability, but rather to competitiveness. A brief on the utilisation of the ISO baseline curve for the second generation of Eurocode 5 were published in 2018. In January 2019, the proposed method for the second generation of Eurocode 5 was published, and the method was implemented and applied in the present work thereafter.

An analysis of the market position of long-span timber floors was performed in the form of a SWOT analysis. The high cost of timber floor elements compared with comparable concrete elements has been significant for the low market share. Furthermore, the arguments for selecting low-emissions designs were insufficient to persuade the sector to adopt timber flooring systems for commercial buildings – a situation that supported the project group’s conclusion. The results of the SWOT analysis exerted a great influence on the research and motivated investigations into how competitiveness should be defined, and how the competitiveness of long-span timber floor elements could be enhanced.

The combined options, conditions and constraints that have to be considered when designing a long-span floor element generate a solution space for which the optimum design can only confidently be identified when computationally explored.

It was found that the challenges related to competitiveness and solution space had the potential to be linked as part of a joint exercise to explore the competitive optimum for timber floor elements as applied in a building. Thus, the final objective and scope of this doctoral project came to address the issue of how to enhance the adaptability and competitiveness of long-span timber floor elements.

The research challenge has been how to quantify competitiveness and develop an approach to the rapid and confident exploration of the solution space of possible combinations of geometries and materials suitable for an adaptable building. Requirements concerning serviceability, support conditions and any significant parameters that influence the use of a floor element in a given building are addressed.

On a methodological level, the objective of this work has been to smooth the way for future research by developing suitable and practical tools and methods. Effort

and focus has thus been directed towards facilitating an enhanced application of the present work by using open source software for programming, by continuously adding thorough comments to the codes written, and by making these codes accessible to future researchers. The present work may be regarded as providing parametric building blocks similar to other recent projects on algorithm-aided design carried out at NTNU.

The research objective of this doctoral study has thus been defined based on the context and experience obtained from a mature research approach, involving research questions duly formulated and answered. The funding agency RCN stated that the product of this research should be a reference work for the use of the Woodsol building system, and this has been a contributing factor in the formulation of the objective and scope of the work.

The academic defence of this doctoral thesis is based on six published articles described in the following. Four of these articles were submitted to peer-reviewed journals, and the last two as contributions to conference proceedings publications.

Paper I: Effect of interconnects on timber floor elements: dynamic and static evaluations of structural scale tests

Floor elements with various configurations and connections are integrated in a flooring system. The connections between the floor elements may offer a cost-effective solution for improvement of the dynamic response of a flooring system without changing the design of the floor element. The results can assist builders in selecting a cost-effective and environmentally beneficial method of increasing floor comfort performance. The work was based on structural scale tests of floor elements arranged both in parallel and in series. It demonstrated that connections between timber elements have significant effects on floor serviceability that may in turn improve the vibration performance of long-span timber floors. The article has been peer-reviewed and accepted by the European Journal of Wood and Wood Products.

Paper II: A study on beam-to-column moment-resisting timber connections

The Woodsol building system was tested in a structural scale model. The building system exhibits a weak direction that may require global building stiffness to be provided by dedicated shear walls or bracings. In the strong direction, stiffness is provided by moment-resisting frames that confer joint stiffness from the columns, the connector, and the embedded edge joists of the floor element. In this study, the moment-resisting frames were subjected to cyclic lateral loading and tested using experimental modal analysis. The lateral stiffness, energy dissipation and fundamental eigen-frequencies of the assembly were measured and quantified, and compared with the results of finite element (FE) analyses. The FE model

demonstrated good agreement with the experimental results. The article has been submitted to the peer-review European Journal of Wood and Wood Products.

Paper III: Competitiveness of timber floor elements: an assessment of structural properties, production, costs and carbon emissions

A method called Item-Driven Activity-Based Consumption (IDABC) has been developed and is presented in this study. The method establishes an accurate relationship between product specifications and overall resource consumption linked to the finished manufactured product. In addition to production time, method outcomes include cost distributions, including labour costs, and carbon emissions for both accrued materials and production line activities. The output serves to quantify competitiveness. The parametric architecture of the method enables implementation in an optimization workflow. The work represents a response to a research gap related to resource consumption and the optimisation of timber floor elements. The IDABC method has been applied to a timber component and assembly line operated by a major manufacturer in Norway, and demonstrates good agreement with empirical data. The article has been peer-reviewed and accepted by the Forest Products Journal.

Paper IV: Optimisation of costs and carbon emission of timber floor elements

The timber industry is under substantial pressure to identify attractive solutions for floor elements with otherwise favourable environmental features. The combined options, conditions and constraints that have to be considered when designing a long-span floor element generate a solution space for which the optimum design can only confidently be explored computationally. In this paper, the cost and ECO2 optimisation of a timber floor element is presented, and the IDABC method is applied to make the calculation possible. A Mixed-Integer Sequential Linearization Procedure (MISLP) is employed to solve the formulated discrete optimisation problem. The results provide insights into the general properties of optimum timber floor elements. The optimisation model is used to analyse the characteristics of optimum designs, and a comparison between the current and the second generation of Eurocode 5 is shown to demonstrate achievable outcomes. The article has been submitted to the peer-review journal of Structural Engineering.

Paper V: Assessing the adequacy of numerical representation for performance optimisation in long-span timber floors

The objective of this study was to describe the effect that variations in the numerical representation of a floor element had on the accuracy of modal analysis and computational effort. Various formulations and combinations of shell and solid members were modelled and subsequently compared with experimental results. The

study succeeded in identifying combinations of element types and sizes resulting in a favourable combination of precision and computational effort, suitable for an optimisation workflow. The article was accepted for the conference proceedings of the World Conference on Timber Engineering, WCTE 2018, Seoul.

Paper VI: Conditions and features of a design tool for long-span timber floor elements

This paper expands on a handbook for timber floor elements using information obtained from architects, engineers and manufacturers. It reviews the factors influencing the competitiveness of timber floor elements for commercial and adaptable buildings, and uses its findings to describe the features and requirements of a design tool that could supply information to a handbook. A SWOT analysis was used to identify indicators of competitiveness, as well as conditions and features that an optimisation tool should include. The paper proposes an architecture that promotes a holistic approach to optimisation and the scoping of solutions with a view to preparing a reference work. The article has been accepted for the conference proceedings of the WCTE 2021, Santiago.

Keywords:

Abaqus; activity-based; adaptable buildings; algorithm aided design; carbon emission; closed hollow sections; competitiveness; COPTICHS; cost optimisation; dynamic performance; engineered wood; expenditure; floor element; flooring system; full-scale test; IDABC; interconnections; ISO baseline; long-span timber floors; mixed-integer sequential linearization procedure (MISLP); moment-resisting timber frames; numerical analysis; optimisation; parametric; production line; PSACHS; python; reference work; serviceability; static performance; stressed-skin panels; timber element manufacturing; wood.

List of publications

- I. Nesheim, S., K. A. Malo and N. Labonnote. 2021. Effect of interconnects on timber floor elements: dynamic and static evaluations of structural scale tests. [1]
Acceptance pending after submitting response to minor revisions in peer-reviewed journal: European Journal of Wood and Wood Products
- II. Vilguts, A., S. Nesheim, H. Stamatopoulos and K. A. Malo. 2021. A study on beam-to-column moment-resisting timber connections, comparing full-scale connection testing and mock-up frame assembly. [2]
Manuscript submitted to peer-reviewed journal: European Journal of Wood and Wood Products
- III. Nesheim, S., K. A. Malo and N. Labonnote. 2021. Competitiveness of timber floor elements: an assessment of structural properties, production, costs and carbon emissions. [3]
Approved for publication in peer-reviewed journal: Forest Products Journal
- IV. Nesheim, S., K. Mela, K. A. Malo and N. Labonnote. 2021. Optimisation of costs and carbon emission of timber floor elements. [4]
Submitted to peer-reviewed journal: Engineering Structures
- V. Nesheim, S. and K. A. Malo. 2018. Assessing adequacy of numerical representation for optimisation performances in long span timber floors. [5]
Published in proceedings of World Conference in Timber Engineering 2018. Seoul.
- VI. Nesheim, S., K. A. Malo and N. Labonnote. 2021. Conditions and features of a design tool for long-span timber floor elements. [6]
Approved for publication in proceedings of World Conference in Timber Engineering 2021. Santiago.

PART I

Synopsis



[7]

Competitive timber floors– PART I: Synopsis

Vær utålmodig menneske!
Langsomt blir allting til.

– Inger Hagerup, "*Vær utålmodig menneske!*", 1947

1 Introduction

1.1 New role for the built environment

1.1.1 The environmental and political backdrop

The built environment has had a significant role in the climate change. This is a role it will continue to have, but with an expected change of character. In the future the role of the construction sector may increasingly be addressed as a measure to decelerate global warming [8]. Currently the construction sector is strongly identified with negative climatic impact, accounting for 36 % of the global energy use and an associated 39 % of the carbon dioxide emissions [9]. Even as 85% of the buildings we will inhabit in 2050 are already built [10], the construction sector is expected to erect or recondition some 230 billion square metres of new construction over the next 40 years [9]. The last three decades the Greenhouse gas (GHG) emissions from the construction sector has increased with 55% and is currently one of the three fastest growing sources [11]. GHG emissions related to the construction sector is likely to be doubled by 2050 [12]. The material use of the construction sector is dominated by concrete. Currently concrete is the second most consumed material in the world surpassed only by water. The much referred benchmark of one cubic meter of concrete per capita per year [13] is outdated. According to the German market and consumer database Statista, it has been a steady growth in the annual cement production until a flattening of the rate in 2013 at 4100 million tonnes per year [14]. This equals an annual consumption of cement-based materials (CBM) of 25 billion tonnes, equivalent to 1.4 cubic meter per capita per year.

This growth comes with a consequence. Our governments are all committed to measures defined by the United Nations Framework Convention on Climate Change (UNFCCC). For the European countries carbon emission targets has steadily grown ambitious from the Kyoto Protocol in 1997 and the Copenhagen Accord in 2009 to the Paris Climate Agreement [15] in 2016 associated with an unconditional reduction of carbon emissions of 40% by 2030 with respect to 1990 levels. In regard to due pledges the European countries are currently performing insufficiently, even trending towards highly insufficiently [16]. Today it is a general understanding that countries cannot meet emission reduction targets without reducing energy consumption in the construction sector. Studies have been conducted in order to reduce the carbon emissions from concrete [17], but to achieve a significant reduction in GHG, steel and concrete must extensively be replaced by timber-based building systems. This is the conclusion in a recent study of material efficiency (ME) strategies for reducing GHG in the construction sector [18]. Whilst the effect of recent political strategies of energy efficiency improvements is seen as reduced GHG

in a lifetime perspective, the embodied GHG of buildings are increasing, as reported by Röck et al [19]. This support the findings in [18] and emphasise the importance of substituting conventional materials and solutions with environmentally friendly building systems.

1.1.2 Timber as a viable building resource for the future

During the last century the amount of Norwegian forests have increased by a factor three, currently holding one billion cubic meters of deciduous and coniferous forest [20, 21]. During 2020 the growth in Norwegian forests was 24 million cubic meters of which only 11 million cubic meters was harvested. [22]. A recent strategy document for the forest sector has pointed out the increased share of forest products in the building industry as a vital drive for a healthy economy [23, 24].

According to mapping of sustainable forests [25], there is a huge potential for industrialization of timber-based products for the European market in the Nordic countries. The availability of raw material in the Nordic countries and Russia is greatly exceeding forest resources of central Europe. Suitable solutions for standardization, agreements on cooperation between Nordic countries as well as necessary political guidelines must be established to release the potential. In North America and Western Europe, the forest is managed and certified. This is however not the case for most forest areas of the world, and manufacturers and suppliers of timber-based products must ensure the use of certified timber. Mapping of certified forests are a helpful means to ensure that the outtake of timber is sustainable [25].

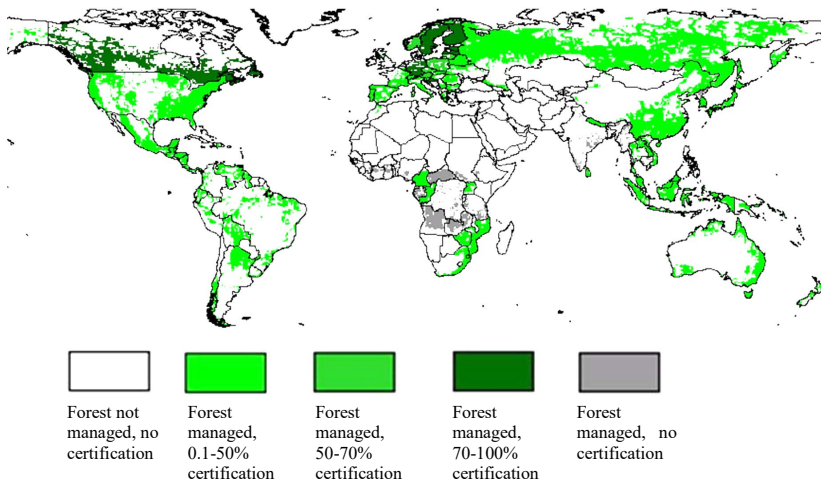


Fig. 1: Certified forest area relative to the forest area under management [25]

In Norway, like in most forests worldwide, the portion of small-diameter trees tend to overstock, and opportunities of utilising this resource is currently studied [26].

1.1.3 Prosperous market potential

City fires from The Great Fire of London to more recent incidents at the beginning of the 20th century, caused national building regulations to have substantial restrictions for use of timber in tall buildings in most European countries. In Norway, the restrictions were relieved as late as 1997 when material-neutral regulations were introduced. In practice this has caused building construction systems of steel and concrete to achieve a substantial lead in developments. The Norwegian Directorate of Public Construction and Property (Statsbygg) has investigated the consequences and concluded that timber-based building systems are associated with higher risk for building contractors in comparison to other materials [27].

Now the trend is more positive. Both in the Nordic countries and in the rest of the world several recent commercial timber-based building projects have forced technical developments ahead [28-31] (see Fig. 2), and the demonstration projects are increasing market trust, as studied in [32]. Throughout the European countries, governmental programmes are established to promote timber-based building systems for commercial and high-rise buildings. The building sector is expected to erect quarter of a trillion square metres of new construction over the next 40 years [9].

The Principles of circular economy and bio-economy strengthens the sustainability of timber construction further, as can be read in the Finnish study of Hynynen [33]. This study also emphasises the timber industry as particularly suitable to stimulate regional economic developments. Opportunities for market growth for timber building systems are associated with the high level of prefabrication, potential in the systematic exploitation of expertise, and in the improved planning [32]. Huge potential is also found in modular commercial building applications, and in a recent review of Ferdous et al. [34], advancement are discussed in terms of challenges and opportunities. A review of new connections for timber structures elaborates on the potential of joining timber components [35]. For both product types a common threat is the lack of standardisation. With respect to the sector of prefabricated concrete elements, the timber sector has very little agreement of standardised solutions for prefabricated modules and timber connections.

Opportunities for timber-based building systems are also associated with timber-concrete composites. The guidelines issued by the COST Action FP1402 [36] are supporting this development, and a positive influence on the market potential is certain, as observed in Germany [37]. In general, the awareness and attention to hybrid timber building systems, is likely to increase market shares of timber, and to improve the environmental performance of the building sector. Joint ventures for buildings in timber in combination with steel, concrete or brick all have the potential of improving the built environment, and the shared knowledge and strengths certainly have the potential to offer common benefits.



Fig. 2: Looking up: Tall wood buildings around the world [38]

Interviews with manufacturers and reviews [32, 39] mention the suitability for industrial applications as one of the main strengths and opportunities for wood. Timber-based building components are accurately and efficiently CNC machined.

The opportunity can be viewed in terms of increased scale and machine-aided operations, where components can be assembled into finalized products. Complete parametric frameworks for design and manufacturing as in the work of Mork et al. [40] and robotic timber manufacturing [41, 42] are some of a range of studies of this topic. Survey of novel timber architecture worldwide has concluded that the opportunities are particularly high for wood [43, 44].

1.1.4 A new generation of timber buildings

The population in Europe is growing and the demography changes. Urbanization takes place and is generally accepted and regarded as a necessary measure to meet reductions in GHG emissions. It is therefore likely that the cities develop towards more compact buildings with more stories. For wood to become an attractive building material in this market, innovative, competitive and industrialized structural concepts with high technical qualities and low economic risk need to be developed, documented and made available. Open architecture and long spanning primary structures will further enhance the competitiveness and environmental performance of timber-based buildings because it increases compliant building functions and typologies. Flooring systems capable of long spans add a high level of indeterminacy to the building and increases possible permutations of internal layouts [45].

A long spanning flooring system also implies that floor elements could be designed with an overcapacity effectively built into the structure as this is erected, to further increase the sustainability of the building. To some extent this would increase immediate costs and emissions, but considerably decrease future resources of adaptations. To further enhance sustainability the building lifetime and adaptability is essential. As reported in Hertwich et al [18] reduced GHG is strongly associated with building lifetime extension, reuse, remanufacturing and recycling.

A tall timber building with an incorporated Designed for Disassembly (DfD) and a flexible plan, meet several of the requirements and can assist in the sustainable development of the built environment.

1.1.5 Rough terrain still ahead

Timber-based building systems exhibit a substantial market potential, and the timber sector is endeavouring to gain market shares for commercial building applications. The advantage timber-based building systems have in terms of carbon emissions is currently not a sufficiently legitimate argument for the construction industry. There is a complex reasoning behind this with many causes linked to a branch that is very little matured with respect to the steel and concrete industry. The construction industry is well-known for risk aversion, and the awareness to the challenges timber-based solutions may have for tall buildings is well expressed. With respect to steel and concrete, timber-based building systems have a disadvantageous ratio of weight

to stiffness causing tall timber buildings to be prone to excessive vibrations both from internal and external sources of excitation.

Wind induced vibrations may cause excessive global deformations and accelerations, whilst human and machine induced vibrations may cause responses to floors and walls exceeding human perception levels for comfort both in terms of tactile and audible vibrations. Restraining structural responses to accepted levels of serviceability and human comfort, is one of the paramount challenges in the design and execution of mid- to high-rise timber-based buildings. Different analysis methods have been used to throw light on future potential for timber-based multi-storey buildings in Europe. In [46], analyses performed in 2014 show high correlation between future potential and the regulatory framework and the construction industry structure. Risk aversion in the value chain of the timber construction industry is assessed to be a significantly larger obstacle than competition from alternative construction principles and materials. The study also argues that competition between manufacturers of timber elements in combination with better cooperation between suppliers of wood products and construction industry is required to increase the competitiveness.

The study supports findings from the timber sector in Norway. A survey presented by the Nordic Network for Tall Wood Buildings and the Norwegian Institute of Wood Technology reports that cooperation between parties is essential to increase market impact [47].

1.2 The Woodsol project

The work performed in this doctoral thesis is funded by the RCN in the Woodsol research project. Woodsol is an acronym for Wood frame solutions for free space design in urban buildings. Woodsol was established to develop industrialized structural solutions for urban buildings [48]. Urban buildings are here commercial buildings in five to ten stories with an open architecture for a flexible plan.

The state of industrialization for timber-based systems for commercial buildings has improved in recent years, particularly in Sweden and in German speaking countries. Although several wooden components are produced effectively by various national vendors, no industrialized solution for the production and assembly of buildings are readily available in Norway. Consequently, building contractors and planners prefer to use other material systems of concrete or steel, believed to represent less risk than timber structures. The Woodsol project was a response to this situation and motivated by political incentives of increasing the use of timber in the construction sector. Additionally, the Woodsol project should be an alternative to building systems of Cross Laminated Timber (CLT) panels. CLT panels have contributed significantly to realization of multi-storey timber buildings up to 10 storeys, but the building system is material consuming and allows limited span lengths.

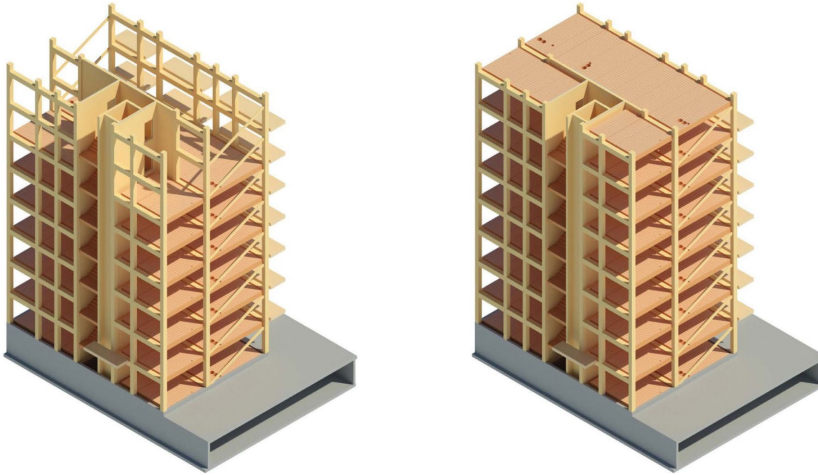


Fig. 3: Woodsol building system as modelled by Løvseth + Partners AS

To facilitate industrial production, the load bearing structure of the Woodsol building system was based on grids and repetitions. The building system has basically one strong and one weak direction for horizontal stabilisation. In the weak direction the stability is solved either by braces or shear walls, but in the strong direction the Woodsol building system offers long span and open facades.

The horizontal stabilisation in the strong direction is based on Moment Resisting Frames (MRF) of columns and beams, with prefabricated couplings to allow rapid erection on site. The Moment Resisting Connectors (MRC) [2, 49] are structurally integrated in the columns and beams by threaded rods [50]. The floor elements are an inherent structural component of the building system as the beams of the MRF are embedded in the longitudinal edges of the floor element. Because the floor element has moment-resisting supports, the span length may be extended without increasing the building height of the floor element [51]. The Woodsol project has a strong focus on the practical documentation of the developed solutions. Hence, a full-scale model was built as part of the project. The scale model was primarily built to assess acoustic properties of the building system [52], but testing of floor elements and building system stiffness was also tested. It was a condition from the RCN that solutions from the research project should be made publicly available, with the aim of providing the building sector with a documented solution for timber-based urban buildings competitive to traditional building systems and solutions. The Woodsol project comprises seven work packages (WP) which will be described in the continuation. The first of these (WP1) was concerning administration and organisation and owned by Kjell Arne Malo (NTNU). In addition to members from

NTNU and SINTEF, the Woodsol project group consisted of members of the following partners of the research project:

- Moelven Limtre AS
- ÅF Advansia AS
- Backe Trondheim AS
- Eggen arkitekter
- Charlottenlund upper secondary school
- Sør-Trøndelag county authority
- Linnéus University
- SP Technical Research Institute of Sweden
- Løvseth + Partner AS
- Sweco Norge AS
- Hochschule für angewandte Wissenschaften Rosenheim

1.2.1 WP2 Production and assembly

The work package was established to define conditions and specifications to meet the desired architectural prospects. Properties concerning story height, span, grid, size of structural elements and openings were addressed. The WP also investigated space for technical installation and requirements for alterations of the components of the building system. Additionally, measures influencing transportation, erection and installation were addressed. The WP was owned by Åge Holmestad (Moelven Limtre AS) and the Woodsol project group was strongly involved in the work.

1.2.2 WP3 Moment resisting frames

The work of fellow doctoral student Aivars Vilguts [2, 49] was linked to WP3. The WP was responsible for the development of Moment Resisting Frames (MRF) based on the use of glulam components connected with long steel rods with timber threads. The WP was formally owned by Kjell Arne Malo (NTNU).

1.2.3 WP4 Flooring systems

The present work is linked to WP4. The scope of WP4 was initially oriented towards enhancing the composite effects of a Timber-Concrete Composite (TCC) for long-span floor elements in MRF applications. With respect to this scope WP4 should address the complete design for long-span floor elements comprising a suitable interface for the structural connection to an MRC in each corner of the floor element, through which moment is transferred between the floor element and the building columns. However, the findings from WP2 strongly influence the scope and objective of WP4. The parallel efforts and achievements of WP3 and WP5 likewise. The WP was formally owned by Kjell Arne Malo (NTNU).

1.2.4 WP5 Acoustics

The WP addressed how the MRF was affecting the transmission of sound and vibrations. The work of fellow doctoral student Simone Conta [52-54] was linked to WP5. The work assessed the structural vibration transmission and how to obtain sufficient sound insulation, depending on the application and code requirements.

1.2.5 WP6 Prototypes

The work package was responsible for the realisation of a full-scale model of the building system. Most of the practical work in this WP was performed by partner Charlottenlund upper secondary school (CVGS), responsible for education and training of carpenters and construction workers in Trondheim, Norway. The WP was formally owned by Petra R  ther (SINTEF).

1.2.6 WP7 Dissemination

The work package was responsible for dissemination of the results and outcomes of the project in a functional and flexible format to increase knowledge among professionals and stakeholders in timber building research, development and construction. A strong emphasis was put to ensure that the end-customers find the format and content valuable in practice. The Research Council of Norway (RCN) who has funded the research project is expecting the deliverable from the project to be a reference work on the use of the Woodsol building system.

1.3 Timber flooring systems in adaptable buildings

1.3.1 Floor layout and available floor element solutions

The term adaptable building is used for buildings that are capable to facilitate and adapt to changes in use and environment. As sustainability has become an increasingly important measure, the concept has been the subject of a series of studies [45, 55-58]. In the present work this term is adopted because it addresses an essential concept in the future role of the built environment, and because it is closely related to the span length. Potential in energy savings and flexibility in use is often lost as floor plan layout is overlooked in early design phase [59]. A building with long spanning primary structures and open architecture increases compliant building typologies and functionality and increases potential permutations of interior layout [45]. Floor elements may affect building adaptability in several ways. By altering the support conditions, orientations of MRF and by utilizing floor elements deviating from rectangular shape flexibility in building plan layouts is possible with timber floor element. See the illustration of a Woodsol plan in Fig. 4. The continuous research on constructive glass argue the case of an increased potential for stabilizing buildings, and the Woodsol project has also executed a study on the topic [60].

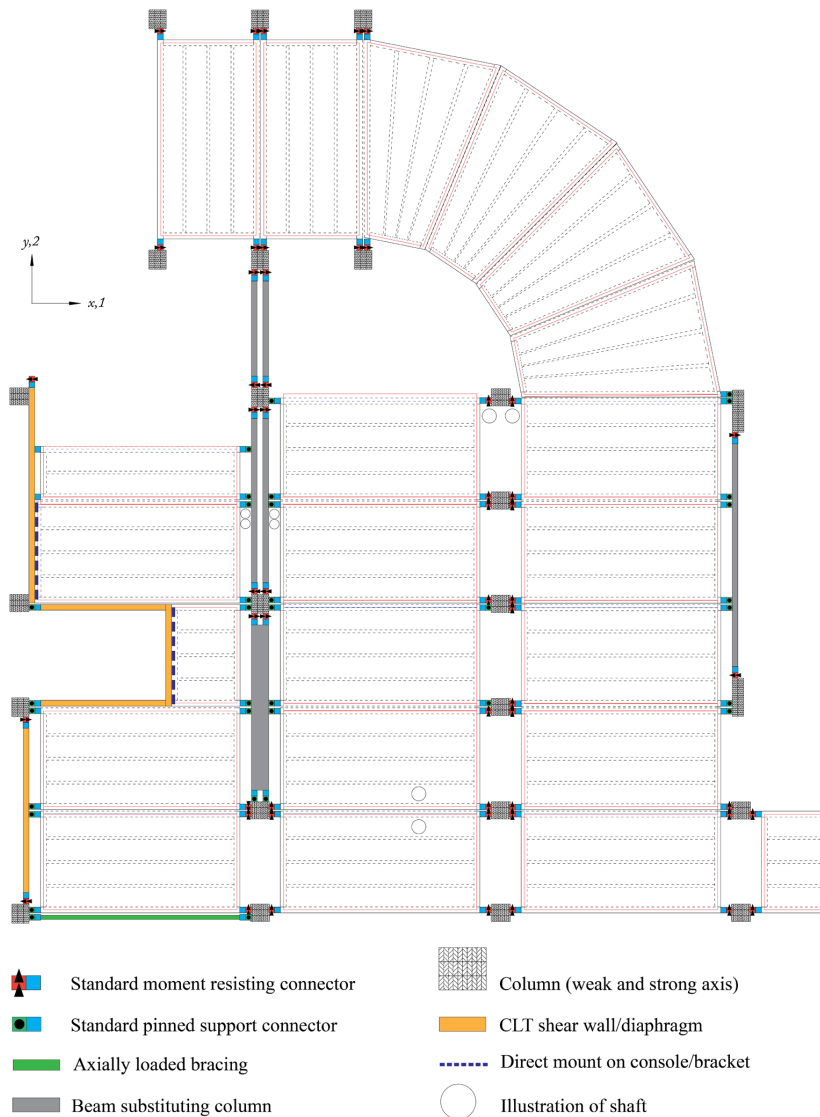


Fig. 4: Variations of support conditions

In the plan of Fig. 4 the important concept of utilizing standardized dimensions of floor element edge joist connectors regardless of mechanical property is envisioned (standard connector with and without moment-resisting capacity) in addition to linear support on console/bracket (girth strip). The concept of standardisation of floor elements and floor element interconnections is shown. Fig. 4 is also showing

the open spaces formed longitudinally between floor elements due to the required space of the columns and the MRCs. Light-frame completion elements (LFCE) are used to fill these openings. The joists of the LFCE may have the same dimensions as the field joists of the floor elements, but the LFCE is typically specified for each building project. Structural bottom flange is typically not required for the LFCE, and it does not contain internal mass unless required for acoustic properties. The top flange of the LFCE is extending onto the adjacent floor element, and the top flange of the LFCE is of identical dimension as the adjacent floor elements. This permits the LFCE to be structurally integrated with the floor elements through interconnections transversally or longitudinally when forming the required lateral stiffness of the flooring system. Simple modifications of floor elements to allow vertical ducts are shown. Modifications of transverse edges of floor elements are not shown. Such modifications are allowed provided that the longitudinal edge joist of the floor elements is intact, and the edge beam is substituted, and the field joists are structurally reintegrated with the substituted edge beam. The modification may require calculation of affected details. Modifications due to horizontal ducts or technical routing longitudinally or transversally is not shown. Such modifications are allowed when prescribed methods are followed. This topic is covered by previous studies at NTNU [61] and not covered in the present work.

The fire resistance design philosophy of the flooring system is that the residual capacity shall be sufficient to withstand actions of accidental limit state with the bottom flange completely charred. The bottom flange is intended either to be exposed to fire or covered by a ceiling system specified for the building project. Rules for structural fire design [62] with guidance from [63-65] and chapter 11 in the Norwegian technical requirements for construction works [66] are used to calculate the required thickness. Hazard class 4 and fire class 3 are used where a complete fire scenario of 90 minutes is presupposed. The minimum thickness of the bottom flange material is then calculated from the charring rate of the material for the fire scenario. Restraining internal mass from fire exposure is not considered.

As concluded in Paper I, standardized floor elements may, to a certain extent, be adapted to required comfort properties by changing the interconnections between the floor elements. The effect of combining strong and weak direction of the floor elements is utilized in addition to brazing and shear walls to provide the required global structural performance of the building. Designing the flooring system with an overcapacity effectively built into the structure as this is erected, will further increase the adaptability of the building [45]. To some extent this would increase immediate costs and emissions, but considerably decrease future resources of adaptations and increase the potential lifetime of the building. Qualities associated with long spanning primary structures are closely related to building lifetime extension, but

may also be linked to improved reuse, remanufacturing and recycling, which are features strongly associated with reduced GHG [18].

For residential buildings, from domestic buildings to mid- and high-rise apartment buildings, span lengths are usually less than 7.2 m. The span lengths for apartment buildings are typically linked to the grid system defined by the basement parking space. To allow an efficient parking¹ the grid size is normally 5.4 or 7.2 m for two or three vehicles within the grid size. As long span lengths and complexity is a cost driver, the floor elements of multi-storey buildings follow the grid, hence the short span lengths even for apartment complexes. The drawback of this is that buildings have low adaptability and are determined to lose market value, or may even be demolished or dismantled, if the required use changes. To ensure that buildings better meet future requirements a longer span is consequently desired. Commercial buildings with open architecture may hold offices or retail or schools which all require longer span to allow the wider range of functions. These buildings may be built as adaptable buildings. Specialised buildings like hospitals or museums or hotels or cultural centres or multifunctional buildings [67] may have similar ambitions. At 9.6 meters the grid size allows both an efficient basement parking space layout with four vehicles within the grid size in addition to a flexible plan. The span of 9.6 m marks a paradigm shift in building plan layout. At this span length few restrictions to functionality exist and may therefore be associated with an adaptable building with only minor expected limitations. At span lengths of 12.6 m, or even at 12.0 m depending on the support conditions and column dimensions, the limitations are substantially smaller and may be associated with a completely adaptable commercial building. In addition to the sources referenced in this section, the span length design premise for adaptable buildings is based on information and discussions during project group workshops. Currently, commercially available timber-based flooring systems are generally offered for span up to six meters (CLT) or eight meters (e.g. Kerto Ripa by MetsaWood or Trä8 by Moelven). Floor element spanning ten meters is also offered (e.g. Lignatur box elements), but with minor potential for high volume commercial building market. For timber floor elements, research and experience is mainly available for 4 to 8 m span lengths, and only limited research has been performed for span lengths exceeding 8 m. Consequently, for the adaptable building market, floor element solutions in concrete and steel are the only competitive solutions available, where span lengths from 6 to 20 m are offered depending on the structural system [68].

¹ Based on information from the research project group, parking space width of 2.4 m is used in the present work. However, current building projects frequently use 2.5 m, and prospect also indicate that 2.6 m is required for modern vehicles. This will affect the floor plan of future adaptable buildings.

While it is technically feasible to design a timber floor of ten metres span with acceptable acoustic performance, the product is generally not an attractive alternative for the construction market. The challenge is therefore to offer the market timber floor elements with competitive cost and designs at an acceptable commercial risk and with proven serviceability.

1.3.2 The structural role of the flooring system

The development of long-spanning flooring systems has the potential to enhance the competitiveness and environmental performance of timber-based buildings. The Woodsol project is one of a handful of research initiatives currently addressing this topic in the Nordic countries, and the initiatives are all investigating timber-based building systems incorporating prefabricated floor elements with an increased structural role. The stability of the buildings is in various manners dependent of the capacity of the flooring system and vice versa, which increases the influence the flooring system has on the overall building robustness and flexibility. Subsequently, as the flooring system is gaining structural influence, volume and complexity, it also receives an increasingly important role in the quest of designing buildings with both low global warming potential and capital expenditures.

1.4 Competitiveness of long-span timber floor elements

The timber sector is endeavouring to gain market shares for commercial and adaptable building applications. As elaborated through section 1.1, timber-based building components exhibit a substantial market potential, with timber-based flooring systems making no exception. However, there exist no competitive timber flooring systems for this segment, and advantages in carbon emissions are currently not a legitimate argument for the construction industry. There is a complex reasoning behind this with many causes linked to a branch that is very little matured with respect to the steel and concrete industry. Timber floor elements are nearly twice the cost of a comparable concrete hollow-core element [69], and the additional challenges of acoustics and serviceability performance are causing the construction sector to be reluctant [46].

For timber floor elements to become an attractive alternative in this market, challenges of serviceability and cost must be addressed. Increased span and improved vibration performances must be achieved whilst keeping consumed resources low.

1.4.1 Material appropriateness

The material properties of wood have both advantages and disadvantages for the use in flooring systems. The adequacy of the material properties is influenced by the span length. Whilst timber is successfully used as a competitive material for flooring

system in domestic buildings and even for mid- to high-rise residential buildings, the properties for a viable option for commercial building applications are demanding. In the following the material properties for timber as an appropriate and viable material for flooring system in commercial and adaptable buildings are briefly elaborated.

In Ashby [70], helpful material selection charts is produced by plotting two key material properties in logarithmic scales. The charts offer valuable information in the process of selecting the appropriate material for a given mechanical application. In the following three charts related to serviceability design of timber floor elements are reproduced by permission from Elsevier. Applied as columns and beams, the ratio of stiffness to cost per unit volume is among the highest for wood, as can be found in Fig. 5. In this figure the dotted line in the middle is the guideline for a stiff beam of minimum cost ($E0.5/C_{v,R}$).

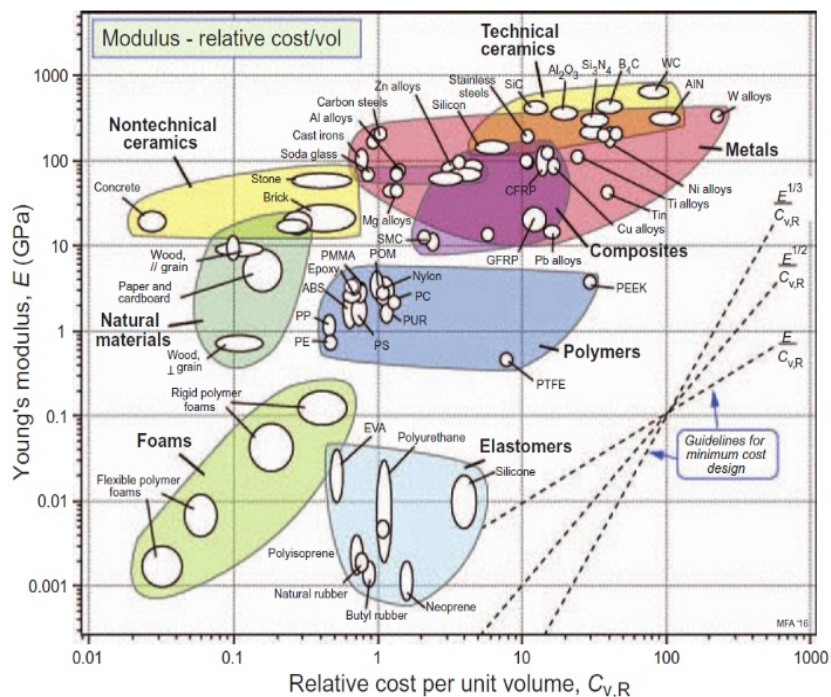


Fig. 5: Chart of stiffness to cost for various materials. Originally published as figure 3.26 in [70]. Reproduced by permission. Copyright Elsevier (2021)

Generally, pronounced advantages are found in the stiffness and carbon emissions (embodied energy) [32]. The environmental performance of wood also shows excellent properties, and as can be seen in Fig. 6, the ratio of stiffness to embodied

energy per unit volume is among the highest for wood. The performance of non-technical ceramics requires tensile armour which will increase cost and carbon emissions with respect to the values used in Fig. 6.

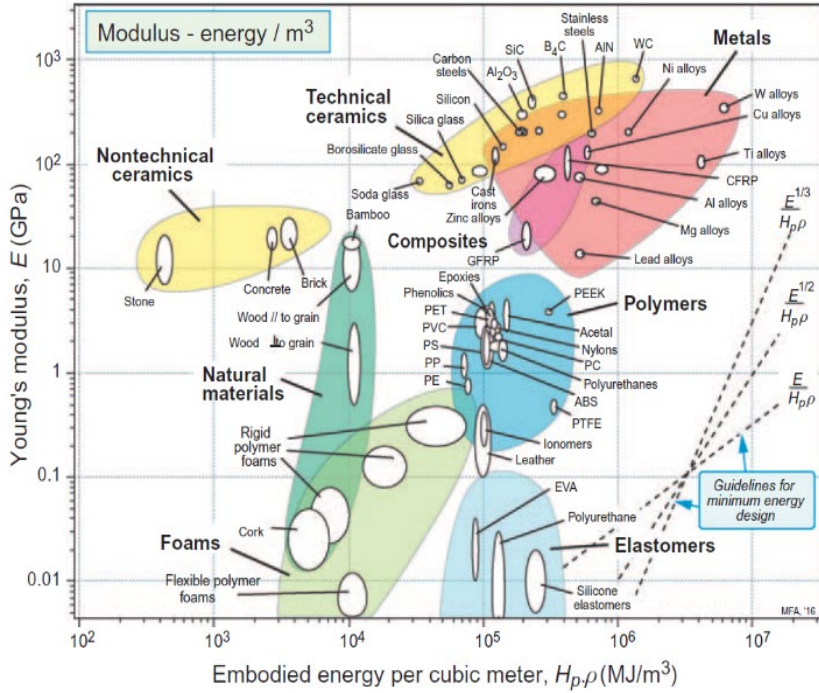


Fig. 6: Chart of stiffness to embodied energy for various materials. Originally published as figure 14.7 in [70]. Reproduced by permission. Copyright Elsevier (2021)

Weaknesses of wood applied to floor elements is associated with vibration performances. Vibration response in terms of human perception can be reduced by increasing stiffness, damping and mass. The most efficient approach depends on the fundamental frequency of the floor.

For a floor element with fundamental frequency above 4.5 Hz, vibration performance responds well to increased mass, but the material properties of wood are not the best candidate to assist. As can be found in the modulus to density plot of Fig. 7, the density of wood is considerably lower than metals and ceramics for the same stiffness. Note that for a stiff beam with a maximum density, a guideline perpendicular to $(E^{0.5}/\rho)$ must be used.

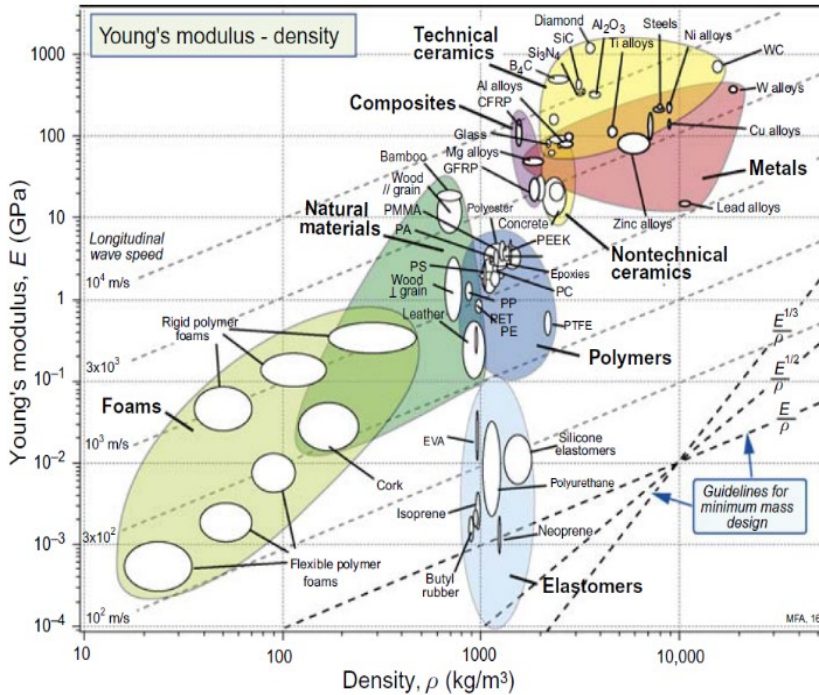


Fig. 7: Chart of stiffness to density for various materials. Originally published as figure 3.3 in [70]. Reproduced by permission. Copyright Elsevier (2021)

Enthusiasm and views on the diverse use of timber and the unexploited potential timber may have for buildings and construction was also found in the following excellent books [31, 42-44, 71-81].

1.4.2 Approaching serviceability consent for structural response

Universally acknowledged criteria for vibration serviceability performance and acceptability is massively debated. Currently, no consensus is obtained and even though the current European timber code, EN 1995-1-1 [82], has guidelines for evaluation of comfort properties of simple floor elements, the requirements are implemented differently in the European countries[83].

Toratti [84] has proposed a design method and classification of floors in vibration classes based on laboratory and in situ tests on steel-, concrete and timber. A work by Hamm and Richter [85] also includes in situ tests of a large number of timber floors together with subjective assessment of floor vibration performance as basis for developing design guidelines for vibration serviceability.

Based on research conducted in North-America on field floors, Hu and Chui [86] published a comfort criterion based solely on 1 kN static deflection and fundamental frequency. The criterion does not recognize damping as a performance parameter.

Measurements of dynamic properties of timber floors have been carried out by many researchers. The work by Homb [87] includes both laboratory and in situ tests on traditional timber joist floors with or without transverse stiffeners, simply supported on two supports or continuous over three supports. The damping ratios of the in situ tested floors were much higher than for the floors measured in the laboratory. Reliable prediction of damping is difficult, although some methods do exist, see e.g. [88].

The interaction with the surrounding parts has an effect on the dynamic properties, and Jarnerö [89] has demonstrated that both the damping ratio and the fundamental frequencies depend on the assembly of structural parts, and they change as the components are added to the structure during construction. A brief overview of this field can be found in Jarnerö [89].

Strengths and weaknesses of the various approaches for evaluation of serviceability have been reviewed by several studies [83, 84, 90-93].

The recent developments on criteria and the limits for vibrations in timber floors by working group WG 3 under CEN TC 250/SC 5 [94] are most interesting and will probably introduce a significant change in how vibration serviceability criteria is treated for timber floor elements. These amendments are likely to be introduced in the second-generation of Eurocode 5, and will give the possibilities of designing flooring systems in performance classes based on analytical calculations involving damping.

The proposed method [95, 96] is based on research efforts over the last 30 years, and has resulted in a new and robust analytical calculation procedure. The approach is based on human perception levels originally developed in the 1930s by Reiher-Meister [97] and later in various forms and for various applications until widely used for steel floors and footbridge structures in the very influential work of Murray [98, 99]. In the modified Reiher-Meister charts the human perception was associated with deflection. See Fig. 8.

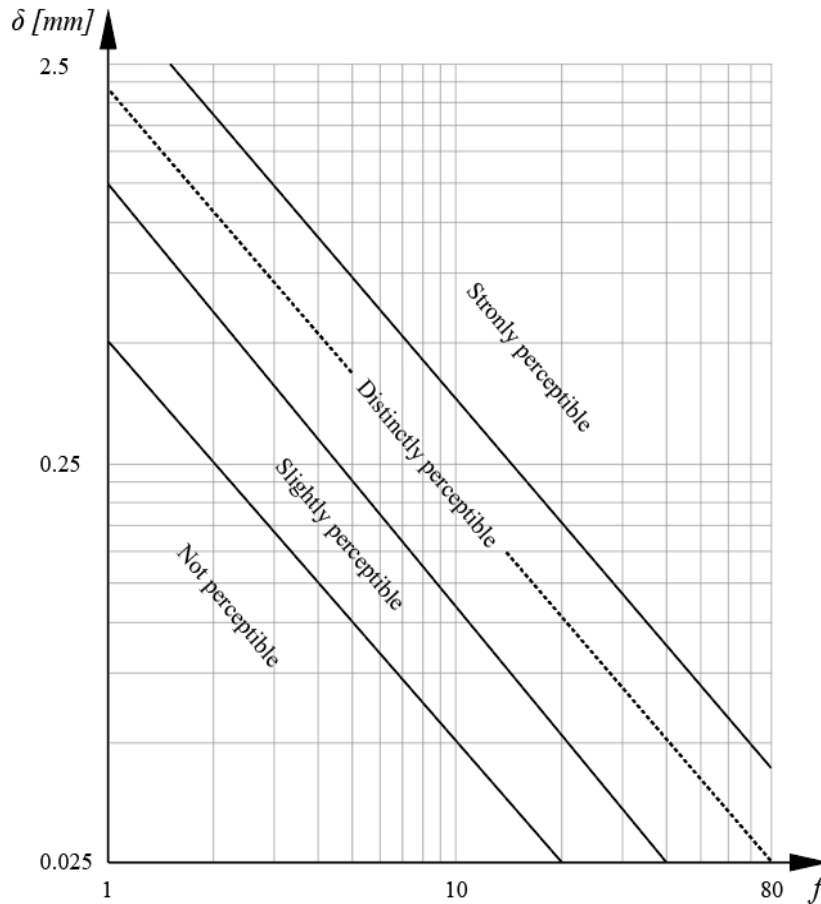


Fig. 8: Reproduction of the modified Reiher-Meister scale

Improved description of human perception is achieved by root mean squared (RMS) acceleration levels. Here levels of acceleration correspond to vibration limit states as defined depending on the use of the building and the associated flooring system. Specific acceleration levels were adopted in early versions of the ISO guideline for the evaluation of human exposure to whole-body vibration in buildings [100]. The same principle is used for the proposed method for the second generation of Eurocode 5, but where the allowable acceleration levels are given by the product of the ISO baseline and a response factor R .

In Fig. 9 this principle is illustrated. Here acceleration levels, which between 4 and 8 Hz dominate the human perception with respect to vibration, are used to quantify the performance of resonant responding floor elements. As can be seen in Fig. 9, the

ISO baseline curve is constant in this frequency at $a_{RMS}=0.005 \text{ m/s}^2$. Above 8 Hz the ISO baseline curve is not constant. By integrating the baseline curve from 8 Hz, the corresponding velocity is constant at $v_{RMS}=0.0001 \text{ m/s}$ [95], and this level is used to quantify performance for transient responding floor elements.

By employing the ISO baseline curve [101] multiples of the curve are used to recommend floor performance levels for the approach proposed for the second generation of Eurocode 5 [102, 103]. Fig. 9 is based on figure C.1 in [101], with floor performance levels as proposed for the final draft of the EN 1995-1-1 [96].

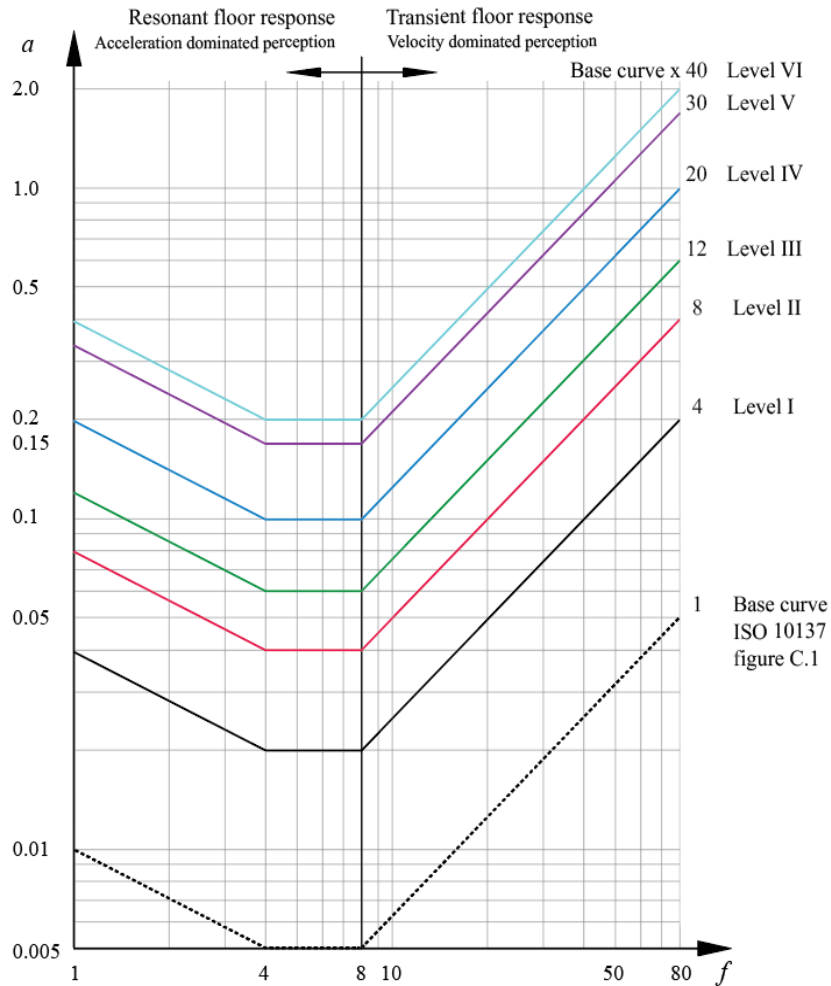


Fig. 9: Floor performance levels with respect to the ISO baseline curve

1.4.3 Determination of floor element response

For CLT or stressed skin panel where the flexural rigidity is well defined in both directions, a floor element with simple support conditions can efficiently and quite precisely be solved analytically. Analytical expressions for continuous floor elements with intermediate supports is also readily available in the guidelines. However, for many building applications Finite Element Analysis (FEA) may often be required to obtain a required level of precision for the floor element response.

The numerical representation of the model depends on the material model and the properties of the structural system, the connections and supports. The combination and properties of finite elements may also impose significant influences on the accuracy of the predicted response. Nevertheless, for floor element responses the load model may impose the greatest challenges and even diverse results.

Several studies are arguing that deterministic methods will produce conservative responses for loads that by nature are stochastic [104, 105], which is the case for footfall [106]. The deterministic models tend to overestimate resonant response particularly when induced by higher order of footfall load harmonics. While improved deterministic models for human induced loading are developed for high-frequency floors [107], this is only marginally helpful for long-span timber floors typically characterised by a resonant floor response. Moreover, since the much-debated cut-off frequency between resonant and transient floor response tends to shift upwards from eight hertz a few years ago to current proposals of 14 Hz [108], long-span timber floors are likely not to utilize these improved models.

Currently, the deterministic analysis approach is conveniently available in several commercial software products for serviceability assessment of floor elements. However, as the above mentioned FEA approaches of computing human induced vibration actually are ignoring Human-Structure Interaction (HSI) [109], alternatives are aspired. In [110] an equivalent moving force based on spring-mass theory is developed to reflect HSI. However, time-step analyses will always be computationally demanding, and when adding HSI the analyses will require even more computational effort. Consequently, time-history FEA is not very suitable, or even incompatible, with optimisation of design where numerous iterations of altering geometry and material composition is required.

An alternative to deterministic methods is to rather model human loading as a stochastic process. In probabilistic methods the interaction of human and the variability in the human step is encountered for. In probabilistic methods a spectral density model is used to represent human induced loads [111]. Such analyses can be performed analytically by employing stochastic vibration theory [112, 113], but the analyses require an accurate mode shape (Eigenvector) to predict the responses.

For CLT or stressed skin panel where the flexural rigidity is well defined in both directions, a floor element with simple support conditions can be solved analytically with modal analyses, but in most building applications FEA is required to obtain reliable results.

Recent studies are promising and appear to have met the level of walking load samples required to generate a spectral density model for stochastic dynamic response of floor elements. In the work of Chen et al [105] Power Spectral Density (PSD) models are generated for single human walking load, and in [114] a similar work is performed to obtain PSD models for jumping load. In a study by Wang et al [115], the development is extended to a PSD model for crowd walking load.

Retaining analytical methods of determination are sought to be required for commonly available guidelines, but the drawbacks of analytical methods increase as the availability and application of FEA increase. Keeping in mind the above-mentioned overestimates of dynamic responses, FEA based on deterministic load models nevertheless produce useful results as reported by many studies [116-118].

The proposed analytical methods in the second generation of Eurocode 5 quantify acceleration and velocity deterministically based on Fourier series assuming the load model from one step to be reproduced by the next in a periodic process [95, 119]. The solutions utilize estimates of damping to improve the description of vibration response, but the precision is consequently sensitive to the level of damping ratio used. Many parameters influence the damping ratio of timber floor elements.

The type of floor element, the support conditions and interconnection between the floor elements, the properties of outfitting, and the use of the building are all influencing parameters.

The continuous assessment of long-span timber floors, either numerically, in-situ or as full-scale laboratory tests, is crucial to build information that will enable a reliable level of damping ratio to be selected for the various floor types and applications.

For long-span timber floor designs, the proposed analytical method for the second generation of Eurocode 5 [95, 96] may offer a good compromise between simplified methods of assessing serviceability [120, 121] and more sophisticated numerical analyses. However, if FEA can be used, the stochastic load models may be a promising way forward. The method is a computationally efficient approach where the precise probabilistic dynamic vibration response directly can be used to assess the performance of the floor with respect to the human perception levels given by the ISO baseline.

1.4.4 Pursuing competitiveness

Information from the Woodsol project group and interviews of members of the Norwegian building and construction sector has emphasised that the cost of long-span timber floor elements is substantially higher than comparable concrete hollow core elements, and the incentive for choosing a flooring system that improves carbon emission accounting is currently not a sufficiently weighty argument to choose timber-based flooring systems for commercial buildings [47]. The much-debated challenge in fire resistance is expressed to be manageable, whilst challenges of acoustics and vibration require attention. These experiences are reflected by the study of Kuzman et al. [32].

Numerous studies have investigated properties related to vibration serviceability of timber floors. The joined forces have reached at a promising approach as presented in section 1.4.2. Also, the acoustic properties are much studied. In recent years frequent studies have addressed timber-concrete or timber-steel composites [122-131], also with valuable outcome [36, 37] as pointed out in section 1.1.3. Many studies have also aimed at redesigning and improving the performance of timber floors [132-138].

However, the cost of the proposed designs and solutions is often either overlooked or treated superficially in terms of bill of materials. In order to increase the market impact of long-span timber floor elements, advancements in competitiveness must be achieved. Consequently, the present work has aimed at filling gap of knowledge and at developing methods and tools that may assist in enhancing competitiveness, either by optimising the floor element or by utilizing other cost-efficient approaches.

1.4.5 Increased competitiveness through optimisation

Timber flooring systems for long-span applications are normally glued thin flange elements with stiffeners and joists constituting the core. The number of joists and stiffeners, the internal added weight and insulation, and the dimensions of all members result in numerous combinations. This number increases drastically when the continuously expanding range of technical wood products and types of bonding are considered. (Fig. 10).

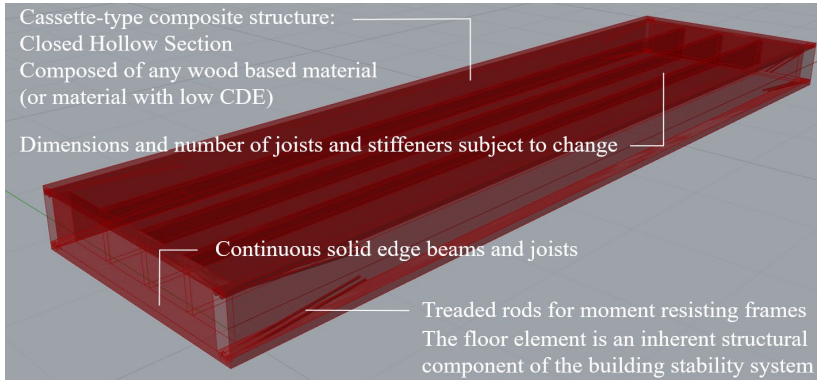


Fig. 10: Timber floor element

When outfitting as overlays and ceiling system is addressed, combinations increase further. And finally, when support conditions and load conditions, serviceability performance levels and building heights are regarded, the solution space is immense (Fig. 11). With this many parameters, finding a competitive design may not be manageable by manual exploration, and the solution space can in practice only confidently be investigated when assessed computationally.

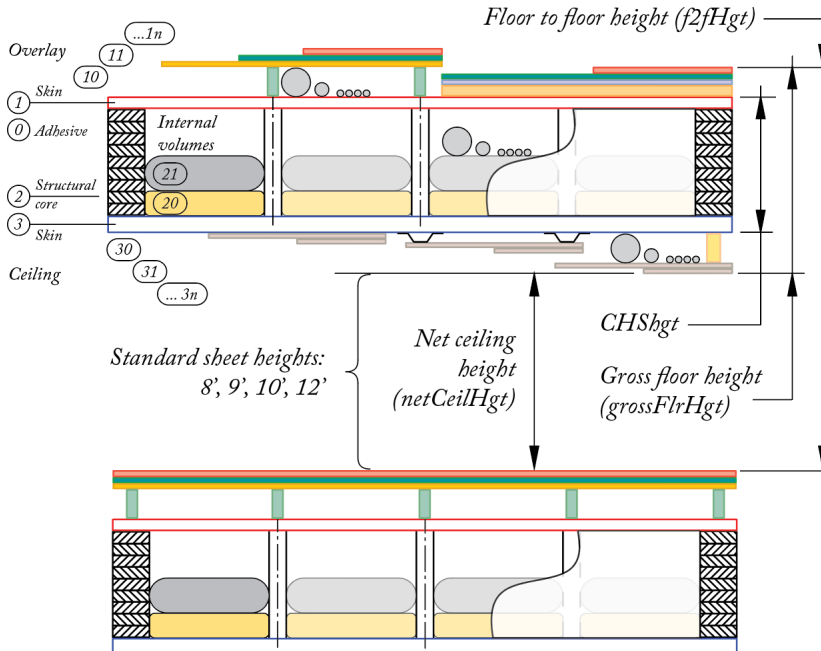


Fig. 11: Some parameters for timber floor element applied in building

As concluded by Forintek and the Canadian Wood Council [139] a precise manufacturing cost accounting in combination with an optimisation workflow can offer an efficient solution for the development of competitive timber floor elements. Findings from informal interviews of parties of the Norwegian timber industry also emphasise the importance of improved knowledge and precisions of costing. This concerns both capital expenditures of manufacturing and construction, and operational expenses throughout the service lifetime.

A parametric accounting method of resources in the manufacturing of timber elements is studied and developed in the present work. The method is called Item-Driven Activity-Based Consumption [Forest Products Journal]. The method may directly be used as an objective function both for cost and the embodied carbon emissions (ECO2) of timber floor elements, and the parametric architecture of the method facilitates for easy implementation in an optimisation workflow. The IDABC-method is employed in a python module that calculates the structural response of the associated floor element as applied in a building [140]. This module is used to describe the timber element subject to optimisation.

By joint forces with the Faculty of Built Environment at Tampere University it was managed to adapt an optimisation algorithm originally developed for cost- and mass-optimisation of steel constructions to cost- and ECO2-optimisation for timber floor elements [141]. In the process of developing the architecture of the workflow, determination of structural response was solved analytically. However, the workflow may employ FEA for a more precise determination of the structural response, hence the effort in the development of a parametric script for an automated generation of Closed Hollow Sections in Abaqus [142]. See Annex A.II. The script was named Python Script for Abaqus for Closed Hollow Sections, herein referred to as PSACHS [143].

Due to the parametric design of the workflow, optimisation of floor element building height is also possible. The building height is also an important indicator of competitiveness for timber floor elements. This is due to the influence the floor elements height has to either the total building height or to the potential loss of number of stories when the building cornice height is constrained.

In Norway an electronic handbook is freely available for concrete floor elements [144]. The handbook readily guides architects and engineers in the use of concrete floor elements. A comparable asset for long-span timber floor elements (LSTFE) would be of significant assistance to increase the market shares of timber floors for commercial building applications. This reference work could have the format of a handbook or a guideline that could be available through a website, possibly with an additional option of a printed version if the market claims this. The data that this

reference should be built upon must comprise competitive designs, and the presented work consequently addresses factors influencing competitiveness of LSTFE.

1.4.6 Environmental challenges

The environmental performances of timber-based building systems are reported to vary. In [145] the differences between a conventional beam and columns to a CLT systems with low global warming potential, show nearly a 10 % reduction in carbon emission in a 50-year service time perspective. A similar consequence is revealed in [146] where carbon emissions in floor elements are studied. Here timber floor elements are found to have lower carbon emissions than comparable floor elements in other material, but it is also shown that a 50-80% higher carbon emissions can be expected for the same timber product if suppliers and components are not selected with care.

The findings address a necessity of an ability of selecting specific building component or direct material between various suppliers, and to see the effect of the selected supplier in the resulting ECO2 for the finalized timber element, and one of many findings entered into the systems analysis of timber floor elements.

2 Research approach

2.1 Background

The scope of the study was initially oriented towards enhancing the composite effects of a Timber-Concrete Composite (TCC) for long-span floor elements in MRF applications. TCC have both advantageous and disadvantageous for floor applications [36, 147]. Whilst TCC may offer longer span, the time-dependent behaviour of the composite, i.e. creep, drying shrinkage, mechano-sorption and thermal and hygroscopic strains, must be addressed for a permanent well performing floor. Full-scale tests at NTNU performed by Skaare [148] (2013), Alm and Frihetsli [149] (2015), and Åby and Hartnes [150] (2016), reported that the disadvantageous early-age behaviour of the concrete flange was difficult to resolve without excessive use of cost or embodied carbon emissions (ECO₂) consuming resources. i.e. reinforcement to counteract creep and shrinkage, or the prefabrication of concrete flanges with cost driving storage during hardening. Of reasons above the focus shifted to flanges of technical timber.

In addition to the main objective of WP4 (see section 1.2.1), the scope of research of the present work was strongly affected by the addressed topics and findings in the research project group during the work on WP2 Production and assembly (see section 1.2.1). The span length and element depth, support conditions, maximum dimensions for transportation, as well as cost and ECO₂ was some of a huge range of topics addressed. The findings from the assessment of buildability and assembly of the Woodsol concept by MSc students Ivar Hoel Monsen and Mathias Nystuen [151] was also considered. The gathered information was sorted and continuously considered during the development of the research approach.

The work of MSc students Henning Bjørge and Terje Kristoffersen was an important background for the present work. Their work [152] included the design and realisation of a full-scale model. This work also included testing and numerical analyses of the floor element. The level of acceptance revealed for a 9 m floor element as measured to various methods of serviceability criterion was influential for the research approach.

Of importance for the research approach was also the ongoing work for a method for floor serviceability for the second generation of Eurocode 5. Reports of utilizing the ISO baseline curve was released in 2018 [102]. In relation to the timeline of the present work, the expected outcome of the new method argued the case of not linking research to current methods for vibration serviceability. In January 2019 the author was informed by Tomi Toratti about details of the proposed method of the second generation of Eurocode 5.

Due to the substantial effort in pursuing the best combination of material and dimensions of the floor element and the associated effort of numerical modelling of the floor element, a script was written to generate the numerical model in Abaqus [142]. Furthermore, due to the high computational time for analysis reported [152], conclusions towards assessing the influence of finite element type and size [153] was also drawn. The objective of assessing how the type and size of finite element will influence the precision and computational effort of solving the numerical model, was consequently addressed (Paper V). This work provided information of what base feature, finite element and element size that would be best for optimisation purposed.

Based on the findings, methods for numerical optimisation using the Abaqus analysis engine was studied. The software developer Dassault was contacted, and the author organised an optimisation workshop at NTNU with Ebbe Smith from PLM Technology. Following the workshop, several undertakings at the Timber Structures Research Group was performed where Abaqus was run from the execution engine iSight [154]. An optimisation workflow for the numerical representation of the floor element was also developed using iSight. The routine proved excellent performances for optimising the dimensions of the members of the floor element based on the Hu & Chui criterion [86] as objective function. However, due to the pending conclusion on serviceability methods, and the increased awareness of cost as a key cause for the low market share for timber floor elements, conclusions that the optimisation workflow requires a cost module was drawn. A literature review related to cost accounting of timber elements identified little compatible research, whilst the reasoning of the value a precise cost accounting would have for the audience of the research work increased.

Attention was brought to the topic of cost accounting for timber elements, whilst the MSc student Sissel Solibakke Mo utilized PSACHS and the optimisation workflow developed in the present work [155]. Mo also used iSight to predict the material model for the flange of the floor element based on laboratory testing. Here the Pointer method in iSight was used, and the information of the material model brought forward in the present work.

During the development of a cost module and essentially a cost object for the floor element, an analytical approach to optimisation using the Galapagos solver for Grasshopper [156] was employed rather than iSight. This was due to benefits from a fast analysis time which was important both for debugging and to assess the results. The development of the cost module was performed in a Python object in Grasshopper to enable the re-implementation in optimisation workflows based on Python coding, which is the case for Abaqus and iSight.

Still the optimisation employed the Hu & Chui criterion for serviceability, but this was done only to have a straightforward assessment of serviceability that always

would return a number during the development of the optimisation. Grasshopper has the same opportunity of selecting different materials and predetermined material dimensions as in iSight, but enables in addition an easy elaboration on the content and results from the Grasshopper workflow. In an early version of the cost module, Grasshopper calculated a number of manufacturing processes and the area of the processed surfaces, with a simplified assessment of the associated costs in addition to the cost and ECO2 of the accrued material. See Fig. 12.

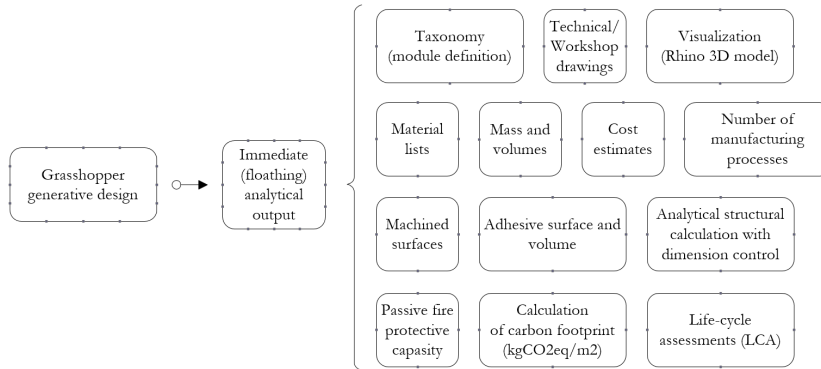


Fig. 12: Outcome from the Grasshopper workflow

However, the cost functions did not produce the required level of accuracy, and a matured literature review on cost and resource consumption from manufacturing was performed. This work was also greatly motivated by the conclusion of Forintek and the Canadian Wood Council [139] stating that a precise manufacturing cost accounting is required to identify competitive solutions for timber floor elements through optimisation.

In spring 2019 Kristo Mela from Tampere University was contacted because of methods applied in cost-optimisation of steel structures. An intent of elaboration was established, and in the autumn, the author stayed two weeks as a researcher in residency at the Tampere University where the Python-based method for optimisation was studied.

The researchers at the Faculty of Built Environment at Tampere University exercised excellent attention to academic common benefits during the cooperation.

2.1.1 Mid-term research approach findings

- Floor elements spanning 10 m between axis is feasible, but finding an optimum solution is demanding
- The construction sector is reluctant to using timber floor elements in commercial applications due to 1) uncertainty of cost estimates, and/or high

costs with respect to comparable alternatives in concrete, and 2) uncertainty in vibration response. Note that at the time of the mid-term conclusions, the recommendation of method for serviceability for the second generation of Eurocode was still pending open hearing.

- Cost is a less studied topic of timber floor elements
- Optimisation requires accurate cost object function
- Computational exploration required to reliably explore the possibilities of available material combinations
- Margins must be pursued throughout the product specifications and in the stages of manufacturing
- The depth of the floor element is an important cost parameter and must be addressed
- Glue pressurizing of flanges using screws are cost-driving

2.1.2 Matured research approach

Quantification of manufacturing resources like production time, cost and ECO2 may serve as indicators for competitiveness, and can be measurable research objectives. Timber-based flooring systems are endeavouring to gain a market share in terms of their use in commercial buildings and cost must be reduced. The challenge of enhancing competitiveness of long-span timber floor elements is substantial and requires the attendance to several goals simultaneously. A matured research approach was consequently defined:

- Certain quantities may serve as indicators of competitiveness and addressed as research objectives.
- Information from the project group must be analysed to identify significant indicators of competitiveness and to ensure that the information is adopted and exploited in terms of conditions for a reference work.
- An optimisation workflow may be built from the compilation of modules for 1) determination of floor element response, 2) quantification of resources from manufacture and materials, and 3) suitable solver for optimisation based on available material types and dimensions.
- The determination of floor element response can be estimated analytically using the proposed guidelines for the second generation for Eurocode 5. The determination should address any significant contributions for the floor element as applied and finalized in a building.
- A parametric quantification of consumed resourced for the floor element as finalized at the factory gates should be developed.
- Elaborate with Tampere University in finding a suitable and robust optimisation solver and workflow for long-span timber floor elements.
- Involve industry in the benchmarking and validation of the work.

- Address topics and concerns related to Design for Disassembly, and criteria to satisfy utilization in adaptable buildings.
- Ensure that the work may be utilized by future students by investing effort in comments and explanations and a clean code.
- The Research Council of Norway (RCN) is expecting a deliverable suitable for a reference work for the Woodsol building system. For the floor element, data for such a reference work must comprise competitive designs to have a market impact.

2.2 Ethical issues

In some areas of the world logging is not sustainable, and outtake are higher than the augmentation. However, political regulations are steadily improving the situation. The recent updates in [25] shows which areas where logging are sustainable, and such sources in addition to assessment of carbon emissions guide in selecting materials that can be combined in a product with high ethical standards.

Simultaneously, the Woodsol building system aims at reducing the amount of required timber as opposed to the more generic CLT solutions and in that manner resembling the efficiency and revolution which the stud frame housing developed because of the timber shortage post-WW2.

Avoiding making timber constructions appear as the more favourable material than what it is, is also an ethical concern. The research project must pursue the best combination of timber with other materials. Timber is not the entire solution but part of the bigger picture. Bridging interests and branches are a shared responsibility, though this is not always the case: Every branch is biased to prioritize own advantages, rather than joining actions and creating a product with less environmental impact even though that could lower profits. It is in this project's interest to show high standards on this matter.

Seeking cooperation with other research institutes and foreign universities has ethical dimensions and will be given attention. Such efforts will build alliances and future projects. Similarly, facilitating for future students to take advantage of the scripts and archive of literature established during the present work is of importance and will gain all parties. This will be achieved by investing efforts in comments and explanations and a clean code and calculation documents.

The vision and strategy of the owners of the research project is kept in mind during the present work. The vision of the Department of Structural Engineering at NTNU is Knowledge for sustainable constructions, and the SINTEF corporate strategy is to contribute to societal benefits, competitiveness and usability. Reflections on these values has been done during the present work.

2.3 Research objective and questions

Timber-based building systems exhibit a substantial market potential, and the timber sector is endeavouring to gain market shares for adaptable building applications. The advantage timber-based building systems have in terms of carbon emissions is currently not a sufficiently legitimate argument for the construction industry. Reductions in greenhouse gas emissions represent a major and universal challenge for the construction sector, and the timber industry is under substantial pressure to find attractive solutions particularly for adaptable buildings that by concept may prove low levels of carbon emissions and overall energy consumption with respect to the expected service life time.

The objective of this doctoral project is to strengthen adaptability and competitiveness of long-span timber floor elements. The challenge is to quantify competitiveness and to develop an approach for a confident and fast exploration of the solution space of possible combinations of geometries and materials suitable for an adaptable building. Requirements concerning serviceability, support conditions and any significant parameter that influences the application of a floor element in the building must be addressed.

The Research Council of Norway (RCN), who has funded this doctoral project, has requested the deliverable from the Woodsol project to be a handbook on the use of the Woodsol building system. This has been a contributing factor in the formulation of the objective and scope of the work. The orientation towards applied research and the aim of demonstrating practicable methods to assist the market for long-span timber floor elements is a response to the request by RCN.

On a methodical level it is an objective that the effort and contribution of this doctoral project should be performed in such a way that it will facilitate for further research based on the tools and approaches developed by the present work.

The elaboration of research objectives has been done based on the context and the experience from a matured research approach. From the research objectives the following research questions have been duly formulated:

- 1) Can timber floor elements be used for span of ten meters, and what parameters are significantly influencing the performance of a timber floor element when applied in a building?
- 2) The cost of timber floor element with respect to comparable alternatives is high. How is this affecting the market share for timber floor elements for commercial buildings, and what can be done to increase the market share?
- 3) The construction industry is well-known for risk aversion, and the awareness of the challenges of long-span timber floor elements is well expressed: How

can this risk be further clarified, and what can be done to reassure the construction sector on this matter?

- 4) Reducing GWP is a paramount responsibility for the construction sector. How can timber floor elements contribute to a sustainable development of the built environment?
- 5) The Research Council of Norway has requested the deliverable from the doctoral work to contribute to a handbook on the use of the Woodsol building system. How can this be addressed? How can the data for a handbook be validated, and what are the conditions and requirements for a handbook related to timber floor elements?
- 6) The amount of new engineered wood products, fasteners and adhesives continuously introduced to the market may be prosperous for the development of a competitive timber floor element, but the availability may also be challenging. How can the solution space be explored efficiently, and what are the requirements for the exploration?
- 7) What can be done to facilitate that methods and tools developed in the present work are utilized by future students at either MSc or doctoral levels for the common best of timber-based solutions as a means of improving the environmental performance of the built environment?

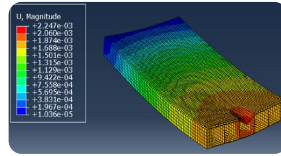
3 Research method

3.1 Methods at a glance

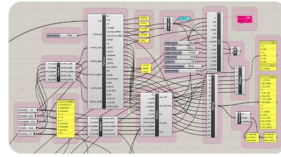
Information retrieval performed through several of the university databases. New information was inquired as the research approach evolved. The information was organised in Endnote. NVivo was used for literature review support.



Numerical analyses performed in crossX for shear flow analyses, and in Abaqus/iSight for numerical determination of responses for floor elements with different support conditions and for two floor elements with interconnections.



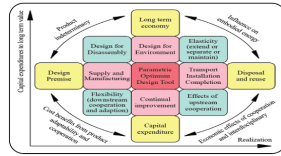
Analytical methods used for determination of responses, frequency analyses, post-processing of numerical results, calculation of resource consumptions and optimisation. The programming language Python was used throughout the study.



Experimental methods for measuring deflections, accelerations and modal shapes. Experiments were performed with different support conditions, and with varying types of interconnections between floor elements to quantify effects.



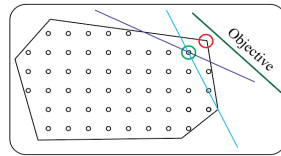
Systems analysis performed to sort and categorise information from the project group. The objective was to ensure that all indicators and parameters was addressed, and to identify features and conditions for competitive timber floor elements.



Real-life approach to involve the industry and to benefit from the knowledge and experience. The dialogue with the industry was important for reality orientation of the present work and in the validation of results.



Optimisation was performed to exploit both the potential of the codes developed in the present work, the potential of long-span timber floor elements, and to essentially comply with the expected outcome of the research.



scientific, technical, medical, and social sciences. Scopus is the most comprehensive abstract and citation database of peer-reviewed literature.

- [ISI Web of Science](#): Consists of seven online databases encompassing more than 50,000 scholarly books, 12,000 journals and 160,000 conference proceedings
- [Compendex/Inspec \(Ei and Engineering Village 2\)](#): Engineering Village is particularly designed for the engineering community and offers access to twelve engineering literature and patent databases providing coverage from a wide range of sources. The most comprehensive of these databases is the Ei Compendex alone offering more than 20 million indexed records
- [Civil Engineering Database \(CEDB\)](#): Free bibliographic database offering records of all publications by American Society of Civil Engineers (ASCE) since 1872. The database is run by the ASCE Library which is offering an online full-text search ranging from peer-reviewed journals, proceedings, e-books, to standards published by the American Society of Civil Engineers.
- [Google Scholar](#): Freely accessible web search engine that indexes the full text or metadata of scholarly literature across an array of publishing formats and disciplines. As of 2014 it is estimated to contain roughly 160 million documents. Google Scholar is similar in function to the freely available CiteSeerX and getCITED.

In addition to library databases the University Library at NTNU was contacted at several occasions for papers not able to available through the subscriptions at NTNU Oria. In addition, several papers from the [Taylor & Francis Group](#) were difficult to retrieve even though listed with NTNU access.

3.2.2 Search inquiry key words

As will be explained in section 2.1 the research approach developed as literature was collected and examined in context of the present project. Each database has its own syntax for truncation and formulation of text search strings, and various options of combining and excluding words or stems of word may be used in addition to other means of conditionally search. Typically, this is to constraints the search to key words and topics, title (exact or approximate), or authors. The search could be constrained to an exact journal, year of publication to mention some. Key words and topics used in the information retrieval is given, but not limited to, the content of Table 1. In several of the groups, various basic terms for limiting the search to e.g. timber floor elements, or long-span timber floor elements, is implemented and not reflected in the search terms. The same apply to the structural type like the terms of Closed Hollow Section or Stressed Skin Panel. Additionally, several inquiries have been performed on specific authors and is not reflected in the table. The key words and topics are presented in groups of literature.

Table 1: Groups of inquired information and related key words

Group	Key word and topic
Adaptable buildings:	Buildings AND adaptable; flexible; sustainable
Composite floor:	Composite; TCC; STC; hybrid;
Cost objective:	(Cost* OR expenditure) AND objective; estimate; competitiveness; economic;
Structural topics:	Shear lag; effective width; Winkler; elastic foundation; horizontal stabilisation; Shear; diaphragm;
Engineered Wood Products:	Glulam; limtre; CLT; Cross laminated; LVL; Laminated timber; Laminated veneer; Laminated strand; EWP;
Experimental Modal Analysis:	Modal; experimental; EMA; MAC; Maxwell reciprocity; rowing hammer;
Fabrication awareness:	Fabrication awareness; manufacturability; buildability; assembly*;
Human induced vibration: Multi-objective:	Human induced; footfall; heeldrop; Low freq*; multi object*; multi paramet*; multi-paramet*; multicriteria design; multicriteria object*
Numerical modelling:	Abaqus; Finite element AND (*selection; *type; *mesh); accuracy; computational effort;
Object function:	Object function; system optimization; structural optimization; design optimization
Optimisation:	Optimisation; Optimization
Parametric study:	Parametric*;
Power Spectral Density:	Power Spectral Density; Power Spectral-Density; Spectral-Density; Spectral Density; PSD; spectral model;
Statistical energy analysis:	Statistical energy; SEA;
Sustainable machining:	Machining AND sustainable; life cycle assessment; LCA; Energy efficiency; sustainability assessment;
Timber construction market potential:	Market; future; potential; industry;
Timber material model:	Mechanical; propert*; modulus; characteristic*; elastic; *tropic; constant*; model; material*
Time-Driven ABC:	time-driven activity
Topology Optimisation:	Topology Optimization; origami;
Vibration serviceability:	Vibration; serviceability; perception; acceptance; structural response; dynamic response; damping*

3.2.3 Interpretation and sorting of literature

During literature analyses and reviews, NVivo [158] was used to ease the interpretation and to gain overview of the collected information. When an assessment or a review was to be made, the relevant Endnote library was imported in to NVivo, and various methods applied. The text search query in NVivo enable a search through the internals (Endnote records where a pdf-file is available) to find occurrences of words or phrases. The text search can filter the library down to occurrences of a subject (e.g. timber AND floor) and store these as a new set, on to which a new text search query or word frequency methods can be run. Queries were run on various file classifications depending on the type of information requested (book, book section, conference paper, journal article, etc.). The result of the NVivo methods is the establishment of a link to each of the occurrences (nodes) where the context of the occurrence is easily found and elaborated on. The use of Word Tree proved very efficient in the process of review, and an example of a timber floor literature set is assessed for the occurrence and context of the word Optimisation with one occurrence selected. See Fig. 14.

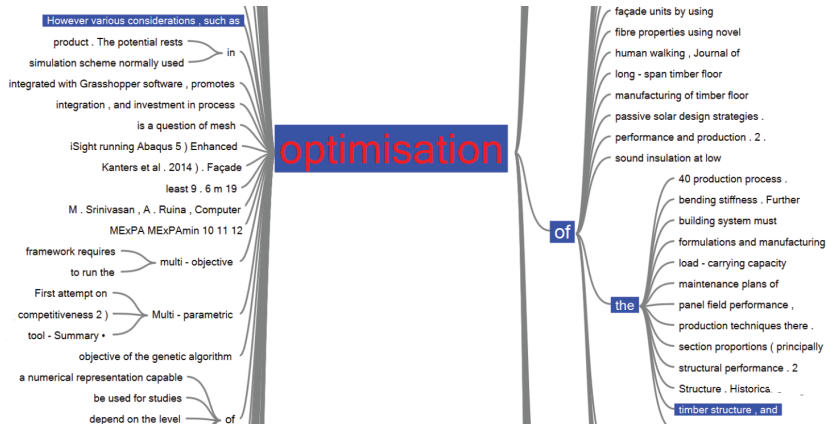


Fig. 14: NVivo Word Tree example

3.2.4 Materials database

A material database is built to support the various codes written in the present work. The database contains both mechanical properties and commercial properties. The material database is built as two Python repositories. See Annex A.I.

The first repository is named *materialFormat*. This repository contains the retail standard material formats of all materials used in the present work. The repository is structured with a mandatory name of the material followed with primary dimensions, secondary dimension and finally production lengths if available. All dimensions are

given as a list even if there are no standard retail dimensions available (bulk material), or if there are only one dimension available. All dimensions in [m].

The second repository is named *materialProperty*. The repository contains the following material properties.

- elasticType: ISOTROPIC or ENGINEERING_CONSTANTS
- elasticProperty: E1, E2, E3, Nu12, Nu13, Nu23, G12, G13, G23 [N/m²]
- density: [kg/m³]
- unitVolCost: unit cost [€/m³]
- unitMassCO2eq and unitMassCO2uptake: unit mass parameters for embodied CO2 emissions (ECO2) and uptake of CO2 equivalents (in g per kg) for materials information modules A1–A3 (Cradle-to-Gate) [gECO2/kg]
- format: Reference to a specific entry in the *materialFormat* repository
- chrRate: None or [mm/min] if available

Quantities of cost and unitMassCO2 (equivalents and uptake) are given as dictionaries. This implies that a supplier must be parsed to retrieve a value of cost or unitMassCO2. This is done because values of cost and unitMassCO2 is prone to differ between suppliers or manufacturers.

The material database is also used to store sources of material properties. The database is primarily based on the following references [69, 77, 146, 159-164].

The Python codes PSACHS [143] and PARAPECHS [140] both read material specifications from this common database.

3.3 Numerical methods

3.3.1 Numerical representation of the flooring system

Throughout the present work a numerical representation of a flooring system was required. The Finite Element Analysis (FEA) software Abaqus [142] was used for this purpose. Due to a cumbersome modelling in combination with changing flooring system specifications, this resulted in the building of a Python Script for Abaqus for Closed Hollow Sections (PSACHS) [143]. This enabled a fast generation of a numerical model with due analyses, post-processing and writing of results to an output file. The specification of the floor element is done in a text file (see Annex A.II). In the current section reference to the parameters of this input file is given as *italic* terms in parenthesis. The script resulted in a complete freedom in the specification of material and dimensions and of number of joists and stiffeners. Full freedom was also given in how to model the base feature of all members (shell or solid), the type of finite element, and the size. Surface layers (applicator and receiver) was added to facilitate easy definition of loading (*ptLoad*, *dstrLoad*) and collecting of responses.

A timber floor element constituting a closed hollow section as shown in Fig. 15. The floor element is created from an edging frame of joists ^① and interconnecting transverse beams ^②. The edge joists are positioned with an optional offset from the flanges. A number of field members (*fldJstNum*) ^③ are fitted between the transverse beams positioned either at even cavity distances (*evenJstCvty* Y/N) or even centre distances. A number of transverse stiffeners (*fldTrnsNum*) may equally be fitted. The centre joist can have particular specifications (*diffCntJst* Y/N). A continuous flange is structurally glued on top ^④ and bottom ^⑤ of the frame. The interaction between the flanges and members of the frame is controlled by stiffness parameters in three directions (*topFlgKnn*, *topFlgKss*, *topFlgKtt*, and *btmFlgKnn*, *btmFlgKss*, *btmFlgKtt*). For the flanges, the number of plies and the direction of the plies may also be specified (*topFlg_plyNum*, *topFlg_plyOrient*, and *btmFlg_plyNum*, *btmFlg_plyOrient*). The Ply orientation apply symmetrically from longitudinal axis with alternating direction of rotation.

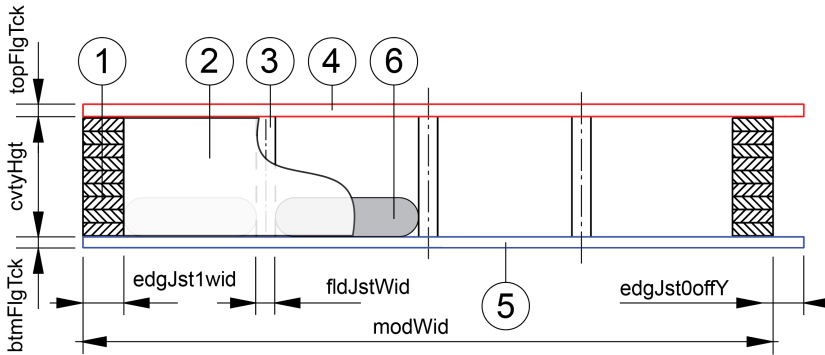


Fig. 15: Cross-section of floor element in PSACHS

Non-structural overlay (*overlayDstrMass*) and internal mass including mass of ceiling system (*cvtyDstrMass*) are represented as distributed mass associated with the top and bottom flange. Mass of fasteners is represented in both or either of these. The script incorporated several types of support conditions as illustrated in Fig. 16.

stiffness in three directions (D_{11} , D_{22} and D_{33}). Skin/Stringer reinforcements (*SCmtrl*) were defined for the joist to represent the load distribution from the MRC to the joists. If the edge joist was defined by solid elements, four cartesian springs was used for each end of the edge joist, while for shell element two cartesian springs was used to generate the required end constraint (see Fig. 17).

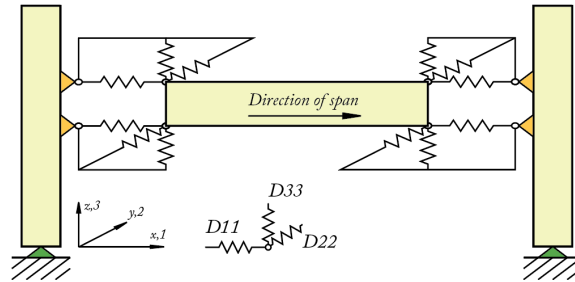


Fig. 17: Definition of cartesian springs

For the cartesian springs, D_{22} and D_{33} was estimated both as an iSight Pointer problem with reference to numbers obtained from experimental testing, and in dialogue with fellow PhD student Aivars Vilguts [2], where the later quantity of $7.425 \cdot 10^6 \frac{N}{m}$ was used. The iSight analysis was based on the deflection from measurements on the structural scale model built at Charlottenlund upper secondary school (CVGS) and showed a stiffness of $5.95 \cdot 10^6 \frac{N}{m}$ in the Z-direction.

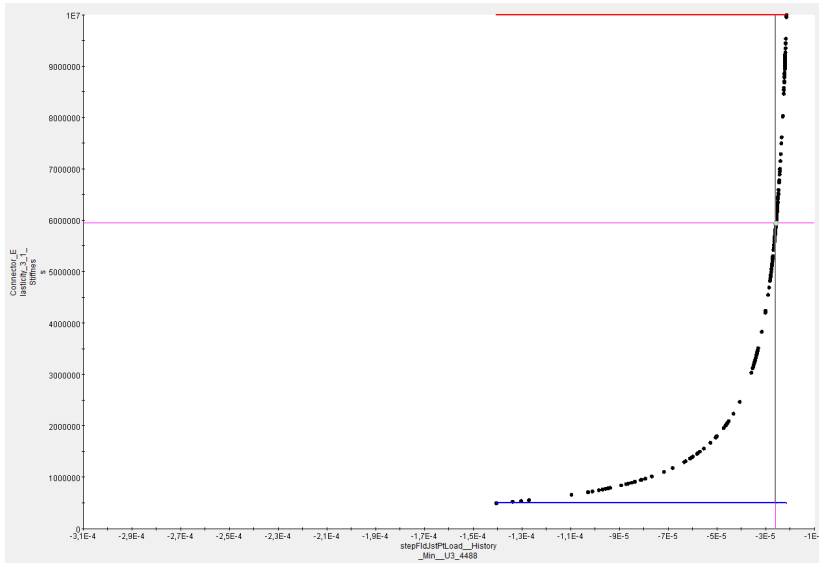


Fig. 18: iSight Pointer target search for vertical stiffness of MRC

For the force couple generating the rotational stiffness of the MRC, the stiffness D_{11} was calculated according to equations of equilibrium as illustrated in Fig. 19, where the elongation of a spring with the stiffness D_{11} is given by u_1 at the applied force F_1 , and where distance between the springs are the height of the edge joist ($cvtyHgt$). See Eq. 1 and Eq. 2.

$$\theta = \frac{2 \cdot u_1}{cvtyHgt} = \frac{2 \cdot \frac{F_1}{D_{11}}}{cvtyHgt} = \frac{2 \cdot F_1}{D_{11} \cdot cvtyHgt}, \text{ where } F_1 = \frac{M}{cvtyHgt} \quad \text{Eq. 1}$$

Substituting force to moment solves the equation with respect to D_{11} .

$$\frac{M}{\theta} = K_{\theta} \xrightarrow{\text{yields}} D_{11} = \frac{2 \cdot K_{\theta}}{cvtyHgt^2} \quad \text{Eq. 2}$$

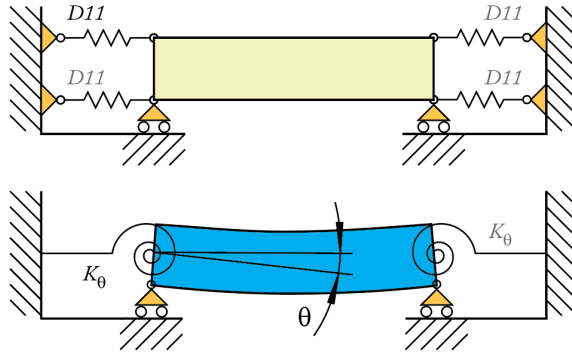


Fig. 19: Principal diagram for rotational stiffness

The output of the floor element analysis when Abaqus was run by the PSACHS-script was in the form of a CSV text file containing the following information:

- Analysis and model identification: *PSACHSver* (version of PSACHS used for the analysis); *pair* (running number parsed from the input file to enable a control that the content of the output file belongs to a given input file), *modelDscr* (manual or automatically generated description of the model), *model_nodesNum* (number of degrees of freedom for the numerical problem)
- First eigenfrequencies (constrained by a total number or a maximum frequency)
- Deflection at midspan due to 1) self-weight measured at the receiver, and 2) point load measured at applicator, for the three positions of: edge joist, field joist closest to longitudinal centre line, and soft spot between two members closest to longitudinal centre line.

3.3.2 Optimisation of the floor element based on FEA

Optimisation of the dimensions of the members of the floor element was performed in iSight. The optimisation workflow comprised a Design Of Experiment (DOE) component and a Simcode component in a loop (see Fig. 20). The workflow instructed Abaqus to create design specifications for the numerical representation of the floor element from the DEO, then run an analysis in a fast-performing non-GUI Abaqus environment and parse the output of the analysis to an analysis record file. The optimisation was performed using the simplified Hu & Chui criterion [86] as objective function.

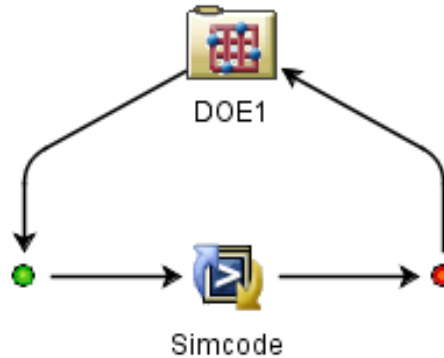


Fig. 20: iSight Design Gateway DEO-Simcode loop

3.3.3 Determination of human induced vibration

The human induced vibration is an essential topic for serviceability performances of flooring systems. In the present work this is mostly described analytically, but numerical analyses are also performed on human induced vibrations and is briefly presented. As described in the introductory section 1.4.2, the load model from footfall is a highly stochastic process and one step is not the same as the next, but the loading, as seen in Fig. 21 [106], may nevertheless be approximated deterministically using a Fourier series.

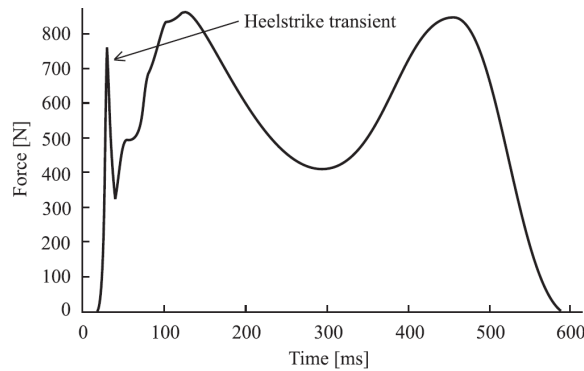


Fig. 21: Vertical load component from foot fall

Related to the present work the MSc students Bjørge and Kristoffersen performed analyses of from human induced vibration from walking load. In this analysis the load function was based on the normalised dynamic load from harmonic terms as given in [165] and reproduced in Eq. 3

$$P_p(t) = \alpha_0 \cdot G + \sum_{i=1}^n \alpha_i \cdot G \cdot \sin(2\pi \cdot i \cdot f_p \cdot t - \varphi_i) \quad \text{Eq. 3}$$

Where G and f_p is the pedestrian weight and step frequency, α_i the Fourier coefficients, and φ_i the phase angle. For details on the parameters see [152]. The analysis of human induced vibrations was performed using implicit dynamic analysis in Abaqus. Here the loading is applied in time domain with a suitable time-increment. The walk stride and step width were 0.75 m and 0.2 m respectively. Depending on definition of damping and the size of time interval, the analysis will produce a time series of the structural response of the floor element from which the acceleration and velocities also can be exposed. The drawback of the method is as described in section 1.4.2 both neglect of human-structure interaction and variability in the human step, as well as the overestimation of responses induced by higher order of footfall load harmonics. The major drawback of the method in the context of the present work is the computational time. Depending on the number of DOF and the time steps, the completion of the analysis may take several hours. Time-domain FEA is therefore not a very suitable option for optimisation where numerous iterations may be required.

A probabilistic FEA was also performed in the present work. Here the interaction of human mass and the variability in the human step is encountered for, and the demanding time-step analyses is replaced by a single domain transformation of the degrees of freedom of the model in question. In probabilistic methods a spectral density model is used to represent human induced loads [111]. Recent studies appear to have met the level of walking load samples required to generate a spectral density model for stochastic dynamic response of floor elements. Based on the work of Chen et al [105] Power Spectral Density (PSD) models may be generated for single human walking load. This is performed in Python (see code in Annex A.IV) for the four first harmonics and subharmonics, and the resulting PSD load model seen in Fig. 22. This load model has been used for random response analyses in Abaqus at an elapsed analysis time of approximately 30 minutes. This a reduction in computational time of a factor 30 with respect to the elapsed analysis time for the deterministic approach, arguing the advantageous for optimisation purposes. The results from the analysis will be presented in a future paper.

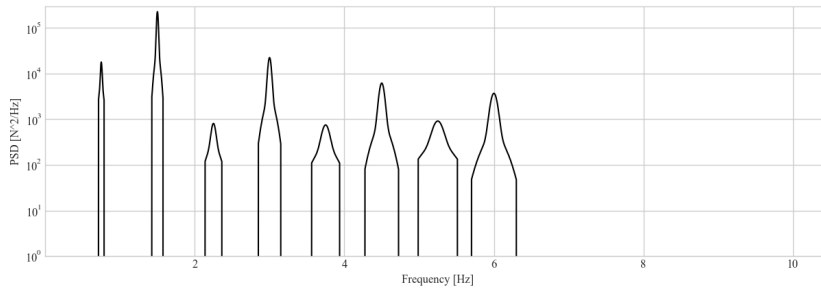


Fig. 22: PSD of individual walking load

3.3.4 Shear flow analysis

At various stages during the present work, an assessment of the shear flow of the floor element was required, either to determine the level of longitudinal shear stress or to assess shear lag. The cross section analysis was performed using CrossX [166]. A screen image from the analysis is given in Fig. 23. The analyses were mostly used as a guidance to decisions of research approach.

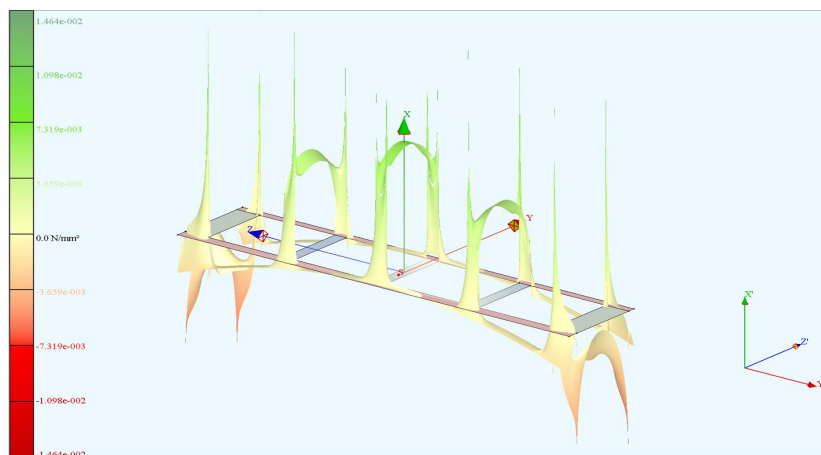


Fig. 23: Image from CrossX analysis

3.4 Analytical methods

3.4.1 Floor serviceability

During the present work the vibration serviceability criteria was calculated either as the first or second generation of Eurocode 5. The serviceability criteria used is summarized in Table 2. Combination 1 is the current common practice for floor

element design in Norway. Combination 2a and 2b is the method proposed for the second generation of Eurocode 5 [96].

Table 2: Floor serviceability criteria and levels

	Current common practice ¹⁾	EC5 proposal	
		Resonant floor response	Transient floor response
$f_{1,min}$ [Hz]	10	4.5	8
$f_{1,max}$ [Hz]	–	8	–
w_{1kN} [mm]	1.3	{0.25 0.25 0.5 0.8 1.2 1.6} ¹⁾	
Dynamic	$HC_{min} = 1$	$a_{rms,max} = 0.005 \cdot R^2$	$v_{rms,max} = 0.0001 \cdot R^2$
$w_{fin,max}$ [m]	$\frac{L}{200}$		
¹⁾	According to SINTEF Building Research Design Guides [167]		
^{2,3)}	Array for Floor Performance Levels (FPL) 1 to 6		
³⁾	Response factor levels [96]: $R(FPL) = \{4 \ 8 \ 12 \ 20 \ 30 \ 40\}$		

3.4.1.1 Determination of bending stiffness

Longitudinal and transversal bending stiffness (EI) is calculated with simple linear elasticity as stated in Eurocode 5 [121], with effective width of flanges b_i and position of neutral axes (a_i) calculated accordingly. The γ factor for composite effect has normally been set to 1.0. See Eq. 4.

$$EI = \sum_{i=1}^3 (E_i I_i + \gamma_i E_i A_i a_i^2) \quad , \text{ where } A_i = h_i b_i \quad \text{Eq. 4}$$

The apparent stiffness (D) of flooring system is calculated as the bending stiffness of the floor section divided by the extent of the section [Nm²/m]. The apparent bending stiffness longitudinal (D_L) and transversally (D_T) is given in Eq. 5 and Eq. 6. The length of the midsection is defined at half the span length of the floor element.

$$D_L = \frac{EI_L}{w_{mod}} \quad \text{Eq. 5}$$

$$D_T = \frac{EI_{T,midSection}}{L_{midSection}} \quad \text{Eq. 6}$$

3.4.1.2 Determination of fundamental frequency

The fundamental frequency has mostly been calculated based on generalized mass and stiffness (Eq. 7 and Eq. 8) with the appropriate expression for the wave function $\psi(x)$ depending on the support conditions.

$$\tilde{m} = \int_0^l m(x) \cdot \psi(x)^2 dx \quad \text{Eq. 7}$$

$$\tilde{k} = \int_0^l EI(x) \cdot \psi''(x)^2 dx \quad \text{Eq. 8}$$

Characteristic equations for respectively simply supported and clamped beams are as stated in Eq. 9 and Eq. 10, where l is the span, and m the distributed mass per unit length. The derivations and wave functions are not shown.

$$f_1 = \frac{\pi^2}{2\pi} \sqrt{\frac{EI}{ml^4}} \quad \text{Eq. 9}$$

$$f_1 = \frac{22.27}{2\pi} \sqrt{\frac{EI}{ml^4}} \quad \text{Eq. 10}$$

Fundamental frequency is also estimated analytically for support condition comprising rotational stiffness. In this case the frequency is calculated according to Eq. 11 as developed in [51]. The estimation of fundamental angular velocity is based on Rayleigh quotient and the corresponding assumed shape function for the vibrational deformations.

$$f_1 = \frac{\sqrt{4290}}{\pi} \cdot \sqrt{\frac{29K_\theta^2 + 116K_\theta + 620}{993K_\theta^2 + 20560K_\theta + 109220}} \cdot \sqrt{\frac{EI}{ml^4}} \quad \text{Eq. 11}$$

Here it can be shown that the floor element gains frequency as the rotational stiffness increase from a pinned support to 10 kNm/rad, before the increase is gradually reduced. In the same range the deflection decreases rapidly as the supports gains rotational stiffness, but at 10 kNm/rad the decrease levels out significantly.

A general form for fundamental frequency was also calculated according to [96] section 9.3.4 (see Eq. 12).

$$f_1 = k_{e,2} \frac{18}{\sqrt{w_{sys}}} \quad \text{Eq. 12}$$

Here the system deformation is due to sum of self-load and partition load (g) and calculated as in Eq. 13.

$$w_{sys} = \frac{5 \cdot g \cdot L^4}{384 \cdot EI_L} + \frac{g \cdot L^2}{8 \cdot GA_L} \quad \text{Eq. 13}$$

The frequency multiplier $k_{e,2}$ is calculated to reflect the effect of the transverse floor stiffness as reproduced in Eq. 14. For the present work the system width B was defined as 1.5 times the span length, unless an actual number of the flooring system width was known.

$$k_{e,2} = \sqrt{1 + \left(\frac{L}{B}\right)^4 \frac{D_T}{D_L}} \quad \text{Eq. 14}$$

Depending on the specification of transverse stiffeners of the floor element the length of the midsection is calculated. When there are no transverse stiffeners in the field of the floor, i.e. only one compartment in the longitudinal direction, and with transverse beams located at the ends of the floor element, the length of the midsection is defined at half the span length of the floor element.

When there are no transverse stiffeners, the transverse bending stiffness of the midsection are approximated. The connection efficiency factor is zero when there are no members between the flanges, hence the neutral axis and Steiner's theorem is not contributing. This is not the best estimate, but it is still used in the optimisation code because of the minor effects it has on the overall performance of the floor element.

The analytical solution for the eigenfrequency of the flooring system deflecting as a standing wave (also referred to as free-free boundary condition) is based on the equation of motion given in Eq. 15.

$$m(x) \frac{\partial^2 u}{\partial t^2} + \frac{\partial}{\partial x} \left(EI(x) \frac{\partial^2 u}{\partial x^2} \right) = 0 \quad \text{Eq. 15}$$

The general form of deflection u with respect to position and time is given by Eq. 16:

$$u(x, t) = \varphi(x) \cdot q(t) \quad \text{Eq. 16}$$

Applied in the equation of motion yield Eq. 17 and Eq. 18.

$$m(x)\varphi(x)q''(t) + q(t)(EI(x)\varphi''(x))'' = 0 \quad \text{Eq. 17}$$

$$\frac{q''(t)}{q(t)} = \frac{(EI(x)\varphi''(x))''}{m(x)\varphi(x)} \quad \text{Eq. 18}$$

Where ω (Eq. 19)

$$\omega^2 = \frac{(EI(x)\varphi''(x))''}{m(x)\varphi(x)} \quad \text{Eq. 19}$$

And β defined as Eq. 20

$$\beta^4 = \frac{\omega^2 \cdot m(x)}{EI(x)} \quad \text{Eq. 20}$$

Yields the general form of the equation of motion of the standing wave (Eq. 21)

$$\varphi(x) = C_1 \sin \beta x + C_2 \cos \beta x + C_3 \sinh \beta x + C_4 \cosh \beta x \quad \text{Eq. 21}$$

Where the constants are solved for the governing boundary conditions to form the particular solution of motion as given in Eq. 22:

$$\varphi(x) = \sinh \beta x + \sin \beta x + \frac{\sin \beta l - \sinh \beta l}{\cosh \beta l - \cos \beta l} (\cos \beta x + \cosh \beta x) \quad \text{Eq. 22}$$

3.4.1.3 Determination of deflection

The deflection from unit point load for respectively pinned, clamped and rotationally stiffened support conditions are approximately calculated as equivalent beam as Eq. 23-Eq. 25.

$$w = \frac{p \cdot L^3}{48 \cdot EI_L} + K_{sfd} \frac{p \cdot L}{4 \cdot GA_L} \quad \text{Eq. 23}$$

$$w = \frac{p \cdot l^3}{192 \cdot EI_L} + K_{sfd} \frac{p \cdot L}{4 \cdot GA_L} \quad \text{Eq. 24}$$

$$w = \left(\frac{p \cdot L^3}{48 \cdot EI_L} + K_{sfd} \frac{p \cdot L}{4 \cdot GA_L} \right) \cdot \frac{K_\theta + 8}{4(K_\theta + 2)} \quad \text{Eq. 25}$$

- p : unit point load 1 kN
- K_{sfd} : constant in prediction of shear force deformations. For rectangular section, $K_{sfd} = 1.2$ [168]
- GA_L : Shear stiffness in longitudinal direction. Only longitudinal members will in practice contribute to the shear capacity from bending, i.e. edge- and field joists of the floor element.

In order to improve the representation of two-way deflection a robust approach based on the Winkler theorem for describing beams on elastic foundation [169, 170] was used. Unit point load at midspan is then estimated as Eq. 26.

$$p = \frac{d^4 w}{dx^4} + k \cdot w \quad \text{Eq. 26}$$

Principally this is done by equating a fictitious Winkler foundation to the uniform deformation w caused by the floor element acting as an equivalent beam (Eq. 23).

By using the effective length of the transverse midsection of the floor element as the length of the foundation (L_{wink}), the Winkler foundation stiffness (k) can be expressed as Eq. 27:

$$k = \frac{p}{\frac{L_{wink}}{w}} \quad \text{Eq. 27}$$

Finally, the deflection constraint due to unit point load is calculated by determining the maximum deflection of the transversal cross section of the floor resting on the elastic foundation as Eq. 28:

$$w_{wink} = \frac{\beta \cdot p}{2 \cdot k} \cdot \frac{2 + \cosh \beta x + \cos \beta x}{\sinh \beta x + \sin \beta x} \quad \text{Eq. 28}$$

Where,

$$\beta = \sqrt[4]{\frac{k}{4 \cdot EI_{T,midSection}}} \quad \text{Eq. 29}$$

3.4.1.4 Determination of dynamic response

The common method for vibration serviceability in Norway is the Ohlsson method of the current Eurocode [121], but where the Hu and Chui criterion [120] (Eq. 30) is applied rather than the unit impulse velocity [167, 171].

$$\frac{\left(\frac{f_1}{18.7}\right)^{2.27}}{w_{1kN}} \geq 1 \quad \text{Eq. 30}$$

A rigorous approach for calculating floor response is proposed in the second generation of Eurocode 5 [95, 96]. The approach relate responses to human perception levels in terms of root mean square acceleration levels of the ISO baseline curve [101]. Acceleration levels dominates the human perception between 4 and 8 Hz. Consequently, the acceleration is used to assess floor performance levels in this frequency range and is calculated as Eq. 31. The ISO baseline curve level is constant in this frequency at $a_{\text{RMS}}=0.005 \text{ m/s}^2$. For human induced vibration, this frequency range is associated with a resonant floor design because the step frequency and the associated four first harmonics may coincide with the first natural frequency of the floor element.

$$a_{\text{rms}} = \frac{\alpha \cdot F}{7 \cdot \zeta \cdot M^*} \quad \text{Eq. 31}$$

- α Fourier coefficient $\alpha = e^{-0.4 \cdot f_1}$
- F Vertical force imposed by walking person (700 N)
- ζ Modal damping ratio of 3 %
- M^* Modal mass $M^* = \frac{mLB}{4}$
- m Mass (kg) of floor per unit area (m^2)

Due to the ratio of stiffness and mass, long-span timber floor elements typically have a first natural frequency above 8 Hz. Above 8 Hz the ISO baseline curve is not constant. As can be seen however, by integrating the baseline curve from 8 Hz, the corresponding velocity is constant at $v_{\text{RMS}}=0.0001 \text{ m/s}$ [95]. This new constant is used as reference for floor performance levels above 8 Hz and is calculated as Eq. 32. For floor elements with first natural frequency above 8 Hz the floor response will be transient when subject to human induced vibration.

$$v_{\text{rms}} = K_{\text{imp}} \cdot \frac{0.7 \cdot I_m}{M^*(x) + 70} (0.65 - 0.01 \cdot f_1)(1.22 - 11 \cdot \zeta) \cdot \eta \quad \text{Eq. 32}$$

$$K_{\text{imp}} \text{ Higher modes multiplier for transient floor response } K_{\text{imp}} = \max \left\{ \begin{array}{l} 0.48 \left(\frac{B}{L}\right) \left(\frac{D_L}{D_T}\right)^{0.25} \\ 1 \end{array} \right.$$

$$l_m \text{ Mean modal impulse } l_m = \frac{42 \cdot f_w^{1.43}}{f_1^{1.3}}$$

$$f_w \text{ Walking frequency (2 Hz)}$$

$$\eta = \begin{cases} 1.52 - 0.55 \cdot K_{imp} & 1.0 \leq K_{imp} \leq 1.5 \\ 0.69 & \text{otherwise} \end{cases}$$

3.4.2 Experimental Modal Analysis

Experimental Modal Analysis (EMA) was performed to determine modal properties of the flooring system. The Rowing Hammer Method (RHM) [172, 173] was applied for this purpose. This method assumes linearity and time-invariance and is based on the Maxwell's reciprocity theorem. The latter simply states that an applied excitation at a given structural position XY causing a response at a structural position $\bar{X}\bar{Y}$, will be identical to a response at $\bar{X}\bar{Y}$ caused by the same excitation at XY , for all frequencies imposed by the excitation source. RHM exposes the modal parameters of frequency, damping ratio and mode shape of the dynamic responses detected. The Frequency Response Function (FRF) H_{ij} (Eq. 33), is the relationship between the Fourier transform of the response $X_i(t)$ and the Fourier transform of the excitation $F_j(t)$. The response $X_i(t)$ is quantified by a stationary accelerometer and the $F_j(t)$ by the impact source.

$$H_{ij}(\omega) = \frac{X_i(\omega)}{F_j(\omega)} \quad \text{Eq. 33}$$

3.4.3 Power Spectral Density

Fast Fourier Transformation (FFT) was performed on the acceleration data from cyclic load tests. However, since a substantial amount of low frequencies is continuously transmitted, the FFT offered only limited assistance to interpret the characteristics of the floor resonances. Due to this the signal was rather analysed by the Welch method [174]. The Welch method is suitable for irregular time-sampled data and for combinations of different wave forms.

The realisation (time series with N samples) is split into K number of (overlapping) segments $X_1(j), \dots, X_K(j)$ of length L of which a modified periodogram is calculated as the finite Fourier transforms $A_1(n), \dots, A_K(n)$ for W data windows (Eq. 34):

$$A_k(n) = \frac{1}{L} \sum_{j=0}^{L-1} X_k(j) \cdot W(j) \cdot e^{-\frac{2kijn}{L}} \quad \text{Eq. 34}$$

See [174] for further details of the segmentation of the realisation (how overlapping is treated). Finally, K modified periodograms is obtained and averaged (Eq. 35):

$$I_k(f_n) = \frac{L}{U} |A_k(n)|^2 \quad \text{Eq. 35}$$

Where

$$f_n = \frac{n}{L}, n = 0, \dots, L/2 \quad \text{and} \quad U = \frac{1}{L} \sum_{j=0}^{L-1} W^2(j) \quad \text{Eq. 36}$$

Is applied to yield an estimation of the Power Spectral Density of the realisation (Eq. 37):

$$PSD(f_n) = \frac{1}{K} \sum_{k=1}^K I_k(f_n) \quad \text{Eq. 37}$$

As can be seen in [174] the area of the spectral window is unity (1) with a width equal to $1/L$.

In practice the PSD describe the power intensity of the accelerations as function of frequency and reveal information on how the flooring system is responding at a given frequency band by assessing the amplitude and width of peaks.

3.4.4 Accounting of consumed resources during manufacture

As reported Paper III, a parametric relationship between the specifications of a timber floor element and the overall resource consumption was developed. This method has similarities to the Time-Driven Activity-Based Costing (TDABC) method [175], and activity-based costing in general [176], but include more information about the resource consumption related to manufacture. The developed method is called Item-Driven Activity-Based Consumption (IDABC).

IDABC resembles the much used Time-driven Activity-Based Costing (TDABC) [175] in how the manufacturing line is modelled as resources combined to perform required activities (Fig. 24). However, where the TDABC uses predetermined duration of activities to calculate costing, the IDABC method utilizes information stored in the items subject to manufacture to calculate durations. For any item the activity requests a specific quantity based on predetermined SI unit associated with the activity, which in turn is used to calculate activity duration. Based on the duration of the activity and the definition of the activity and the underlying resources, manufacturing resources are determined.

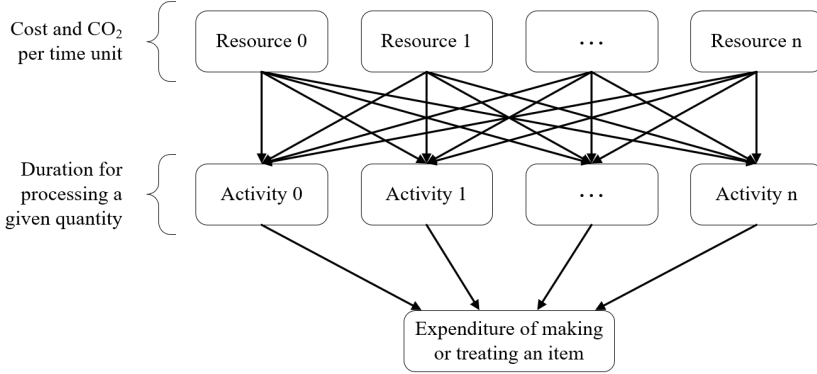


Fig. 24: Activity-based accounting in general. The relationship between resources, activity and expenditures

In the method an expenditure vector V_η is computed for all items at every activity the item is subject to during the manufacturing. The vector contains the duration T_η [s], cost C_η [€], the part of cost associated with labour LC_η [€], and the ECO2 [kgCO₂eq], where η represent an item in the floor element (see Eq. 38).

$$V_\eta = \{T_\eta \quad C_\eta \quad LC_\eta \quad ECO2_\eta\} \quad [s \quad \text{€} \quad \text{€} \quad \text{kgCO}_2\text{eq}] \quad \text{Eq. 38}$$

The total expenditure of the floor element is the accumulated expenditures for all items (bodies and assemblies) of the product (Eq. 39). This is the outcome of the method and may be utilized as an objective function in an optimisation workflow, or it may serve to quantify competitiveness.

$$V_{product} = \sum_{i=0}^{numBody} \sum_{j=0}^{numAct} V_{i,j} + \sum_{k=0}^{numAsmby} \sum_{l=0}^{numAct} V_{k,l} \quad \text{Eq. 39}$$

3.5 Experimental methods

3.5.1 Experimental Modal Analysis (EMA)

During the present work various modal analyses was performed using the Rowing Hammer Method (RHM). The eigen frequency of the floor element was tested by supporting the floor element on soft air cushions (see Fig. 25). This was a useful approach because it simplified the boundary conditions of the system, hence improving the accuracy in modelling of the governing boundary conditions numerically. The EMA with free-free boundary conditions therefore provided better data for the calibration and validation of the numerical models.

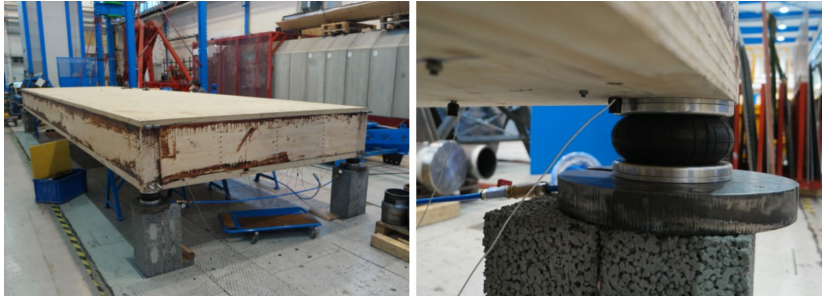


Fig. 25: Floor element resting on air cushions

Support conditions is essential of a flooring system and the RHM was also used for more realistic boundary conditions. In the laboratory a 9 m floor element was tested with pinned support conditions (floor element corners or linear along the transverse edge), and with moment-resisting end constraints. This work was performed as part of the MSc of Bjørge and Kristoffersen [152].

A structural scale model (also referred to as mock-up) was built in cooperation with Charlottenlund upper secondary school (CVGS). Carpenter students at CVGS built the floor elements and the PhD students of the Woodsol project assembled the mock-up with assistance from Leif Joar Lassesen at CVGS, all according to an assembly manual [177]. Fig. 26 and Fig. 27 show the conceptual sketch and the completed mock-up at CVGS. Extensive use of the RHM was performed during the full-scale test.

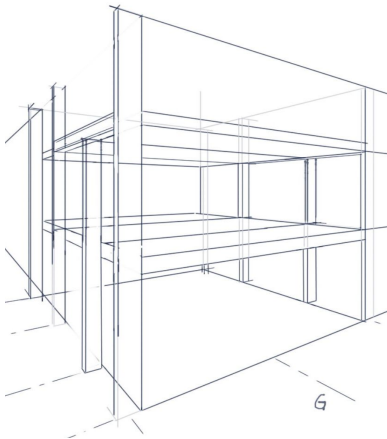


Fig. 26: Mock-up conceptual sketch



Fig. 27: Mock-up as-built

On the structural scale model, the present work tested the effect of various interconnections between the floor elements. Fig. 28 show the cross-section of two floor elements structurally related by one of the interconnections designed for the test.

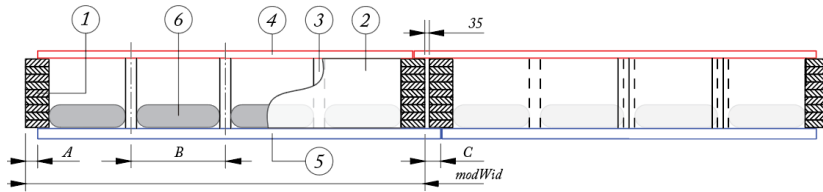


Fig. 28: Section view (in direction of span) of one of the interconnections tested

For the structural scale model EMA was performed to determine both in-plane and out-of-plane deformation modes and their related modal parameters. The results from the exercise are found in Paper I and Paper II. Fig. 29 and Fig. 30 show the excitation grid and position of the accelerometer the out-of-plane EMA.

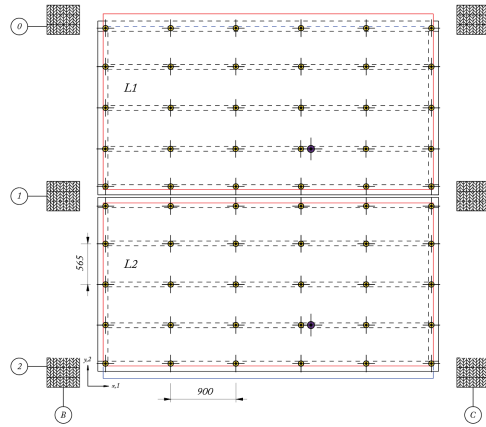


Fig. 29: Rowing hammer grid for floor elements in parallel

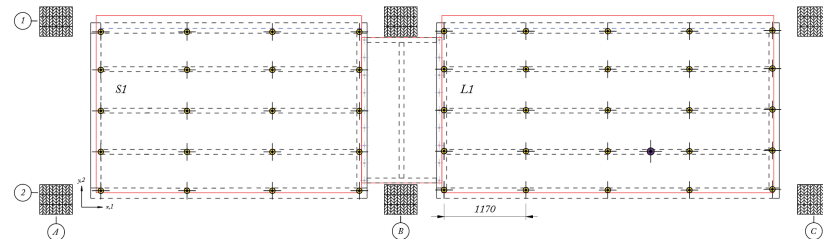


Fig. 30: Rowing hammer grid for floor elements in series

3.5.2 Deflection tests

Deflection tests were performed on the structural scale model at CVGS. A series of deflection sensors was positioned in relation to both the loaded and unloaded floor element. Point load was applied at the centre of the top flange through tension bars towards the underside of the floor element to where load cell and charge was located. The load on the floor element was distributed from the upper 16 mm adapter steel plate

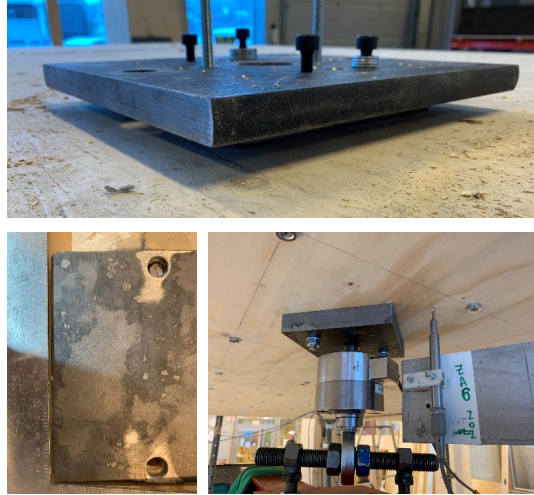


Fig. 31: Load and load cell application

to an underlying 200 cm² load pad as advised in the timber floors test method [178] (see Fig. 31). Three different loading protocols were developed and employed at site. The first protocol used a water tank for loading advantageous for the steady rate of change of load, but the method was time consuming. The second and third protocol differs from the first in ramp time and type of charge, replacing the water tank by a precise chain hoist anchored in the workshop floor. The drawback of the charge was the difficulty to maintain a steady rate of change of load, but the advantage was the ability of taking fast series of onloading and offloading.

The deflection tests suffered from low amplitude response due to short span floor elements primarily built for testing acoustic performances [36]. Because of this and the complexity in the deformation due to the number of parameters affecting the deflection, a statistical evaluation was performed to reveal main effects and the level of significance each factor had on the response of the flooring system. The statistical assessment was performed in Minitab [179], with the following figures exposed:

- Pareto chart to express the absolute values of standardized effects in ascending order aiding to determine the magnitude and importance of the effects of the factor.
- Main effect chart to show how the fluctuation in mean response as the level of a factor moves between its extremes.
- Interaction chart to express the relationship between one factor and the continuous response depending on the value of a second factor.

For further details see Paper I.

3.5.3 Cyclic load

The structural scale model was also subjected to cyclic load. An eccentric mass vibrator (EMV) [180] was used to excite the floor element dynamically from 5 Hz to 30 Hz during a 2 min sweep. The EMV was mounted to one of the floor elements both for floor elements in parallel and in series, The EMV was anchored to the loaded floor element through the same adaptor plate as used for the deflection tests, which was tied to the floor element at the mid span. See Fig. 32.

Two accelerometers monitored the response; one at EMV (applicator) and one at immediate proximity to the centre of the bottom flange (receiver). In addition to floor accelerations the exciter frequency was recorded. The force from the exciter varied from 50 N to 1250 N as function of frequency. For further details see Paper I.

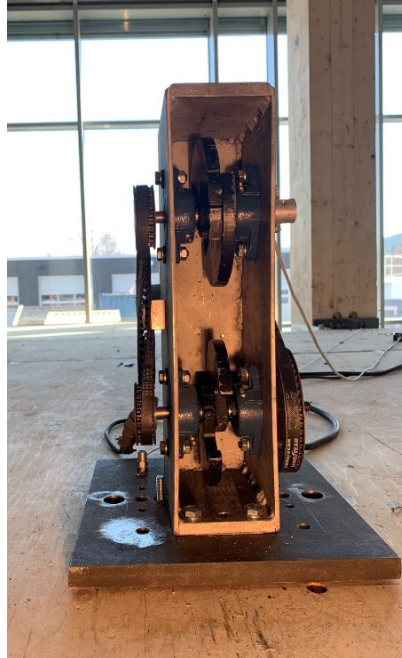


Fig. 32: EMV anchored to floor element

3.6 Systems analysis

The project group associated with the Woodsol research project comprised manufacturers of wood components, architects, building and construction companies, and research institutes. The project group represents a valuable resource and information and knowledge from the group must be utilized. During the work on WP2 Production and assembly, the project group addressed a range of topics for a successful flooring system. Also findings from the assessment of buildability and assembly of the Woodsol concept by Monsen and Nystuen [151] was taken into account. The collected material consisted of more than one hundred drivers and conditions and factors that a successful long-span timber floor element should regard. This information was regarding the floor element specification, advantageous and disadvantageous of manufacturing processes, and topics related to transport, installation and completion, adaptability and reuse.

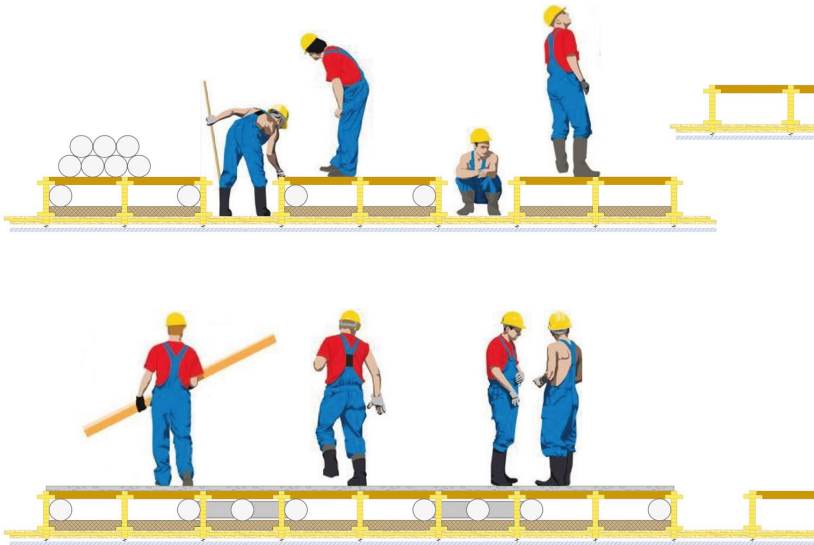


Fig. 33: Illustration of a possible completion scenario of early floor design

In order to analyse the information, a framework was needed where the information could be sorted and arranged. Several approaches were attempted before a conclusion was drawn for both a strategy and a framework for information analysis.

The strategy was to base the analysis of information on the concept of an optimisation tool that would collect information and produce an optimum solution for a given application. As can be studied in Paper VI the optimisation tool was envisioned to produce information to a reference work (possibly in the form of a handbook for long-span timber floor elements). Due to this the optimisation tool was placed in the centre of a system that should be able to produce optimum solutions, i.e. competitive solutions.

The framework of how the information could be analysed was then addressed. This took the form of a simplified systems analysis established to categorize topics influencing the market impact of timber floor elements for commercial building applications. The analysis was used to elaborate the purpose and scope of a ready reference work, and to gain overview of the possible features and requirements of a design tool that this reference could be based upon.

As described in Paper VI, the indicators proposed to quantify competitiveness for a floor element finalized at the factory is the consumed resources (manufacturing time, cost and ECO₂). Linked to a floor element applied in a building, additional indicators serve to quantify its competitiveness. The combined performance of resource

consumption from manufacture and the required resources linked to adaptability of the floor element was therefore selected as one of the axes of the framework. Because resource consumption has different units of quantity, the resources consumption was assessed in terms of economy. Along the other axis of the framework the phases of realization were placed, from design and manufacture, via installation and completion, to adaption, reuse and disposal. The systems analysis was executed by sorting topics related to resource consumption, in economic terms, in entities along the ordinate axis, and topics related to realization processes in entities along the abscissa axis.

Due to the nature of the selected axis (short to long term economic on the ordinate axis, and phases of realization along the abscissa axis), interactions occur when information is transferred between entities in the framework diagram (Fig. 34). This offered perspectives and help in interpreting how the various information would affect both the role of the floor element when this is a part of the built environment, and for the conceptualisation of an optimisation tool that should produce data to a relevant reference work for the market.

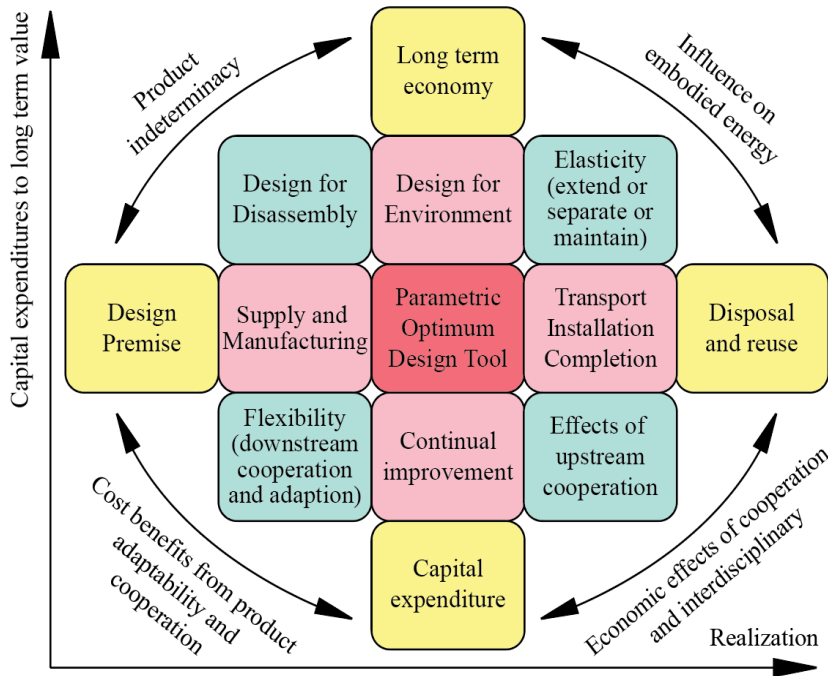


Fig. 34: Framework of realization processes and economic impacts influenced by an optimisation tool for long-span timber floor element

3.7 Real-life approach

Dialogue with the industry was held during various phases of the present work. The factory visits at the Trä8 floor element production line at Moelven Töreboda AB and at the Splitkon AS production line gave valuable insight. An extensive presentation and demonstration at Stora Enso Oyj in Helsinki was also helpful to understand the market of commercial timber products.

However, the explanation of the production line and the bilateral workshop at Moelven Limtre AS was essential for scoping and outcome of Paper III. During this session quantification of resources and activities was carried following extensive dialogue with a production line manager with thorough understanding of the operations that take place on the production line.

3.8 Optimisation

3.8.1 Method

The optimisation workflow developed in the present work consists of three modules as indicated in Fig. 35: i) Design premise; ii) Item-Driven Activity-Based Consumption; and iii) Optimisation. The output from IDABC is the cost and ECO2, and the design premise state the constraint function values. Both these modules are included in a common code named Parametric Resources and Performance of CHS (PARAPECHS) [140]. This information is input to the optimisation module (MISLP Optimise in Fig. 35). The output of the optimisation module is the optimised product.

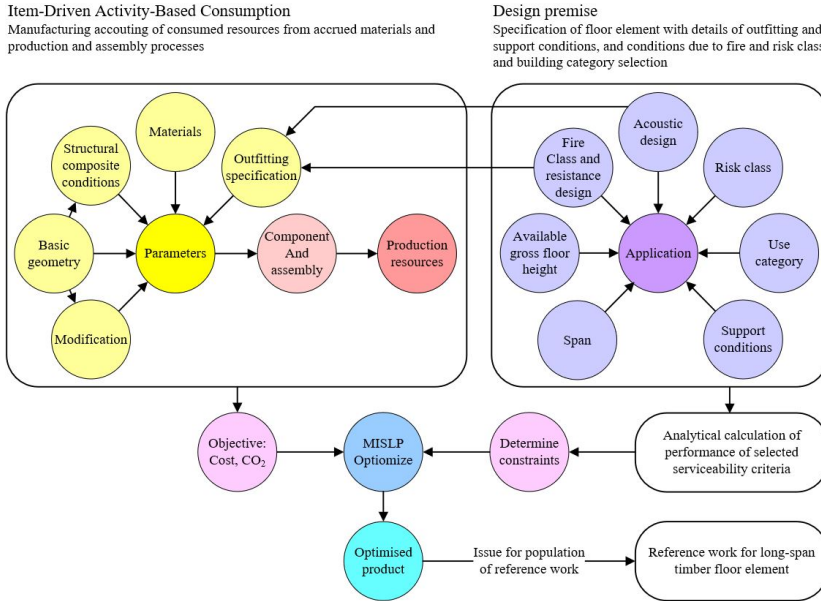


Fig. 35: Flow chart of optimisation framework

The optimisation method employed in this study is based on solving a sequence of linear mixed-integer optimisation problems. This method is a discrete extension of the well-known sequential linear programming (SLP) approach [181]. At each iteration point, the nonlinear functions are approximated by their linearization. The design variables are treated as continuous variables when solving the linearization. In the present work five dimensions related to the cross-section of the floor element are taken as design variables, collated as a vector denoted by \mathbf{x} (Eq. 40).

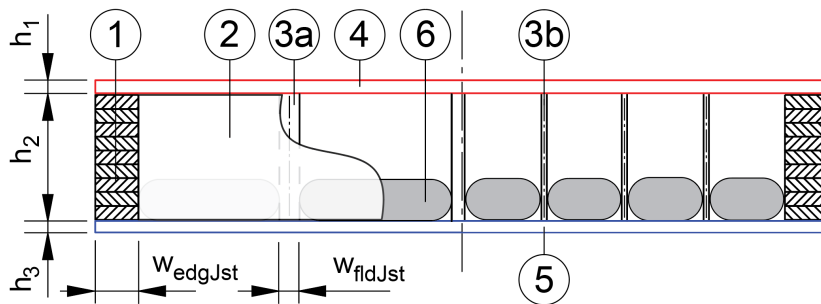


Fig. 36: Cross-section for floor element subject to optimisation

$$\mathbf{x} = \{h_1 \quad h_2 \quad h_3 \quad w_{edgJst} \quad w_{fldJst}\} \quad [mm] \quad \text{Eq. 40}$$

3.8.2 Theory

Discrete values can be enforced by introducing binary variables as follows. Let x be a discrete variable with the allowable values $X = \{\hat{x}_1, \hat{x}_2, \dots, \hat{x}_d\}$. The binary variables are then introduced, $y_j \in \{0,1\}$, $j = 1, 2, \dots, d$. The variable x can be forced to have one of its allowable values by adding the following linear constraints to the optimization problem:

$$x = \sum_{j=1}^d \hat{x}_j y_j \quad \text{Eq. 41}$$

$$\sum_{j=1}^d y_j = 1 \quad \text{Eq. 42}$$

The latter equation ensures that exactly one binary variable takes the value 1, whereas the former equation sets the discrete value corresponding to the non-zero binary variable for x . Each discrete variable is supplemented with its own binary variables and constraints of Eq. 41 and Eq. 42.

Consider the following optimization problem

$$\begin{aligned} & \min_{\mathbf{x}} f(\mathbf{x}) \\ & \text{such that } g_i(\mathbf{x}) \leq 0, i = 1, 2, \dots, m \\ & \quad \mathbf{Ax} \leq \mathbf{b} \\ & \quad \mathbf{Cx} = \mathbf{d} \end{aligned} \quad \text{Eq. 43}$$

where g_i are nonlinear and continuously differentiable functions, and the matrices \mathbf{A} and \mathbf{C} as well as the vectors \mathbf{b} and \mathbf{d} are constants. The vector of design variables, \mathbf{x} , includes both continuous and discrete variables.

In one iteration of the *mixed-integer sequential linearization procedure* (MISLP), the original optimisation problem is linearized at the current iteration point, \mathbf{x}^k :

$$\begin{aligned} & \min_{\mathbf{x}} f(\mathbf{x}^k) + \nabla f(\mathbf{x}^k)^T (\mathbf{x} - \mathbf{x}^k) \\ & \text{such that } g_i(\mathbf{x}^k) + \nabla g_i(\mathbf{x}^k)^T (\mathbf{x} - \mathbf{x}^k) \leq 0, i = 1, 2, \dots, m \\ & \quad \mathbf{Ax} \leq \mathbf{b} \\ & \quad \mathbf{Cx} = \mathbf{d} \end{aligned} \quad \text{Eq. 44}$$

The problem of equation Eq. 44 is a mixed-integer linear optimisation problem (MILP), which can be solved, for example, by the branch-and-cut method that is implemented in various optimisation software packages.

It is well-known that the SLP as well as the MISLP method may not converge in its basic form. The method can be stabilised by introducing so-called *move limits* that restrict the feasible set of the linearized problem. The move limits are written as additional bound constraints for the design variables. the move limits can be expressed as a portion of the total range of the variable, or in terms of local allowable change, say 15% of the current value. In any case, the move limits can be written as

$$\underline{\Delta}_i^k \leq x_i - x_i^k \leq \overline{\Delta}_i^k \quad \text{Eq. 45}$$

where $\underline{\Delta}_i^k$ and $\overline{\Delta}_i^k$ are the prescribed bounds. In this study, the bounds are related to the range of variable values, i.e.

$$\begin{aligned} \underline{\Delta}_i^k &= C_1(\overline{x}_i - \underline{x}_i) \\ \overline{\Delta}_i^k &= C_2(\overline{x}_i - \underline{x}_i) \end{aligned} \quad \text{Eq. 46}$$

where C_1 and C_2 are constants. In this study, the initial values $C_1 = 0.5$ and $C_2 = 0.5$ were used. Over the iterations, these constants are updated by the following rule

$$C_i \leftarrow (1 - \gamma)C_i \quad \text{Eq. 47}$$

where $\gamma = 0.001$ was used in this study.

For the application of the MISLP method on the timber floor optimisation problem see Paper IV. As for the modules of objective and constraint, the modelling of the optimisation problem is performed in Python [182], and the Google AI OR-Tools for Python [183] are used to solve the MILP sub-problem.

3.8.3 Results and implications

The performance of the MISLP optimisation technique was evaluated by comparing the design obtained by MISLP to the global minimum found by manual exploration of the solution space. This was a huge endeavour because of the possible combination of the solution space. As can be studied in see Paper IV, finding the optimum solution with brute force (global exploration of the solution space) used an average of 600 minutes per case. In comparison the average duration of the optimisation approach was less than two seconds per case. The mean error between the global optimum and the optimum found by the MISLP-optimisation was 1.5%.

The implications of the study are that the MISLP optimisation method may be run directly from a server to generate immediate designs based on parameters collected from the user interface. Other implications are that cost- or ECO2 optimised solutions may be found for a set of changing parameters like span, or maximum

values of building depth, to mention some. In the following figure this is exemplified by the showing the cost-optimum solution whilst varying span and serviceability constraints, to see the effect on the depth of the floor element. See Fig. 37. In this figure the current common method of Hu and Chui is compared to the new method proposed for the second generation of Eurocode. The dashed lines represent resonant floor element design ($4.5 \leq f_1[Hz] < 8$), continuous lines represent transient floor element designs ($f_1[Hz] \geq 8$), and the dash-dot line representing the current common method. This figure is discussed in Paper IV. Example of other practical implications directly addressing the sought delivery of the present work is found in Paper IV.

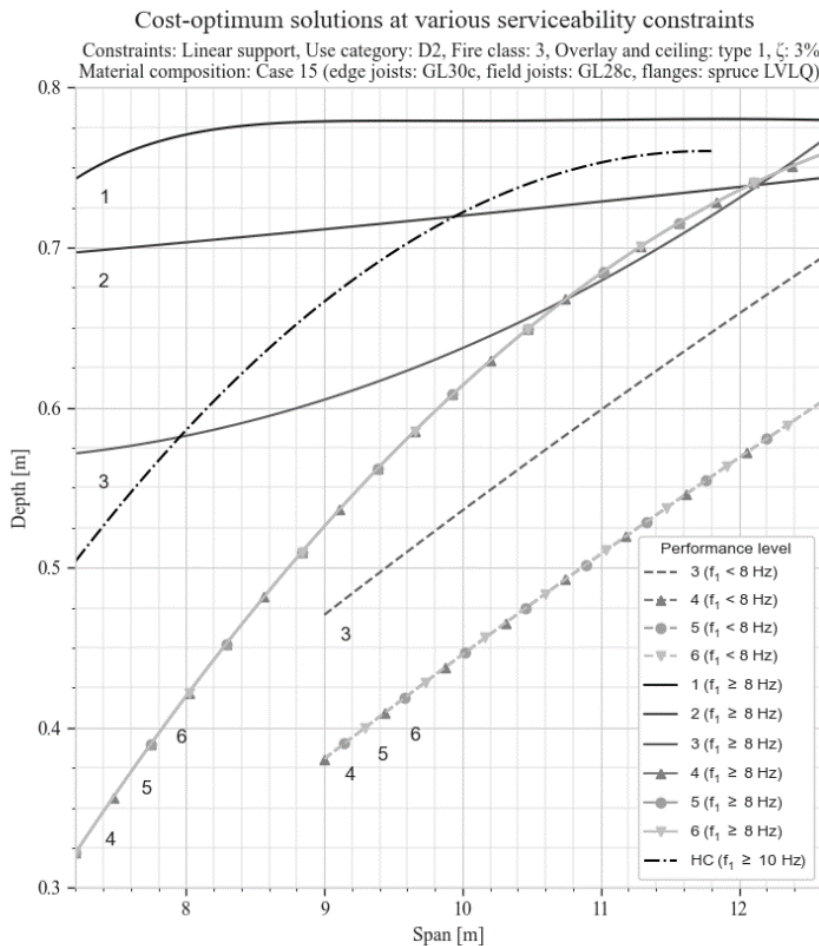


Fig. 37: Cost-optimum solutions at various serviceability constraints

4 Research

4.1 Objectives and findings

4.1.1 Paper I

Effect of interconnects on timber floor elements: dynamic and static evaluations of structural scale tests.

When assembling floor elements together to form a functional flooring system, various connections and configurations can be used. These connections can be a cost-effective solution to improve the dynamic response of a flooring system without changing the design of the floor element. The result can aid in choosing a cost and environmentally advantageous method to increase the performance related to floor comfort properties. This was the background and motivation of the study. The objective was to investigate how interconnections between timber floor elements could be used as the basis for a resource-efficient approach to enhance serviceability performance.

Full-scale floor elements were positioned in a variety of configurations and tested for static and dynamic performance using different types of interconnections. The interconnections were mounted both transversally and longitudinally and tied to floor element edge members while varying the number of fasteners.

A major part of the study was to see how the damping ratio was affected by changing interconnections through different mode shapes. Whilst material damping may be estimated from the strain energy method [184, 185], the structural damping is difficult to predict because it is linked to detailing in the design and execution of the floor element and its supporting structures [186]. Full-scale tests are therefore an important yet expensive measure to obtain credible values of total damping.

The observed effects of interconnection types vary according to the configuration and direction of mode shapes, and were assessed in terms of shift in frequency, damping and resonant energy. In general, a strong interconnection will increase fundamental frequency with respect to an isolated similar floor element and increase the performance of the flooring system as quantified by the Hu & Chui criterion. For resonant floor design situations (acceleration dominated perception) increased stiffness of the interconnection will increase damping and consequently reduce accelerations. Depending on the fundamental frequency, it is a likely measure to shift acceleration levels considerably down. For transient floor design situations (velocity dominated perception) both increased damping and increased fundamental frequency will contribute to decrease velocity response. The concurrent effect from both would contribute effectively to decrease velocity response.

The present work demonstrated that connections between timber elements have significant effects on timber floor serviceability and may offer interesting solutions to improve the vibration performance of long-span timber floors.

4.1.2 Paper II

A study on beam-to-column moment-resisting timber connections

In the structural scale model at CVGS the Woodsol building system was tested. The building system has one weak direction (y-direction) where the global building stiffness must be provided by dedicated shear walls or bracings. In the strong direction (x-direction) the Moment Resisting Frames (MRF) comprising the joint stiffness of columns, the Moment Resisting Connector (MRC) and the embedded edge joists of the floor element provide the global building stiffness. In the study of Paper II, the moment-resisting frames were subjected to both cyclic and monotonic loading, and the rotational stiffness and the energy dissipation were determined based on full-scale cyclic tests. The mock-up frame assembly was subjected to cyclic lateral loading and tested with experimental modal analysis. The lateral stiffness, the energy dissipation and the fundamental eigen-frequencies of the frame assembly were measured and quantified and compared with the FE analyses.

Experimental Modal Analysis of both weak and strong direction was performed. The dynamic structural damping ratios measured with experimental modal analysis were 2.1% and 3.9% in x- and y-directions. The FE model shows good agreement between the experimental results and the analytical model.

For more information about additional tests performed to assess the beam-to-column stiffness on the mock-up frame assembly, see Paper II.

4.1.3 Paper III

Competitiveness of timber floor elements: an assessment of structural properties, production, costs and carbon emissions

Cost reductions for timber floor elements to competitive levels must be pursued throughout the product details and in the stages of manufacturing. As new wood products are introduced to the market, solution space is increased to levels that demand computerised optimisation models, which require accurate expenditure predictions. To meet this challenge, a method called Item-Driven Activity-Based Consumption (IDABC) has been developed and presented in this study. The method establishes an accurate relationship between product specifications and overall resource consumption linked to finished manufactured products. In addition to production time, method outcomes include cost distributions, including labour costs, and carbon emissions for both accrued materials and production line activities. A novel approach to resource estimation linked to assembly friendliness is also

presented. IDABC has been applied to a timber component and assembly line operated by a major manufacturer in Norway and demonstrates good agreement with empirical data.

The objectives of the present work was to explore a parametric method for quantification of consumed resources in the manufacture of timber elements. The output of the method should serve as a quantification of competitiveness. The findings of Paper VI and a dedicated review have identified production time, cost, labour cost and ECO2 as indicators of competitiveness. The method should be parametric and have features that makes it suitable as an objective function in optimization workflows. The method should be based on principles that keep the effort of implementation low.

In compliance with the objective the method established a parametric link between the specification of a timber element and the quantification of manufacturing expenditures. Also, in compliance with the objective, the output of the method serves to quantify competitiveness in terms of production time, total cost, labour cost and carbon emissions. The parametric architecture of the method enables the implementation in an optimization workflow for timber elements. This was one of the main motivation of Paper III. The attention to means of reducing implementation effort, as addressed in the objective, led to the item-driven approach that utilizes information stored in the items being processed to calculate duration of the various activities of the manufacturing.

4.1.4 Paper IV

Optimisation of costs and carbon emission of timber floor elements

Long-span timber floor elements may increase the sustainability and adaptability of a building and exhibit a significant market potential. The timber sector is currently endeavouring to meet this potential, but building projects employing long-span timber floors have encountered drawbacks. High costs and vibration performance are challenging, and the timber industry is under substantial pressure to find attractive solutions for building components with otherwise favourable environmental features.

Timber flooring systems for long-span applications are normally glued thin flange elements with stiffeners and joists constituting the core. The number of joists and stiffeners, the internal added weight and insulation, and the dimensions of all members result in numerous potential combinations to be examined. This number increases drastically when the range of wood products and types of bonding are considered. When outfitting such as overlays and ceiling system is addressed, the number of combinations increase further. And finally, when support and load conditions and serviceability performance levels are regarded, the solution space is

immense. With this many parameters, finding a competitive design may not be manageable by manual exploration, and the solution space can in practice only confidently be investigated when assessed computationally.

Optimisation is useful when there are conflicting criteria, and when different objectives cause disagreeing designs. This is also the case for timber floor elements. The constraints and objective of an optimum solution may differ from project to project. For one project the pursued optimum would be towards minimum cost, while another project would pursue minimum ECO2 or building depth.

The objective of the present work has been to assist in the commercialisation of timber floor elements suitable for adaptable building applications. The recent development of a novel parametric accounting method for manufacturing of timber elements [3] has contributed to realize this study. As concluded by Forintek and the Canadian Wood Council [139] a precise manufacturing cost accounting in combination with an optimisation workflow can offer an efficient solution for the development of competitive timber floor elements, and this is what Paper IV has endeavoured.

In this study, the cost and ECO2 optimisation of a novel timber floor element is presented. A mixed-integer sequential linearization procedure is employed to solve the formulated discrete optimisation problem. Various material combinations and constraint combinations are treated. The optimisation framework provides a tool for rapid design exploration that can be used in general design situations. The results of the calculations carried out in this study provide insight on the general trends of optimum floor elements. The optimisation model is used to analyse the characteristics of the optimum designs, and a comparison between the current and the second generation of Eurocode 5 is shown to demonstrate implications.

The MISLP optimisation method demonstrates adequate properties and performances required to be run directly from a server to generate immediate designs based on parameters collected from the user interface. The ability to confidently explore a solution space in a rapid growing market of novel engineered wood products opens a range of opportunities and implications.

4.1.5 Paper V

Assessing adequacy of numerical representation for optimisation performances in long-span timber floors

The objective of this study was to describe the effect variations in the numerical representation of a floor element had on the accuracy of modal analysis and computational effort. The expected outcome of the study was to find the adequate numerical representation for optimisation workflows for timber floor elements. The variations of the numerical representation was 1) the base feature of the members of

the floor element (shell or solid), 2) the type of element, and 3) the size of the element. The effect was measured as the combined RMS error between the predicted and the measured eigen frequency, and the computational effort as quantified by the number of DOF.

For the solid base feature the following elements was included in the Design Of Experiment (DOE): C3D8, C3D8R, C3D20R, C3D8I and SC8R (here the continuum shell was modelled as a solid and consequently listed here). The shell elements assessed was S4, S4R, and S8R. From these compatible combinations was generated. The seed size changed from 0.025 m to 0.07 m in four steps. The analysis was performed in Abaqus/Standard, and the PSACHS code [143] was generating the numerical representations and executing the analysis based on an excel file where the Design Of Experiment was modelled.

The finding of the study was the identification of combinations of element types and element sizes that render a favourable combination of precision and computational effort, suitable for an optimisation workflow. The finding were that 1) Moderately thick to thick joists should be modelled as C3D8 in combination with flanges modelled as conventional S4. 2) A robust field joist formulation accepting varying thicknesses should be formulated with the S8R element in combination with C3D20R for thick edge joists and beams and with S8R in the flanges. 3) A linear version of the same base feature should be modelled with field joists in S4 in combination with C3D8I for edge joists and beams and with the S4 formulation for the flanges. 4) A solid flange formulation would favourably be modelled with the continuum shell in combination with C3D20R given relatively thick joists and flanges.

4.1.6 Paper VI

Conditions and features of a design tool for long-span timber floor elements

A handbook for long-span timber floor elements would be of significant assistance to increase the market shares of timber floors for commercial building applications. Based on collected information from architects, engineers and manufacturers, the study elaborates on the contents of a ready reference. The presented study also reviews factors influencing the competitiveness of timber floor elements for commercial and adaptable buildings, and combines the findings to scope the features and requirements of a design tool that could supply information to a handbook.

The objective of the present work was to suggest a design approach for a calculation tool that could be used to generate useful and reliable data for a reference work for long-span timber floor elements, and to uncover gaps and further developments required to realize this tool. A literature review in the form of a SWOT-analysis was performed as part of the study.

The study has contributed to the development of a method of optimisation suitable for producing data for a reference work for long-span timber floor element. The contribution comprises the architecture of a holistic method of optimisation, identification of indicators for competitiveness, identification of conditions and features that an optimisation tool should apprehend, and the scoping of solutions to realize a reference work.

4.2 Answers to research questions

Based on research objectives stated in section 2.3 due research questions were formulated. In the continuation these are quoted in bold following a condensed answer based on the findings of the papers of the present work.

1) Can timber floor elements be used for span of ten meters, and what parameters are significantly influencing the performance of a timber floor element when applied in a building?

It is technically feasible to design a timber floor of ten metres span with acceptable acoustic performance. Findings in Paper IV suggest that lengths of 12.6 meters may also be achieved (based on analytical determined accelerations and velocities), but the cost tend to increase considerably from approximately ten meters span. Designing floor elements as an inherent structural component in moment-resisting frames is achievable. Moment resisting end constraint will increase the span length without increasing the building depth of the floor element depending on the rotational stiffness of the connector and the columns. The moment-resisting connector transferring rotational stiffness between column and floor element introduce loads to connected members in an arrangement of threaded rods. The structural interface between the threaded rods and edge joists of the floor element is flexible and practicable. The threaded rods can be installed during floor element manufacture. The design specification for floor element related to the interface with the MRC is a balance of the interrelated parameters of building height, loading, number of bays of MRF, span, and floor element depth. The outcome of the balance is an arrangement and dimension of threaded rods and dimensions that must be fitted in the edge joist where required edge spacing is taken into account. In order to harmonize rules, the height of the edge joist is used as the extremes of the accommodating volume for the threaded rods, but during tests the threaded rods has entered at flange level, and is a doable option that may increase the rotational stiffness of the MRF. Vibration serviceability is enhanced by increasing stiffness, damping and modal mass. The most efficient approach to influence serviceability depends on the fundamental frequency of the floor.

2) The cost of timber floor element with respect to comparable alternatives is high. How is this affecting the market share for timber floor elements for commercial buildings, and what can be done to increase the market share?

Timber floor elements are nearly twice the cost of a comparable concrete hollow-core element, and the advantages in carbon emissions are currently not a legitimate argument for the construction industry. There is a complex reasoning behind this with many causes linked to a branch that is very little matured with respect to the steel and concrete industry. For timber floor elements to increase the market share, innovative, competitive and industrialized elements with high technical qualities and low economic risk need to be developed, documented and made available. The floor elements must respond to the requirements for adaptable buildings (see section 1.3.1) and enter into a process of standardisation of building components for timber building systems. The increased focus on ISO baseline curve for serviceability, with dynamic responses either determined analytically or numerically, is likely to increase the precision in vibration performance without regard to span length, and the possibility of varying floor performance levels will increase flexibility in design. In Paper I the effect of connections between floor elements was assessed as a resource-efficient approach to modify serviceability performance.

3) The construction industry is well-known for risk aversion, and the awareness of the challenges of long-span timber floor elements is well expressed: How can this risk be further clarified, and what can be done to reassure the construction sector on this matter?

In Paper VI a due SWOT-analysis was performed where key indicators of both risk and competitiveness was identified. Findings from the timber industry emphasise the importance of improved knowledge and precisions of costing. This concerns both capital expenditures of manufacturing and construction, and operational expenses throughout the service lifetime. Threats may predominately be associated with the lack of standardisation in timber building system. Opportunities are found in the level of prefabrication, potential of systematic feedback of expertise, and in the improved responsibility in planning and construction. Substantial potential is also found in modular commercial building applications and method for of joining timber components. The lack of precise methods for cost estimation of timber element manufacturing led to the development of a parametric accounting approach for estimation of manufacturing resources for timber elements.

4) Reducing GWP is a paramount responsibility for the construction sector. How can timber floor elements contribute to a sustainable development of the built environment?

The reference to adaptable buildings is adopted in the present work because it addresses an essential concept in the future role of the built environment, and because it is closely related to the design of floor elements. The potential in energy savings and flexibility in use is often lost as floor plan layout is overlooked in early design phase. A building with long spanning primary structures and open architecture increases compliant building typologies and functionality and increases potential permutations of interior layout. Due to the attention to reduced GWP, the parametric accounting of manufacturing resourced developed in the present work is also addressing embodied carbon emissions (ECO₂), and as can be seen in Paper III and Paper IV be used to optimised floor element with respect to ECO₂.

5) NFR has requested the deliverable from the doctoral work to contribute to a handbook on the use of the Woodsol building system. How can this be addressed? How can the data for a handbook be validated, and what are the conditions and requirements for a handbook related to timber floor elements?

The present work has been devoted to the request from the NFR on a handbook. This deliverable is assessed to be most advantageous for the general development of timber floor elements. As demonstrated in all kind of technical developments, the exposure of solutions to the market is the most effective method to force developments ahead. Due to this, there has been a strong orientation towards applied research and the aim of demonstrating practicable methods to assist the market for long-span timber floor elements.

In Norway an electronic handbook is freely available for concrete floor elements, readily guiding architects and engineers in the use of concrete floor elements. A comparable asset for long-span timber floor elements may be of significant assistance to increase the market shares of timber floors for adaptable buildings. This reference work could have the format of a handbook or a guideline that could be available through a website. In the process of answering to this request, information from architects, engineers and manufacturers was collected and elaborated with respect to the contents of a handbook. The data that such reference work should be based upon must comprise competitive designs, and the present work addressed both this topic and the conceptualisation of an optimisation framework that could be used to generate required data in Paper VI.

In Paper III an object function quantifying indicators of competitiveness is developed, and the method is applied to a timber component and assembly line operated by a major manufacturer in Norway and demonstrates good agreement with empirical data. In Paper IV the optimisation framework is built and executed and implications with respect to a ready reference work discussed.

6) The amount of new engineered wood products, fasteners and adhesives continuously introduced to the market may be prosperous for the development of a competitive timber floor element, but the availability may also be challenging. How can the solution space be explored efficiently, and what are the requirements for the exploration?

Timber flooring systems for long-span applications are normally glued thin flange elements with stiffeners and joists constituting the core. The number of joists and stiffeners, the internal added weight and insulation, and the dimensions of all members result in numerous potential combinations to be examined. This number increases drastically when the range of wood products and types of bonding are considered. When outfitting such as overlays and ceiling system is addressed, the number of combinations increase further. And finally, when support and load conditions and serviceability performance levels are regarded, the solution space is immense. With this many parameters, finding a competitive design is not manageable by manual exploration, and the solution space can in practice only confidently be investigated when assessed computationally. Based on this context, awareness of indicators of competitiveness and manufacturing cost-drivers, a holistic approach of exploring the solution space was conceptualised and developed. The approach incorporates:

- parametric relationship between the specifications of a timber floor element and the overall resource consumption in the format of an objective function for optimisation
- Quantification of added cost due to complexity of the floor element assembly (quantification of directionality)
- Utilization of the retail assortment of standard material formats of applicable materials
- Determination of vibration serviceability based on the method proposed in the second generation of Eurocode 5 implying 1) span length is not critical for the determination of performance, 2) utilisation of the ISO baseline curve increasing flexibility in floor design, and 3) the computation is fast and, based on

statement in [95], offers a good compromise to more sophisticated numerical analyses.

- Implementation of a suitable optimisation solver compatible with integer material dimensions

The optimisation framework has demonstrated the possibility of a holistic design approach for timber floor elements incorporating all significant parameters for the optimum design of the floor element as applied in a building.

The development of an automated numerical modelling of floor elements based on the same parametric system for geometric specification as for the analytical approach applied in Paper IV represents an unexplored potential. In combination with the probabilistic load model developed for use with Abaqus for human induced vibration (Annex A.IV) has the potential of increase precision when the importance of moment-resisting end constraints is apparent. This may not be adequately addressed in the analytical approach even though expressions for rotational stiffness in end constraints is implemented in the determination model [140].

7) What can be done to facilitate that methods and tools developed in the present work are utilized by future students at either MSc or doctoral levels for the common best of timber-based solutions as a means of improving the environmental performance of the built environment?

This will be achieved by writing codes in a language much used by engineers and architects, and by making codes available. The codes incorporate a high level of commenting along the codes.

The codes are written parametrically with the utilisation of common input files and customizable material databases, to facilitate collaboration between modules. The work may be implemented in BIM and the Architecture of Architecture (e.g. implemented in tools like Spacemaker).

The codes may be considered as an early step to allow for the implementation of machine learning in the computational design of optimised timber floor elements, where feedback from customers/users can build a training set for improves timber floor performance

4.3 Further work

- 1) The present work can be used as a basis for comparing the structural response in terms of acceleration and velocity and the associated computational effort for a range of floor elements and spans, as determined for the following three methods:

- a. The proposed analytical method for the second generation of Eurocode 5.
- b. Numerical analysis based on deterministic load models (time-domain implicit analysis)
- c. Numerical analysis based on probabilistic load models (frequency domain random response analysis)

The comparison should categorise the various floor element designs in the Floor Performance Level table of [96]. The effect of changing damping coefficient and the effect of changing internal mass could also be addressed. The tools and methods developed in the present work have prepared for this comparative analysis to be easily performed. By utilizing PSACHS for the generation of numerical models and the use of PARAPECHS for the analytical model, the same floor element can be built and assessed. The two codes use the same input file for specification of the floor element. The cumbersome definition of the probabilistic load model is given in Annex A.IV, and the deterministic load model with references to required parameters found in section 3.3.3.

- 2) Timber floor elements is completion friendly. For timber floor elements with a continuous bottom flange, completion is particularly convenient. Time to completion, and consequently cost, is therefore associated with competitiveness with respect to comparable alternatives in concrete. The cost of transportation and installation must also be addressed as means of increased competitiveness. Due to the lower mass of long-span timber floor elements, the number of elements per transporting vehicle will be higher for timber than for concrete floor elements. This affects cost and carbon emissions. The required capacity of building crane will due to weight also be lower for timber than for concrete floor elements. The calculation can also be extended to comprise figures for adaption, dismantling and reuse of timber floor elements which in all cases has impact on competitiveness both in terms of cost and ECO2. The topic can be addressed, and comparisons made to provide more numbers of competitiveness of timber floor elements.
- 3) There is a substantial potential for standardisation of timber building systems. Much work has been done on the topic, but efforts are scattered on a range of more or less particular cases. A comprehensive review of the topic must be performed, including related guidelines, and the scoping and conceptualisation of standardisation of timber elements, connectors and interfaces must be performed. An obvious part of the standardisation is Design for Disassembly and reuse. The standardisation must comprise requirements for adaptable buildings.

- 4) A floor element with thin field webs were designed and built during the present work. However, the doctoral project newer found resources to test this floor element in order to determine the accuracy of the numerical representation of floor elements with thin field webs. The floor element is stored at NTNU and may be used in future research. Technical drawings of the floor element is included in

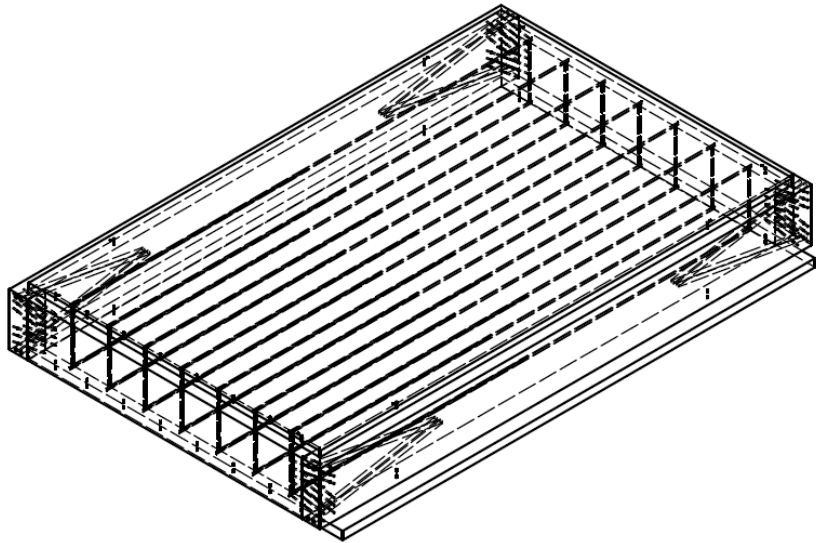


Fig. 38: Thin field web floor element

5 Reproducibility and information access

Transparency and reproducibility in articles may be aided by making associated data and codes available. As argued in the present work, and in accordance with the proposal for future research, data is shared and reuse invited.

The data from measurements and codes used herein is made available under standard publication license Attribution 4.0 International (CC BY 4.0) at <https://bird.unit.no/>

This license lets others distribute, remix, tweak, and build upon the work, even for commercial purposes, as long as the work using the resource credit the original creation.

BIRD is a digital service that collects, preserves, and distributes digital material. Repositories are important tools for preserving an organization's legacy; facilitating digital preservation and scholarly communication. BIRD is a part of Unit (Norwegian Directorate for ICT and Joint Services in Higher Education and Research) and is a part of a national strategy on access to and sharing of research data.

- The data from testing and codes for analysing structural response for the work on effects of interconnection between timber floor elements (relating to the work of Paper I) is made available here:
<https://hdl.handle.net/11250/2724776>
- The material data base, the PSACHS code for modelling and analysing timber floor elements in Abaqus, and required input files is made available here:
<https://hdl.handle.net/11250/2724786>
- The literature archive used in the present work is made available at the Timber Structures Research Group at NTNU.

6 References

- [1] S. Nesheim, K. A. Malo, and N. Labonnote, "Effect of interconnects on timber floor elements: Dynamic and static evaluations of structural scale tests," *Eur. J. Wood Wood Prod.*, 2021.
- [2] A. Vilguts, S. Nesheim, H. Stamatopoulos, and K. A. Malo, "A study on beam-to-column moment-resisting timber connections, comparing full-scale connection testing and mock-up frame assembly," *Eur. J. Wood Wood Prod.*, 2021.
- [3] S. Nesheim, K. A. Malo, and N. Labonnote, "Competitiveness of timber floor elements: An assessment of structural properties, production, costs and carbon emissions," *Forest Prod. J.*, 2021.
- [4] S. Nesheim, K. Mela, K. A. Malo, and N. Labonnote, "Optimisation of costs and carbon emission of timber floor elements," *Forest Prod. J.*, vol. 71, no. 2, 2021, Art no. 20-00067, doi: 10.13073/FPJ-D-20-00067.
- [5] S. Nesheim and K. A. Malo, "Assessing adequacy of numerical representation for optimisation performances in long span timber floors," presented at the World Conference in Timber Engineering 2018, Seoul, 2018.
- [6] S. Nesheim, K. A. Malo, and N. Labonnote, "Conditions and features of a design tool for long-span timber floor elements (Manuscript submitted for publication)," presented at the World Conference in Timber Engineering 2021, Santiago, 2021.
- [7] C.-D.-J. Eisen, "Vitruvian primitive hut," ed. Frontispiece from *Essai sur l'architecture*, second edition: DOME / MIT Library collections, 1755.
- [8] U. Iyer-Raniga, "Zero Energy in the Built Environment: A Holistic Understanding," *Applied Sciences*, vol. 9, p. 3375, 08/16 2019, doi: 10.3390/app9163375.
- [9] UN Environment and International Energy Agency (IEA), "Towards a zero-emission, efficient, and resilient buildings and construction sector. Global Status Report 2017.," UNEP 188, 2017. [Online]. Available: http://www.worldgbc.org/sites/default/files/UNEP%20188_GABC_en%20%28web%29.pdf
- [10] T. Dixon, J. Connaughton, and S. Green, *Sustainable Futures in the Built Environment to 2050: A Foresight Approach to Construction and Development*. John Wiley & Sons, 2018.
- [11] M. Ge and J. Friedrich. "4 Charts Explain Greenhouse Gas Emissions by Countries and Sectors." World Resources Institute. <https://www.wri.org/blog/2020/02/greenhouse-gas-emissions-by-country-sector> (accessed).
- [12] F. Pomponi and A. Moncaster, "Embodied carbon mitigation and reduction in the built environment – What does the evidence say?," *Journal of*

- Environmental Management*, vol. 181, pp. 687-700, 2016/10/01/ 2016, doi: <https://doi.org/10.1016/j.jenvman.2016.08.036>.
- [13] EcoSmart. "Statistics." http://ecosmartconcrete.com/?page_id=208 (accessed).
- [14] Statista. "Cement production globally and in the U.S. from 2010 to 2019." <https://www.statista.com/statistics/219343/cement-production-worldwide/> (accessed).
- [15] UNFCCC. "The Paris Agreement." UNFCCC secretariat. <https://unfccc.int/process-and-meetings/the-paris-agreement/the-paris-agreement> (accessed).
- [16] Climate action tracker. "Climate action tracker Europe." <https://climateactiontracker.org/countries/eu/> (accessed).
- [17] J. de Brito and R. Kurda, "The past and future of sustainable concrete: A critical review and new strategies on cement-based materials," *J. Clean. Prod.*, p. 123558, 2020/09/16/ 2020, doi: <https://doi.org/10.1016/j.jclepro.2020.123558>.
- [18] E. G. Hertwich *et al.*, "Material efficiency strategies to reducing greenhouse gas emissions associated with buildings, vehicles, and electronics—a review," *Environmental Research Letters*, vol. 14, no. 4, p. 043004, 2019.
- [19] M. Röck *et al.*, "Embodied GHG emissions of buildings – The hidden challenge for effective climate change mitigation," *Applied Energy*, vol. 258, p. 114107, 2020/01/15/ 2020, doi: <https://doi.org/10.1016/j.apenergy.2019.114107>.
- [20] S. Helle, "Skogen som veks og veks," in *Dag og Tid*, ed. Dag og Tid: Dag og Tid, 2020.
- [21] G. Hylen. "Nye rekordtall for skogen i Norge." Norsk institutt for bioøkonomi (NIBIO). <https://www.nibio.no/nyheter/nye-rekordtall-for-skogen-i-norge> (accessed).
- [22] (2011). *Meld. St. 9, Melding til Stortinget, Landbruks- og matpolitikken. Velkommen til bords.* [Online] Available: <https://www.regjeringen.no/no/dokumenter/meld-st-9-20112012/id664980/>
- [23] (2015). *SKOG22 Nasjonal strategy for skog og trenæringen.* [Online] Available: <https://www.regjeringen.no/no/dokumenter/skog-22--nasjonal-strategi-for-skog--og-trenaringen/id2363770/>
- [24] Pöyry Management Consulting, "Markedsanalyse av Skognæringen i Norge," Innovasjon Norge, October 6. 2014 2014. [Online]. Available: <http://www.innovasjonnorge.no/PageFiles/992303/MARKEDSANALYSE%20SKOGSN%C3%86RING%20I%20NORGE1610.pdf>
- [25] F. Kraxner *et al.*, "Mapping certified forests for sustainable management - A global tool for information improvement through participatory and collaborative mapping," *Forest Policy and Economics*, vol. 83, pp. 10-18, 2017/10/01/ 2017, doi: <https://doi.org/10.1016/j.forpol.2017.04.014>.

- [26] A. Bukauskas *et al.*, "Whole timber construction: A state of the art review," *Construction and Building Materials*, vol. 213, pp. 748-769, 2019/07/20/ 2019, doi: <https://doi.org/10.1016/j.conbuildmat.2019.03.043>.
- [27] (2013). *Tre for bygg og bygg for tre. Kunnskapsgrunnlag for økt bruk av tre i offentlige bygg.* [Online] Available: <https://www.regjeringen.no/no/dokumenter/tre-for-bygg-og-bygg-i-tre/id721773/>
- [28] R. B. Abrahamsen and K. A. Malo, "Structural design and assembly of" Treet"—A 14-storey timber residential building in Norway," in *World conference on timber engineering*, 2014, vol. 2014, no. 8.
- [29] R. Abrahamsen and M. L. AS, "Mjøstårnet-Construction of an 81 m tall timber building," in *International House Forum*, 2017.
- [30] M. Keskiä, "Use of tension rods in wood construction—14 storeys with laminated veneer lumber as shear walls: Lighthouse Joensuu," in *Internationales Holzbau-Forum IHF 2018*, 2018, pp. 6-7.
- [31] A. V. Jensen and N. Craig, *Wood in Construction-25 cases of Nordic Good Practice*. Nordic Council of Ministers, 2019.
- [32] M. K. Kuzman and D. Sandberg, "A new era for multi-storey timber buildings in Europe," presented at the Forest Products Society International Convention : 26/06/2016 - 29/06/2016, Madison, 2016, 2016. [Online]. Available: <http://urn.kb.se/resolve?urn=urn:nbn:se:ltu:diva-31108>.
- [33] A. Hynynen, "Future in Wood? Timber Construction in Boosting Local Development," (in English), *European Spatial Research and Policy*, vol. 23, no. 1, p. 127, 01 Jun. 2016 2016, doi: <https://doi.org/10.1515/esrp-2016-0007>.
- [34] W. Ferdous, Y. Bai, T. D. Ngo, A. Manalo, and P. Mendis, "New advancements, challenges and opportunities of multi-storey modular buildings – A state-of-the-art review," *Eng. Struct.*, vol. 183, pp. 883-893, 2019/03/15/ 2019, doi: <https://doi.org/10.1016/j.engstruct.2019.01.061>.
- [35] K.-U. Schober and T. Tannert, "Hybrid connections for timber structures," *Eur. J. Wood Wood Prod.*, vol. 74, no. 3, pp. 369-377, 2016.
- [36] A. Dias, *Design of Timber-concrete Composite Structures: A State-of-the-art Report by COST Action FP1402/WG 4*. Shaker Verlag, 2018.
- [37] M. Knauf, "Market potentials for timber-concrete composites in Germany's building construction sector," *Eur. J. Wood Wood Prod.*, vol. 75, no. 4, pp. 639-649, 2017/07/01 2017, doi: 10.1007/s00107-016-1136-9.
- [38] Think Wood, "Looking up: Tall wood buildings around the world," ed, 2017.
- [39] L. Eliasson, S. Berg, and D. Sandberg, "Some aspects on the more efficient use of wood in the industrial manufacture of single-family timber houses," *Pro Ligno*, vol. 11, no. 4, pp. 418-425, 2015.

- [40] J. H. Mork, M. Luczkowski, S. H. Dyvik, B. Manum, and A. Rønquist, "Generating timber truss bridges—examining the potential of an interdisciplinary parametric framework for architectural engineering," 2016.
- [41] J. Willmann, M. Knauss, T. Bonwetsch, A. A. Apolinarska, F. Gramazio, and M. Kohler, "Robotic timber construction — Expanding additive fabrication to new dimensions," *Automation in Construction*, vol. 61, pp. 16-23, 2016/01/01/ 2016, doi: <https://doi.org/10.1016/j.autcon.2015.09.011>.
- [42] Y. Weinand, *Advanced Timber Structures: Architectural Designs and Digital Dimensioning*. Birkhäuser, 2017.
- [43] N. Aage, O. Amir, A. Clausen, L. Hadar, D. Maier, and A. Søndergaard, "Advanced topology optimization methods for conceptual architectural design," in *Advances in Architectural Geometry 2014*: Springer, 2015, pp. 159-179.
- [44] J. Mayo, *Solid wood: case studies in mass timber architecture, technology and design*. Routledge, 2015.
- [45] J. Gosling, P. Sassi, M. Naim, and R. Lark, "Adaptable buildings: A systems approach," *Sustainable Cities and Society*, vol. 7, pp. 44-51, 2013/07/01/ 2013, doi: <https://doi.org/10.1016/j.scs.2012.11.002>.
- [46] E. Hurmekoski, R. Jonsson, and T. Nord, "Context, drivers, and future potential for wood-frame multi-story construction in Europe," *Technological Forecasting and Social Change*, vol. 99, pp. 181-196, 2015/10/01/ 2015, doi: <https://doi.org/10.1016/j.techfore.2015.07.002>.
- [47] "Taking wood to the top," Nordic Network for Tall Wood Buildings and Norwegian Institute of Wood Technology (NTI), Eds., ed. Survey at Green Building Conference Copenhagen, 2018.
- [48] H. Stamatopoulos and K. Malo, "Wood frame solutions for free space design in urban buildings (WOODSOL)," in *7th Forum Wood Building Nordic*, Växjö, Sweden, 2018.
- [49] A. Vilguts, K. A. Malo, and H. Stamatopoulos, "Moment resisting frames and connections using threaded rods in beam-to column timber joints," in *World Conference on Timber Engineering*, Seoul, Republic of Korea, 2018.
- [50] K. A. Malo and H. Stamatopoulos, "Connections with threaded rods in moment resisting frames," in *WCTE 2016 - World Conference on Timber Engineering*, 2016. [Online]. Available: <https://www.scopus.com/inward/record.uri?eid=2-s2.0-85010952856&partnerID=40&md5=a5f3aa5e8bac9a6f848eed69c244d78>. [Online]. Available: <https://www.scopus.com/inward/record.uri?eid=2-s2.0-85010952856&partnerID=40&md5=a5f3aa5e8bac9a6f848eed69c244d78>
- [51] K. A. Malo and J. Köhler, "Vibrations of timber floor beams with end restraints," in *2nd International Conference on Structures and Architecture, ICSA 2013, July 24, 2013 - July 26, 2013*, Guimaraes, Portugal, 2013: CRC Press/Balkema, in *Structures and Architecture: Concepts, Applications and*

- Challenges - Proceedings of the 2nd International Conference on Structures and Architecture, ICSA 2013, pp. 181-189.
- [52] S. Conta and A. Homb, "Sound radiation of hollow box timber floors under impact excitation: An experimental parameter study," *Applied Acoustics*, vol. 161, p. 107190, 2020/04/01/ 2020, doi: <https://doi.org/10.1016/j.apacoust.2019.107190>.
- [53] S. Conta, "Experimental modal analysis on Woodsol prototype floor element," NTNU, Trondheim, Norway, 2017.11.12 2017.
- [54] S. Conta and A. Homb, "Challenges and limitations using the Integral Transform Method to obtain the impact noise level of timber floors," 2018.
- [55] A. Manewa, M. Siriwardena, A. Ross, and U. Madanayake, "Adaptable buildings for sustainable built environment," *Built Environment Project and Asset Management*, vol. 6, no. 2, Supplement 1, 2016.
- [56] K. Beadle, A. Gibb, S. Austin, A. Fuster, and P. Madden, "Adaptable futures: sustainable aspects of adaptable buildings," in *ARCOM (Association of Researchers in Construction Management) Twenty-Fourth Annual Conference*, 2008, pp. 1-3.
- [57] A. Gidlund, "The Diagrid: Adaptable housing with timber construction," ed, 2020.
- [58] J. Gosling, M. Naim, P. Sassi, L. Iosif, and R. Lark, "Flexible buildings for an adaptable and sustainable future," in *Procs 24th Annual ARCOM Conference*, 2008: Association of Researchers in Construction Management Cardiff, pp. 1-3.
- [59] T. Dogan, E. Saratsis, and C. Reinhart, "The optimization potential of floor-plan typologies in early design energy modeling," 2015.
- [60] B. Dalen and C. H. Stenberg, "Horizontal stiffening with glass field," NTNU, Trondheim, 2017.
- [61] E. Orrestad Nilsen and L. M. Hovden, "Kapasitetsanalyse av limtrebjelker med store utsparinger-Analytisk og numerisk analyse," NTNU, 2015.
- [62] *NS-EN 1995-1-2:2004+NA:2010*, CEN, Brussels, Belgium, 2010. [Online]. Available: <http://www.standard.no/no/Nettbutikk/produktkatalogen/Produktpresentasjon/?ProductID=418958>
- [63] B. Östman and S. P. S. t. forskningsinstitut, *Brandsäkra trähus 3 : nordisk-baltisk kunskapsöversikt och vägledning*, Version 3. ed. (SP rapport (Sveriges provnings- och forskningsinstitut)). Stockholm: SP Sveriges Tekniska Forskningsinstitut, 2012.
- [64] SP, *Fire safety in timber buildings : technical guideline for Europe* (SP rapport (Sveriges provnings- och forskningsinstitut)). Stockholm: SP Technical Research Institute of Sweden SP Träteknik, 2010.

- [65] K. L. Friquin, S. Nesheim, B. G. Olsø, and J. M. Hisdal, "Brannsikkerhet i trebygg over 4 etasjer - Bruk av trekonstruksjoner i brannklasse 3," SINTEF Building and Infrastructure, Trondheim, 2016.12.12 2016.
- [66] DIBK, "Regulations on technical requirements for construction works TEK17," in *Norwegian Building Authority*, ed, 2017.
- [67] M. Gerigk, "Multi-Criteria Approach in Multifunctional Building Design Process," in *IOP Conference Series: Materials Science and Engineering*, 2017, vol. 245, p. 052085.
- [68] D.-I. M. Oppe, "Conceptual design and design examples for multi-storey buildings."
- [69] Norconsult Informasjonssystemer AS and Bygganalyse AS, *Norsk prisbok: et oppslagsverk for byggebransjen*, 2019-02 ed. (Norsk prisbok: et oppslagsverk for byggebransjen). Sandvika: Norconsult informasjonssystemer AS i samarbeid med AS Bygganalyse, 2019.
- [70] M. F. Ashby, *Materials selection in mechanical design*, Fifth edition ed. Butterworth-Heinemann, 2017.
- [71] B. Kucera and R. M. Næss, *Tre: naturens vakreste råstoff*. Landbruksforlaget Oslo, Norway, 1999.
- [72] S. Thelandersson, "Wood as Construction Material," in *Timber Engineering*, S. Thelandersson and H. J. Larsen Eds.: Wiley, 2003.
- [73] Norske limtreprodusenters forening, K. Bell, and H. Liven, *Limtreboka* (Design of glulam structures). Bergen: John Grieg Norske limtreprodusenters forening, 2015.
- [74] A. Menges, T. Schwinn, and O. D. Krieg, *Advancing wood architecture: a computational approach*. Routledge, 2016.
- [75] A. Lyons, *Materials for Architects and Builders (Third Edition)*. Oxford: Butterworth-Heinemann, 2006, pp. 1-31.
- [76] O. P. Larsen and A. Tyas, *Conceptual structural design : bridging the gap between architects and engineers*. London: Thomas Telford, 2003.
- [77] D. Jones and C. Brischke, *Performance of bio-based building materials*. Woodhead Publishing, 2017.
- [78] Forest Product Laboratory, U. S. D. o. Agriculture, Ed. *Wood Handbook: Wood as an Engineering Material*. United States Department of Agriculture, 2010.
- [79] J. Bodig and B. A. Jayne, *Mechanics of Wood and Wood Composites*. Krieger Publishing Company, 1993.
- [80] H. J. Blaß and C. Sandhaas, H. u. S. V. Versuchsanstalt für Stahl, Ed. *Timber Engineering - Principles for Design*. Karlsruhe: KIT Scientific Publishing (in English), 2017, p. 644.

- [81] G. Orheim, "Tradisjonell bruk av treslag på vestlandet," ed. Volda: Høgskulen i Volda, 2000.
- [82] CEN, European committee for standardization, "EN 1995-1-1:2004: Design of timber structures. Part 1-1: General-Common rules and rules for buildings," ed. Brussels, Belgium, 2004.
- [83] B. Zhang, B. Rasmussen, A. Jorissen, and A. Harte, "Comparison of vibrational comfort assessment criteria for design of timber floors among the European countries," *Engineering Structures*, vol. 52, pp. 592-607, 2013, doi: 10.1016/j.engstruct.2013.03.028.
- [84] T. Toratti and A. Talja, "Classification of human induced floor vibrations," *Building Acoustics*, vol. 13, no. 3, pp. 211-221, 2006, doi: 10.1260/135101006778605370.
- [85] P. Hamm, A. Richter, and S. Winter, "Floor vibrations - New results," in *11th World Conference on Timber Engineering 2010, WCTE 2010*, 2010, vol. 4, pp. 2765-2773. [Online]. Available: <https://www.scopus.com/inward/record.uri?eid=2-s2.0-84870471459&partnerID=40&md5=16ca66cebad48f9b672138952edae98d>. [Online]. Available: <https://www.scopus.com/inward/record.uri?eid=2-s2.0-84870471459&partnerID=40&md5=16ca66cebad48f9b672138952edae98d>
- [86] L. J. a. C. Hu, Y.H., "Development of a design method to control vibrations induced by normal walking action in wood-based floors.," presented at the 8th World Conference on Timber Engineering 2004, WCTE 2004, Lahti, Finland, 2004.
- [87] A. Homb, "Low frequency sound and vibrations from impacts on timber floor constructions.," PhD, NTNU Norwegian University of Science and Technology, 2006.
- [88] N. Labonnote, A. Rønquist, and K. A. Malo, "Prediction of material damping in timber floors, and subsequent evaluation of structural damping," *Materials and Structures/Materiaux et Constructions*, vol. 48, no. 6, pp. 1965-1975, 2015, doi: 10.1617/s11527-014-0286-7.
- [89] K. Jarnerö, A. Brandt, and A. Olsson, "Vibration properties of a timber floor assessed in laboratory and during construction," *Eng. Struct.*, vol. 82, pp. 44-54, 2015, doi: 10.1016/j.engstruct.2014.10.019.
- [90] C. Jaafari and J. Mohammadi, "Floor Vibration Control as a Serviceability Requirement in Design Standards and Practices," *Practice Periodical on Structural Design and Construction*, vol. 23, no. 2, p. 04018003, 2018.
- [91] J. Negreira, A. Trollé, K. Jarnerö, L. G. Sjökvist, and D. Bard, "Psychovibratory evaluation of timber floors - Towards the determination of design indicators of vibration acceptability and vibration annoyance," *Journal of Sound and Vibration*, Article vol. 340, pp. 383-408, 2015, doi: 10.1016/j.jsv.2014.12.001.

- [92] I. Glisovic and B. Stevanovic, "Vibrational behaviour of timber floors," in *11th World Conference on Timber Engineering 2010, WCTE 2010, June 20, 2010 - June 24, 2010*, Trentino, Italy, 2010, vol. 4: Trees and Timber Institute, in 11th World Conference on Timber Engineering 2010, WCTE 2010, pp. 2785-2793.
- [93] A. Ebrahimpour and R. L. Sack, "A review of vibration serviceability criteria for floor structures," *Computers & Structures*, vol. 83, no. 28, pp. 2488-2494, 2005/11/01/ 2005, doi: <https://doi.org/10.1016/j.compstruc.2005.03.023>.
- [94] *EN 1995-1-1 SC5.T3 milestone draft 2 Revised section 9.3*, CEN, Brussels, 2018.
- [95] I. Abeysekera, P. Hamm, T. Toratti, and A. Lawrence, "Development of a floor vibration design method for Eurocode 5," *New Zealand timber design*, vol. 27, no. 1, 2019.
- [96] *EN 1995-1-1 SC5.T3 Final draft prEN*, CEN, Brussels, 2020.04.30 2020.
- [97] H. Reiher and F. J. Meister, "The Effect of Vibration on People," *Forsch. Geb. Ing. Wes.*, vol. 2 (11) 381-6, 1931.
- [98] T. M. Murray and B. Davis, "Evaluation of problem floors because of human induced vibrations," in *Proceedings of the 8th International Conference on Structural Dynamics, EURO DYN 2011*, 2011, pp. 1009-1013. [Online]. Available: <https://www.scopus.com/inward/record.uri?eid=2-s2.0-84885394098&partnerID=40&md5=e6642222a0423fdd16acc155fa941f48>. [Online]. Available: <https://www.scopus.com/inward/record.uri?eid=2-s2.0-84885394098&partnerID=40&md5=e6642222a0423fdd16acc155fa941f48>
- [99] T. M. Murray, "Floor vibrations: The human tolerance side of the equation," in *Proceedings of the International Modal Analysis Conference - IMAC*, 1999, vol. 1, pp. 1-6. [Online]. Available: <https://www.scopus.com/inward/record.uri?eid=2-s2.0-0032671499&partnerID=40&md5=0f6c11d530948b55c69dabffa8dc04bc>. [Online]. Available: <https://www.scopus.com/inward/record.uri?eid=2-s2.0-0032671499&partnerID=40&md5=0f6c11d530948b55c69dabffa8dc04bc>
- [100] *ISO 2631-2:2003 Mechanical vibration and shock - Evaluation of human exposure to whole-body vibration - Part 2: Vibration in buildings (1 Hz to 80 Hz)*, ISO, Lysaker, 2003.
- [101] *ISO 10137:2007 Bases for design of structures - Serviceability of buildings and walkways against vibrations*, ISO, 2007.
- [102] L. Hu, Y. H. Chui, P. Hamm, T. Toratti, and T. Orskaug, "Development of ISO baseline vibration design method for timber floors," in *WCTE 2018 - World Conference on Timber Engineering*, 2018. [Online]. Available: <https://www.scopus.com/inward/record.uri?eid=2-s2.0-85058141638&partnerID=40&md5=695a602fc32566953133d03404c74212>. [Online]. Available: <https://www.scopus.com/inward/record.uri?eid=2-s2.0-85058141638&partnerID=40&md5=695a602fc32566953133d03404c74212>

- [103] G. Sedlacek *et al.*, "Design of floor structures for human induced vibrations," Luxembourg : OPOCE, Luxembourg, 1018-5593, 2009.
- [104] A. Paskalov and S. Reese, "Deterministic and probabilistic floor response spectra," *Soil Dynamics and Earthquake Engineering*, vol. 23, no. 7, pp. 605-618, 2003/10/01/ 2003, doi: [https://doi.org/10.1016/S0267-7261\(03\)00064-2](https://doi.org/10.1016/S0267-7261(03)00064-2).
- [105] J. Chen, J. Wang, and J. M. Brownjohn, "Power spectral-density model for pedestrian walking load," *Journal of Structural Engineering*, vol. 145, no. 2, p. 04018239, 2019.
- [106] V. Racic, A. Pavic, and J. M. W. Brownjohn, "Experimental identification and analytical modelling of human walking forces: Literature review," *Journal of Sound and Vibration*, vol. 326, no. 1, pp. 1-49, 2009/09/25/ 2009, doi: <https://doi.org/10.1016/j.jsv.2009.04.020>.
- [107] C. J. Middleton and J. M. W. Brownjohn, "Response of high frequency floors: A literature review," *Eng. Struct.*, vol. 32, no. 2, pp. 337-352, 2010/02/01/ 2010, doi: <https://doi.org/10.1016/j.engstruct.2009.11.003>.
- [108] A. S. Mohammed, A. Pavic, and V. Racic, "Improved model for human induced vibrations of high-frequency floors," *Eng. Struct.*, vol. 168, pp. 950-966, 2018/08/01/ 2018, doi: <https://doi.org/10.1016/j.engstruct.2018.04.093>.
- [109] E. Shahabpoor, A. Pavic, and V. Racic, "Interaction between Walking Humans and Structures in Vertical Direction: A Literature Review," *Shock and Vibration*, vol. 2016, p. 22, 2016, Art no. 3430285, doi: 10.1155/2016/3430285.
- [110] E. Ahmadi, C. C. Caprani, and A. Heidarpour, "An equivalent moving force model for consideration of human-structure interaction," *Applied Mathematical Modelling*, vol. 51, no. Supplement C, pp. 526-545, 2017/11/01/ 2017, doi: <https://doi.org/10.1016/j.apm.2017.06.042>.
- [111] J. M. Brownjohn, A. Pavic, and P. Omenzetter, "A spectral density approach for modelling continuous vertical forces on pedestrian structures due to walking," *Canadian Journal of Civil Engineering*, vol. 31, no. 1, pp. 65-77, 2004.
- [112] A. K. Chopra, *Dynamics of structures : theory and applications to earthquake engineering*, 4th ed. ed. (Prentice-Hall international series in civil engineering and engineering mechanics). Boston, Mass: Prentice Hall, 2012.
- [113] E. N. Strømmen, *Structural dynamics*. Springer, 2014.
- [114] J. Xiong and J. Chen, "Power spectral density function for individual jumping load," *International Journal of Structural Stability and Dynamics*, vol. 18, no. 02, p. 1850023, 2018.
- [115] J. Wang, J. Chen, Y. Yokoyama, and J. Xiong, "Spectral Model for Crowd Walking Load," *Journal of Structural Engineering*, vol. 146, no. 3, p. 04019220, 2020.

- [116] H. Xiong, J. Kang, and X. Lu, "Finite element analysis on dynamic behavior of timber floor subjected to pedestrian-induced force," in *World Conference on Timber Engineering 2012, WCTE 2012*, 2012, vol. 2, pp. 508-515. [Online]. Available: <https://www.scopus.com/inward/record.uri?eid=2-s2.0-84871964544&partnerID=40&md5=d45b64083016ad2688f0d362b62ba1cf>. [Online]. Available: <https://www.scopus.com/inward/record.uri?eid=2-s2.0-84871964544&partnerID=40&md5=d45b64083016ad2688f0d362b62ba1cf>
- [117] C. C. Caprani and E. Ahmadi, "Formulation of human–structure interaction system models for vertical vibration," *Journal of Sound and Vibration*, vol. 377, no. Supplement C, pp. 346-367, 2016/09/01/ 2016, doi: <https://doi.org/10.1016/j.jsv.2016.05.015>.
- [118] M. M. Ebadi, G. Doudak, and I. Smith, "Finite-Element Modeling and Parametric Study of Glulam Beam-and-Deck Floors," *Journal of Structural Engineering (United States)*, Article vol. 143, no. 9, 2017, Art no. 04017106, doi: 10.1061/(ASCE)ST.1943-541X.0001844.
- [119] M. R. Willford, P. Young, and M. CEng, *A design guide for footfall induced vibration of structures*. Concrete Society for The Concrete Centre, 2006.
- [120] L. J. Hu and Y. H. Chui, "Development of a design method to control vibrations induced by normal walking action in wood-based floors," presented at the Proceedings of the 8th World Conference on Timber Engineering, Lahti, Finland, 2004.
- [121] *NS-EN 1995-1-1:2004+A1:2008+NA:2010*, CEN, Brussels, 2010. [Online]. Available: <http://www.standard.no/no/Nettbutikk/produktkatalogen/Produktpresentasjon/?ProductID=436137>
- [122] O. Neve, "Shear connectors for thin topping timber-concrete composite floors," *Structural Engineer*, vol. 87, no. 17, pp. 21-23, 2009.
- [123] R. Selle, K. Holschemacher, and B. Heiden, "An alternative approach for hybrid floors made of timber and concrete (TCCS)," in *10th International Conference on Modern Building Materials, Structures and Techniques, May 19, 2010 - May 21, 2010*, Vilnius, Lithuania, 2010: Vilnius Gediminas Technical University, in 10th International Conference Modern Building Materials, Structures and Techniques, pp. 778-786.
- [124] K. Crews, S. John, C. Gerber, A. Buchanan, T. Smith, and S. Pampanin, "Innovative engineered timber building systems for non-residential applications, utilising timber concrete composite flooring capable of spanning up to 8–10 m," *Forest and Wood Products Australia Report PNA012-0708*. ISBN, pp. 978-1, 2010.
- [125] M. Fragiacomano and E. Lukaszewska, "Development of prefabricated timber-concrete composite floor systems," *Proceedings of the Institution of Civil Engineers: Structures and Buildings*, Article vol. 164, no. 2, pp. 117-129, 2011, doi: 10.1680/stbu.10.00010.

- [126] T. Sartori and R. Crocetti, "Prefabricated timber-concrete composite floors," *Eur. J. Wood Wood Prod.*, vol. 74, no. 3, pp. 483-5, 05/ 2016, doi: 10.1007/s00107-016-1007-4.
- [127] V. Schmid, D. Zauft, and M. A. Polak, "Bonded timber-concrete composite floors with lightweight concrete," in *2016 World Conference on Timber Engineering, WCTE 2016, August 22, 2016 - August 25, 2016*, Universitätsring 1, Vienna, Austria, 2016: Vienna University of Technology, in WCTE 2016 - World Conference on Timber Engineering.
- [128] S. E. Zimmer and M. Augustin, "Timber-steel-composite - A possibility for hybrid structures of long span timber floors," in *2016 World Conference on Timber Engineering, WCTE 2016, August 22, 2016 - August 25, 2016*, Universitätsring 1, Vienna, Austria, 2016: Vienna University of Technology, in WCTE 2016 - World Conference on Timber Engineering.
- [129] C. Loss and B. Davison, "Innovative composite steel-timber floors with prefabricated modular components," (in English), *Eng. Struct.*, Article vol. 132, pp. 695-713, Feb 2017, doi: 10.1016/j.engstruct.2016.11.062.
- [130] T. Tannert, B. Endacott, M. Brunner, and T. Vallée, "Long-term performance of adhesively bonded timber-concrete composites," *International Journal of Adhesion and Adhesives*, Article vol. 72, pp. 51-61, 2017, doi: 10.1016/j.ijadhadh.2016.10.005.
- [131] D. Riccadonna, K. Walsh, G. Schiro, M. Piazza, and I. Giongo, "Testing of long-term behaviour of pre-stressed timber-to-timber composite (TTC) floors," *Construction and Building Materials*, vol. 236, p. 117596, 2020/03/10/ 2020, doi: <https://doi.org/10.1016/j.conbuildmat.2019.117596>.
- [132] K. McGunnigle *et al.*, "Development of light timber frame floor/ceiling systems with good low frequency performance," in *12th International Congress on Sound and Vibration 2005, ICSV 2005, July 11, 2005 - July 14, 2005*, Lisbon, Portugal, 2005, vol. 5: International Institute of Acoustics and Vibrations, in 12th International Congress on Sound and Vibration 2005, ICSV 2005, pp. 4636-4643.
- [133] K. Salmela and A. Olsson, "Dynamic properties of a sawn timber floor element with high transverse bending stiffness," *Building Acoustics*, Article vol. 13, no. 4, pp. 295-310, 2006, doi: 10.1260/135101006779320500.
- [134] K. Salmela and A. Olsson, "Vibration properties of a floor system with high transverse stiffness," in *9th World Conference on Timber Engineering 2006, WCTE 2006*, 2006, vol. 1, pp. 726-729. [Online]. Available: <https://www.scopus.com/inward/record.uri?eid=2-s2.0-84870026664&partnerID=40&md5=9433483a7b5f1cff6bd2e00d3676302e>. [Online]. Available: <https://www.scopus.com/inward/record.uri?eid=2-s2.0-84870026664&partnerID=40&md5=9433483a7b5f1cff6bd2e00d3676302e>
- [135] B. Zhang, A. Kermani, and T. Fillingham, "Vibrational performance of timber floors constructed with metal web joists," *Eng. Struct.*, vol. 56, pp. 1321-1334, 2013, doi: 10.1016/j.engstruct.2013.07.011.

- [136] H. Chung and G. Emms, "Vibration reduction in lightweight floor/ceiling systems with a sand-sawdust damping layer," in *INTERNOISE - Int. Congr. Noise Control Eng.: Improv. World Through Noise Control*, 2014. [Online]. Available: <https://www.scopus.com/inward/record.uri?eid=2-s2.0-84923546015&partnerID=40&md5=4925d246e98d8f36d043d0127a69aa5f>. [Online]. Available: <https://www.scopus.com/inward/record.uri?eid=2-s2.0-84923546015&partnerID=40&md5=4925d246e98d8f36d043d0127a69aa5f>
- [137] W. G. Montgomery, S. D. Schiff, and W. Pang, "Hollow massive timber panels: A high-Performance, long-span alternative to Cross Laminated Timber," in *WCTE 2014*, 2014. [Online]. Available: <https://www.scopus.com/inward/record.uri?eid=2-s2.0-84924955612&partnerID=40&md5=0ae159ff80d9f01d359ace90e9016cc2>. [Online]. Available: <https://www.scopus.com/inward/record.uri?eid=2-s2.0-84924955612&partnerID=40&md5=0ae159ff80d9f01d359ace90e9016cc2>
- [138] K. Lewis, B. Basaglia, R. Shrestha, and K. Crews, "The use of cross laminated timber for Long span flooring in commercial buildings," in *2016 World Conference on Timber Engineering, WCTE 2016, August 22, 2016 - August 25, 2016*, Universitätsring 1, Vienna, Austria, 2016: Vienna University of Technology, in *WCTE 2016 - World Conference on Timber Engineering*.
- [139] L. J. Hu, R. Desjardins, and E. Jones, "Systems approach for optimizing wood-based floor construction," in *9th World Conference on Timber Engineering 2006*, Portland, OR, United states, August 6, 2006 - August 10, 2006 2006, vol. 3: Oregon State University Conference Services, in *9th World Conference on Timber Engineering 2006, WCTE 2006*, pp. 2069-2076.
- [140] *Parametric Resources and Performance of CHS*. (2020). NTNU. Accessed: 2020.11.22.
- [141] *Competitiveness Optimizer for CHS*. (2020). NTNU. Accessed: 2020.12.01.
- [142] *Abaqus CAE*. (2017). Dassault Systèmes Simulia corp. [Online]. Available: <https://www.3ds.com/products-services/simulia/products/abaqus/abaquscae/>
- [143] *Python Script for Abaqus for Closed Hollow Sections (PSACHS)*. (2018). NTNU. Accessed: 2018.05.01.
- [144] Betongelementforeningen. "Betongelementboka." Online. <https://betongelementboka.betongelement.no/betongapp/default.html> (accessed).
- [145] A. Dodoo, L. Gustavsson, and R. Sathre, "Lifecycle carbon implications of conventional and low-energy multi-storey timber building systems," *Energy and Buildings*, vol. 82, pp. 194-210, 2014/10/01/ 2014, doi: <https://doi.org/10.1016/j.enbuild.2014.06.034>.
- [146] C. Skaar, B. Solem, and P. Rütther, "Composite floors in urban buildings: Options for a low carbon building design," presented at the Forum Wood Building Nordic, Trondheim Norway, 2017.

- [147] D. Yeoh, M. Fragiaco, M. De Franceschi, and K. Heng Boon, "State of the art on timber-concrete composite structures: Literature review," *Journal of structural engineering*, vol. 137, no. 10, pp. 1085-1095, 2011.
- [148] M. K. Skaare, K. A. Malo, and T. Kanstad, "Vibrations in Composite Timber-Concrete Floor Systems," MSc, Fakultet for Ingeniørvitenskap og Teknologi; Institutt For Konstruksjonsteknikk, NTNU, Trondheim, 2013. [Online]. Available: <http://hdl.handle.net/11250/237395>
- [149] O. Frihetsli and O. Alm, "Wood-Concrete Composite Floor," MSc, NTNU, 2015. [Online]. Available: <http://hdl.handle.net/11250/2357971>
- [150] K. A. Åby, M. Hartnes, and K. A. Malo, "Timber composite floor," NTNU, 2016. [Online]. Available: <http://hdl.handle.net/11250/2433669>
- [151] I. H. Monsen and M. Nystuen, "Buildability and Assembly of the WoodSol Concept," NTNU, 2018. [Online]. Available: <http://hdl.handle.net/11250/2568524>
- [152] H. Bjørge and T. Kristoffersen, "Conceptual study of wooden composite floors with possibility of rigid attachment to glulam column," NTNU, 2017. [Online]. Available: <http://hdl.handle.net/11250/2614916>
- [153] Dassault Systèmes, "Element selection in Abaqus," ed: Dassault Systèmes Simulia corp., 2007.
- [154] *iSight and Simulia Execution Engine*. (2017). Dassault Systèmes Simulia corp. [Online]. Available: <https://www.3ds.com/products-services/simulia/products/isight-simulia-execution-engine/>
- [155] S. S. Mo, "Modelling of long Span Wooden Floors with Finite Element Method," NTNU, 2018. [Online]. Available: <http://hdl.handle.net/11250/2571483>
- [156] *Grasshopper*. (2007). Robert McNeel and associates. [Online]. Available: <https://www.grasshopper3d.com/>
- [157] *EndNote Reference management*. (2020). Clarivate Analytics, Philadelphia. [Online]. Available: endnote.com
- [158] *Nvivo*. (2020). QSR International, Melbourne, Australia. [Online]. Available: <https://www.qsrinternational.com/nvivo-qualitative-data-analysis-software/home>
- [159] B. D. Kristian and F. F. I. O. T. I. F. K. Norges Teknisk-Naturvitenskapelige Universitet, "Mechanical properties of clear wood from Norway spruce," Norges teknisk-naturvitenskapelige universitet, Fakultet for ingeniørvitenskap og teknologi, Institutt for konstruksjonsteknikk, 2009.
- [160] J. Hakkarainen, "Properties of Kerto LVL for FEM calculations," ed: Metsä Wood, 2016.

- [161] D. I. f. Bautechnik, "Board BauBuche S/Q German technical approval," in *Z-9.1-838*, P. F. GmbH, Ed., ed. Berlin: Deutsches Institut für Bautechnik, 2016, p. 10.
- [162] Norgips, "EPD Norgips Fireboard," ed, 2020.
- [163] Moelven Töreboda AB, "EPD Glulam beams and pillars," ed, 2016.
- [164] C. Sandhaas and J. Van de Kuilen, "Material model for wood," *Heron*, vol. 58, no. 2/3, p. 173, 2013.
- [165] H. Bachmann, F. Deischl, W. J. Ammann, and SpringerLink, *Vibration Problems in Structures: Practical Guidelines*: Birkhäuser Basel, 1995.
- [166] *CrossX*. (2003). Norwegian University of Science and Technology.
- [167] A. Homb, "Kriterier for opplevde vibrasjoner i etasjeskillere. Delrapport fra prosjektet «Comfort properties of timber floor constructions»,", ed, 2007.
- [168] P. Aune, *Trekonstruksjoner : 1 : Materialer, dimensjonering, forbindelser*. Trondheim: Tapir, 1992.
- [169] J. Clastornik, M. Eisenberger, D. Z. Yankelevsky, and M. A. Adin, "Beams on Variable Winkler Elastic Foundation," *Journal of Applied Mechanics*, vol. 53, no. 4, pp. 925-928, 1986, doi: 10.1115/1.3171882.
- [170] D. Froio and E. Rizzi, "Analytical solution for the elastic bending of beams lying on a variable Winkler support," *Acta Mechanica*, vol. 227, no. 4, pp. 1157-1179, 2016.
- [171] SINTEF Community. 522.351 Trebjelkelag. Dimensjonering og utførelse [Online] Available: https://www.byggforsk.no/dokument/334/trebjelkelag_dimensjonering_og_utfoerelse
- [172] P. Pavelka, R. Hunady, M. Hagara, and F. Trebuna, "Reciprocity in Experimental Modal Analysis," *American Journal of Mechanical Engineering*, vol. 3, no. 6, pp. 252-256, 2015. [Online]. Available: <http://pubs.sciepub.com/ajme/3/6/20>.
- [173] N. Labonnote, "Modal hammer for dummies 1.2," S. Nesheim, Ed., Version 1.2 ed: NTNU, 2018.
- [174] P. Welch, "The use of fast Fourier transform for the estimation of power spectra: a method based on time averaging over short, modified periodograms," *IEEE Transactions on audio and electroacoustics*, vol. 15, no. 2, pp. 70-73, 1967.
- [175] R. S. Kaplan and S. R. Anderson, "Time-Driven Activity-Based Costing," *Harv. Bus. Rev.*, Article vol. 82, no. 11, pp. 131-138, 2004. [Online]. Available: <http://search.ebscohost.com/login.aspx?direct=true&db=bth&AN=14874836&site=ehost-live>.

- [176] C. Drury, "Activity-based costing," in *Management and Cost Accounting*: Springer, 1992, pp. 273-288.
- [177] S. Nesheim, "Monteringsanvisning Woodsol dekkeelementer ved Charlottenlund VGS," ed. Trondheim, Norway: NTNU, 2018.
- [178] *EN 16929 Test methods - Timber floors - Determination of vibration properties*, CEN, 2018.
- [179] Minitab Inc, *Getting Started with Minitab 18*. Minitab, 2018.
- [180] I. Anco Engineers, "Operating manual for the MK-102 eccentric mass vibrator system," ed. Boulder Colorado: Anco Engineers Inc., 2010, p. 26.
- [181] J. S. Arora, *Introduction to Optimum Design*. Elsevier Academic Press, 2004.
- [182] *The Python Language*. (2003). Network Theory Ltd. [Online]. Available: www.python.org
- [183] *OR-Tools*. (2019). Google. Accessed: 2019-7-19. [Online]. Available: <https://developers.google.com/optimization/>
- [184] R. D. Adams and D. Bacon, "Measurement of the flexural damping capacity and dynamic Young's modulus of metals and reinforced plastics," *Journal of Physics D: Applied Physics*, vol. 6, no. 1, p. 27, 1973.
- [185] E. E. Ungar and E. M. Kerwin Jr, "Loss factors of viscoelastic systems in terms of energy concepts," *The Journal of the acoustical Society of America*, vol. 34, no. 7, pp. 954-957, 1962.
- [186] N. Labonnote, A. Ronnquist, and K. A. Malo, "Prediction of material damping in timber floors, and subsequent evaluation of structural damping," *Materials and Structures*, vol. 48, no. 6, pp. 1965-75, 06/ 2015, doi: 10.1617/s11527-014-0286-7.
- [187] H. Wierix, "Christuskind helpt Jozef met zagen," ed, 1563.
- [188] S. Nesheim, Asplan Viak Oslo. Experience from timber based flooring systems at NTNU. (20170914). [Presentation].
- [189] S. Nesheim, NTNU Wood Workshop 2018. Closed hollow wood sections in long-span flooring systems. (20180606). [Presentation].
- [190] S. Nesheim, Tampere University Finland. Optimisation strategies for timber floor element. (20190923). [Presentation].
- [191] S. Nesheim, NTNU Wood Workshop 2019. Brief on Woodsol floor developments. (20190605). [Presentation].
- [192] S. Nesheim, "Norge nå," in *Mjøstårnet - verdens høyeste trehus*, NRK, Ed., ed: Norwegian Broadcasting Corporation, 2019.
- [193] A. Dürer, "Melencolia I," ed, 1514.

PART II

Dissemination



[187]

Competitive timber floors – PART II: Dissemination

Vågar du tro på ett höghus av trä?

– bob hund “Raketmaskinen”, 1998

1 Peer-reviewed articles

1.1 Paper I

Effect of interconnects on timber floor elements: Dynamic and static evaluations of structural scale tests.

Sveinung Nesheim, Kjell Arne Malo, Nathalie Labonnote

For publication in: European Journal of Wood and Wood Products

Submitted: 28th September 2020

Accepted: Pending after submitting response to minor revisions

Credit author statements

For the Original article presented herein, all authors have contributed to its preparation as described in the below statement:

Sveinung Nesheim: Conceptualization, Methodology, Software, Validation, Investigation, Resources, Writing - Original Draft, Writing - Review & Editing, Visualization, Project administration.

Kjell Arne Malo: Writing - Review & Editing, Supervision, Funding acquisition.

Nathalie Labonnote: Writing - Review & Editing, Supervision.

Effects of interconnections between timber floor elements

Dynamic and static evaluations of structural scale tests

Abstract

Long-span timber floor elements increase the flexibility of a building and exhibit a significant market potential. Timber floor elements are endeavouring to fulfil this potential, but building projects employing long-span timber floors have encountered drawbacks. High costs and vibration performance are challenging, and the timber industry is under substantial pressure to find attractive solutions for building components with otherwise favourable environmental features. Only a few existing studies have investigated serviceability sensitivity in relation to timber floor connections. Interconnections are inexpensive to produce and install and may offer a resource-efficient approach to improving serviceability performance. In the present study, the effect of interconnections is investigated in a full-scale structural test. Floor elements positioned in different configurations have been tested for static and dynamic performance using different types of interconnections. The observed effects of interconnection types vary according to the configuration and direction of mode shapes, and are assessed in terms of shift in frequency, damping and resonant energy. These can all be utilised in combination with observed differences in the deflection parameter. The present work demonstrates that connections between timber elements have significant effects on timber floor serviceability and may offer interesting solutions to improve the vibration performance of long-span timber floors.

Keywords

Long-span timber floors; interconnections; full-scale test; static performance; dynamic performance; serviceability.

1 Introduction

The greater utilisation of timber in the building sector has the potential to contribute to reductions in greenhouse gas (GHG) emissions, which represent a major and universal challenge to the sector. Global population growth and urbanization are placing increasing demands on a need for multi-storey, space-efficient, sustainable and flexible buildings. For timber to become an attractive building material under

current market conditions, innovative and competitive concepts must be developed, proven and effectively marketed. The development of open architectures and long-spanning primary structures has the potential to enhance the competitiveness and environmental performance of timber-based buildings. Such features increase the scope of compliant building typologies, functionality and potential interior layout permutations (Gosling et al. 2013). It is currently technically feasible to design a timber floor of ten metres span with acceptable acoustic performance. The challenge is however to offer the market floor elements with competitive designs at an acceptable commercial risk with proven static and dynamic performance of serviceability.

Numerous criteria may be used to assess timber floor serviceability, and although the physical principles are similar to human discomfort during horizontal motion, the topic is less matured and no international agreement of evaluating serviceability have been established. In general terms, floor serviceability criteria involve the use of a deflection constraint for flatness, and a frequency constraint that addresses human perception. The criterion commonly used by Hu and Chui (Hu 2004) is based solely on these two constraints. However, most other approaches employ a dynamic constraint, either in the form of a Vibration Dose Value (ISO 2007), an RMS-acceleration for resonant response (Smith et al. 2009), or an RMS-velocity for transient response (Ohlsson 1988) that serves to improve the description of what are perceived to be troublesome vibrations. Recent developments resulting from work carried out in Working Group 3 of the CEN TC 250/SC 5 (CEN 2018) are likely to introduce more adaptable criteria that incorporate categorisation into performance classes. As is clear from published reviews (Zhang et al. 2013, Negreira et al. 2015), all documented methods exhibit benefits and drawbacks and will lead to different floor designs for the same application.

The second major challenge facing the timber floor construction sector is how to boost serviceability and market competitiveness while keeping resource consumption low. A focused exploration of the solution space related to typologies and innovatively engineered timber products is a challenging task. A less studied approach has been the assessment and utilisation of performance differences when comparing single floor elements with contiguous flooring systems. The assembly of floor elements to form a functional flooring system may involve the use of a variety of connections and configurations. The use of connections may represent a cost-effective approach to altering the dynamic response of a flooring system without changing the overall design of the basic floor element.

Only very few investigations have been published on the topic of connections, and generally with the aim of establishing guidelines governing the cost-efficient adaptation of floor elements to different applications. Comparisons of differences in performance of floor elements with continuous and discontinuous sheeting have

been presented in (Burch et al. 2016), and similar results are expected for comparisons between floor elements. Weckendorf et al. (Weckendorf and Smith 2012) present a study of the effects of both interconnecting elements and intermediate supports in the context of Cross Laminated Timber (CLT) construction. Ebadi et al. (Ebadi et al. 2016, Ebadi 2017) document the results of a study of the low-amplitude dynamic responses of a one-way spanning floor element. One out of nine floor configurations (Floor 5 in their study), demonstrated the effect of interconnected adjacent floor elements contributing towards increased composite action. This study concluded that the first fundamental frequency and deflection parameters remain unchanged, but that frequency spacing between adjacent modes decrease for higher mode shapes. In another study carried out by Weckendorf et al. (Weckendorf et al. 2016), mode shapes, frequencies and damping are interpreted to be strongly dependent on the construction details of end and edge restraints, as well as the method of interconnection between the elements making up the flooring system. In Weckendorf et al. (Weckendorf et al. 2016), the authors address the influence on boundary conditions of timber floors in the context of both design strategies and damping. Ignoring the semi-rigid connections between CLT elements, by assuming either an absence of connections or full continuity, leads to significant inaccuracies in predictions of mode shapes and frequencies. This is also pointed out in a study by Ussher (Ussher et al. 2017), which investigated half-lap screwed interconnections. In Labonnote et al. (Labonnote and Malo 2010), a main effects analysis indicated that connection stiffness and element width exert a significant influence on the Hu and Chui (Hu and Chui 2004) criterion. This study demonstrated that the vibration properties of floor elements improve with increasing width, and that the influence of interconnections between elements is closely related to element width. Weckendorf (Weckendorf et al. 2014) investigated the effects of on-site horizontal transmissions within floor substructures forming contiguous flooring systems, but the boundary conditions are not comparable.

The objective of this study is to adapt the comfort performance of elements in a flooring system in a way that reduces costs and environmental impact. This has been achieved by investigating whether interconnections between timber floor elements can be used as the basis for a resource-efficient approach to enhance serviceability performance. Full-scale floor elements are positioned in a variety of configurations and then tested for static and dynamic performance using different types of interconnections. Interconnections are mounted both transversally and longitudinally, and tied to floor element edge members while varying the number of fasteners. Comfort properties for floor elements are related to damping, but the quantification of damping is challenging. Total damping consists of material damping and structural damping. Whilst material damping may be estimated from the strain energy method (Ungar and Kerwin Jr 1962, Adams and Bacon 1973), the structural damping is difficult to predict because it is linked to detailing in the design

and execution of the floor element and its supporting structures (Labonnote et al. 2015). Full-scale tests are therefore an important yet expensive measure to obtain credible values of total damping. To the authors' knowledge, the present study is the only investigation to date addressing interconnections between cassette type timber floor elements.

2 Materials and Methods

2.1 Geometry and material properties

Three Closed Hollow Section (CHS) floor elements with two different spans are studied: Two identical long floor elements (L) and one short floor element (S). A cross-section of two parallel floor elements viewed in the direction of the span is shown in Fig. 1. The floor element cross-section and material selection was based on studies reported in (Nesheim and Malo 2018). Each of the floor elements has a continuous frame of two joists ① and transverse end beams ② in 405 x 140 GL30c. In the main load carrying direction three field joists ③ in 405 x 66 GL28c are fitted between the end beams. The cavities are filled with gravel type 8/16 ⑥ with mass corresponding to a distributed 100 kg/m² for improved acoustic performance. The floor has a continuous top ④ and bottom ⑤ flange of 43 and 61 mm Kerto-Q, respectively. The frame including field joists is both glued and screwed with liquid gap filling phenol-resorcinol adhesive (Dynea 2017) and self-tapping double threaded fastener (SFS WT-T 8.2 x 220), whilst the flanges were structurally glued together with the same adhesive, but without fasteners. When floor elements are combined laterally, they are referred to as flooring system, and in current study the flooring system is simplified and arranged as two elements either in parallel or series. The floor elements of the Woodsol building system is an inherent structural component in the Moment Resisting Frames (MRF), joined to the columns with Moment Resisting Connectors (MRC). In the current study the columns were 405 x 450 GL30c, stretching 450 mm in the direction of the span. The MRC consisted of two parts connected with M30 grade 12.9 friction bolts with a rated tightening torque of 2.5 kNm. The parts of the MRC are connected by threaded rods to the floor element edge joists, and columns. See light blue and dark blue dashed lines of Fig. 2. The length of the MRC was 285 mm in the direction of span. The long elements (L) were 4.7 m between end supports, designed at half the span of a typical floor element for the Woodsol building system (Stamatopoulos and Malo 2018), while the short floor (S) was 3.8 m long. The corresponding system lengths (centre of columns) was 5.72 and 4.82 m. The length of the floor elements and the quantity of internal mass was based on assessments related to acoustic testing (Conta and Homb 2020).

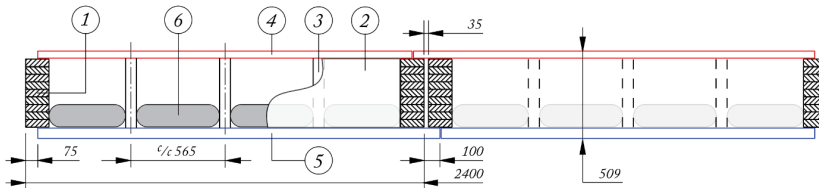


Fig. 1 Floor element cross-section (configuration 3)

2.2 Test specimen configurations

At floor level each face of a column can accommodate one MRC, hence parallel floors share an MRC, whilst elements in series are connected to separate MRC. Principally the floor element is suspended as illustrated in Fig. 2. and the MRC is represented by a set of normal springs with various stiffness in the cartesian directions. In Fig. 2. the x -direction spring (D_1) is visible. The columns are supported on hinges with no rotational stiffness about the Y -axis. In the test the floor elements were mounted with the bottom of construction levelled 2 m above ground. Details on the MRC can be found in (Vilguts et al. 2018).

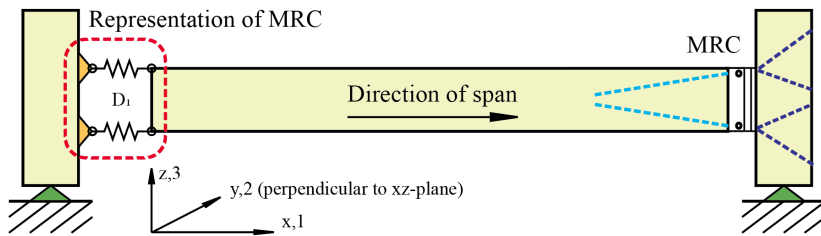


Fig. 2 Spring arrangement for deck in longitudinal direction (left: principle of MRC, right: physical realization)

Four different configurations of floor elements were tested. Configuration one through three have floor elements in parallel, whilst configuration four have floor elements in series. See Fig. 3 and Fig. 4, respectively.

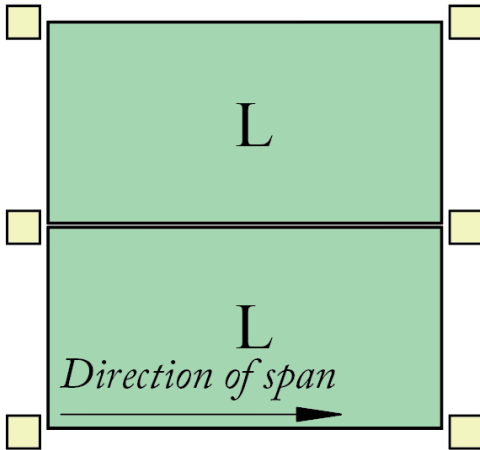


Fig. 3 Plan of configuration 1 through 3 (floor elements in parallel)

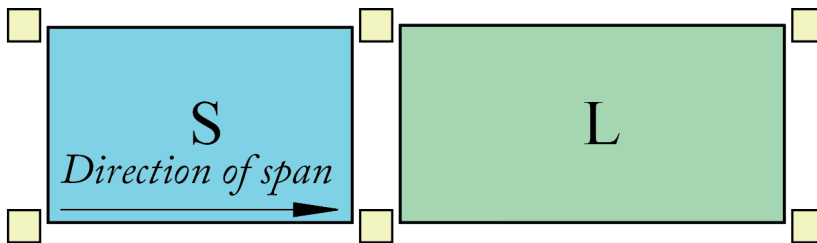


Fig. 4 Plan of configuration 4 (floor elements in series)

When floor elements are mounted in parallel, the flooring system differs only by the type of interconnection between the elements. Fig. 5 show the three different connections used for floor elements in parallel.

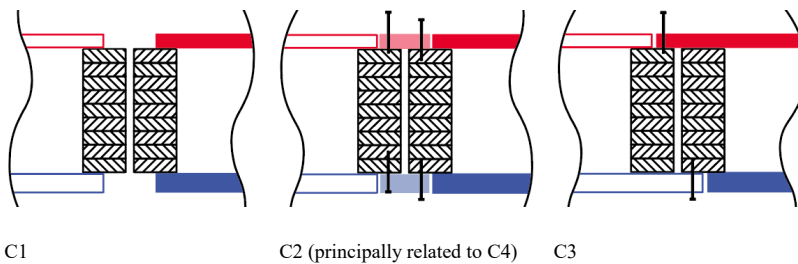


Fig. 5 Section view (in direction of span) of element interconnections: C1: No connection, C2: Board/bridge connection with twin row of fasteners at top and bottom level, C3: Intersecting connection with single row of fasteners at both levels.

In configuration 1 (C1) there are no interconnection between elements, and the elements are structurally related only through common columns. In configuration 2 (C2), a section similar to the upper and lower flange is attached between adjacent longitudinal edge joists with a number of screws, and in configuration 3 (C3) the top and bottom flange is respectively extended and retracted to facilitate an intersecting connection with the flanges of the adjacent floor element. The torque on the bolts of the MRC is affecting the rotational stiffness between column and floor element. Configurations C1 and C2 is tested with rated torque on the bolts of the MRC. Because the rated tightening torque of the M30 bolts require hydraulic torque tools, the bolts of the MRC were tightened to 1 kNm achievable by manual labour for the remainder of the tests.

In configuration 4 (C4) floor element S is mounted in series with element L. The C4 test sequence starts with floor elements connected only through their common columns, advancing with the installation of a bridging component mounted as a transverse interconnection between the floor elements, principally like C2, but with shear capacity. The bridging component covers the open space caused by the columns and the required space of the MRC (see Fig. 6). The bridging component is constructed from a central transverse web and two longitudinal edge webs all in GL28c 66 x 405 mm. The flange plates are identical to the flanges of the floor elements. The bridge piece was not filled with additional mass.

The pattern of fasteners is chosen from combined considerations of required edge spacing, a desired fastener at mid span, even centre to centre distance, and allowance for systematic increase in the number of fasteners. For C2 and C3 fasteners was positioned according to Fig. 7 and Fig. 8, and for C4 according to Fig. 6. For C2 the minimum amount of fasteners was three per row, at two rows per board. For C3 and C4 the minimum amount was one fastener per row. The sequence of fastening was: one central screw when applicable, three fasteners by adding one screw at each end of the row. Further fastening was then achieved by adding screws between existing screws.

The screw pattern distance was 245 mm for longitudinal interconnections (C2 and C3), and 240 mm for transverse interconnection (C4). The fastener used was a partial threaded flange head Ø8 mm by 160 mm for top flange, and 180 mm for the bottom flange (SFS-HT-T-FH-PT). The nail plate used in C4 was a Rothoblaas LBV 2.0 x 1200 x 100 mounted in series to cover the width of the bridge. Rows of 50 screws per meter was mounted at each longitudinal edge of the nail plate.

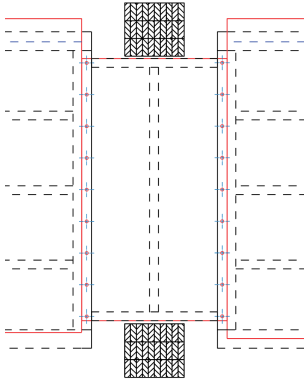


Fig. 6 Fasteners C4 (9 screws at each row and level)

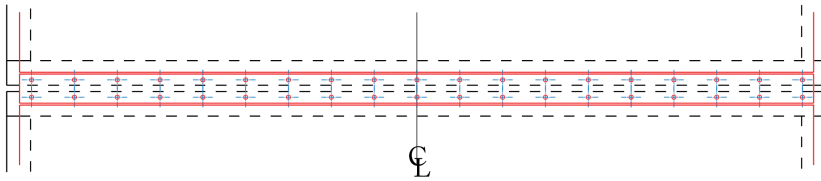


Fig. 7 Fasteners position for C2 (19 screws at each row and level)

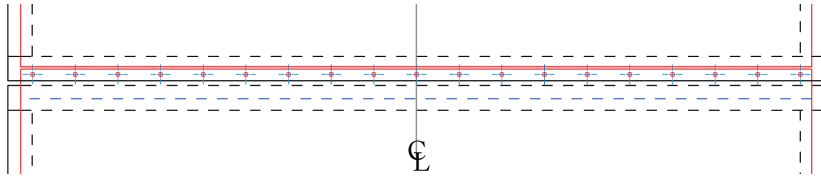


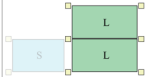
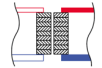
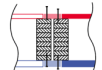
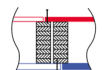
Fig. 8 Fasteners position for C3 (19 screws at each level)

2.3 Design of experiments

The design of experiments is presented in Table 1 and Table 2. Both tables follow the same setup: ID column are configuration identifiers separated by a running number. Interconnection columns contain number of screws per row, and an additional parameter specifying the particulars of the interconnection: For floor elements in parallel stating the MRC torque, and for floor elements in series stating whether nail plates are used. For C4 top and bottom flange fastening has separate columns. Performed tests are given in the last three columns. The selected tests were designed to study variation in deflection and modal parameters as the interconnection between the floor elements was altered. Due to limitations of time and changing boundary conditions, not all tests was performed for the various configurations and interconnections. As can be seen only a few rowing hammer tests was performed.

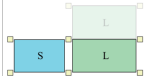
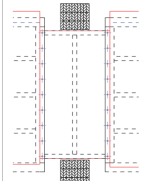
For floor element in parallel rowing hammer tests was performed only for the weakest and strongest connection where the MRC is tightened at rated torque. The shaded area identifies factors used in the statistical analysis of structural response as described in section 2.6.

Table 1 Test sequence of floor elements in parallel

	ID	Interconnection		Static point load	EMV ¹⁾	Rowing hammer
		Screw	Torque [kNm]			
	c1_0	0	2.5	✓	✓	✓
	c1_1	0		✓	✓	
	c1_2	0		✓	✓	
	c2_0	3	1.0	✓	✓	
	c2_1	5		✓	✓	
	c2_2	9		✓	✓	
	c2_3	19	2.5	✓	✓	✓
	c2_4	19		✓	✓	
	c2_5	19		✓	✓	
	c3_0	0	1.0	✓	✓	
	c3_1	1		✓		
	c3_2	3		✓		
	c3_3	5		✓		
	c3_4	9		✓		
	c3_5	19		✓	✓	

¹⁾ Eccentric Mass Vibrator

Table 2 Test sequence of floor elements in series

	ID	Interconnection				Static point load	EMV	Rowing hammer
		Screw		Nailplate				
		Top	Btm	Top	Btm			
	c4_1	0	0	No	No	✓	✓	✓
	c4_2	1	1	No	No	✓		
	c4_3	3	3	No	No	✓	✓	
	c4_4	5	5	No	No	✓	✓	✓
	c4_5	9	9	No	No	✓	✓	
	c4_6	9	9	Yes	No	✓	✓	
	c4_7	9	9	Yes	Yes	✓	✓	✓
	c4_8	9	0	Yes	No	✓	✓	✓

2.4 Data collection

2.4.1 Weight and moisture content

Weight of the floor elements was $m_L = 2450$ kg and $m_S = 1865$ kg, including additional mass. Weight of the MRC parts were 4 pieces of 18 kg and the associated threaded rods were 16 pieces of 1.5 kg, in addition to weight of adhesive and fasteners (~10 kg). Moisture content was 10.5 % for glulam, and 11.0 % for LVL.

2.4.2 Excitations

Two dynamic and one static excitation test protocol was designed for the study. Types and positions of sensors and excitation source are given in Annex A.II.

2.4.2.1 Experimental Modal Analysis (EMA)

Rowing Hammer Method (RHM) (Labonnote 2018) was applied to quantify out-of-plane deformation modes and damping. The method assumes linearity and time-invariance to fulfil the Maxwell's reciprocity theorem (Pavelka et al. 2015). The response was measured by a stationary ceramic/quartz impedance accelerometer type 8770A50 (Kistler 2008), and the excitation by the 8210 sledge (Brüel & Kjær 2012). With a mass of 5.44 kg and with the soft impact tip it produces a 10 mS duration impulse with a maximum force of 500 N. The excitation grids and position of the accelerometer for the tested configurations are given in Annex A.I.

2.4.2.2 Cyclic load

An Eccentric Mass Vibrator (EMV) (Anco Engineers 2010) was used to excite the floor element dynamically from 5 Hz to 30 Hz during a 2 min sweep. The EMV was mounted to the floor element through an adaptor plate tied to the floor element at mid-point. Two accelerometers monitored the response; one at EMV (applicator) and one at immediate proximity to the centre of the bottom flange (receiver). Both accelerometers was type 8770A50 (Kistler 2008). In addition to floor accelerations, the exciter frequency was recorded. The force from the exciter varied from 50 N to 750 N depending on frequency. Data were recorded at 1200 Hz. The dynamic loading was produced by four rotating weights on two shafts. The weights counter-rotate to retain a uni-directional force. The magnitude of the dynamic loading is controlled by the eccentricity of the weights. By turning the angles of the weights, the eccentricity can be adjusted from 0% to 100%, corresponding to the range from zero to 0.12 kg · m. The weights were chosen with 30% eccentricity.

2.4.2.3 Point load deformation

A point load was applied at the centre of the top flange via two Ø8 mm tension bars connected to load cell and with the loading located under the floor element. The tension bars was affixed to a 16 mm steel plate distributing the load to the underlying 200 cm² load pad as advised in the timber floors test method (CEN 2018). Because the cross section of the floor element was designed for twice the span, the standard unit load of 1kN was increased to 10 kN. The point load idled at maximum load for 5 min to expose creep, before it was released to the unloaded state. The rate of loading and unloading was 6 ⅔ N/s for floor elements in parallel (loading from water balloon as illustrated in Fig. 9), and ⅓ kN/s for floor elements in series (loading from hoist anchored to ground). The response was sampled at 2Hz.

A 50 kN load cell was used (HBM 2019), and the displacements were recorded with Linear Variable Differential Transformers (LVDT) (HBM 2019), see Fig. 9.

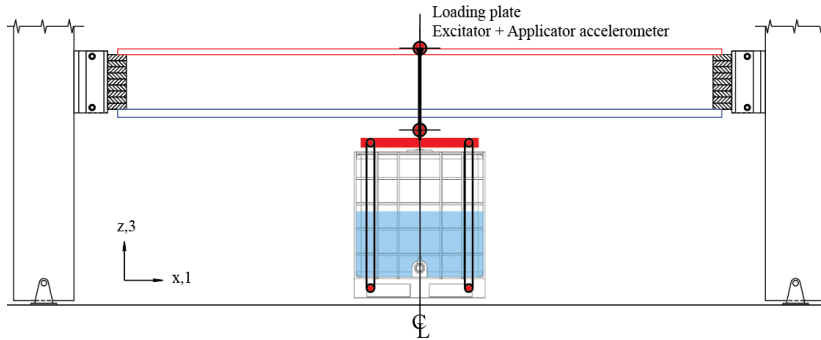


Fig. 9 Illustration of load and load cell application



Fig. 10: Static load test situation image

2.5 Numerical representation

Numerical analysis was performed using Abaqus (Dassault Systèmes 2017). Members of the core were modelled as solids, while shell elements were used for flanges. The interconnections were modelled by shell members tied to the flanges. The representation differs from the study performed in (Ebadi et al. 2017), where connecting elements and joists are modelled as simplified 2D quadratic Timoshenko orthotropic element and spring elements for interconnections were used. Particular care was taken for the numerical model to be able to represent accurate eigen frequencies and bending modes, and the selection of elements was done in accordance with (Nesheim and Malo 2018). Eight-node brick element (C3D8) were used for all members of the core, whilst four-node shell element (S4) was used for

flanges. A surface was put on top and bottom of the floor elements to manage loads and responses. These are modelled with the four-node quadrilateral surface element (SFM3D4). Columns are modelled with solids in C3D8. Each of the four threaded rods of the MRCs was modelled as a linear cartesian connector with the following properties with respect to the global axis system, where 1 is longitudinal, 2 is transversal and 3 is vertical direction:

$$\mathbf{D} = \{D_1 \quad D_2 \quad D_3\} = \{12.2 \quad 3.715 \quad 7.425\} \cdot 10^6 \begin{bmatrix} N \\ m \end{bmatrix}$$

The modelling did not consider variation in tensioning of the bolts on the MRC, and \mathbf{D} was computed to represent a constant rotational stiffness of 2 MNm/rad between the column and each end of the edge joists of the floor element. To allow a realistic force employment from the point loads of the MRC, a reinforced skin modelled as a S4 shell was attached to timber faces covered by the MRC. The skins were all modelled as 27 mm S355 steel plate. Added weight of 100 kg/m² was applied to the bottom flange to represent internal mass, whilst 15 kg/m² was added to top flange to represent adhesive and fasteners.

2.6 Statistical evaluation

A statistical evaluation was performed to reveal main effects and the level of significance each factor had on the response of the flooring system. The design of experiment, as explained in section 3.3, was transformed to matrices of factors (columns) and runs (rows) corresponding to the shaded area of Table 1 and Table 2. The statistical assessment was performed in Minitab. Hu and Chui (Hu and Chui 2004) criterion (1) was used to evaluate changes in performance as alterations in the interconnections changed fundamental frequency (f_1) and unit point load deflections (w). Similarly, changes in dynamic responses was evaluated using the expressions for root mean square of acceleration (2) and velocity (3) as described in (Abeysekera et al. 2019).

$$\frac{\left(\frac{f_1}{18.7}\right)^{2.27}}{w} > 1 \quad (1)$$

$$a_{rms} = \frac{\alpha \cdot F_0}{7 \cdot \zeta \cdot M^*} \quad (2)$$

- | | |
|--|--|
| α Fourier coefficient $\alpha = e^{-0.4 \cdot f_1}$ | F_0 Vertical force imposed by walking person (700 N) |
| ζ modal damping ratio | M^* modal mass $M^* = \frac{mLB}{4}$ |
| m Mass (kg) of floor per unit area (m ²) | L span of floor (m) |
| B Width of floor (m) | |

$$v_{rms} = K_{imp} \cdot \frac{0.7 \cdot I_m}{M^* + 70} (0.65 - 0.01 \cdot f_1)(1.22 - 11 \cdot \zeta) \eta \quad (3)$$

$$K_{imp} \text{ Higher modes multiplier for transient response } K_{imp} = \max \left\{ 0.48 \left(\frac{B}{L} \right) \left(\frac{EI_L}{EI_T} \right)^{0.25}, 1 \right\}$$

EI_L Longitudinal bending stiffness (Nm²/m) EI_T Transverse bending stiffness (Nm²/m)

l_m Mean modal impulse $l_m = \frac{42 \cdot f_w^{1.43}}{f_1^{1.3}}$ f_w Walking frequency (Hz)

$$\eta = \begin{cases} 1.52 - 0.55 \cdot K_{imp} & 1.0 \leq K_{imp} \leq 1.5 \\ 0.69 & \text{otherwise} \end{cases}$$

3 Results

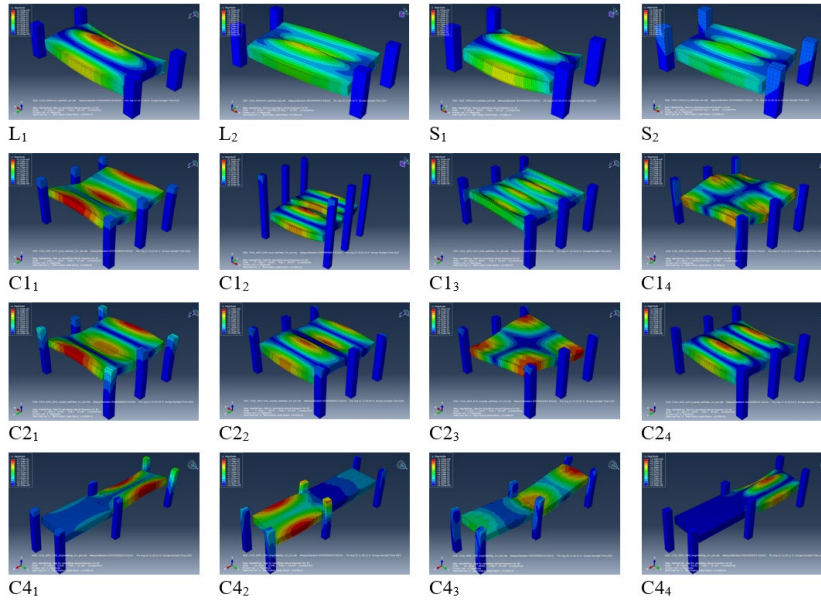
3.1 Numerical analysis

Eigen frequencies from finite element analysis (FEA) are presented in Table 3. The first column of the table contains a reference to the images in Table 4 for the associated modal shapes. No differences were made in the numerical representation of floor elements with longitudinal interconnection (C2 and C3), and the numerical representation is of C2 with 19 screws. The direction of view is arranged to match the view of corresponding configurations in Table 5. Due to the wide edge joists made to accommodate the threaded rods, the longitudinal bending stiffness (EI_L) is higher at the element edges compared to the field. Furthermore, since the bending stiffness transversally (EI_T) is low, transverse mode orders dominates the mode shapes, typically in combination with first longitudinal mode of the field of the floor element.

Table 3 FEA fundamental frequency analyses

Table 4	Boundary condition	Frequency [Hz]	Description of mode shape	
L ₁	Single element attached to column through MRC	L	38.83	1 st transversal (element)
L ₂			50.36	2 nd transversal (element)
S ₁		S	46.21	1 st transversal (element)
S ₂			56.86	2 nd transversal (element)
C1 ₁	C1 (uncoupled elements type L)		22.82	1 st transversal (diaphragm) / RB roll (element)
C1 ₂			38.87	2 nd transversal (elements out-of-phase viewed)
C1 ₃			50.38	3 rd transversal
C1 ₄			52.06	1 st torsional
C2 ₁	C2 19s (coupled elements type L)		24.61	1 st transversal (diaphragm)
C2 ₂			32.72	2 nd transversal
C2 ₃			37.7	1 st torsional
C2 ₄			39.42	3 rd transversal
C4 ₁	C4 (L and S in series) modelled as nail plates on top and bottom		23.57	L-dominated 1 st torsional (element roll)
C4 ₂			29.96	S-dominated 1 st torsional (element roll)
C4 ₃			35.15	1 st longitudinal (L-dominated)
C4 ₄			39.36	L-dominated 1 st transversal

Table 4 FEA fundamental frequency mode shapes



3.2 Rowing Hammer experiments

Table 5 presents governing mode shapes from 1 to n with corresponding frequencies (f_n) and damping (ζ_n) for the flooring system as measured by rowing hammer testing. The grids for the rowing hammer positions are visualized in Annex A.I Fig. 17 and Fig. 18 for floor elements in parallel and series, respectively. Due to the low vertical stiffness of the MRC, rigid body motions were large with respect to modal deformations. Furthermore, since the objective of the present work is focusing at the relative movement between the floor elements, the rigid body motions was excluded.

Table 5 EMA frequency and damping results floor elements in parallel

ID	f_1 [Hz]	ζ_1	f_2 [Hz]	ζ_2	f_3 [Hz]	ζ_3	f_4 [Hz]	ζ_4	f_5 [Hz]	ζ_5	f_6 [Hz]	ζ_6	f_7 [Hz]	ζ_7	f_8 [Hz]	ζ_8
C1.0																
	22.03	0.70	23.38	0.75	28.13	1.31	34.03	1.58	37.70	2.08	40.76	1.27	45.90	2.58	53.67	2.95
C2.3																
	24.77	0.73	27.05	1.32	30.89	2.13	32.96	1.15	35.57	2.28	37.97	3.04	40.66	2.53	45.67	2.15

Table 6 EMA frequency and damping results floor elements in series

ID	f_1 [Hz]	ζ_1	f_2 [Hz]	ζ_2	f_3 [Hz]	ζ_3	f_4 [Hz]	ζ_4	f_5 [Hz]	ζ_5
C4.1	23.96	1.17	26.28	1.69	28.56	1.55	32.60	1.93	39.72	2.15
C4.4	24.82	1.07	26.90	1.58	30.23	1.60	35.63	4.05	40.00	1.52
C4.7	25.00	1.55	27.05	1.75	30.45	2.00	35.78	2.39	39.85	2.23
C4.8	24.60	0.98	27.77	1.57	29.44	0.87	35.51	1.19	41.10	1.51

3.3 Cyclic loading experiments

Responsive energy is characterised by Power Spectral Density (PSD) of accelerations of the floor elements due to imposed dynamic loading is charted in Fig. 11 and Fig. 12. Corresponding peak values is given in Table 7. The magnitude of dynamic loading as generated by the EMV is controlled by the crank weight, eccentricity (set at 30%), and angular frequency squared as given in (4).

$$F_{EMV}(f) = 0.12kgm \cdot 30\% \cdot (2\pi f)^2 \quad (4)$$

Responses below 20 Hz are related to rigid body motions and are disregarded. These are succeeded by modal shapes associated with behaviour of the floor elements, starting with responses for the floor acting as a common diaphragm from 22 to 25 Hz. The vertical motions of the floor elements are mainly caused by deflections in the MRCs, which were large compared to deformations associated with the floor elements. Hence, modal properties of the isolated flooring system were not obvious from a standard FFT-analysis. However, by applying Welch's method (Welch 1967) the modal deformations associated with the flooring system appear distinctly in the PSD charts as seen in Fig. 11 and Fig. 12. For C4, the peaks at 30 Hz is disregarded. These peaks are associated with resonance in the EMV due to a frequency sweep out of range.

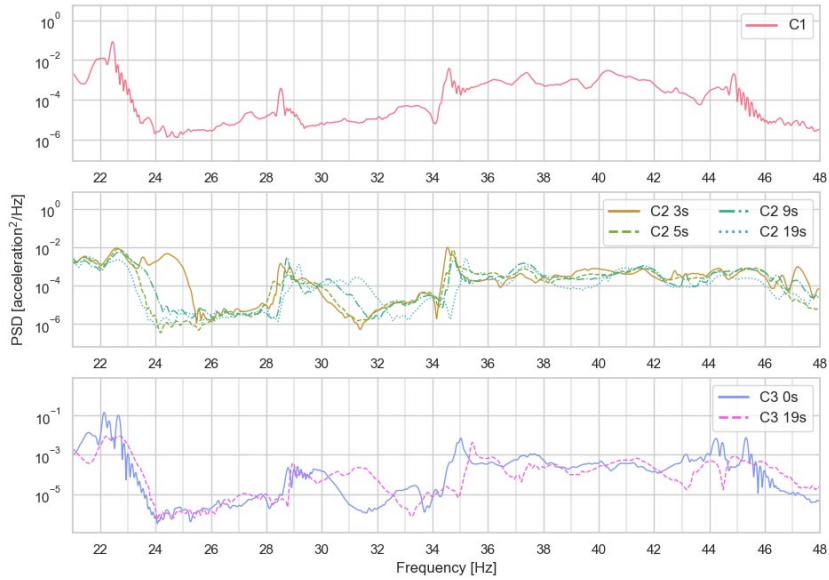


Fig. 11 Logarithmic plot of PSD for responses in configurations 1 to 3

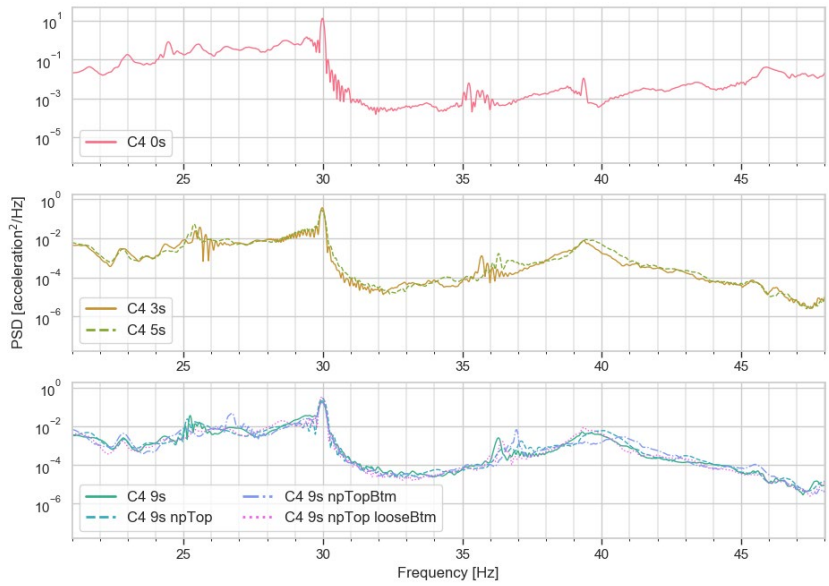


Fig. 12 Logarithmic plot of PSD for responses in configuration 4

Table 7 Dominant resonant peak properties from Welch method

Description	ID	1st dominant		2nd dominant	
		Frequency	Value	Frequency	Value
		[Hz]	[(m/s ²)/Hz]	[Hz]	[(m/s ²)/Hz]
C1	c1_2	34.60	0.0038	37.38	0.0024
C2 3s	c2_0	34.54	0.0097	37.18	0.0005
C2 5s	c2_1	34.73	0.0072	37.44	0.0008
C2 9s	c2_2	34.78	0.0021	37.28	0.0015
C2 19s	c2_5	35.11	0.0026	37.39	0.0010
C3 0s	c3_0	35.02	0.0071	37.52	0.0011
C3 19s	c3_5	35.44	0.0043	37.49	0.0004
C4 0s	c4_1	35.12	0.0062	39.34	0.0180
C4 3s	c4_3	35.69	0.0013	39.35	0.0077
C4 5s	c4_4	36.30	0.0017	39.43	0.0088
C4 9s	c4_5	36.29	0.0026	39.30	0.0052
C4 9s npTop	c4_6	37.11	0.0018	40.05	0.0061
C4 9s npTopBtm	c4_7	36.93	0.0068	40.79	0.0030
C4 9s npTop looseBtm	c4_8	36.42	0.0018	39.35	0.0087

3.4 Unit load deflection

As explained in 3.4.2.3, due to assumed linearity the point load was increased to 10 kN to have measurable deformations. Deformations at unit load (1 kN) were then calculated by regression analyses of the measured deformations from the entire loading protocol. R^2 were typically above 96%. Relative deflection and Root Mean Square Error (RMSE) were calculated for all response parameters and compiled into tables. Table 8 and Table 9 contain dimensionless responses as relative deformations with respect to C1_A for floor elements in parallel, and to C4_1 for floor elements in series. In Annex B Table 11 and Table 12. RMSE from the regression analyses is found. Only the most relevant measurements are displayed in Table 8 and Table 9. Compression of sensors yield positive number.

3.4.1 Floor elements in parallel

The reference denoted C1_A is the average structural responses of C1_0 and C1_1. Similarly, C2_3 and C2_4 is replaced with an average C2_A. C1_A and C2_A are the tests where the friction bolts of the MRC are tightened at rated prestressing torque (2.5 kNm). Note that $Z_{Amean1and4}$ is the mean value of ZA1 and ZA4. RY_{atCon} and RX_{btwFlr} is respectively relative rotation in radians about Y-axis between column and edge of floor element, and relative rotation about X-axis between longitudinal adjacent floor elements.

Table 8 Relative deflection of selected positions with respect to C1_A

ID	ZA0	ZA2	ZAmean1/4	ZA5	ZA6	ZR0	RYatCon	RXbtwFlr
	[1]	[1]	[1]	[1]	[1]	[1]	[1]	[1]
c1 A	1	1	1	1	1	1	1	1
c1 2	1.062	1.353	1.168	0.733	1.057	1.156	0.059	Invalid
c2 0	1.062	1.096	1.108	0.728	0.980	0.582	-2.154	1.386
c2 1	1.025	1.208	1.035	0.721	0.983	0.475	-2.776	1.128
c2 2	1.016	1.092	1.018	0.703	0.976	0.316	-0.861	2.056
c2 A	0.976	1.189	0.858	0.959	0.984	0.017	-0.545	2.129
c2 5	1.038	1.129	0.990	0.697	0.983	0.126	-2.102	2.353
c3 0	0.800	1.099	0.986	0.861	1.000	0.551	-0.809	0.326
c3 1	0.952	1.328	0.815	0.881	1.024	0.254	-0.212	0.644
c3 2	0.868	1.060	0.800	0.834	1.014	0.063	-1.415	0.766
c3 3	0.880	1.325	0.918	0.869	1.023	0.116	-0.665	0.822
c3 4	0.913	1.270	0.797	0.849	1.031	0.000	-1.258	1.214
c3 5	0.878	1.399	0.880	0.879	1.022	0.000	-1.215	1.814

3.4.2 Floor elements in series

Note that $Z_{Amean0and4}$, $Z_{Amean3and9}$ and $Z_{Amean7and8}$ is the mean value of ZA0 and ZA4, ZA3 and ZA9, and ZA7 and ZA8, respectively. RY_{btwFlr} is the relative rotation in radians about Y-axis between the two end beams (transversal part of floor element frame) facing the bridging component.

Table 9 Relative deflection of selected positions with respect to C4-1

ID	Z _{Amean0/4}	ZA1	ZA2	Z _{Amean3/9}	ZA5	ZA6	Z _{Amean7/8}	RY _{btwFlr}
	[1]	[1]	[1]	[1]	[1]	[1]	[1]	[1]
c4 1	1	1	1	1	1	1	1	1
c4 2	0.991	1.043	1.194	1.039	0.991	0.991	1.107	0.995
c4 3	0.986	2.753	2.249	0.961	0.997	1.021	3.740	0.801
c4 4	0.961	2.912	2.857	0.957	0.976	1.009	3.993	0.826
c4 5	0.971	2.969	2.288	0.943	0.983	1.026	4.392	0.718
c4 6	0.906	3.704	2.593	0.888	0.922	0.996	5.521	0.452
c4 7	0.823	4.210	3.099	0.992	0.927	1.004	8.078	-0.066
c4 8	0.841	3.153	2.516	0.996	0.949	1.018	5.355	0.938

3.5 Statistical assessment

A full factorial analysis was generated based on the dimensionless responses from the point load. The included terms in the model were seven terms for floor elements in parallel (three factors: See shaded columns of Table 1), and 15 for floor elements in series (four factors: See shaded columns of Table 2). Two-sided confidence level for all intervals was set to 95%. Data from the analyses was exposed in three charts:

- 1) Pareto chart to expresses the absolute values of standardized effects in ascending order aiding to determine the magnitude and importance of the effects of the factor. The reference line in the chart indicate which factor that is statistically significant at the given significance level.

- 2) Main effect chart to show how the fluctuation in mean response as the level of a factor moves between its extremes.
- 3) Interaction chart to express the relationship between one factor and the continuous response depending on the value of a second factor. An interaction implies that the response due to one factor depends on the level of the other factor.

These charts are the results of the analysis, and the charts are used in the discussion. The charts are given in Annex C.

4 Discussion

4.1 Comparison of dynamic responses

The most significant effect of tying the floor elements together is the advancing formation of modal shapes where the elements are responding as a common diaphragm. In mode shapes where energy is dissipated in the interconnection, structural damping is increasing, and frequency is shifted depending on the direction of the mode and the mode order. Mode interactions is complicating the interpretation. To assist in the assessment of the influence of interconnection, the responsive energy is therefore examined: The power intensity of the accelerations as function of frequency, as described by the PSD, reveal information on how the flooring system is responding at a given frequency band by assessing the amplitude and width of peaks. The influence on human perception of vibration is in the present work evaluated from a combined examination of shift in frequency, damping and responsive energy, and the floor elements in parallel and in series are discussed separately. In the discussion, reference to mode shapes are made with respect to Table 5 and Table 6. Interpretation of the PSD are challenging because the peaks are separated with nearly equal spacing, indicating that the peaks can be associated with harmonic components of the same mode. Furthermore, the frequency range of the EMV was not high enough to actively stimulate the vibrations of interest, and the analysis was trusting random vibrations of higher harmonics to be developed by the vibration source.

For both floors in parallel and in series, the effect of tying floor elements together is characterized in the PSD as a flattening of the resonant energy. This has the effect of reducing the susceptibility of fundamental frequencies responding as a distinct peak, making the flooring system less disposed to resonance from a single frequency source. The peaks tend to agree with fundamental mode orders starting with transverse mode.

4.1.1 Floor elements in parallel

The longitudinal interconnection constrains relative movements between floor elements, and depending on the mode shape, the interconnection will be subjected to axial and shear stresses. For modal deformations longitudinally, the effect of the interconnection on bending stiffness is neglectable, and it is evident that the modal mass increases with respect to the bending stiffness causing a reduction in frequency. This mechanism is reflected in the numerical analyses where eigen frequencies for first common mode decreases with 15.8 %. This is also demonstrated in the experimental results where eigen frequencies from EMA suggest a decrease by 19.1 % from $f_{6, C1_0}$ (40.8 Hz) to $f_{4, C2_3}$ (33.0 Hz) for modes dominated by longitudinal deformations. This interpretation supports findings in (Ebadi et al. 2016, Ebadi 2017). No significant change in damping was observed for this mode.

For transverse mode shapes the trend is different: The increase in bending stiffness of the flooring system caused by the interconnection is significant with respect to the limited bending stiffness the floor element has transversally. From uncoupled to coupled elements (C2_3), the numerical analysis yields a shift in eigen frequency for first transversal mode upwards from 22.8 Hz to 24.6 Hz (7.9 %), comparable to the EMA which changes from 22.0 Hz for $f_{1, C1_0}$ to 24.8 Hz for $f_{1, C2_3}$ (12.4 %). For this mode for C2_3, the interconnection is activated in-plane and perpendicular to the length of the interconnection, and the axial stress cause no significant change in damping.

For the second transversal mode (f_2), the interconnection is activated for shear stress perpendicular to plane and the damping ratio is increased from 0.75 % to 1.32 %. As can be seen from comparing the matching first two transversal modes (f_1 and f_2) of C1_0 and C2_3, it is evident that the shift is attributed structural damping in the interconnection. Shear deformation of both the interconnector and the floor elements generally render high damping. This supports the findings in (Labonnote et al. 2013).

Advancing to f_3 , torsion of the floor elements is causing shear dominant stresses, and the damping of C1_0 where there is no interconnection, are also generating high damping. When tying the floor elements together, the same mode is seen in $f_{3, C2_3}$, and structural damping from the shear stressed connection is increasing the total damping from 1.31 % to 2.13 % as system boundaries alter. The torsional modes are however significantly stimulated by the low vertical stiffness of the MRC, and would undoubtedly be less evident if the vertical motion of the floor element supports was more constrained.

In mode order five, the damping is high for both configurations: For C1_0, the mode is the second transverse mode. The damping is higher than for the first transverse mode, and lower than for the third transverse mode ($f_{8, C1_0}$), strengthening the finding

of increased damping for increasing mode order, supporting the findings in (Labonnote et al. 2013).

For floor elements in parallel, as stiffness in the interconnection is increased, the frequency spacing between adjacent modes decrease, supporting findings in (Ebadi et al. 2016).

4.1.2 Floor elements in series

Due to the geometry and the support conditions, the interconnection is only subject to axial stresses, and shear due to bending from connected floor elements. Shear stresses from deflection is predominantly transferred to the columns. The bridging component requires both top and bottom flange to be connected to increase the bending stiffness of the flooring system. This is observed in the EMA particularly for C4_1 (loose bridge) from which the frequency is slight increasing with increasing stiffness of the bridging component. However, no significant interaction was observed between frequency spacing of adjacent modes and stiffness of the interconnection.

For 1st transverse (f_1), longitudinal (f_2) and transverse (f_3), as well as for 2nd transverse (f_5), increasing stiffness generally cause higher damping.

The damping tends to be higher with nail plates than with a number of larger screws, even as the screwed connection is causing a comparable shift in frequency, hence arguing a comparable increase in bending stiffness. The exception from this tendency is seen in the 2nd longitudinal mode where high damping already is found in the loose bridge ($f_{4, C4_1}$), and increasing from 1.93 % to 4.05 % with a screwed connection, whilst it only increases slightly with nail plates. This is difficult to explain, but this is the only mode shape where the curvature is changing direction across the bridging component, and shear stress is predominantly transferred to the columns.

For the last EMA test, the bridging component is fastened with nail plates at the top flange, but the bottom flange is loose. This test was performed because it represents a favourable method of installing and fastening the bridging component. However, the performance of the flooring system is unfortunate, and damping is generally low. In comparison, even a completely loose bridging component tend to cause higher damping.

4.2 Point load deflection

The following discussion is based on statistical analyses of the deflection tests as described in section 3.5. The charts used as background for the discussion are found in Annex C.

4.2.1 Floor elements in parallel

The propagation of deflection from loaded to unloaded floor element, increase by up to 30% as the interconnection gain stiffness. (Fig. 22) (RMSE considered). The pareto chart shows significance for type of configuration and torque of MRC bolts (Fig. 23). Main effects clearly state that the C3 interconnection is the most effective connection to even out deflection between floor elements. For rated prestressing torque, response of unloaded floor tends to increase from configuration 1 to 2, whilst for 1.0 kNm torque, the same response tends to decrease from configuration 1. Not immediately expected this indicates that the deflection of the unloaded floor to be vulnerable not only to intersecting flanges of C3, but also to the stiffness of the connection to the columns (torque on MRC bolts). See Fig. 24.

The relative vertical deflection between adjacent floor elements unveil the most distinctive results from the test (see Fig. 13 and Annex C.I.b). The pareto chart (Fig. 25) show significance of both configuration and screws as expected. Furthermore, the magnitude as expressed in the main effects chart (Fig. 26) is unambiguous and easy to interpret. Upper left panel of the interaction chart show valuable information (Fig. 27): For configuration domain 1 to 2: Changing torque has less significance for the first configuration. Effect of an increasing number of screws are not as apparent for C3 as for C2. With respect to unconnected elements, five screws in C3 will cause an 80% reduction of the displacement between adjacent floor elements, while it for C2 only causes 50% reduction. Bear in mind C2 require four rows of screws whilst C3 only two, hence C2 will consume twice the amount of workforce and screws as C3 for installation.

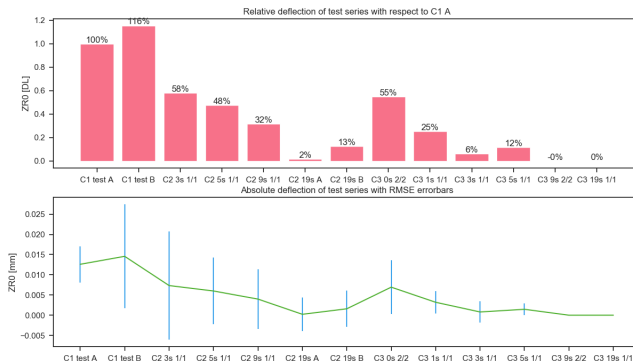


Fig. 13 Relative and absolute deflection with errorbar for ZR0

Concerning the rotation about longitudinal axis between adjacent edges (see Annex C.I.c), torque is as expected not significant, but the configuration and the shear capacity of the connection (i.e. number of screws) is dominating (see Fig. 28). The main effects plot (Fig. 29) clearly shows the effect of configurations and the number

of screws and that the rotation is increasing from C1 to C2 as the flanges are increasingly tied together with loose flange boards, and that the same effect is seen for C3. The deformation pattern is as expected because adjacent longitudinal edges follow a quadrilateral pattern for C2, whilst for C3 vertical deformation from the loaded floor is efficiently transferred to the unloaded floor. For C3 this causes the unloaded floor to be deformed more, thus increasing the relative rotation between the floors because the stiffness of the intersecting flange is smaller than the stiffness of the floor elements. See Fig. 14. The analysis of rotational deflection indicates that neither of the present longitudinal interconnections can transfer significant bending moment between the floor elements.

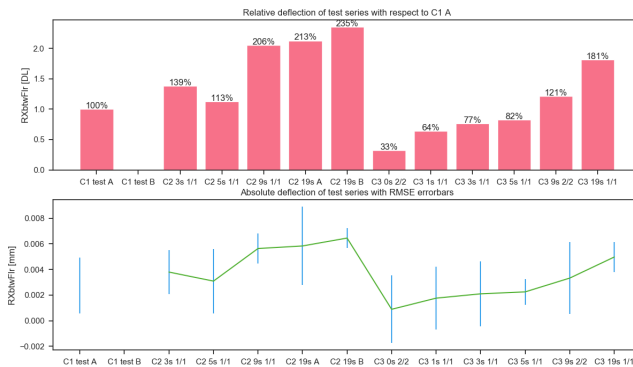


Fig. 14 Rotation about longitudinal axis between adjacent edge joists (RXbtwFlr)

4.2.2 Floor elements in series

For floor elements in series the following trends are seen: Both ZA1 and ZAmean7and8 is responding similarly and with similar statistical results. The discussion is based on charts for the latter (see Fig. 15). The deflection is responding rapidly on the first number of screws particularly on top of the bridge. Already at three screws the deflection is transmitted from loaded floor to unloaded floor with 80% of the expected potential. The observed effect of bottom nail plate with respect to nail plate on top for transmitting deflection, is likely to be connected to the censoring point which are on the bottom flange (Fig. 30). The response shows no noteworthy interaction of factors, hence not discussed.

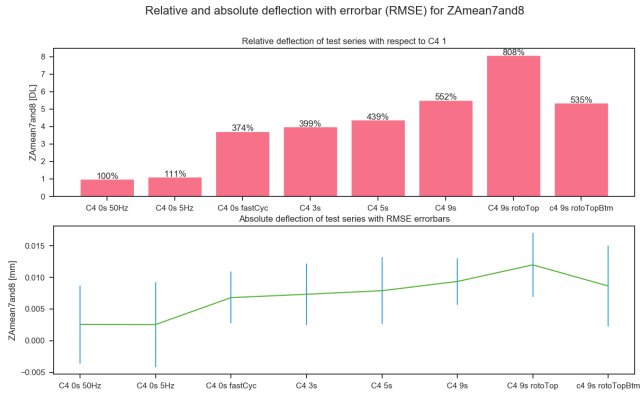


Fig. 15 Relative and absolute deflection with errorbar for Z_Amean7and8

As for the deflection of the unloaded floor (Annex C.II.b), the midspan deflection is also responding rapidly on the first number of screws (Fig. 31), but the responding mechanisms are different: The deflection is increasing as the floors are tied together, but as the moment stiffness is further increased either with nine screws at top and bottom, or nail plates on both levels, the deflection decreases (Fig. 32). This phenomenon is as expected and is distinctively also seen in the relative rotation between the floor elements in section 5.1.2.4.

As can be seen on Fig. 16 the relative rotation is responding nicely to increased stiffness between the floor elements, but the effect requires nine screws to be substantial (45 % of the rotation of the unconnected case). The nail plate added on the three last runs on is equally efficient as nine screws, but it requires as expected a force couple on top and bottom (see difference on two runs to the right of Fig. 16 as well as left panel on the interaction chart Fig. 33).

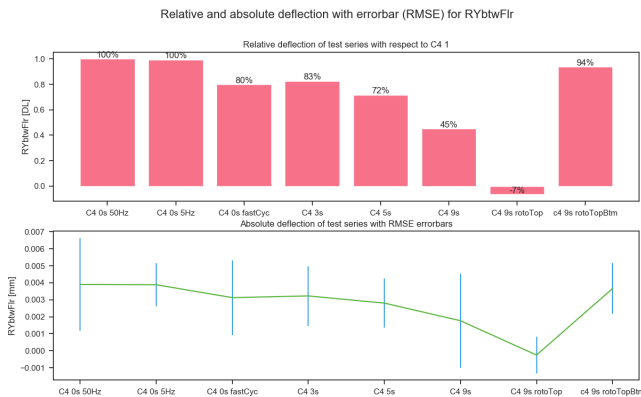


Fig. 16 Relative and absolute deflection with errorbar for RYbtwFlr

4.3 Numerical modelling of interconnection

The numerical modelling of the floor elements used in the present work is studied in (Nesheim and Malo 2018). The modelling of the MRC was done in accordance with results from testing of the MRC (Vilguts et al. 2021). The interconnections were modelled as simplified shell elements tied to the flanges also modelled as shell elements as no alterations was studied in the numerical representation of the interconnections. Interconnections can more accurately be modelled as spring elements to better reflect changes in the stiffness of the interconnection, but for the present work the simplified modelling sufficed to see the dominating variations between the different configurations. If, however changes to a particular interconnection was to be studied, the numerical modelling must have been modelled more accurately.

5 Conclusions

Dynamic and static evaluations of the effect of interconnection on various configurations of two full-scale floor elements have revealed several discoveries. Investigation of results have focused on effects that can aid as resource-efficient approach of manipulating vibration serviceability performance without any significant increase in cost or carbon emission for the flooring system. The present work can aid in the understanding on how the dynamic responses shift as interconnections and orientations of floor elements change, and the principle can aid in standardization of floor elements as one design can be utilized in flooring systems with amendable comfort properties. Generally, fundamental mode shapes of the floor elements acting as unconnected entities are observed to persist, but their resonant energy is lowered depending on the interconnection. Ignoring the effects of interconnections may cause considerable misjudgement in the assessment of vibration serviceability performance of the flooring system. Due to the range of configurations and effects, key findings are condensed from the discussion and presented schematically in Table 10. The table is split to have floor elements in parallel and series in separate columns, and with category of effects in separate rows. Each of the key findings of Table 10 contains a reference to the associated paragraph of the discussion.

Table 10 Schematic presentation of key findings

Effect	Floor elements in parallel	Floor elements in series
Frequency	Increased interconnection stiffness reduces eigen frequency of longitudinal mode shapes, shifting towards resonant response. (4.1.1¶1).	For each mode order, both longitudinally and transversally, the eigen frequency is increasing with increasing bending stiffness of the interconnection. (4.1.2¶1).
	Increased interconnection stiffness yields a shift in eigen frequency of transverse mode shapes upwards close to 10 %. (4.1.1¶2).	
	Frequency spacing between adjacent modes decrease with increasing stiffness of the interconnection. (4.1.1¶6).	No significant correlation is observed between the stiffness of the connection and the frequency spacing of adjacent modes.
Damping generally	Damping increase with increasing mode order. (4.1.1¶5, 4.1.2¶2).	
	For comparable mode shapes, damping increase with increasing stiffness of interconnection, provided that both shear and bending is transferred. (4.1.1, 4.1.2).	No information available
Material damping	Mode shapes associated with bending generally cause low damping (see 4.1.1¶1)	
	Mode shapes associated with floor element torsion efficiently increase damping. (4.1.1¶4).	
Structural damping	Mode shapes activating interconnection axial stress cause no significant contribution to damping. (4.1.1¶2).	
	Mode shapes activating shear stress either in the interconnection or the floor elements render high damping. (4.1.1¶3).	
Resonant energy	Resonant energy is flattened as interconnection gain stiffness: Susceptibility to resonance from single frequency source is reduced as the response characteristics are flattened. (4.1¶2)	
Deflection transfer	Intersecting flanges (C3) is the proposed solution for design situations requiring good load distribution. Screws are more effectively utilised in C3 than in board interconnection. Only five screws in C3 will cause an 80% reduction of the displacement between adjacent floor elements. (4.2.1¶1,2)	Already at three screws per row on the bridging component, deflection from loaded to unloaded floor element is transmitted with 80% of the expected potential. Adding more screws is likely not an economic measure. (4.2.2¶1)
Bending transfer	The longitudinal interconnections do not have the structural capacity of transferring significant bending moment between the floor elements. (4.2.1¶3)	The interconnection must transfer moment to realize significant effect. (4.1.2¶4). Either nine screws or nail plates on both top and bottom suffice. Further fastening is likely not cost-effective. (4.2.2¶3)

In general, a strong interconnection will increase fundamental frequency with respect to an isolated similar floor element and increase the performance of the flooring system as quantified by the Hu & Chui criterion. For resonant floor design situations (acceleration dominated perception) increased stiffness of the interconnection will increase damping and consequently reduce accelerations. Depending on the fundamental frequency, it is a likely measure to shift acceleration levels considerably down. For transient floor design situations (velocity dominated perception) both increased damping and increased fundamental frequency will contribute to decrease velocity response. The concurrent effect from both would contribute effectively to decrease velocity response.

Experiments executed in this study suffer from low amplitude dynamic response due to short span floor elements primarily built for testing acoustic performances (Conta and Homb 2020). Several sensors have readings lower than the accuracy of the sensor and is disregarded. For a future opportunity of full-scale testing of long spanning floor elements, a design of experiment that can validate the findings herein would be valuable. Keeping all floor elements of same size would help in revealing mechanisms with enhanced general validity. An interesting topic could also be to investigate the effect of combining strong and weak direction of the floor elements, both due to the flexibility the configuration may add to the floor plan, but also due to the increased system and torsional damping. Due to the findings of damping related to torsion, combining floor elements in reciprocal configurations that induce torsional deflections may yield flooring system with high damping. These studies would all provide valuable information for resource-efficient measures of adapting standardized floor elements to a wide range of applications.

Acknowledgements

This work is part of the four-year project “WoodSol – Wood frame solutions for free space design in urban buildings” realized through the research grant from The Research Council of Norway (254699/E50). The support is gratefully acknowledged. The authors would also like to acknowledge the contribution by fellow doctoral students Aivars Vilguts and Simone Conta in the preparation and execution of the work.

Transparency and reproducibility

The data from measurements and codes used herein is made available under standard publication license Attribution 4.0 International (CC BY 4.0) at <https://bird.unit.no/>

The data from testing and codes for analysing structural response for the present work is found here: <https://hdl.handle.net/11250/2724776>

References

- Abeyssekera, I., P. Hamm, T. Toratti and A. Lawrence. 2019. Development of a floor vibration design method for Eurocode 5. *New Zealand timber design* 27(1).
- Adams, R. D. and D. Bacon. 1973. Measurement of the flexural damping capacity and dynamic Young's modulus of metals and reinforced plastics. *Journal of Physics D: Applied Physics* 6(1): 27.
- Anco Engineers, I. 2010. Operating manual for the MK-102 eccentric mass vibrator system. Boulder Colorado, Anco Engineers Inc.: 26.
- Brüel & Kjær. 2012. Heavy Duty Impact Hammer - Type 8210, Brüel&Kjær Sound & Vibration Measurement A/S.
- Burch, H., S. Sanchez and A. Ebrahimpour. 2016. Serviceability sensitivity analysis of wood floors allowing for sheathing discontinuities. *Wood and Fiber Science* 48: 17-21.
- CEN. 2018. EN 1995-1-1 SC5.T3 milestone draft 2 Revised section 9.3. Revised section 9.3. Brussels, European committee for standarization.
- CEN. 2018. EN 16929 Test methods - Timber floors - Determination of vibration properties, European Committee for Standardization.
- Conta, S. and A. Homb. 2020. Sound radiation of hollow box timber floors under impact excitation: An experimental parameter study. *Applied Acoustics* 161: 107190.
- Dassault Systèmes. 2017. Abaqus CAE, Dassault Systèmes Simulia corp.
- Dynea. 2017. Prefere 4094 Technical Data Sheet. Liquid, gap filling phenol-resorcinol adhesive for the wood industry, Dynea.
- Ebadi, M. M. 2017. Vibration Behaviour of Glulam Beam-and-Deck Floors. PhD Article, Univ. of Ottawa.
- Ebadi, M. M., G. Doudak and I. Smith. 2016. Dynamic characteristics of glulam beam and deck-element floors. 2016 World Conference on Timber Engineering, Vienna University of Technology.
- Ebadi, M. M., G. Doudak and I. Smith. 2017. Finite-Element Modeling and Parametric Study of Glulam Beam-and-Deck Floors. *Journal of Structural Engineering (United States)* 143(9).
- Gosling, J., P. Sassi, M. Naim and R. Lark. 2013. Adaptable buildings: A systems approach. *Sustainable Cities and Society* 7: 44-51.
- HBM. 2019. Inductive Standard Displacement Transducers WA2, Hottinger Baldwin Messtechnik GmbH.
- HBM. 2019. U2B 50 kN Force Transducer, Hottinger Baldwin Messtechnik GmbH.

- Hu, L. J. and Y. H. Chui. 2004. Development of a design method to control vibrations induced by normal walking action in wood-based floors. Proceedings of the 8th World Conference on Timber Engineering. Lahti, Finland. 2: 217-222.
- Hu, L. J. a. C., Y.H. 2004. Development of a design method to control vibrations induced by normal walking action in wood-based floors. 8th World Conference on Timber Engineering 2004, WCTE 2004. Lahti, Finland.
- ISO. 2007. ISO 10137:2007 Bases for design of structures - Serviceability of buildings and walkways against vibrations, International Organization for Standardization.
- Kistler. 2008. Ceramic/Quartz Impedance Head for Modal Analysis Type 8770A. 8770A_000-252-07.08. Switzerland, Kistler Group.
- Labonnote, N. 2018. Modal hammer for dummies 1.2. S. Nesheim, NTNU.
- Labonnote, N. and K. A. Malo. 2010. Vibration properties of cross laminated timber floors. *Structures and architecture*: 428-435.
- Labonnote, N., A. Ronnquist and K. A. Malo. 2015. Prediction of material damping in timber floors, and subsequent evaluation of structural damping. *Materials and Structures* 48(6): 1965-1975.
- Labonnote, N., A. Rønquist and K. A. Malo. 2013. Experimental evaluations of material damping in timber beams of structural dimensions. *Wood Science and Technology* 47(5): 1033-1050.
- Negreira, J., A. Trollé, K. Jarnerö, L. G. Sjökvist and D. Bard. 2015. Psycho-vibratory evaluation of timber floors - Towards the determination of design indicators of vibration acceptability and vibration annoyance. *Journal of Sound and Vibration* 340: 383-408.
- Nesheim, S. and K. A. Malo. 2018. Assessing adequacy of numerical representation for optimisation performances in long span timber floors. World Conference in Timber Engineering 2018. Seoul.
- Ohlsson, S. 1988. Springiness and human-induced floor vibrations. A design guide. *Document D12 - Swedish Council for Building Research*(12).
- Pavelka, P., R. Hunady, M. Hagara and F. Trebuna. 2015. Reciprocity in Experimental Modal Analysis. *American Journal of Mechanical Engineering* 3(6): 252-256.
- Smith, A. L., S. J. Hicks and P. J. Devine. 2009. Design of floors for vibration: A new approach. *SCI, Ascot, Berkshire*.
- Stamatopoulos, H. and K. Malo. 2018. Wood frame solutions for free space design in urban buildings (WOODSOL). 7th Forum Wood Building Nordic, Växjö, Sweden.
- Ungar, E. E. and E. M. Kerwin Jr. 1962. Loss factors of viscoelastic systems in terms of energy concepts. *The Journal of the acoustical Society of America* 34(7): 954-957.

- Ussher, E., K. Arjomandi, J. Weckendorf and I. Smith. 2017. Prediction of motion responses of cross-laminated-timber slabs. *Structures* 11: 49-61.
- Vilguts, A., K. A. Malo and H. Stamatopoulos. 2018. Moment resisting frames and connections using threaded rods in beam-to column timber joints. World Conference on Timber Engineering, Seoul, Republic of Korea.
- Vilguts, A., S. Nesheim, H. Stamatopoulos and K. A. Malo. 2021. A study on beam-to-column moment-resisting timber connections, comparing full-scale connection testing and mock-up frame assembly (Manuscript submitted for publication). *Eur. J. Wood Wood Prod.*
- Weckendorf, J., G. Hafeez, G. Doudak and I. Smith. 2014. Floor vibration serviceability problems in wood light-frame buildings. *Journal of Performance of Constructed Facilities* 28(6).
- Weckendorf, J. and I. Smith. 2012. Dynamic characteristics of shallow floors with cross-laminated-timber spines. World Conference on Timber Engineering 2012, WCTE 2012.
- Weckendorf, J., T. Toratti, I. Smith and T. Tannert. 2016. Vibration serviceability performance of timber floors. *Eur. J. Wood Wood Prod.* 74(3): 353-367.
- Weckendorf, J., E. Ussher and I. Smith. 2016. Dynamic response of CLT plate systems in the context of timber and hybrid construction. *Compos. Struct.* 157: 412-423.
- Welch, P. 1967. The use of fast Fourier transform for the estimation of power spectra: a method based on time averaging over short, modified periodograms. *IEEE Transactions on audio and electroacoustics* 15(2): 70-73.
- Zhang, B., B. Rasmussen, A. Jorissen and A. Harte. 2013. Comparison of vibrational comfort assessment criteria for design of timber floors among the European countries. *Eng. Struct.* 52: 592-607.

Annex A. Methods & materials

Annex A.I EMA

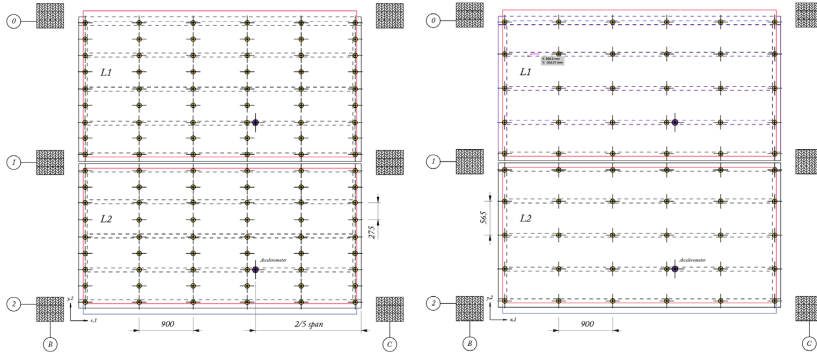


Fig. 17 The 18 by 9 (left) and 10 by 9 rowing hammer grid for C1 and C2

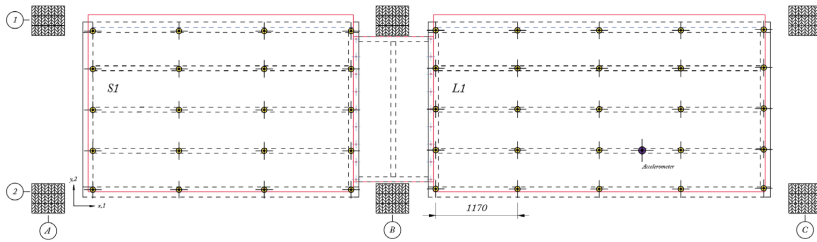


Fig. 18 The 9 by 5 rowing hammer grid for C4

Annex A.II Positioning of monitoring equipment

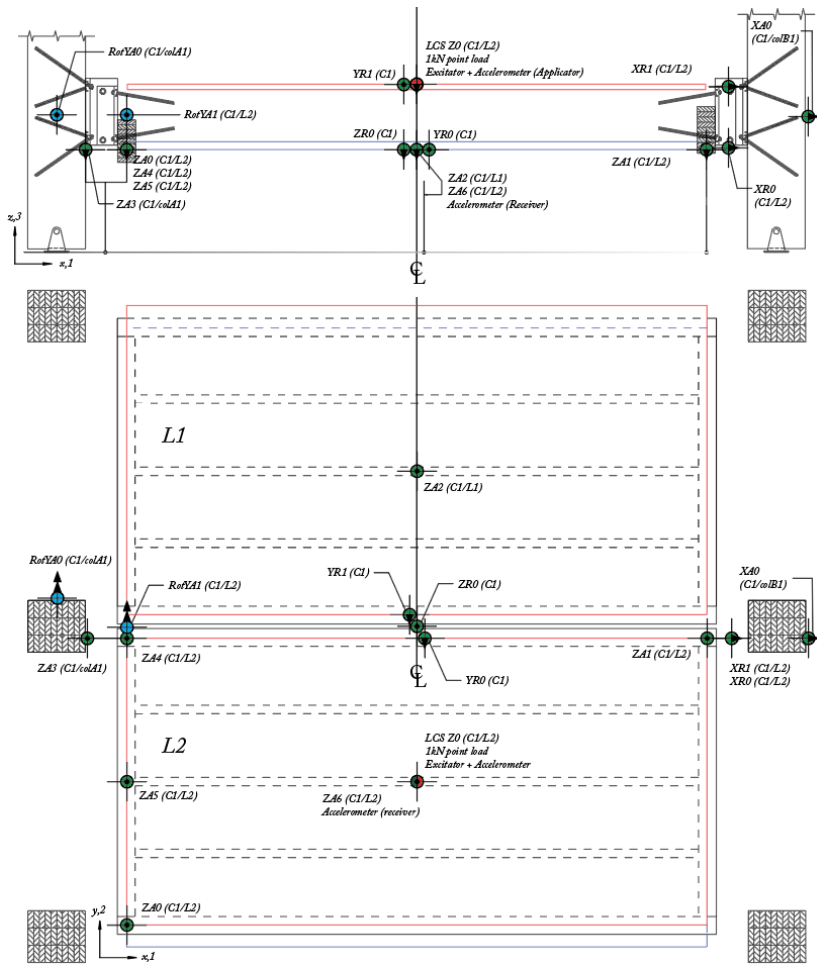


Fig. 19 Position and type of sensors for floor elements in parallel

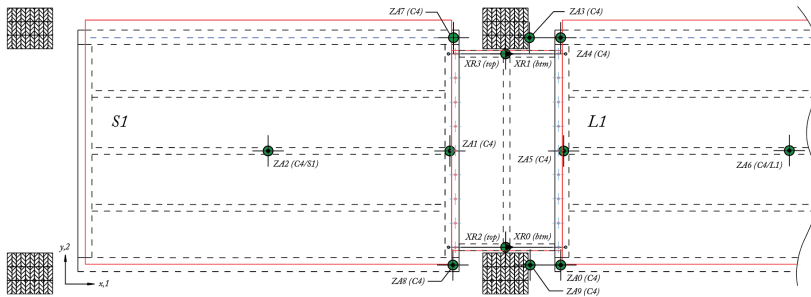


Fig. 20 Position and type of sensors for floor elements in series

Sensor label taxonomy is explained in **Fig. 21**:

- Linear displacement (green): First letter is direction of measurement.
- Inclinometer (blue): Prefix Rot following the axis of which the rotation is measured about.
- Accelerometers and position for cyclic load are only marked with their specific colour.
- General: The letter A designate absolute measurements, and R for relative deformation. The trailing digit is a running number.

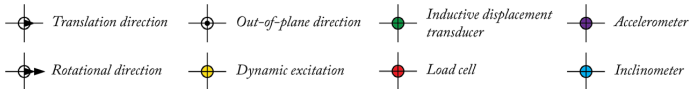


Fig. 21 Marker identification chart

Annex B. Results from unit load deflection

Table 11 Root Mean Square Error (RMSE) of selected positions

ID	ZA0 [m]	ZA2 [m]	ZAmean1and4 [m]	ZA5 [m]	ZA6 [m]	ZR0 [m]	RYatCon [rad]	RXbtwFlr [rad]
c1_A	4.31E-06	1.72E-06	6.65E-06	5.71E-06	1.82E-05	4.50E-06	6.31E-06	2.18E-06
c1_2	1.67E-05	5.70E-06	2.16E-05	1.17E-05	2.37E-05	1.29E-05	1.65E-06	NaN
c2_0	1.39E-05	1.57E-06	1.41E-05	1.01E-05	1.77E-05	1.34E-05	2.87E-06	1.72E-06
c2_1	1.51E-05	1.37E-06	2.89E-05	1.15E-05	1.88E-05	8.23E-06	2.80E-06	2.50E-06
c2_2	1.53E-05	1.58E-06	2.15E-05	9.57E-06	1.67E-05	7.40E-06	6.37E-07	1.18E-06
c2_A	6.08E-06	1.59E-06	8.88E-06	5.22E-06	1.72E-05	4.18E-06	2.26E-06	3.06E-06
c2_5	1.57E-05	7.54E-07	1.78E-05	7.53E-06	1.99E-05	4.51E-06	2.61E-06	7.68E-07
c3_0	1.32E-05	2.33E-06	1.32E-05	1.05E-05	1.54E-05	6.71E-06	2.51E-06	2.64E-06
c3_1	1.21E-05	7.70E-06	1.55E-05	4.74E-06	1.17E-05	2.78E-06	1.69E-06	2.43E-06
c3_2	2.06E-05	6.92E-06	1.99E-05	1.32E-05	1.74E-05	2.64E-06	2.23E-06	2.53E-06
c3_3	1.47E-05	3.17E-06	8.14E-06	6.15E-06	1.76E-05	1.44E-06	7.43E-07	1.01E-06
c3_4	1.41E-05	8.29E-06	9.14E-06	5.80E-06	1.48E-05	5.99E-08	2.35E-06	2.80E-06
c3_5	1.57E-05	7.21E-07	1.57E-05	1.08E-05	1.63E-05	0.00E+00	1.72E-06	1.16E-06

Table 12 Root Mean Square Error (RMSE) of selected positions of C4

ID	ZAmean0and4 [m]	ZA1 [m]	ZA2 [m]	ZAmean3and9 [m]	ZA5 [m]	ZA6 [m]	ZAmean7and8 [rad]	RYbtwFlr [rad]
c4_1	1.22E-05	4.86E-06	6.79E-06	7.41E-06	9.18E-06	1.86E-05	6.13E-06	2.75E-06
c4_2	1.41E-05	3.65E-06	3.05E-06	7.05E-06	1.00E-05	1.71E-05	6.75E-06	1.27E-06
c4_3	9.43E-06	2.41E-06	2.43E-06	3.34E-06	8.81E-06	1.80E-05	4.09E-06	2.21E-06
c4_4	8.81E-06	3.01E-06	2.29E-06	4.84E-06	7.38E-06	1.47E-05	4.83E-06	1.76E-06
c4_5	9.42E-06	2.88E-06	2.83E-06	4.55E-06	9.09E-06	2.45E-05	5.25E-06	1.44E-06
c4_6	5.33E-06	1.96E-06	3.15E-06	5.30E-06	5.31E-06	1.17E-05	3.66E-06	2.78E-06
c4_7	6.76E-06	1.91E-06	2.18E-06	3.35E-06	6.69E-06	1.93E-05	5.07E-06	1.07E-06
c4_8	1.09E-05	2.84E-06	2.74E-06	5.17E-06	8.97E-06	1.82E-05	6.39E-06	1.49E-06

Annex C. Results from statistical assessment

Annex C.I Floor elements in parallel

Annex C.I.a Midspan deflection of adjacent unloaded floor (ZA2)

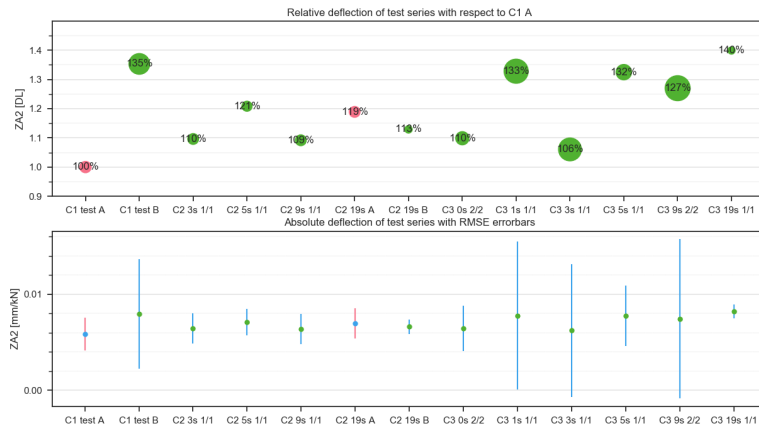


Fig. 22 Relative and absolute deflection with errorbar for ZA2

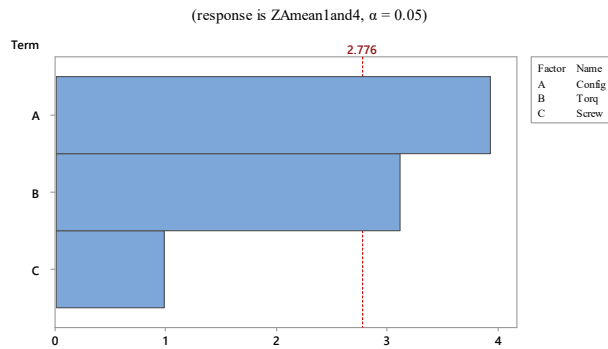


Fig. 23 Pareto

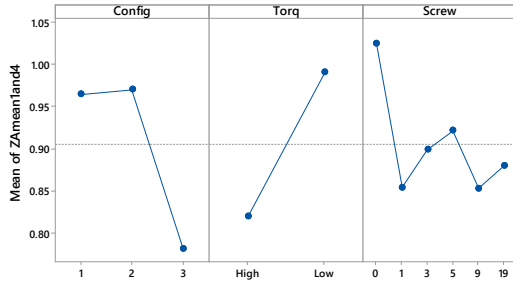


Fig. 24 Main effects

Annex C.I.b Relative vertical deflection between adjacent floor elements (ZRO)

(response is ZRO, $\alpha = 0.05$)

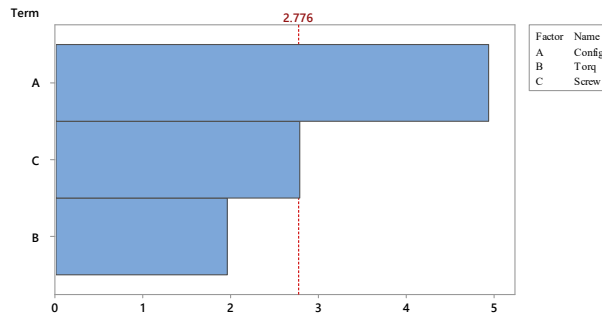


Fig. 25 Pareto

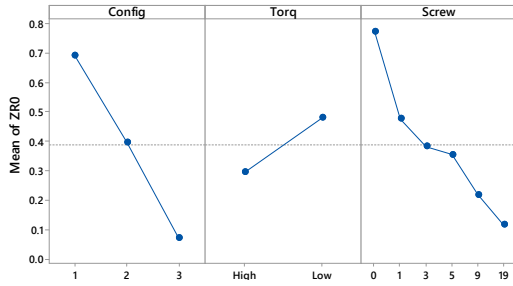


Fig. 26 Main effects

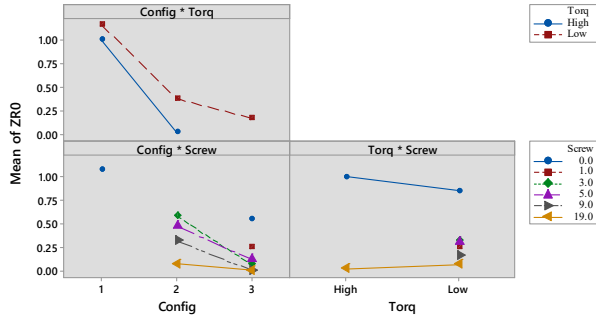


Fig. 27 Interaction

Annex C.I.c Rotation about longitudinal axis between adjacent edge joints (RXbtwFlr)

(response is RXbtwFlr, $\alpha = 0.05$)

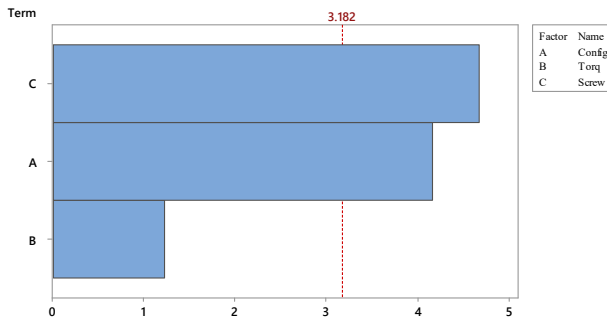


Fig. 28 Pareto

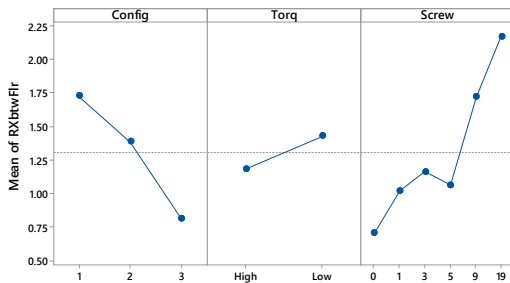
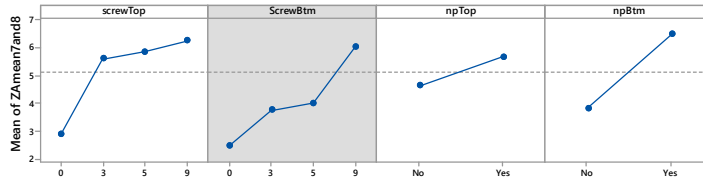


Fig. 29 Main effects

Annex C.II Floor elements in series

Annex C.II.a Deflection of unloaded floor towards bridging



A gray background represents a term not in the model.

Fig. 30 Main effects

Annex C.II.b Midpoint of unloaded floor element

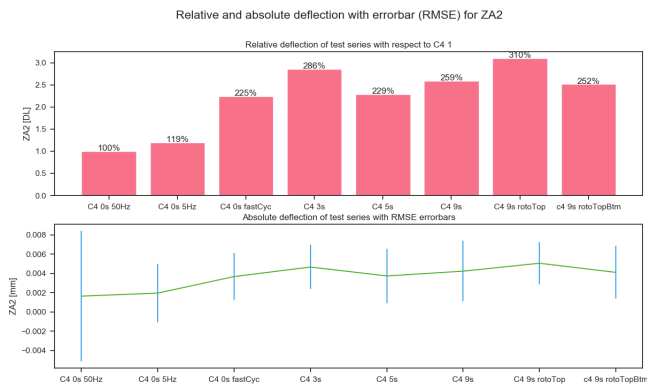
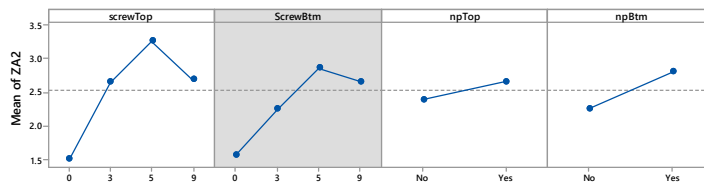


Fig. 31 Relative and absolute deflection with errorbar for ZA2



A gray background represents a term not in the model.

Fig. 32 Main effects

Annex C.II.c Rotation about transverse axis between adjacent floors

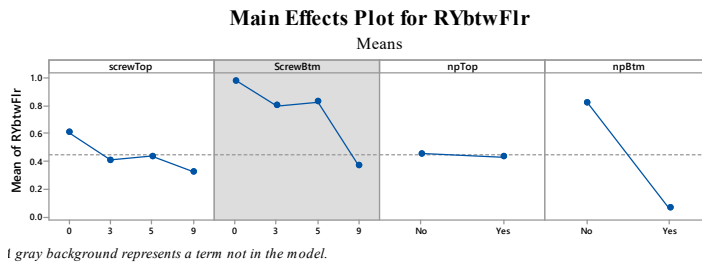


Fig. 33 Main effects

1.2 Paper II

A study on beam-to-column moment-resisting timber connections, comparing full-scale connection testing and mock-up frame assembly

Aivars Vilguts, Sveinung Ørjan Nesheim, Haris Stamatopoulos, Kjell Arne Malo

For publication in: European Journal of Wood and Wood Products

Submitted: 17th December 2020

Accepted: Pending after submitting response to minor revisions

Credit author statements

The 1st author has written the paper (including figure preparation), performed all experimental static tests of the moment-resisting connections and mock-up frame assembly, Finite Element simulations and performed all calculations. The 1st and 2nd contributed to the mock-up frame assembly process. The 2nd author has performed experimental modal analysis of the mock-up-frame assembly. The 3rd and 4th author have contributed to the concept/content development and have critically reviewed the manuscript. The 1st authors have developed the original concept of steel coupling part based on L-profiles and friction bolts. The 4th author has developed the conceptual design of the experimental protocol and energy dissipation determination and has developed the original concept of moment-resisting beam-to-column connections based on inclined threaded rods. The 3rd author has developed the component method and derived equations. All authors have seen and approved the manuscript and have contributed significantly to its preparation.

A study on beam-to-column moment-resisting timber connections, comparing full-scale connection testing and mock-up frame assembly

Abstract

A new timber frame structural system consisting of continuous columns, prefabricated hollow box timber decks and beam-to-column moment-resisting connections is investigated. The hollow box timber decks allow long spans with competitive floor height and efficient material consumption. To achieve long spans, semi-rigid connections at the corners of deck elements are used to join the columns to the deck elements. In the present paper, experimental investigations of a semi-rigid moment-resisting connection and a mock-up frame assembly are presented. The semi-rigid connection consists of inclined screwed-in threaded rods and steel coupling parts, connected with friction bolts. Full-scale moment-resisting timber connections were tested under monotonic and cyclic loading to quantify rotational stiffness, energy dissipation and moment resistance. The mock-up frame assembly was tested under cyclic lateral loading and with experimental modal analysis. The lateral stiffness, energy dissipation, rotational stiffness of the connections and the eigen-frequencies of the mock-up frame assembly were quantified based on the experimental tests in combination with a Finite Element model, i.e. the model was validated with experimental results from the rotational stiffness tests of the beam-to-column connections. Finally, the structural damping measured with experimental modal analysis was evaluated and compared with FE model by use of material damping of timber parts and equivalent viscous damping measured of the moment-resisting connections.

Keywords

Moment-resisting timber connection, Damping, Experimental modal analysis, Equivalent viscous damping, Lateral stiffness, Full-scale tests.

1 Introduction

1.1 Background

The main aim of the Norwegian research project WOODSOL is to develop industrialised structural solutions based on moment-resisting timber frames and hollow box timber decks for urban buildings up to ten storeys allowing for greater architectural flexibility. The moment-resisting frames, the hollow box timber decks, the moment-resisting connections and the acoustic properties of the buildings are the research objectives of the project. The structural system consists of moment-resisting timber frames with continuous columns and hollow box timber decks connected to columns via semi-rigid beam-to-column connections.

The main purpose of a building's structural system is to carry vertical and lateral loads to the foundation. The type of structural system is chosen taking architectural and structural restrictions into account and a system based on moment-resisting timber frames with semi-rigid beam-to-column connections can be an interesting alternative. Timber frames offer many opportunities such as constructability, low environmental footprint and high strength-to-mass ratio (Kasal et al. 2014, Gohlich et al. 2018). Hollow box timber decks can be very effective floor elements and are further improved when connected by moment-resisting connections to the columns. Malo and Köhler (Malo and Köhler 2013) showed that semi-rigid end restraints of beams can be exploited to achieve enhanced performance against human-induced vibrations and therefore makes longer spans possible.

To increase the span length of hollow box timber decks and to satisfy the structural requirements of buildings, the semi-rigid connection stiffness should be sufficient. The research presented in (Vilguts et al.) concluded that required connection stiffness for mid- and high-rise timber buildings with moment-resisting frames should be around 10000-15000 kNm/rad, respectively. The moment-resisting timber connection with screwed-in, inclined threaded rods with wood screw threads and steel coupling parts has been presented in (Lied and Nordal 2016, Vilguts et al. 2018). Based on tests of these connection types, rotational stiffness values up to approx. 8000 kNm/rad can be achieved for two planes of rods. Therefore, the required stiffness values can be achieved with approx. 2-6 planes of rods.

1.2 Outline

In the present paper, the experimental results from full-scale tests of a moment-resisting connection with inclined threaded rods and steel coupling parts are presented. The connections as shown in Figure 1 (a) were subjected to both cyclic and monotonic loading and the rotational stiffness, moment resistance and energy

dissipation in the low-intensity domain were quantified. The experimental results from monotonic loading tests were compared to an analytical component model (Stamatopoulos and Malo 2020). Moreover, a mock-up frame assembly with columns and hollow box timber decks connected with the moment-resisting connections, see Figure 1 (b), was used to evaluate the properties of the connections in the frame assembly. The frame assembly was subjected to cyclic lateral loading and the lateral stiffness, energy dissipation and rotational stiffness of the connections were evaluated. In addition, the energy dissipation was estimated in the longitudinal and transversal directions of the frame assembly using the modal hammer technique followed by experimental modal analysis. The experimental results from the tests were input to Finite Element (abbr. FE) simulations, where the experimentally measured rotational stiffness and energy dissipation of the beam-to-column connections were used to model the behaviour of the connections in the mock-up frame assembly. Finally, the static and dynamic properties from experimental testing were evaluated and compared with results from FE modelling.

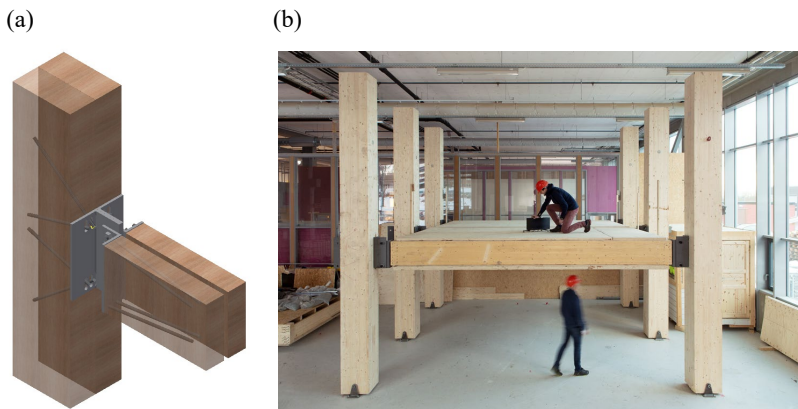


Fig. 1: (a) Moment resisting connection with inclined threaded rods and steel coupling parts comprising of L-profiles inter-connected with friction bolts. (b) Mock-up frame assembly, photo: SINTEF/A.-L.Bakken

2 Materials and methods

2.1 Moment-resisting connections

2.1.1 Experimental set-up and specimens

Three full-scale moment-resisting timber connections were tested under cyclic loading, to evaluate rotational stiffness and energy dissipation. One out of these three

tests was tested until failure to explore the complete behaviour with respect to rotational stiffness and moment resistance. The experimental set-up is shown in Figure 2 with corresponding pictures in Figure 3. In total 3 columns, 2 beams and 3 steel coupling parts were used to assemble the connection specimens.

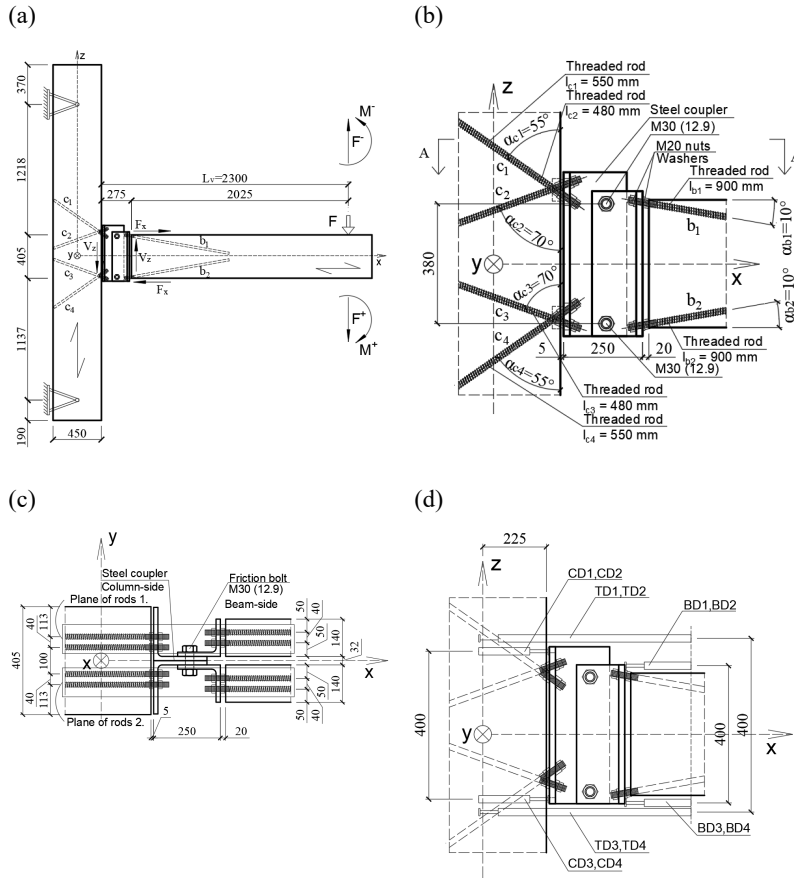


Fig. 2: Experimental set-up: (a) beam-to-column moment-resisting connection, (b) technical layout of the connection, (c) section A-A, (d) location of instrumentation

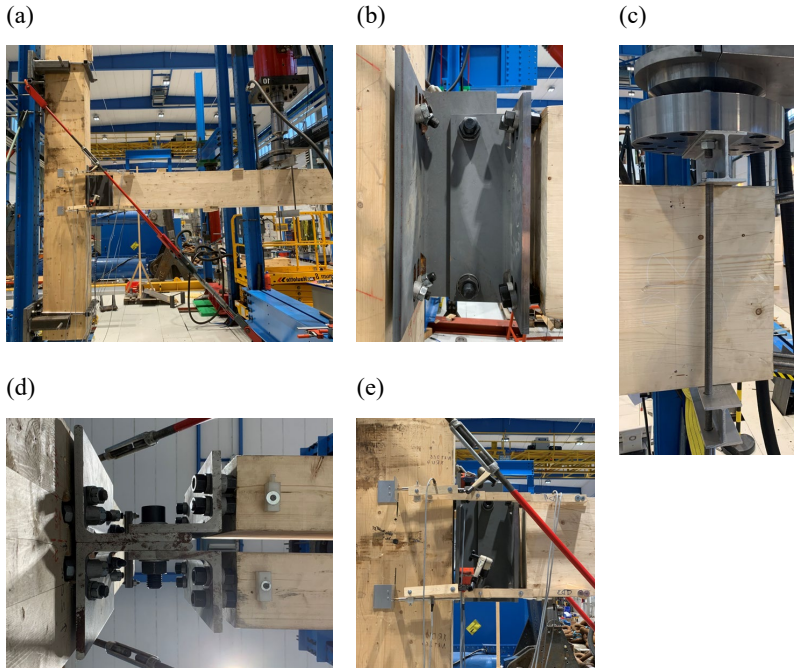


Fig. 3: Detailed experimental set-up: (a) experimental set-up, (b) steel coupling part, (c) load application, (d) bottom-view of the connection, (e) locations of LVDTs

The beam-to-column moment-resisting connection consists from two timber beams, steel coupling parts and a timber column. The threaded rods at the beam-side were installed with rod-to-grain angle of 10 degrees, while in the column-side 55 and 70 degrees were used, as shown in Figure 2 (b). The threaded rods were screwed in predrilled holes with diameter 17 mm. The rods were manufactured with two types of threads at their ends: wood screw threads in one end and M20 metric threads at the other end, as shown in Figure 4. The inner and outer diameter of the wood screw threads were $d_1 = 16.1$ mm and $d = 22$ mm, respectively. The mean ultimate strength of the rods was $f_{u,mean} = 952$ MPa (Lied and Nordal 2016).

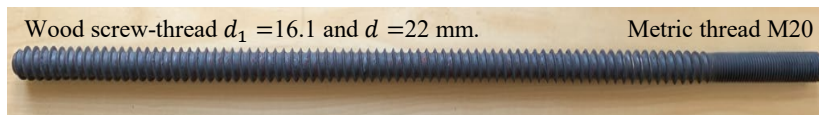


Fig. 4: Threaded rod

The steel coupling parts at the beam-side and column-side were connected to the rods by use of purpose-made steel washers and M20 nuts, as shown in Figure 2 (b).

The steel coupling parts were made from standard L200x200x16 profiles (strength class S355) with oversized holes, to allow better fitting to the inclined threaded rods. The steel coupling parts were fastened to the column and beams with 5 mm and 20 mm gaps respectively, as shown in Figure 2 (b). These intended gaps ensured that the forces were transferred solely by the threaded rods. The beam- and column-side steel coupling parts were connected with two M30 high strength friction bolts of strength class 12.9. The pre-stressing torque applied of the bolts was 2500 Nm. The rod-to-grain angles α_i , embedment lengths of rods l_i , and the free length of the rods $l_{0,i}$ (i.e. the distance between the entrance point on wood and the fixing point in the steel plates) for tests are summarized in Table 1. The values in Table 1 are given for positive moment according to Figure 2 (a).

Table 1: Parameters for experimental set-up according to Figure 2

α_{c1} = α_{c4}	α_{c2} = α_{c3}	α_{b1} = α_{b2}	l_{c1} = l_{c4}	l_{c2} = l_{c3}	l_{b1} = l_{b2}	$l_{0,c1}$ a	$l_{0,c2}$ a	$l_{0,c3}$ a	$l_{0,c4}$ a	$l_{0,b1}$ a	$l_{0,c2}$ a	z
(deg)	(deg)	(deg)	(mm)	(mm)	(mm)	(mm)	(mm)	(mm)	(mm)	(mm)	(mm)	(mm)
55	70	10	550	480	850	65	55	40	45	45	25	400
^a $l_{0,c1} \neq l_{0,c4}$, $l_{0,c2} \neq l_{0,c3}$ and $l_{0,b1} \neq l_{0,b2}$ despite geometrical symmetry: the tensile forces at the top edge are transferred by contact between fixing washers and the interior surface of steel plates, while in the bottom edge the compressive forces are transferred by contact of fixing washers and the exterior surface of steel plates.												

Columns and beams were Glued-laminated timber (abbr. glulam) elements made from Norwegian spruce (*Picea Abies*) with strength class GL30c (CEN 2013) and lamination thickness 45 mm. The cross-sectional dimensions of the columns were 405 x 450 mm² (i.e. block glued glulam), while the beams were 140 x 405 mm², confer Figure 2 (a), (c). The timber specimens were conditioned at temperature of 20°C and 65% relative humidity, resulting in approximately 12 % moisture content in the wood.

The supports at both ends of the column were pinned. To prevent splitting perpendicular to grain, steel brackets were mounted at both supports, as shown in Figure 3 (a). The point loading was applied on the beams by a clamp of two aluminium profiles (Figure 3 (c)), which allowed both positive and negative point loading.

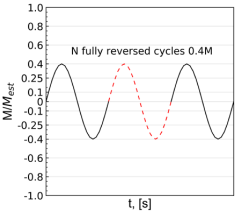
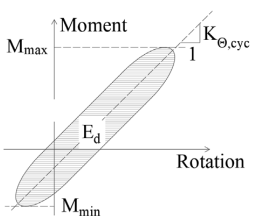
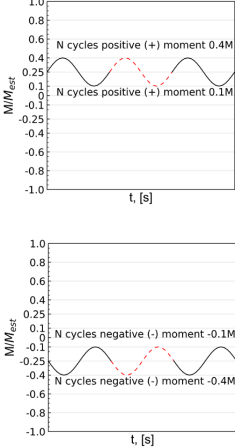
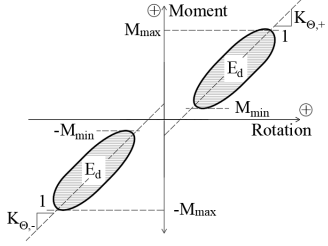
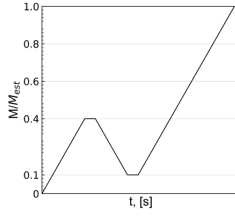
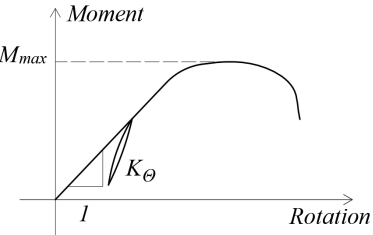
The deformation in beams, column and steel coupling parts was measured by a total of 12 displacement transducers (abbr. LVDTs), confer Figure 2 (d). The relative horizontal deformation between the column and the beams was measured with four LVDTs (TD1, TD2, TD3, TD4). Four LVDTs measured the relative horizontal deformation between the column and the steel coupling parts at column-side (CD1, CD2, CD3, CD4), and four LVDTs measured the relative horizontal deformation between the beam and the steel coupler at beam-side (BD1, BD2, BD3, BD4).

2.1.2 Loading protocol

In total, four loading protocols were applied, as shown in Table 2 :

- Fully reversed cyclic loading in range from +30 to -30 kNm. The cyclic rotational stiffness $K_{\theta,cyc}$ was obtained by fitting a straight line to the hysteresis loops giving a representative stiffness for a connection subjected to cyclic alternate loading (typical in structures subjected to vibration). The area enclosed in each hysteresis loop is the energy dissipation per cycle E_d .
- Cyclic loading with positive moment ranging from +7.5 to +30 kNm and cyclic loading with negative moment ranging from -7.5 to -30 kNm. These loading schemes do not give alternating signs, that is, the moment does not go through zero moment. The cyclic rotational stiffness and the energy dissipation are determined for each side. separately.
- Monotonic loading until failure according to EN 26891:1991 ([CEN 1991](#)).

Table 2: Imposed moment vs Rotation for the moment-resisting beam-to-column connections according to the various loading schemes

Loading scheme	Measured response
<p>1</p> 	
<p>2</p> 	
<p>3</p> 	

2.1.3 Equivalent viscous damping

To quantify energy dissipation in the connection subjected to cyclic loading, the equivalent viscous damping ratio is estimated according to Eq. (1) (Chopra 2012):

$$\xi_{eq} = \frac{1}{4\pi} \frac{E_d}{\Delta E_{el}} \quad (1)$$

where E_d is the dissipated energy per cycle and ΔE_{el} – is the corresponding change in elastic energy per cycle. The dissipated energy E_d per cycle can be found from the measured enclosed area in the hysteresis loop, visualised in Table 2. The maximum elastic change ΔE_{el} during a cycle is:

- In case of moment-rotation:

$$\Delta E_{el} = \frac{1}{2} \frac{M_a^2}{K_{\theta,cyc}} \quad (2)$$

- In case of force-displacement:

$$\Delta E_{el} = \frac{1}{2} \frac{F_a^2}{K_{ax,cyc}} \quad (3)$$

where $M_a = 1/2 \cdot (M_{max} - M_{min})$ and $F_a = 1/2 \cdot (F_{max} - F_{min})$, M_{max} and M_{min} – are the maximum and minimum moments in the hysteresis loop, F_{max} and F_{min} – are the maximum and minimum applied forces in the hysteresis loop, $K_{\theta,cyc}$, $K_{ax,cyc}$ – are the linear stiffnesses obtained by fitting a straight line to all points in the hysteresis loop, using the method of least squares.

2.1.4 Analytical methods

2.1.4.1 Rotational stiffness of connection

The analytical model proposed in (Stamatopoulos and Malo 2020) is used in the present paper to calculate the rotational stiffness and resistance of the connection. The analytical model considers the connection in three separate parts: column-side, beam-side and steel coupling part.

The horizontal force component F_x is obtained by moment equilibrium, as shown in Figure 2:

$$F_x = \frac{M}{z} \quad (4)$$

where M – is the moment acting on the connection and z – is the lever are of the connection.

The rotational stiffness about y-axis of the connection at the column-side is obtained using the following equation (Stamatopoulos and Malo 2020):

$$K_{\theta,y,c} = \frac{M_y}{\theta_{y,c}} = \frac{z_c^2}{(S_{xx,c}^{(c1-c2)} + S_{xx,c}^{(c3-c4)}) + (S_{xz,c}^{(c3-c4)} - S_{xz,c}^{(c1-c2)}) \cdot \frac{z_c}{2 \cdot L_v}} \quad (5)$$

$$S_{xx,c}^{(c1-c2)} = \frac{\cos^2 \alpha_{c1} / K_{ax,c2} + \cos^2 \alpha_{c2} / K_{ax,c1}}{(\cos \alpha_{c1} \cdot \sin \alpha_{c2} + \cos \alpha_{c2} \cdot \sin \alpha_{c1})^2} \quad (6)$$

$$S_{xx,c}^{(c3-c4)} = \frac{\cos^2 \alpha_{c3} / K_{ax,c4} + \cos^2 \alpha_{c4} / K_{ax,c3}}{(\cos \alpha_{c3} \cdot \sin \alpha_{c4} + \cos \alpha_{c4} \cdot \sin \alpha_{c3})^2} \quad (7)$$

$$S_{xz,c}^{(c1-c2)} = \frac{\cos \alpha_{c1} \cdot \sin \alpha_{c1} / K_{ax,c2} - \cos \alpha_{c2} \cdot \sin \alpha_{c2} / K_{ax,c1}}{(\cos \alpha_{c1} \cdot \sin \alpha_{c2} + \cos \alpha_{c2} \cdot \sin \alpha_{c1})^2} \quad (8)$$

$$S_{xz,c}^{(c3-c4)} = \frac{\cos \alpha_{c3} \cdot \sin \alpha_{c3} / K_{ax,c4} - \cos \alpha_{c4} \cdot \sin \alpha_{c4} / K_{ax,c3}}{(\cos \alpha_{c3} \cdot \sin \alpha_{c4} + \cos \alpha_{c4} \cdot \sin \alpha_{c3})^2} \quad (9)$$

where $K_{ax,c1}, K_{ax,c2}, K_{ax,c3}, K_{ax,c4}, K_{ax,j}$ are the axial stiffness of rods $c1-c4$ (see Section 2.1.4.3), z_c – is the lever arm between threaded rods at column-side.

The rotational stiffness about y-axis of the connection at the beam-side is given by the following equation (Stamatopoulos and Malo 2020):

$$K_{\theta,y,b} = \frac{M_y}{\theta_{y,b}} = \frac{z_b^2}{(S_{xx,b1} + S_{xx,b2}) + (S_{xz,b2} - S_{xz,b1}) \cdot \frac{z_b}{2 \cdot L_v}} \quad (10)$$

$$S_{xx,b1} = \frac{\sin^2 \alpha_{b1}}{K_{v,b1}} + \frac{\cos^2 \alpha_{b1}}{K_{ax,b1}} \quad (11)$$

$$S_{xx,b2} = \frac{\sin^2 \alpha_{b2}}{K_{v,b2}} + \frac{\cos^2 \alpha_{b2}}{K_{ax,b2}} \quad (12)$$

$$S_{xz,b1} = \sin \alpha_{b1} \cdot \cos \alpha_{b1} \cdot \left(\frac{1}{K_{v,b1}} - \frac{1}{K_{ax,b1}} \right) \quad (13)$$

$$S_{xz,b2} = \sin \alpha_{b2} \cdot \cos \alpha_{b2} \cdot \left(\frac{1}{K_{ax,b2}} - \frac{1}{K_{v,b2}} \right) \quad (14)$$

where $K_{ax,b1}$, $K_{ax,b2}$, $K_{v,b1}$, $K_{v,b2}$ are the axial and lateral stiffness of threaded rods (see Section 2.1.4.3), z_b – is the lever arm between threaded rods at beam-side.

The steel connector has coupling parts both at the column- and beam-side, which are inter-connected by friction bolts. The rotational stiffness of the steel connector can be measured or derived from FE model, see Section 3.1.1.

The total rotational stiffness of the connection can be calculated according to Eq. (15):

$$K_{\theta,y} = \left(\frac{1}{K_{\theta,c}} + \frac{1}{K_{\theta,b}} + \frac{1}{K_{\theta,con}} \right)^{-1} \quad (15)$$

2.1.4.2 Capacity of threaded rods and column

The threaded rods are mainly axially loaded and the axial capacity per threaded rod is given by the following equation:

$$F_{ax,R} = \frac{n_{ef}}{n} \cdot \min \left\{ \begin{array}{l} F_{ax,a,R} \\ F_{tens,R} \end{array} \right. \quad (16)$$

where $n_{ef} = n^{0.9}$ – is the effective number of threaded rods acting together according to EN1995-1-1 (CEN 2010) and $F_{tens,R} = A_s \cdot f_{u,mean}$ is the tensile capacity of each rod.

On the column-side, the axial forces in each rod can be estimated according to Eqs. (17-20) (Stamatopoulos and Malo 2020):

$$F_{ax,c1} = \frac{1}{n} \cdot \frac{\cos \alpha_{c2} + \sin \alpha_{c2} \cdot \frac{z_c}{2 \cdot L_v}}{\cos \alpha_{c1} \cdot \sin \alpha_{c2} + \cos \alpha_{c2} \cdot \sin \alpha_{c1}} \cdot \frac{M}{z_c} \quad (17)$$

$$F_{ax,c2} = \frac{1}{n} \cdot \frac{\cos \alpha_{c1} - \sin \alpha_{c1} \cdot \frac{z_c}{2 \cdot L_v}}{\cos \alpha_{c1} \cdot \sin \alpha_{c2} + \cos \alpha_{c2} \cdot \sin \alpha_{c1}} \cdot \frac{M}{z_c} \quad (18)$$

$$F_{ax,c3} = -\frac{1}{n} \cdot \frac{\cos \alpha_{c4} - \sin \alpha_{c4} \cdot \frac{z_c}{2 \cdot L_v}}{\cos \alpha_{c3} \cdot \sin \alpha_{c4} + \cos \alpha_{c4} \cdot \sin \alpha_{c3}} \cdot \frac{M}{z_c} \quad (19)$$

$$F_{ax,c4} = -\frac{1}{n} \cdot \frac{\cos \alpha_{c3} + \sin \alpha_{c3} \cdot \frac{z_c}{2 \cdot L_v}}{\cos \alpha_{c3} \cdot \sin \alpha_{c4} + \cos \alpha_{c4} \cdot \sin \alpha_{c3}} \cdot \frac{M}{z_c} \quad (20)$$

On the beam-side, the axial forces in each rod can be estimated according to Eqs. (21) and Eq. (22) (Stamatopoulos and Malo 2020):

$$F_{ax,b1} = \frac{1}{n} \cdot \left(\cos \alpha_{b1} + \sin \alpha_{b1} \cdot \frac{z}{2 \cdot L_v} \right) \cdot \frac{M}{z} \quad (21)$$

$$F_{ax,b2} = -\frac{1}{n} \cdot \left(\cos \alpha_{b2} + \sin \alpha_{b2} \cdot \frac{z}{2 \cdot L_v} \right) \cdot \frac{M}{z} \quad (22)$$

2.1.4.3 Analytical predictions of axial and lateral stiffness and capacity of screwed-in threaded rods

The axial stiffness of threaded rod is one of the most important parameters. The withdrawal stiffness of threaded rods can be approximated by Eqs. (23) and (24) (Stamatopoulos and Malo 2020):

$$K_{ser,ax} \approx \frac{50000 \cdot \left(\frac{d}{20}\right)^2 \cdot \left(\frac{\rho_m}{470}\right)^2 \cdot k_{lenght,K}}{0.40 \cdot \cos^{2.3} \alpha + \sin^{2.3} \alpha} \quad (23)$$

$$k_{lenght,K} = \min \left[\left(\frac{l}{300} \right)^{0.75}, 1.0 \right] \quad (24)$$

where d – is the outer-thread diameter of the rod in mm, ρ_m – is the wood density in kg/m³, α – is the rod-to-grain angle and l – is the embedment length in mm.

The axial stiffness of the free part (non-embedded) of the threaded rod is given by the following equation:

$$K_{ax,l0} = A_s \cdot E_s / l_0 \quad (25)$$

where $A_s = \pi \cdot d_1^2 / 4$; $E_s = 210000$ MPa, d_1 – is the inner-diameter of threaded rod, l_0 – is the free length of the rod not embedded in timber (i.e. the length between the entrance point in wood and the fastening point in the steel coupling parts).

The total axial stiffness of the threaded rods is given by the following equation:

$$K_{ser,ax,tot} = \frac{K_{ser,ax} \cdot K_{ax,l0}}{K_{ser,ax} + K_{ax,l0}} \quad (26)$$

The lateral stiffness of a threaded rod subjected to lateral loading depends on the rotation of the end of the rod at the connecting point to the steel coupling part (Stamatopoulos and Malo 2020). For fixed end, the following expression can be used:

$$K_{ser,v,tot} = \frac{3 \cdot m \cdot k_v \cdot l_{ch} \cdot (\lambda_0 + m)}{\lambda_0^4 + 4 \cdot \lambda_0^3 \cdot m + 6 \cdot \lambda_0^2 \cdot m^2 + 6 \cdot \lambda_0 \cdot m^3 + 3 \cdot m^4} \quad (27)$$

where $k_v \approx 300 \text{ N/mm}^2$ is the foundation modulus of timber (Qazi 2020), $m = d_{net}^4/d_1^4$, $\lambda_0 = l_0/l_c$, $l_{ch} = \sqrt[4]{4 \cdot E_s \cdot I_s/k_v}$. The flexural stiffness of the embedded part screw is $E_s \cdot I_s = E_s \cdot \pi \cdot d_1^4/64$, $d_{net} = 0.9 \cdot 20 = 18 \text{ mm}$ is the diameter of the non-embedded part.

A simplified expression, derived in (Stamatopoulos and Malo 2020), can be used to estimate mean withdrawal capacity of threaded rods:

$$F_{ax,a,R} \approx 15.0 \cdot d \cdot l \cdot \left(\frac{\rho_m}{470}\right) \quad (28)$$

2.2 Mock-up frame assembly

2.2.1 Experimental set-up and specimens

The mock-up frame assembly shown in Figure 5 was used to evaluate the properties of connections in moment-resisting frame. The mock-up frame assembly consisted of six glulam columns and two hollow 4.7 m long box timber deck elements. The connections were similar to those presented in Section 2.1, as shown in Figure 5 (b) and (c). A cross-section of two parallel floor elements in direction of the span is shown in Figure 5 (d). Each of the deck elements consisted of two external parallel glulam beams (1) of GL30c with cross section of $140 \times 405 \text{ mm}^2$ and three internal glulam beams (2) of GL28c with cross section of $66 \times 405 \text{ mm}^2$. The top (3) and bottom (4) flanges were made from Kerto-Q LVL plates with thickness of 43 mm and 61 mm, respectively. The elastic material properties are given in Table 3.

Table 3: Material properties (Kristoffersen and Bjørge 2017)

	$P,$	$E_L,$	$E_t,$	$E_R,$	$G_{LR},$	$G_{LT},$	$G_{RT},$
	[kg/m ³]	[MPa]	[MPa]	[MPa]	[MPa]	[MPa]	[MPa]
GL30c	430	13000	300	300	600	600	30
LVL (Kerto-Q)	510	10500	2400	130	600	120	22

The flange plates (Kerto-Q) were glued to beams with phenol-resorcinol adhesive and therefore rigid behaviour at the interface was assumed. The deck elements were installed to the columns with the bottom flange 2 m above the floor level.

The columns were 5.2 m high with a block glued cross-section of 405 x 450 mm². The columns used in this set-up were the same columns as used for the beam-to-column moment-resisting tests described in Section 2.1. The columns were installed on the concrete floor with brackets, which allowed rotation about y-axis, as shown in Figure 5 (a), that is, the connections to the floor were pinned about y-axis.

The hollow box decks elements were connected to the columns with the moment-resisting connections described in Section 2.1. Two M30 high strength friction bolts (grade 12.9) with applied prestressing torque on the bolts of 2500 Nm. Both floor elements shared the central column (C_2) with the double-sided connection shown in Figure 5 (b), while the connections to the corner columns were a single-sided version of the same connection, as shown in Figure 5 (c).

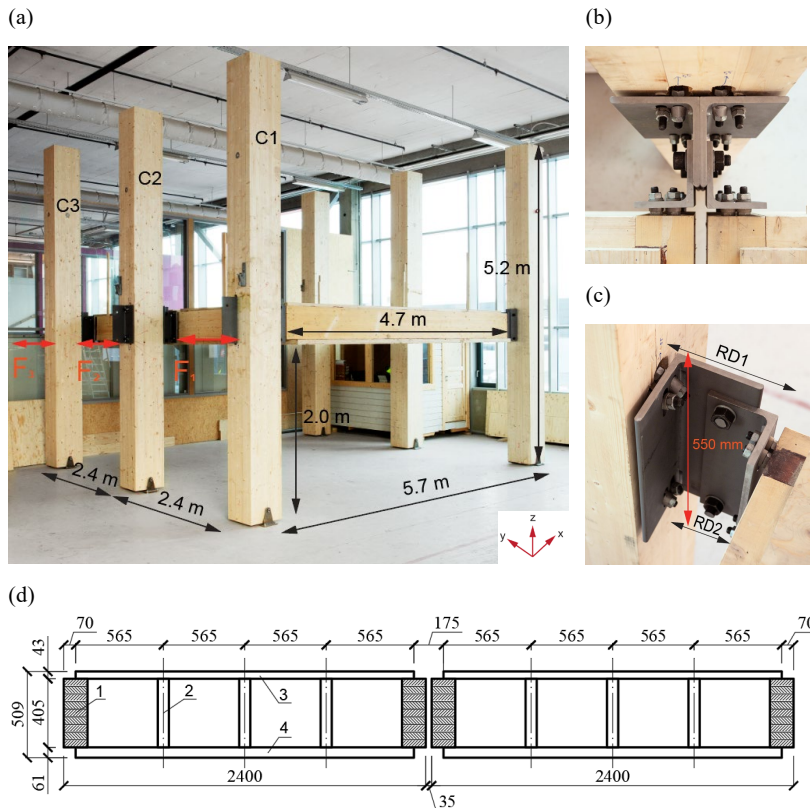


Fig. 5: The mock-up frame assembly set-up. (a) over-view of the construction, (b) connection between floors and centre columns (C2), (c) connection between floors and edge columns (C1 and C3), (d) cross-section of the floor elements. Photo (a), (b) and (c): SINTEF/A.-L.Bakken

2.2.2 Loading protocol and instrumentation

In order to evaluate lateral stiffness, energy dissipation and some dynamic properties of the frame assembly, the following tests were performed:

- 1) Cyclic loading from 0 to +11/12 kN. The load was applied two meters above concrete floor. This loading was applied on each one of the columns (C1, C2, C3) separately, that is, three test series were performed in total.
- 2) Experimental modal analysis (abbr. EMA), by use of the roving hammer technique using one reference accelerometer and a defined grid of hammering points. The impact loads were imposed at the level of the moment-resisting connections as shown in Figure 6 (b); in the direction of moment-resisting connections (x-axis),

and in the transversal direction (y-axis). An impact hammer with a soft rubber cap was used to excite the structure. Two impacts at each point of the gird were executed, recorded and averaged. The experimental modal analysis was limited to the two horizontal directions.

The lateral deformations of the prototype frame construction were measured by a total of 9 LVDTs. Three LVDTs measured the absolute displacements (x-axis) of the columns (C_1, C_2, C_3) two meters from the concrete floor. Two LVDTs for each column (RD1, RD2, RD3, RD4, RD5, RD6) were used to measure the relative displacements between the columns and floor elements at the top and bottom levels of the moment-resisting connections at columns C_1, C_2, C_3 , as shown in Figure 5 (c), which allowed to determine of their rotations.

2.2.3 Finite Element analysis

Finite Element analysis of frame assembly was carried out by SAP2000 Finite Element software (Wilson and Habibullah 1997, SAP 2003), where the rotational stiffness of moment-resisting connections on the mock-up frame assembly is the emphasized issue. The obtained results are compared to the experimental tests. The layout of 3D frame structure is shown in Figure 6 (a).

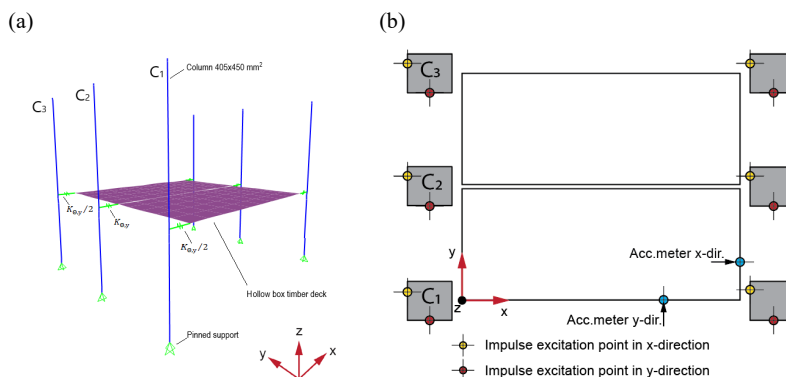


Fig. 6: (a) 3D FE model of frame structure, (b) horizontal cross-section of the frame assembly showing the locations of accelerometers and excitation points

The glulam columns were modelled with linear elastic beam elements with mean elastic moduli equal to: $E_{0,mean,c} = 13000$ MPa and $G_{mean,c} = 650$ MPa for GL30c according to EN14080 (CEN 2013), see Table 3. The floor elements were modelled as thick shell elements with effective bending stiffness of $EI_{f,longitudinal} = 6.7 \cdot 10^{13}$ N-mm² in the longitudinal x-direction (Conta and Homb 2020) and $EI_{f,transversal} = 4 \cdot 10^{13}$ N-mm² in the transversal y-direction (Kristoffersen and Bjørge 2017). These effective bending stiffness values in longitudinal and transversal directions were measured experimentally.

The moment-resisting connections between columns and floor elements were modelled as semi-rigid with respect to the rotational degrees of freedom (abbr. DOF) about x- and y-axis. Linear-elastic rotational springs with spring constants $K_{\theta,x}$ and $K_{\theta,y}$ represented the moment-resisting connections. The translational DOFs were fixed between columns and decks in all directions, while the rotation about z-axis was released (pinned). The rotational stiffness values $K_{\theta,y}$ used for FE analysis were taken from the experimental tests of the moment-resisting connections. For the centric columns (C₂) the rotational stiffness was $K_{\theta,y}$, but for the connections at the corner columns (C₁ and C₃) $K_{\theta,y}/2$ was used. The connections for the C₂ columns consist of the double amount of threaded rods and steel coupling parts compared to the connections at the corner columns.

2.2.4 Analytical predictions of connection stiffness about x-axis

The rotational stiffness about x-axis $K_{\theta,x}$ were estimated from the following expressions as the total connection rotational stiffness, column-side stiffness and beam-side stiffness, respectively:

$$K_{\theta,x} = \frac{K_{\theta,x,c} \cdot K_{\theta,x,b}}{K_{\theta,x,c} + K_{\theta,x,b}} \quad (29)$$

$$K_{\theta,x,c} = \frac{M_x}{\theta_{x,c}} = z_{x,c}^2 \cdot \left(\frac{1}{K_{v,y,c}} + \frac{1}{K_{v,y,c}} \right)^{-1} \quad (30)$$

$$K_{\theta,x,b} = \frac{M_x}{\theta_{x,b}} = z_{x,b}^2 \cdot \left(\frac{1}{K_{v,y,b}} + \frac{1}{K_{v,y,b}} \right)^{-1} \quad (31)$$

where $K_{v,y,c}, K_{v,y,b}$ – are the lateral stiffness of threaded rods (see Section 2.1.4.3) and $z_{x,c}, z_{x,b}$ – are the lever arms between threaded rods in column and beam, respectively.

2.2.5 Free damped vibrations of mock-up frame assembly

One major objective in the present research was to explore possible prediction of structural damping based on knowledge of mass, stiffness and damping characteristics of each of the components constituting a complete structure. The mock-up frame assembly, see Figure 1 (b), was modelled with the FE model shown in Figure 6 (a). The following values (in parenthesis) were used for the material damping in the various components; timber columns (0.5%) (Labonnote et al. 2013), hollow box timber decks (1.5%) (Conta and Homb 2020) and the stiffness and mass were modelled by their representative tabulated mean values. The moment-resisting connections were modelled as linear-elastic rotational springs with the average values of spring stiffness from the cyclic tests of the connections. The equivalent

viscous damping of the connections in the FE model was modelled by the damping coefficient (c) as stiffness-proportional damping (Chopra 2012):

$$c = \beta \cdot K_{\theta,y} \quad (32)$$

where $\beta = 2\xi_{eq}/\omega_{n,x}$, ξ_{eq} – is the experimentally measured equivalent viscous damping for the connections (equivalent viscous damping assumed equal for all the connection in FE model), and $\omega_{n,x} = 2\pi \cdot f_{n,x}$, $f_{n,x}$ – is the undamped fundamental eigen-frequency obtained from FE simulations along x-direction. In calculations of damping coefficient (c), the rotational stiffness of connections on centric columns (C_2) $K_{\theta,y}$ were taken from cyclic experimental tests of the moment-resisting connections, while the rotational stiffness on the corner columns (C_1 and C_3) were taken as $K_{\theta,y}/2$.

Using the FE model and initial conditions (applied displacement on columns along x-axis), a damped free vibration was obtained in the x-direction of the mock-up frame assembly. The structural damping from the damped simulation was estimated using the method with logarithmic decrement, leading to Eq. (33) (Chopra 2012):

$$\xi = \frac{1}{2\pi j} \ln \frac{u_i}{u_{i+j}} \quad (33)$$

where j – is the number of cycles for evaluation, u_i – is the maximum displacement of i -th cycle and u_{i+j} – is the (decreased) displacement of $(i + j)$ -th cycle.

From the free vibrational response of the FE model the by applying the material and connection mechanical properties, the vibrational frequency and the structural damping for the structure were determined.

3 Results and discussion

3.1 Moment-resisting connection

3.1.1 Experimental monotonic loading tests

One full scale moment-resisting beam-to-column timber connection was tested under monotonic loading until failure. The result from the monotonic test is presented in Figure 7. The capacity of the connection was by slips (loss of friction) between the steel coupling parts. The recorded maximum moment resistance was 100.6 kNm. No initial slip was observed in the test. The estimated axial forces in the threaded rods at failure were lower than the estimated withdrawal capacities, confer Table 4. Analytical predictions of the forces in the threaded rods at maximum moment are given in Table 4, while the prediction of the connection stiffness is summarized in Table 6.

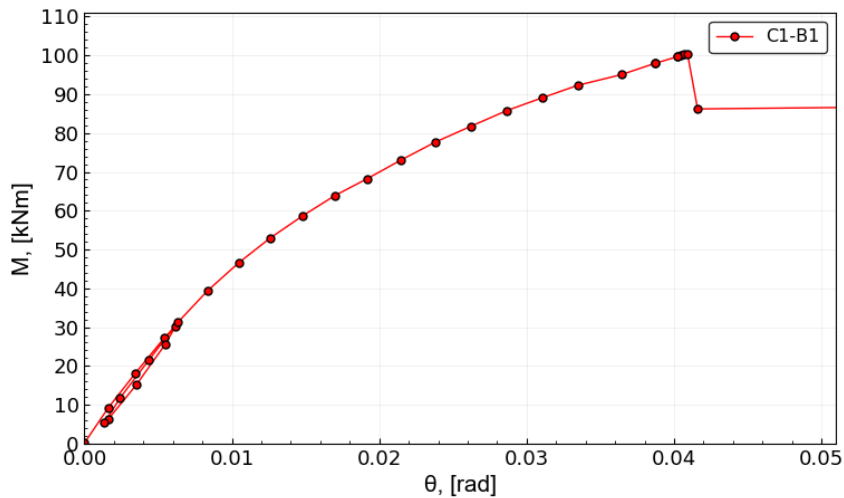


Fig. 7: Moment-rotation curve from monotonic loading test

Table 4: Analytical predictions at failure

Parameter	Reference	C1-B1	Units
Maximum moment, M_u	Figure 7	100.6	(kNm)
$F_{ax,c1}$	Eq. (17)	65.0	
Utilization, withdrawal, %	Eq. (17)	42.0%	(kN)
steel, %	Eq. (16)	28.8%	
$F_{ax,c2}$	Eq. (18)	77.1	
Utilization, withdrawal, %	Eq. (18)	57.0%	(kN)
steel, %	Eq. (16)	34.1%	
$F_{ax,c3}$	Eq. (19)	-77.1	
Utilization, withdrawal, %	Eq. (19)	57.0%	(kN)
steel, %	Eq. (16)	34.1%	
$F_{ax,c4}$	Eq. (20)	-65.0	
Utilization, withdrawal, %	Eq. (20)	42.0%	(kN)
steel, %	Eq. (16)	28.8%	
$F_{ax,b1}$	Eq. (21)	125.7	
Utilization, withdrawal, %	Eq. (21)	49.6%	(kN)
steel, %	Eq. (16)	55.6%	
$F_{ax,b2}$	Eq. (22)	-125.7	
Utilization, withdrawal, %	Eq. (22)	49.6%	(kN)
steel, %	Eq. (16)	55.6%	
Maximum axial force at failure in the connection, F_x	Eq. (4)	251.5	(kN)
Steel capacity of a single rod: $F_{tens,R} = A_s \cdot f_{u,mean} = (\pi \cdot 16.1^2 / 4) \cdot 952 \cdot 10^{-3} \cdot (n_{ef}/n) = 180.8 \text{ kN}$			

3.1.2 Finite Element simulations of steel coupling part

The axial stiffness and resistance of the steel coupling parts were evaluated by use of Finite Element (abbr. FE) software ABAQUS (Corp. 2014). The FE model is shown in Figure 8. The simulations were performed for both tensile loading (Figure 8 (a)) and compressive loading (Figure 8 (b)). The steel coupling parts were meshed with eight-node linear full integration brick elements. The modelled material properties for the steel parts are given in Table 5. Possible plasticity in the steel was taken into account by stress-plastic strain relationship according to DNV (2013) for S355. The contact between the steel coupling parts was modelled by use of “hard”

contact behaviour in the normal direction, while isotropic tangential behaviour with friction coefficient of 0.3 (steel-to-steel) were used in the contact plane. The friction bolts were modelled linearly isotropic with assumed $E = 210$ GPa and $\nu = 0.3$. The pre-stressing force was applied in the middle of the bolts as a pre-stressing force F depending on the torque level. The pre-stressing force was calculated according to Eq.(34) (Oskouei and Chakherlou 2009):

$$F = \frac{T}{k \cdot d_{bolt}} \quad (34)$$

where T – is the applied torque, $k = 0.20$ and is the torque coefficient defined as the term which depends on friction coefficients and d_{bolt} – is the nominal diameter of the bolt.

The FE results are summarized in Figure 9. According to Figure 9, the elastic axial stiffness values with respect to horizontal displacements in tension and compression are $K_{ax,con,1} = 460$ kN/mm and $K_{ax,con,2} = 500$ kN/mm, respectively. Based on the values for $K_{ax,con,1}$ and $K_{ax,con,2}$ the rotational stiffness about y-axis was determined as follows:

$$K_{\theta,con} = \frac{M}{\theta_{con}} = z_{con}^2 \cdot \left(\frac{1}{K_{ax,con,1}} + \frac{1}{K_{ax,con,2}} \right)^{-1} \quad (35)$$

where $z_{con} = 380$ mm, as shown in Figure 2 (b).

The rotational stiffness of the steel coupling part is 34595 kNm/rad. The friction slip between steel coupling part occurred at about 260 kN, which also was observed from monotonic loading tests, where F_x at maximum moment was 251.5 kN, confer Table 4.

Table 5: Material properties for steel S355, 16mm < t < 40mm (2013)

E , [MPa]	ν , [-]	σ_p , [MPa]	σ_{y1} , [MPa]	σ_{y2} , [MPa]	σ_{ult} , [MPa]	ε_p , [-]	$\varepsilon_{p,y1}$, [-]	$\varepsilon_{p,y2}$, [-]	$\varepsilon_{p,ult}$, [-]
21000	0.	311.0	346.9	355.9	541.6	0.000	0.004	0.019	0.139
0	3					0	0	7	1

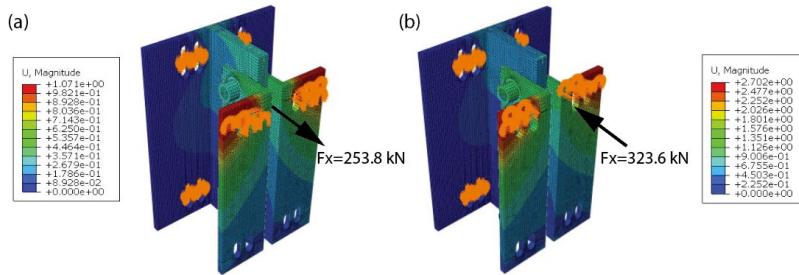


Fig. 8: Finite element model of steel coupling part subjected to axial forces: (a) tensile loading, (b) compressive loading

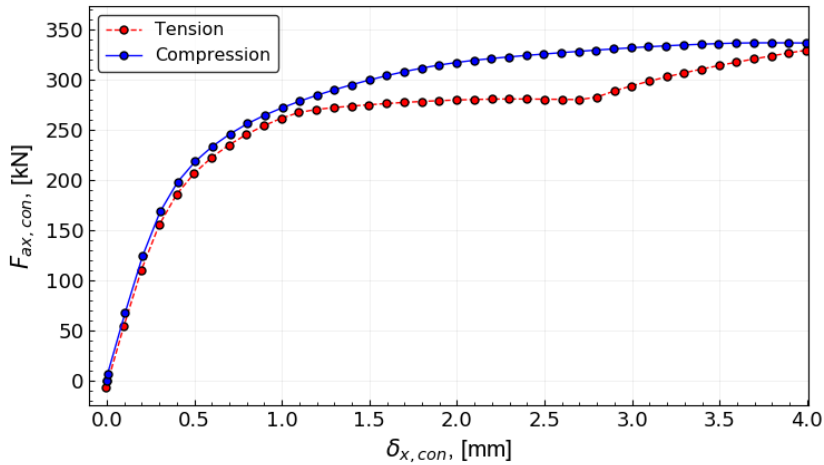


Fig. 9: Force-displacement curve for steel coupling part according to FE simulations

The experimental results and the analytical predictions of the component method with respect to rotational stiffness are summarized in Table 6, which give the resulting values from evaluations of the analytical expressions given in Section 2.1.4. The experimentally measured rotational stiffness value of the connection under monotonic loading was $K_{\theta,y} = 4761$ kNm/rad and the analytical prediction gave 7137 kNm/rad. The analytical prediction overestimates the total stiffness of the connection, which can be related to the high rotational stiffness of simulated steel coupling part. The analytical expressions slightly underestimate the rotational stiffness on the beam-side and slightly overestimate rotational stiffness on the column-side.

Table 6: Analytical predictions of rotational stiffness compared to experimental result from monotonic test

Property	Reference	Specimen	Units
$K_{ax,c1}$ ($K_{ser,ax,c1}/K_{ax,l0,c1}$)		62.6 (68.1/822.1)	
$K_{ax,c2}$ ($K_{ser,ax,c2}/K_{ax,l0,c2}$)	Eq. (25)	53.4 (56.2/1068.7)	
$K_{ax,c3}$ ($K_{ser,ax,c3}/K_{ax,l0,c3}$)	In parenthesis: $K_{ser,ax}/K_{ax,l0}$	53.7 (56.2/1187.1)	(kN/mm)
$K_{ax,c4}$ ($K_{ser,ax,c4}/K_{ax,l0,c4}$)	Eq. (23)/ Eq. (25)	65.6 (68.1/1781.3)	
$K_{ax,b1}$ ($K_{ser,ax,b1}/K_{ax,l0,b1}$)		113.3 (125.3/1179.4)	
$K_{ax,b2}$ ($K_{ser,ax,b2}/K_{ax,l0,b2}$)		118.4 (125.3/2137.6)	
$K_{v,c1}$		4.9	
$K_{v,c2}$		5.9	
$K_{v,c3}$	Eq. (27)	8.2	(kN/mm)
$K_{v,c4}$		7.3	
$K_{v,b1}$		7.3	
$K_{v,b2}$		11.1	
$K_{\theta,c}$	Eq. (5)	12627 (per plane of rods: 6330)	(kNm/rad)
	Tests	11223	
$K_{\theta,b}$	Eq. (10)	31250 (per plane of rods: 7813)	(kNm/rad)
	Tests	35006	
$K_{\theta,con}$	FE Results	34595	(kNm/rad)
	Tests	-	
$K_{\theta,y}$	Eq. (15)	7137	(kNm/rad)
	Tests	4761	

3.1.3 Cyclic loading tests

Initially, cyclic tests were performed on the moment-resisting connections using the loading protocols presented in Section 2.1.2. For each cyclic loading case 10 cycles were performed. The experimentally recorded moment-rotation hysteresis loops for each specimen are shown in Figure 10, where first column gives the total rotational stiffness for the test set-ups, while the second and third columns visualise the contributions from beam-side and column-side, respectively. Table 7 summarizes the

experimentally recorded cyclic stiffness values, the (average) energy dissipation per cycle and the equivalent viscous damping ratios according to Eq. (2) for the connection and for each part separately.

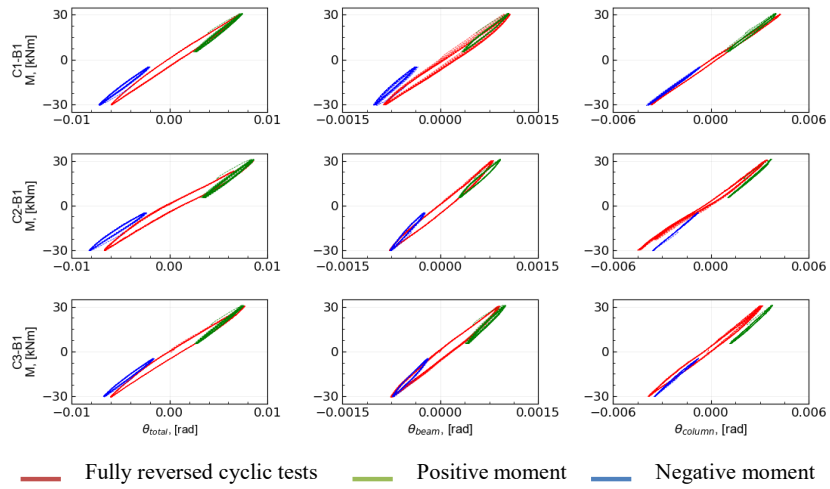


Fig. 10: Moment-rotation curves from cyclic tests of the connections

Table 7: Experimental results of connections subjected to cyclic testing

Entire connection									
Test ID.	Fully reversed cyclic			Negative moment			Positive moment		
	$K_{\theta,cyc}$, [kNm/rad]	E_d , [kNm]	ξ_{eq} , [%]	$K_{\theta,-}$, [kNm/rad]	E_d , [kNm]	ξ_{eq} , [%]	$K_{\theta,+}$, [kNm/rad]	E_d , [kNm]	ξ_{eq} , [%]
C1-B1	4465	0.052	4.1	4675	0.010	4.7	5028	0.010	4.7
C2-B1	3774	0.067	4.4	4090	0.014	5.5	4677	0.012	5.5
C3-B1	4287	0.054	4.1	4676	0.010	4.4	4993	0.008	3.8
Mean	4175	0.058	4.2	4480	0.011	4.9	4900	0.010	4.7
CoV, [%]	8.6	13.4	4.3	7.5	19.2	11.4	4.0	22.3	18.9
Beam-side connection									
Test ID.	Fully reversed cyclic			Negative moment			Positive moment		
	$K_{\theta,b,cyc}$, [kNm/rad]	E_d , [kNm]	ξ_{eq} , [%]	$K_{\theta,b,-}$, [kNm/rad]	E_d , [kNm]	ξ_{eq} , [%]	$K_{\theta,b,+}$, [kNm/rad]	E_d , [kNm]	ξ_{eq} , [%]
C1-B1	30869	0.004	3.3	37089	0.001	3.2	33684	0.001	2.9
C2-B1	36774	0.004	2.5	45341	0.001	3.3	37323	0.001	3.5
C3-B1	35458	0.004	2.8	43388	0.001	3.4	40918	0.001	3.1
Mean	34367	0.004	2.8	41939	0.001	3.3	37308	0.001	3.2
CoV, [%]a	9.0	9.7	14.7	10.3	8.8	2.2	9.7	11.8	10.2
Column-side connection									
Test ID.	Fully reversed cyclic			Negative moment			Positive moment		
	$K_{\theta,c,cyc}$, [kNm/rad]	E_d , [kNm]	ξ_{eq} , [%]	$K_{\theta,c,-}$, [kNm/rad]	E_d , [kNm]	ξ_{eq} , [%]	$K_{\theta,c,+}$, [kNm/rad]	E_d , [kNm]	ξ_{eq} , [%]
C1-B1	8292	0.012	2.8	7500	0.003	2.2	7982	0.006	4.8
C2-B1	8567	0.017	2.0	8635	0.004	2.7	9106	0.004	3.6
C3-B1	8529	0.020	2.9	8887	0.003	2.3	9356	0.003	3.1
Mean	8463	0.016	2.6	8341	0.003	2.4	8815	0.005	3.8
CoV, [%]	1.8	22.8	19.0	8.9	27.6	10.2	8.3	29.9	22.9

The mean rotational stiffness measured for fully reversed cyclic loading $K_{\theta,cyc} = 4175$ kNm/rad is slightly lower compared to mean values of the rotational stiffness for positive moment ($K_{\theta,+} = 4900$ kNm/rad) and negative moment ($K_{\theta,-} = 4480$ kNm/rad). Furthermore, the measured stiffness values from monotonic loading (4761 kNm/rad) are quite similar to all the values recorded from the cyclic tests. The mean rotational stiffness on the column-side connection ranges from 8341 to 8815 kNm/rad and on the beam-side connection the mean rotational stiffness ranges from 34367 to 41939 kNm/rad.

The mean equivalent damping ratios are similar for fully reversed loading (4.2%), positive moment (4.7%) and negative moment (4.9%) with variability coefficient of 13.4%, 18.9% and 11.4, respectively. The mean equivalent viscous damping ratios for the beam-side connection are approximately two times higher compared to column-side, both for fully reversed loading (5.7% vs 2.6%), cyclic loading under

positive moment (6.3% vs 3.8%) and cyclic loading under negative moment (6.6% vs 2.4%). This finding may be related to the fact that more threaded rods are used on the beam-side possibly resulting in larger energy dissipation.

3.2 Mock-up frame assembly

3.2.1 Cyclic loading tests

The experimental results from cyclic loading tests are given in Figure 11 in terms of force-displacement hysteresis loops for each loading point and displacement measurement. The displacements in x-direction were monitored by the LVDTs attached to the columns C_1 , C_2 and C_3 , as shown in Figure 5 (a). Consequently, Figure 11 can be interpreted as a graphical 3x3 stiffness matrix. As it may be observed, the off-diagonal elements are fairly symmetric and indicates the degree of coupling effects between the three columns. The corresponding values for lateral stiffness (K_{frame}), energy dissipation (E_d), viscous damping coefficient (ξ_{eq}), bending moments (M_c) and rotational stiffness of connections ($K_{\theta,y}$) are summarized in Table 8. Furthermore, the experimental results were compared with the FE model shown in Figure 6 (a).

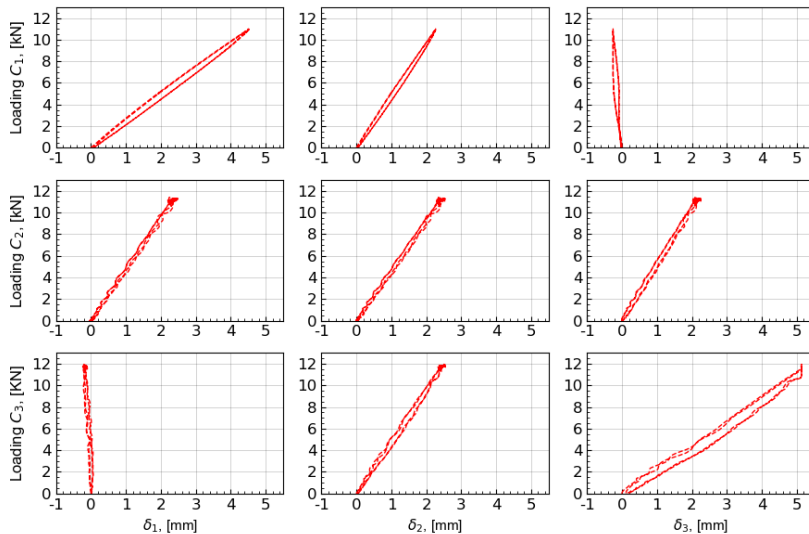


Fig. 11: Force-displacement curves from lateral cyclic tests of the mock-up frame assembly

Table 8: Experimental and FE results of mock-up frame assembly subjected to lateral cyclic loading

Property	Units	Loading C ₁			Loading C ₂			Loading C ₃		
		C1	C2	C3	C1	C2	C3	C1	C2	C3
F_{\max}	[kN]	11.00	-	-	-	11.40	-	-	-	12.00
K_{frame}	[kN/mm]	2.43	-	-	-	4.49	-	-	-	2.33
E_d	[kN]	2.46	-	-	-	1.15	-	-	-	4.53
ξ_{eq}	[%]	3.11	-	-	-	2.62	-	-	-	4.65
M_c^a	[kNm]	5.30	5.03	0.36	2.63	5.10	2.63	0.42	5.48	5.73
M_c/θ	[kNm/rad]	1895	4535	2006	1822	4400	1932	1711	4166	1900
δ_{tests}	[mm]	4.52	2.27	-0.26	2.49	2.54	2.26	-0.26	2.55	5.14
δ_{FE}^a	[mm]	5.26	2.46	-0.27	2.51	2.56	2.51	-0.30	2.68	5.73

^a FE results assuming: $K_{\theta,y} = 4200$ kNm/rad, $K_{\theta,x} = 1184$ kNm/rad on centric columns and $K_{\theta,y} = 2100$ kNm/rad, $K_{\theta,x} = 592$ kNm/rad on corner columns.

As shown in Table 8, the lateral stiffness of the mock-up frame assembly for loading in C₁, C₂, C₃ were measured to 2.43, 4.49, 2.33 kN/mm, respectively. The lateral stiffness is smallest when the load is applied on the corner columns, presumably due to torsion caused by the eccentric loading. Furthermore, the frame assembly showed considerable energy dissipation with equivalent viscous damping coefficients for all loading cases (3.11%, 2.62% and 4.65%).

3.2.2 Finite Element evaluations

In order to examine the effects of the transversal (x-axis) rotational stiffness of the connections, a series of FE simulations of the frame assembly were carried out varying the ratio between the rotational stiffness about x-axis (transversal) and y-axis $K_{\theta,x}/K_{\theta,y}$. The rotational stiffness ($K_{\theta,y}$) about y-axis were fixed to 4200 and 2100 kNm/rad for centric and corner columns, respectively (i.e. the average rotational stiffness from the cyclic loading tests). The FE results are presented in Figure 12. The stiffness ratio range of $K_{\theta,x}/K_{\theta,y} = 0.2-0.3$, which is highlighted in Figure 12, give good agreement regardless of load condition and is valid both for static and dynamic response. The rotational stiffness of connection about x-axis does not affect horizontal displacements when the loading is applied on the centric column, confer Figure 12. Furthermore, the mean rotational stiffness of connection measured in laboratory was 4175 kNm/rad, but for the mock-up frame assembly the measurements gave rotational stiffness from 4166 to 4535 kNm/rad. The mean rotational stiffness of connection for corner columns was measured to 1878 kNm/rad. The FE model with the stiffness ratio $K_{\theta,x}/K_{\theta,y}$ in the range 0.20-0.30 gave also good agreement for the fundamental eigen-frequency in the y-direction compared to the experimentally obtained value of 1.81 Hz (Table 9), see the rightmost plot on Figure 12. The corresponding vibrational modes from FE simulations are shown in Figure 13.

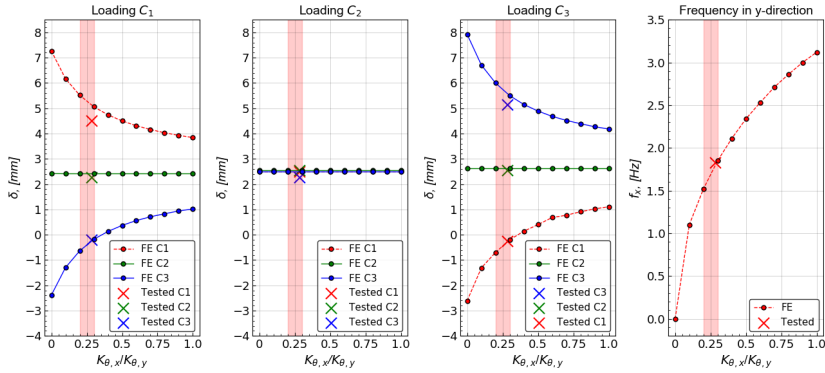


Fig. 12: Lateral displacements according to FE analyses of the frame assembly as function of the ratio $K_{\theta,x}/K_{\theta,y}$

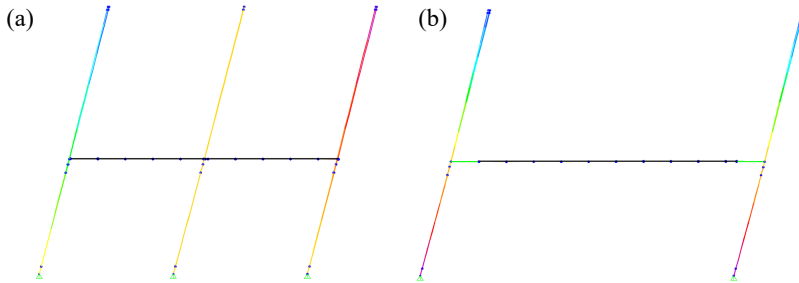


Fig. 13: Mock-up frame assembly mode shapes from FE software SAP2000: (a) First mode in transversal y-direction with frequency of 1.80 Hz; (b) Second mode in longitudinal x-direction with frequency of 3.34 Hz

3.2.3 Free damped vibration evaluation

The fundamental eigen-frequencies and damping ratios with respect to translation in x- and y-directions obtained from experimental modal analysis and FE simulation are given Table 9. The fundamental eigen-frequency with EMA was recorded to be 1.81 Hz along the y-direction and 3.55 Hz along the x-direction with structural damping ratios of 2.1% and 3.9%, respectively. No experiment on energy dissipation in the connections for transverse direction (y-direction) was performed, and hence no comparison of FE and EMA is available for y-direction.

Table 9: The fundamental eigen-frequencies and structural damping from EMA and FE simulations

Test method	$f_{n,y}$, [Hz]	ξ_y , [%]	$f_{n,x}$, [Hz]	$\omega_{n,x}$, [rad/sec]	ξ_x , [%]
EMA	1.81	2.10	3.55	22.30	3.90
FE	1.80	-	3.34	20.98	3.88

To evaluate the structural damping with FE simulations as discussed in Section 2.2.5, the applied material damping values of the timber columns and hollow box timber decks and damping coefficients of the moment-resisting connections are presented in Table 10 and damping coefficient estimated according to Eq. (32). The free damped vibration results from FE simulation are presented in Figure 14 in terms of displacement vs time and compared with free damped vibration test results from values obtained with EMA by applying the equation of motion for damped structures:

$$u(t) = e^{-\xi_x \omega_{n,x} t} \left[u(0) \cos \omega_{d,x} t + \frac{\dot{u}(0) + \xi_x \omega_{n,x} u(0)}{\omega_{d,x}} \sin \omega_{d,x} t \right] \quad (36)$$

$$\omega_{d,x} = \omega_{n,x} \sqrt{1 - \xi_x^2} \quad (37)$$

where ξ_x – is the structural damping from EMA, $\omega_{n,x}$ – is the natural frequency, $u(0)$ – is the initial displacement, $\omega_{d,x}$ – is the damped natural frequency, $\dot{u}(0)$ – is the initial velocity.

Table 10: Material and equivalent viscous damping ratios for FE simulation

Structural part	Material damping, [%]	Equivalent viscous damping, [%]	Damping coefficient (c), [N·s/mm]
Timber columns	0.5	-	-
Hollow box timber decks	1.5	-	-
Moment-resisting connections on centric columns	-	4.2	16816.0
Moment-resisting connections on corner columns	-	4.2	8408.0

FE simulations assuming: $K_{\theta,y} = 4200$ kNm/rad on centric columns and $K_{\theta,y} = 2100$ kNm/rad on corner columns. Undamped natural frequency $\omega_{n,x} = 2\pi \cdot f_{n,x} = 2\pi \cdot 3.34 = 20.98$ rad/sec.

The initial displacement on the centric and corner columns at the level of hollow box timber decks $u(0) = 5.0$ mm and initial velocity $\dot{u}(0) = 0$ m/s were applied to measure free damped vibrations. The structural damping of FE frame assembly model according to Eq. (33) and Figure 14 is 3.88%.

As it may be observed from Table 9, as well as from Figure 14, a minor difference in the fundamental frequency $f_{n,x}$ between the FE model (with measured component values) and the EMA results (of the mock-up frame assembly) is present. The FE model give $f_{n,x} = 3.34$ Hz, while $f_{n,x} = 3.55$ Hz is obtained from EMA. Probably this is due to small differences in the rotational stiffness of the connections. The resulting deviation in frequency is consistent with the fact that the connection stiffness obtained from the mock-up (and consequently in the EMA) were slightly larger than the stiffness measured in the connection component tests. It should also be kept in mind that there are experimental variations in the performance of the connections, both in the component tests as well as in the mock-up frame assembly tests. The use of material damping and equivalent viscous damping from the cyclic connection tests show very good agreement and this approach can successfully be used to predict the structural damping of complete frame assemblies.

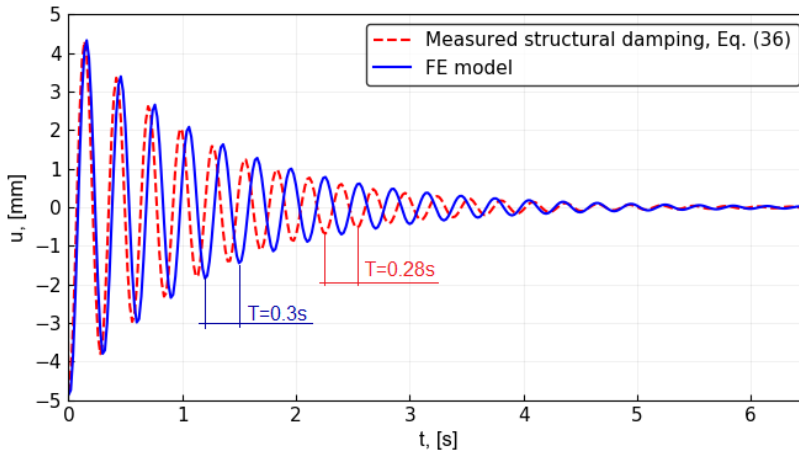


Fig. 14: EMA and FE free damped vibration results in x-direction

4 Conclusions

The performance of beam-to-column moment-resisting timber connections with inclined threaded rods and steel coupling parts connected with friction bolts has been investigated by use of full-scale tests and a mock-up frame assembly. The moment resisting connections were subjected both to cyclic and monotonic loading. The rotational stiffness and the energy dissipation properties were determined on the basis of the three full-scale cyclic tests. In addition, the rotational stiffness and the moment resistance were measured under monotonic loading and compared with analytical predictions based on an analytical model (Stamatopoulos and Malo 2020). The mock-up frame assembly was subjected to cyclic lateral loading and also tested with experimental modal analysis. The lateral stiffness, energy dissipation, fundamental eigen-frequencies and structural damping of the frame assembly were measured and quantified and compared with FE analyses. The following main conclusions are drawn:

- The rotational stiffness of present connection measured from monotonic loading test was 4761 kNm/rad. The maximum moment resistance was 100.6 kNm limited by friction between the steel plates. No initial slip was recorded, and the connection demonstrated initial load take-up.
- The rotational stiffness of connections for fully reversed loading and single-sided positive and negative moment tests were 4175, 4480 and 4900 kNm/rad, respectively with coefficient of variation around in range from 4.0

to 8.6%, and hence only minor differences are exhibited by this type of connections.

- The mean rotational stiffness of connection from laboratory tests and from tests with mock-up frame assembly were in average 4175 kNm/rad and 4367 kNm/rad, respectively. Therefore, the measured values for connection properties obtained in the laboratory are also achievable in full-scale assemblies for this type of connections.
- The rotational stiffness of connections obtained from fully reversed cyclic loading tests are very suitable for FE simulations. The FE model shows good agreement between the experimental results and the analytical model.
- For unsymmetrical loading conditions when torsional rotation of the frame assembly is introduced, the transversal rotational stiffness of the connections should be considered. The transversal rotational stiffness value of these moment-resisting connections can be assumed to be around $0.20-0.30 \cdot K_{\theta,y}$.
- The moment-resisting connections and mock-up frame assembly tests under cyclic loading showed high energy dissipation; 4.2% and 3.5% in terms of equivalent viscous damping, respectively.
- Cyclic energy dissipation from quasi-static component tests can be used to predict the structural damping in moment-resisting frames. Provided that the amount of material damping is known in the components, the damping caused by the connections can be modelled by equivalent viscous damping in FE models and consequently the structural damping in framed structures can be predicted.

Acknowledgments

This study has been carried out within the (WOODSOL) project, a project funded by The Research Council of Norway and led by Kjell Arne Malo at NTNU (NFR Grant 254699). The project includes research at NTNU and SINTEF Building & Infrastructure and the PhD grant for the first and second author of this paper, which is gratefully acknowledged. Petra R  ther at SINTEF was work package leader for “WP6 Prototype”, which made the prototype possible. Simone Conta, the PhD student at NTNU and member of the Woodsol project, was involved in the design and construction of the WOODSOL prototype. Leif Joar Lasseesen and students from Charlottenlund Videreg  ende skole in Trondheim (NO) greatly supported us during the construction of the prototype.

References

2013. Determination of structural capacity by non-linear fe analysis methods. from <https://rules.dnvgl.com/docs/pdf/DNV/codes/docs/2013-06/RP-C208.pdf>.
- CEN. 1991. EN 26891:1991 (ISO 6891:1983): Timber structures- Joints made with mechanical fasteners-General principles for the determination of strength and deformation characteristics. Brussels, Belgium, European Committee for Standardization.
- CEN. 2010. NS-EN 1995-1-1:2004+A1:2008+NA:2010. Design of timber structures - Part 1-1: General - Common rules and rules for buildings. Brussels, European committee for standarization.
- CEN. 2013. EN 14080-2013: Timber structures- Glued laminated timber and glued solid timber - Requirements. Brussels, Belgium, European Committee for Standardization.
- Chopra, A. K. 2012. Dynamics of structures: theory and applications to earthquake engineering. . 4th ed. red. Upper Saddle River, N.J.: Prentice Hall.
- Conta, S. and A. Homb. 2020. Sound radiation of hollow box timber floors under impact excitation: An experimental parameter study. *Applied Acoustics* 161: 107190.
- Corp., D. S. S. 2014. Abaqus analysis user's guide, Version 6.14.
- Gohlich, R., J. Erochko and J. E. Woods. 2018. Experimental testing and numerical modelling of a heavy timber moment-resisting frame with ductile steel links. *Earthquake Engineering & Structural Dynamics* 47(6): 1460-1477.
- Kasal, B., P. Guindos, T. Polocoser, A. Heiduschke, S. Urushadze and S. Pospisil. 2014. Heavy laminated timber frames with rigid three-dimensional beam-to-column connections. *Journal of Performance of Constructed Facilities* 28(6).

- Kristoffersen, T. and H. Bjørge. 2017. Konseptstudie av trebaserte komposittdykker med mulighet for innspenning til limtresøyler. (Conceptual studies of wood based floor with semi-rigid supports), NTNU.
- Labonnote, N., A. Rønnquist and K. A. Malo. 2013. Experimental evaluations of material damping in timber beams of structural dimensions. *Wood science and technology* 47(5): 1033-1050.
- Lied, K. and K. Nordal. 2016. A conceptual study of glulam connections using threaded rods and connecting circular steel profiles. Trondheim, Norway, NTNU Norwegian University of Science and Technology.
- Malo, K. A. and J. Köhler. 2013. Vibrations of timber floor beams with end restraints. Structures and Architecture: Concepts, Applications and Challenges - Proceedings of the 2nd International Conference on Structures and Architecture, ICSA 2013.
- Oskouei, R. and T. Chakherlou. 2009. Reduction in clamping force due to applied longitudinal load to aerospace structural bolted plates. *Aerospace Science and Technology* 13(6): 325-330.
- Qazi, J. 2020. Embedment strength and stiffness of threaded rods in softwood (in Norwegian). *Norwegian University of Science and Technology: Trondheim, Norway*.
- SAP, C. 2003. Analysis reference manual. *Computers and Structures, Inc., Berkley, California, USA*.
- Stamatopoulos, H. and K. A. Malo. 2020. Analysis of moment-resisting beam-to-column timber connections with screwed-in threaded rods. *WOODSOL internal report*.
- Stamatopoulos, H. and K. A. Malo. 2020. On strength and stiffness of screwed-in threaded rods embedded in softwood. *Construction and Building Materials* 261: 119999.
- Vilguts, A., K. A. Malo and H. Stamatopoulos. 2018. Moment resisting frames and connections using threaded rods in beam-to column timber joints Proceedings of WCTE 2018 - World Conference on Timber Engineering. Seoul, Republic of Korea.
- Vilguts, A., H. Stamatopoulos and K. A. Malo. Parametric analyses and feasibility study of moment-resisting timber frames under service load. *Engineering Structures* 228: 111583.
- Wilson, E. L. and A. Habibullah. 1997. SAP2000 integrated finite element analysis and design of structures. *Computers and Structures Inc., Berkeley, California*.

1.3 Paper III

Competitiveness of timber floor elements: an assessment of structural properties, production, costs and carbon emissions

Sveinung Nesheim, Kjell Arne Malo, Nathalie Labonnote

For publication in: Forest Products Journal

Submitted: 5th September 2020

Accepted: 23rd January 2021

Credit author statements

For the Original article presented herein, all authors have contributed to its preparation as described in the below statement:

Sveinung Nesheim: Conceptualization, Methodology, Software, Validation, Investigation, Resources, Writing - Original Draft, Writing - Review & Editing, Visualization, Project administration.

Kjell Arne Malo: Writing - Review & Editing, Supervision, Funding acquisition.

Nathalie Labonnote: Writing - Review & Editing, Supervision.

Competitiveness of timber floor elements

An assessment of structural properties, production, costs and carbon emissions

Abstract

As long-spanning timber floor elements attempt to achieve a meaningful market share, proof of serviceability continues to be a demanding task as international consensus remains unsettled. Initiatives to improve vibration levels are achievable, but a lack of confidence in the market is resulting in increases in margins for both manufacturers and contractors. State-of-the-art concrete alternatives are offered at less than half the price, and even though timber floors offer reduced completion costs and low carbon emissions, the market is continuously reserved. Cost reductions for timber floor elements to competitive levels must be pursued throughout the product details and in the stages of manufacturing. As new wood products are introduced to the market, solution space is increased to levels that demand computerised optimisation models, which require accurate expenditure predictions. To meet this challenge, a method called Item-Driven Activity-Based Consumption (IDABC) has been developed and presented in this study. The method establishes an accurate relationship between product specifications and overall resource consumption linked to finished manufactured products. In addition to production time, method outcomes include cost distributions, including labour costs, and carbon emissions for both accrued materials and production line activities. A novel approach to resource estimation linked to assembly friendliness is also presented. IDABC has been applied to a timber component and assembly line operated by a major manufacturer in Norway and demonstrates good agreement with empirical data.

Keywords

Activity-based; assembly; component; carbon emissions; cost; expenditure; floor; forest products; optimization; production; timber; wood.

1 Introduction

Timber flooring systems are endeavoring to gain a market share in commercial buildings. In this market cost is the dominant selling point, hence cost reductions for timber floor elements to competitive levels must be pursued throughout the product

details and in the stages of manufacturing. However, future competitiveness is not an issue of cost only. The construction sector currently contribute to global energy use and carbon emissions by 36 % and 39 %, respectively (UN Environment and International Energy Agency (IEA) 2017), and emission reduction targets are likely not to be met without a reduction of the energy consumption in the sector. 85% of the buildings we will use in 2050 are currently built (Dixon et al. 2018). Still projections indicate that 230 billion square meters of buildings will be erected or reconditioned by 2060 (UN Environment and International Energy Agency (IEA) 2017). Estimates suggest that greenhouse gas (GHG) emissions is likely to double in the same period (Pomponi and Moncaster 2016). Material Efficiency (ME) analyses have been performed to form strategies for reducing GHG by substituting steel and concrete with timber (Hertwich et al. 2019). Studies of energy efficient buildings show a reduction of GHG in the service lifetime, but an increase in embodied GHG of the building itself (Röck et al. 2020). As political incentives are encouraging the use of environmental beneficially materials (Hill and Dibdiakova 2016), the market potential for timber elements gain strength. However, the construction industry is expectant and more research is required to improve timber floor systems and simultaneously reduce GHG emissions and cost.

As new wood products are introduced, computerized optimization models may be required to find the optimum solution both to cost and embodied carbon emissions. Forintek and the Canadian Wood Council (Hu et al. 2006) concluded that an accurate accounting of the expenditure of manufacturing is required to formulate methods of optimization of timber floor elements.

Assessment of estimation methods for major construction cost factors provide evidence of the importance of accurate accounting. (Akintoye 2000). The study reports that construction and buildability constitute critical factors, and that precise estimates of cost and delivery of prefabricated components such as floor elements are essential.

Cost of direct material (material from supplier) and labor cost is key indicators of competitiveness, but better description of machining processes may further enhance competitiveness (Ratnasingam et al. 1999). The study brings understanding of the furniture wood machining and related machining cost, and argues that machining costs may be calculated using Activity-Based Costing (ABC) (Drury 1992). The study has many similarities to the present work, but the level of detail may not be suitable for heavy timber product manufacture. Implementation of lean manufacturing in the secondary wood industry increase competitiveness, according to (Velarde et al. 2011). Depending on the factory, lean manufacturing requires specific systems, and the implementation of new systems can be a burden for a factory. However, the outcome may reduce excess production time, increase the efficiency of the factory floor and the utilization of direct material.

The United States Department of Agriculture and the Wood Components Manufacturers Association developed a product cost quotation tool for timber component manufacturers (Andersch et al. 2013, Andersch et al. 2014). This is a robust framework for costs accounting but is based on traditional costing methods and historical data taken from the company applying the method. It is neither parametric, nor does it facilitate the calculation of carbon emissions linked to manufacturing. As such, it cannot be applied as part of an optimization algorithm without extensive redesign. Other studies have been carried out with the aim of developing methods to assist sawmill operators in estimating product costs (Howard 1988), but such methods are not representative of cost calculations used in timber element manufacturing.

An outline of basic manufacturing costing methods is presented in (Moore and Creese 1990). In this study, costs are assigned to specific activities and the methods described share similarities with the frequently applied models using Activity-Based Costing (Yongqian et al. 2010) and Time-Driven Activity-Based Costing (Namazi 2016). Applied for product manufacturing, the Activity-Based Costing methods all define activities along the production line as resources that combine to perform operations in the manufacture or processing of a given item. The drawback of these models is that they are not parameterized, and requires input in the form of predetermined values of activity durations. More advanced mathematical methods are able to model demand-driven manufacturing. The method described in (Kalaiarasi and Rajarathnam 2015) addresses inventories and not activities, while (Durga Prasad et al. 2014) describe an approach involving a mathematical representation of quality control, value engineering and target costs. In the latter approach, product cost management during the conceptual phase is studied as a means of balancing costs and quality, and the mathematical relationships are analyzed and solved to support optimization procedures during product development.

The manufacturing of timber-based floor elements is a machine-driven production process. The machining industry is increasingly required to record and reduce its carbon emissions. The energy consumption of timber element manufacturers is moderate compared to sectors such as the metallurgical and chemical industries, where the levels of energy consumption and carbon emissions are excessive. However, the topic still has relevance for the timber components and assembly sector. In (Cai et al. 2018, Hu et al. 2018, de Souza Zanuto et al. 2019) methods to manage carbon emissions related to consumables is studied, whilst (Du et al. 2015) study operational models for low-carbon manufacturing processes to assist in strategic work to reduce carbon emissions in the machinery manufacturing industry.

Cost of manufacturing of steel-based flooring systems is reported in (Klanšek and Kravanja 2006). The study includes cost of accrued materials, energy consumption

and labor, and is a relevant study because it embraces the holistic approach of measuring a wider range of resource consumption. The costing method applied in (Mela and Heinisuo 2014) where feature-based cost centers is controlled by processing units, the approaches described in (Klanšek and Kravanja 2006, Mela and Heinisuo 2014), combined with the Time-Driven Activity-Based Costing (TDABC) method (Kaplan and Anderson 2003), have all provided valuable input to the method developed in the present work.

Objectives of the present work are to explore a parametric method for quantification of consumed resources in the manufacture of timber elements. The output of the method should serve as a quantification of competitiveness. The review has identified production time, cost, labor cost and ECO2 as indicators of competitiveness. The method should be parametric and have features that makes it suitable as an objective function in optimization workflows. The method should be based on principles that keep the effort of implementation low.

2 Materials and methods

2.1 Background and principle

The method developed and presented in this study has similarities to the aforementioned Time-Driven Activity-Based Costing (TDABC) method (Kaplan and Anderson 2004). However, while TDABC uses predetermined values as input for activity duration, the method described here uses the parametric properties of the items being processed to calculate durations. Moreover, the outcome is not limited to costings, but also to a more detailed calculation of consumption in terms of time, overall costs, labor costs, and carbon emissions. To acknowledge its relationship with the TDABC approach, the method developed during the present study is called Item-Driven Activity-Based Consumption (IDABC). Its relationship with the TDABC method and the differences between the two are explained in the following, subsequent to key definitions and programming concept:

Activity-based costing in general (Hoozée and Hansen 2014), as applied for product manufacturing, defines activities along a production line as resources that combine to perform operations in the manufacture or processing of a given item. Resources are the theoretical definition of apparatus and personnel that can contribute in an activity, whilst an activity is the physical realization to a given item. An activity is performing an operation on an item, and an item is either direct material in the manufacturing of a component, or a component in the assembly or processing of the final product. See Figure 1.

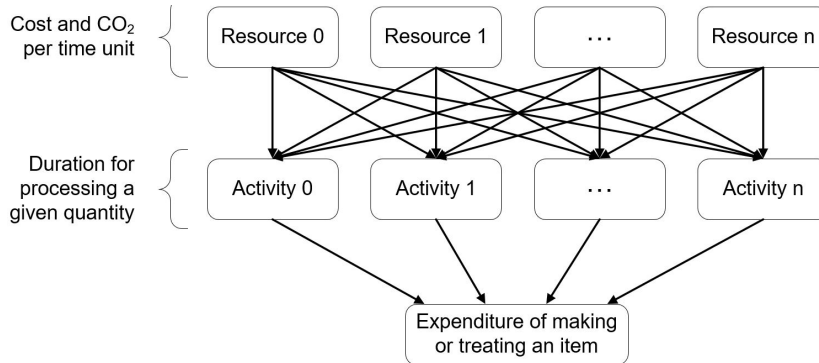


Figure 1: Activity-based accounting in general. The relationship between resources, activity and expenditures

Object-Oriented Programming (OOP) was applied in the programming of the IDABC. OOP is generally much used in modelling of real-life applications and the concept of classes in OOP is convenient and offers excellent levels of control when a programming operation shall be repeated multiple times. Classes were defined for resources and activities, sections, bodies and assembly, and the instantiation of any of these classes generates a unique object based on a set of attributes. The object can then be treated by what is known as methods of the class, to perform various programming operations of that object. OOP is not compulsory when implementing IDABC, but is mentioned to give some understanding of how the programming was performed.

The TDABC approach employs two parameters for the estimation of cost-driver rates. These are the cost per unit time of resources, and the time required to perform a given activity (Kaplan and Anderson 2004). In situations involving the costs of product manufacture, the TDABC approach would multiply cost-center rates with the duration of the relevant activities. This requires the duration of all activities to be predetermined. Any permutations from a planned manufacturing framework will impose additional planning production costs on the manufacturer during product cost determination.

The IDABC approach allows more indeterminacy, and features levels of flexibility and information content that enable the parametric accounting of manufacturing expenditures linked to the systematic and repeated manufacture of components constituting an assembly.

The initial parameter used in the IDABC method is cost of resources per unit time (C_R), where R denotes a resource. In addition to cost rate, the IDABC method also includes the rate of production of CO₂ equivalents (CO_{2R}). This is required for the completion of an Environmental Product Declaration (EPD), which is an

increasingly important factor in customer purchase motivation (Del Borghi 2013, Thies et al. 2019).

The second parameter used in the TDABC method is the predetermined duration of an activity. In the IDABC approach this is substituted by a parametric function in the activity object (the programmed representation of the activity). When an item is subject to an activity, the activity object is parsing the predefined processing SI unit of the activity, and the item is returning the requested quantity processed by the activity. In the activity object a series of methods serve to compute an expenditure vector associated with the processing of the item. For example, during the lifting of a given item, the weight of the item in [kg] is requested. During a sawing process, depending on which saw activity that is used, either the number of items being cut [1], or the cutting area [m²], is requested.

The expenditure vector V_η (Eq. 1) contains the duration of an activity T_η [s], overall costs C_η [€], labor costs LC_η [€], and the amount of CO₂ equivalents GWP_η [kgCO₂eq] associated with the item. The subscript η denotes a specific item subject to a given activity. Overall costs represent the total costs linked to the activity, while labor costs constitute that part of the costs associated with labor.

$$V_\eta = \{T_\eta \ C_\eta \ LC_\eta \ GWP_\eta\} \quad [s \ \text{€} \ \text{€} \ \text{kgCO}_2\text{eq}] \quad \text{Eq. 1}$$

Principally, an item inherits an expenditure vector for each activity to which it is subjected during the production process. The total expenditure linked to manufacture of the product ($V_{assembly}$) is the sum of expenditures for the activities completed as the items pass along the production line and operations for building the assembly are performed (Eq. 2). $V_{assembly}$ is the output of the method, and comprise the selected indicators for competitiveness.

$$V_{assembly} = \sum_{i=0}^{numBody} \sum_{j=0}^{numAct} V_{i,j} + \sum_{k=0}^{numAsmby} \sum_{l=0}^{numAct} V_{k,l} \quad \text{Eq. 2}$$

2.2 Description of the process

The IDABC process is initiated by specifying the SI units associated with the activities, and the energy sources linked to the resources. This is followed by definitions of the unique sections that constitute the product. These sections are defined on the basis of the product's general specifications as illustrated in the two upper rows in Figure 2. The IDABC approach divides the manufacturing into two subprocesses. The first of these involves the manufacture of bodies (“Body Level”), and the second is the assembly process that produces the final product (“Assembly Level”). The term body is introduced here as a more general expression also covering

e.g. coating and adhesive, and will be used to address the physical components of an assembly. Introductory, the term component was used because it better communicates the physical meaning, but this term will henceforth be used in reference to vector components (elements of a linear array). In a flowchart the process is divided into four subprocesses (Figure 2):

- Input: definitions of fasteners and sections based on specifications, materials selection, accounting figures, the energy source for resources, and the SI units associated with the activities.
- Cost centers: Identification of activities and associated resources in the production line
- Body Level: bodies are made from direct materials
- Assembly Level: bodies are assembled to make the final product

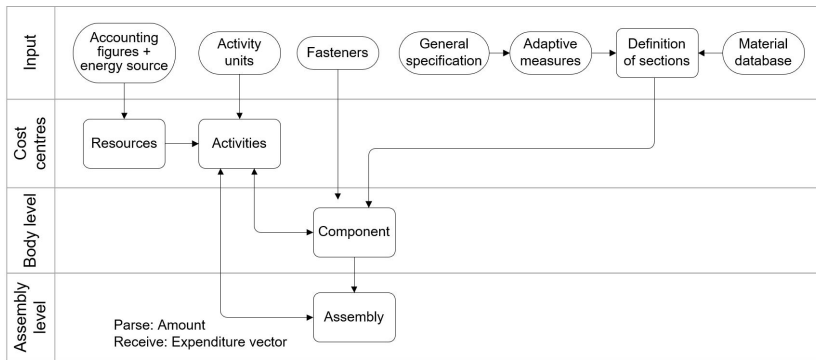


Figure 2. IDABC method process flowchart

Resources defined for the present study:

- Operators: human resources employed at the factory. Most activities require operators.
- Joinery saw: 5D CNC machine used for linear cutting and milling operations. Direct materials used by this resource are either standard lengths or predetermined lengths from the supplier.
- Sheet panel saw: device used to cut structural plates. A plate is defined as a section with an aspect ratio above a given threshold.
- Overhead crane: Handling of items weighing above a given threshold.
- Element inverter: equipment inverting structural plates or sub-assemblies through 180 degrees.
- Robotic arm: device used to operate screwing and nailing modules.

- Glue center: in this study, only manual gluing operations are considered, and gluing is associated with operator resources. However, most technical timber product manufacturing processes employ an automatic glue center.
- Glue press: this is an optional resource by which a product is subjected to pressure during glue hardening. In this study, the resource is not included because pressure in conjunction with glue hardening is applied using screws.
- Overhead: this resource parameter encompasses costs linked to carbon emissions from the factory building, including lighting, heating, ventilation, and air conditioning (HVAC), and the use of hand tools.

In the case considered in this study, the resources used are combined to form fifteen activities performed at “Body Level” and “Assembly Level” (Figure 2). As is illustrated in the flowchart in Figure 3, it is possible for any given resource to contribute to a given activity, and for any given activity to contribute towards producing a given body. Furthermore, once manufactured, any given body can be incorporated into an Assembly Level activity, and any Assembly Level activity can contribute towards the assembly process. In Figure 3, to avoid confusion arising from an excessive number of connecting lines, only two linkage combinations (separated by continuous and dotted lines) are included for the upper three processes. The relevant resources and activities are explained in more detail in sections 2.3 and 2.5.

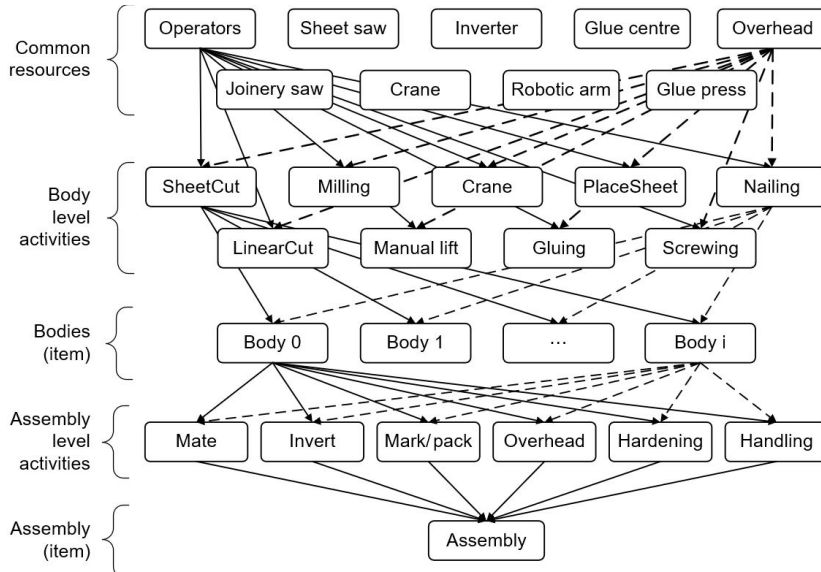


Figure 3. Resource flow chart for the IDABC method

2.3 Materials database

A materials database is required as input to the method. The database contains supplier-specific information regarding the delivery format, density, unit cost (in Euros per cubic meter), and unit mass parameters for embodied CO₂ emissions (ECO₂) and uptake of CO₂ equivalents (in g per kg) for materials information modules A1–A3 (Cradle-to-Gate). The delivery format is structured with the primary dimension listed first, followed by the secondary dimension and optionally lengths.

2.4 Definition of factory resources

2.4.1 General form

Factory resources are associated with two consumables; the rate of cost, and rate of CO₂ emissions. The rate of cost is given as cost per second and is written on general form for a given resource R in Eq. 3:

$$C_R = \left(\frac{C_A}{(T_{SOW} \cdot T_{OPW} - T_{USDt}) \cdot T_{EUT}} \right) \cdot \frac{1}{3600} \quad \left[\frac{\text{€}}{\text{s}} \right] \quad \text{Eq. 3}$$

where C_A is the annual cost of the resource as it appears in factory accounting figures, inclusive of payments on associated loans, capital consumption allowance, and the cost of scheduled maintenance and operation. T_{SOW} and T_{OPW} are the annual scheduled weeks of operation, and the scheduled hours of operation per week, respectively. T_{USDt} represents the number of hours of unscheduled downtime, and T_{EUT} is the expected uptime per time unit.

The rate of CO₂ emissions from factory operations is obtained from a combination of ECO₂ from the machinery, and emissions resulting from power consumption. Several papers, including (Du et al. 2015) and (Liu et al. 2017), address the issue of emissions from machining tools, but very little information is available on how the ECO₂ generated by any given machine is treated and distributed across the products it produces. Our approach is to calculate machinery-related ECO₂ by first distributing the effective ECO₂ from a given machine along its service time and then redistributing it to the activities that utilize the resource. Both the ECO₂ and the service lifetime are parameters that are specific for a machinery and the maintenance strategy of the factory, and must be entered into the method. Effective CO₂ emissions are calculated by subtracting the upstream ECO₂ (as installed) from the downstream ECO₂ (documented recovery as replaced or disposed) for the machinery, and then adding an estimate of the ECO₂ emitted by consumer durables, parts, and maintenance work carried out during the service lifetime of the machine. This approach provides the factory with an incentive to maintain residual service capacity in its resources, which would be the case when leasing machinery. It will also serve

to reduce CO₂ emissions associated with manufacturing by encouraging late-phase maintenance and ensuring that residual CO₂ in the machinery is sustained.

The amount of CO₂ produced by a resource is a function of its energy consumption (P_R) and the energy source used in production. As is illustrated by the typical machining power profile published in reference (Shin et al. 2017), power consumption is kept constant for the duration of the operation. The approach fails to take into consideration standby power consumption, but succeeds in taking high levels of power consumption during idle operations into account (Schudeleit et al. 2016). Emissions levels from various energy sources are defined in (Schlömer et al. 2014). Median energy values from hydropower are used in the calculations performed in this study (Table 1).

Table 1. Median values for emissions derived from selected electricity supply technologies (gCO₂eq/kWh) (Schlömer et al. 2014).

$$\frac{\text{gCO}_2\text{eq}}{\text{kWh}} \Big|_{\text{source}} = \begin{bmatrix} \text{coal} & \text{gas} & \text{solar} & \text{hydro} & \text{nuclear} & \text{wind}_{\text{ocean}} & \text{wind}_{\text{land}} \\ 820 & 490 & 41 & 24 & 12 & 11 & 12 \end{bmatrix}$$

The CO₂ produced by a given resource is given by the general expression in Eq. 4:

Eq. 4

$$\text{CO}_{2R} = \left(\frac{\frac{\text{CO}_{2\text{emb,ef}}}{T_{SL}}}{(T_{SOW} \cdot T_{OPW} - T_{USD T}) \cdot T_{EUT}} + \frac{\frac{\text{gCO}_2\text{eq}}{\text{kWh}} \Big|_{\text{source}}}{1000} \cdot P_R \right) \cdot \frac{1}{3600} \left[\frac{\text{kgCO}_2\text{eq}}{\text{s}} \right]$$

2.4.2 Case study resources

Table 2 lists the specific values used in the resource equations for the production line investigated in the present study. The values are defined from both empirical and probability data and are based on interviews with the Production Line Manager. The values will change between factories depending on a variety of factors, including level of loan financing and efficiency of premises and installed inventory, salary, working hours, lean manufacture implementation levels, and maintenance strategy to mention some.

Table 2. Factory resource specification

Name of factory resource	Effective ECO2 ¹	Service lifetime	Power consumption	Annual Resource Cost	Annual Scheduled Operation	Weekly scheduled operation	Expected Uptime Per Time Unit	Annual Unscheduled Downtime
	ECO _{2,ef}	T _{SL}	P _R	C _A	T _{SOW}	T _{OPW}	T _{EUT}	T _{UDT}
	[kgCO ₂ eq]	[yrs]	[kw]	[€/yr]	[wks/yr]	[hrs/wk]	[DL]	[hrs/yr]
Factory operators	1000	3	0	60000	1750 ² /37.5	37.5	0.85	16
Joinery saw	10000	10	10	100000	45	40	0.85	10
Sheet panel saw	10000	10	12	75000	45	40	0.5	10
Overhead crane	10000	20	2	5000	45	40	0.75	10
Element inverter	1000	15	3	5000	45	40	0.1	10
Robotic tool arm	5000	8	5	10000	45	40	0.75	10
Glue center	10000	15	3	10000	45	40	0.5	10
Glue press	10000	15	10	15000	45	40	0.5	10
Overhead	50000	25	50	75000	45	40	1	10

1) Upstream (as installed) minus downstream (documented recovery as alternated) ECO2 values for the machinery, with added estimate of the CO₂ emitted by consumer durables, parts, and maintenance work carried out during the service lifetime of the machine.

2) Full-time equivalent for operators

2.5 Definition of factory activities

2.5.1 General form

Costs and CO₂ emissions are a function of the duration of the activity. The duration of an activity is a parametric function of processed quantity and an associated Index of Effort (IoE). The processed quantity is activity-specific and is defined according to how the underlying resources operate. The SI units associated with a processed quantity may be Piece [ea.], Weight [kg], Length [m], Area [m²], Volume [m³] or Time [s]. The IoE is typically expressed in terms of machineability (feed rate), which influences the time taken to process the processed quantity. The duration of an activity is the first component of the expenditure vector (\mathbf{V}), expressed in its general form in Eq. 5:

$$\mathbf{V}[1] = T(QTY, IoE) = T_{PRE} + T_{uQTY}(IoE) \cdot QTY + T_{CLS} \quad [s] \quad \text{Eq. 5}$$

where T_{PRE} is the preparation time for the activity, T_{uQTY} is the processing rate of the activity in time per unit quantity (as a function of IoE), QTY is the processed quantity, and T_{CLS} is the time taken to close the activity. The second component of \mathbf{V} is the associated overall cost of the activity, and is calculated using Eq. 6, where C_{NonTD} is the non-time-dependent initial cost of the activity, n_{OP} is the number of operators, $C_{operators}$ is the cost rate of the operator, and C_R is the rate of cost, as defined in Eq. 3.

$$V[2] = C(T) = C_{NonTD} + (C_R + n_{OP} \cdot C_{operators}) \cdot T \quad [€] \quad \text{Eq. 6}$$

The third component of V comprises labor costs and is calculated in Eq. 7.

$$V[3] = CL(T) = n_{OP} \cdot C_{operators} \cdot T \quad [€] \quad \text{Eq. 7}$$

CO₂ emissions constitute the last component of V and are a function of energy source (in gCO₂eq per kWh) and resource power consumption (in kW), expressed in Eq. 8.

Eq. 8

$$V[4] = CO_2 \left(T, \frac{gCO_2eq}{kWh} \Big|_{source} \right) = (CO_{2R} + n_{OP} \cdot CO_{2operators}) \cdot T \quad [kgCO_2eq]$$

A sheet panel saw is used as an example. The saw is operated by two persons and the unit of processing quantity is cutting area. It takes 100 seconds to prepare, and an additional 20 seconds to close the saw cut process. A fixed non-time-dependent cost of 5 Euros is added to the process. Depending on the density of the material, sawing takes 25, 50, or 100 seconds per unit area (1m²) based on a power consumption of 12 kW averaged across the time taken to complete the process. For a unit cutting area of 1m² at lowest IoE, the consumption functions return the following expenditure vector: [145, 11.16, 2.78, 11.6e-3] in [s, €, €, kgCO₂eq]

2.5.2 Case study activities

For the product investigated in the present study the activity specifications and dependent resources are summarized in Table 3. The values are based on interviews with the Production Line Manager and a process of calibration. The number of operators, preparation- and closure times and the non-time-dependent costs will change between factories. The values are influenced by the factory floor infrastructure, operation friendliness of depending resources, and operation strategies to mention some. Furthermore, it requires documentation or understanding of the activity processes to properly define the representative processing SI unit and the processing time rate, optionally with a level of effort. Note that for the LinearCut activity, the underlying resource is not influenced by machineability because the parameter $T_{uQTY}(IoE)$ has identical values for all three components. These are adaptations based on interviews with the Production Line Manager.

Table 3. Factory activity specification

Factory activity	Type of operator	Number of operators	SI units of processing quantity ¹⁾	Preparation time	Time per unit quantity (function of IoE)	Closure time	Non-time-dependent initial cost	Resource(s)
	C _{operators}	n _{op}		T _{PRE}	T _{uQTY} (IoE)	T _{CLS}	C _{NonTD}	
				[s]	[s/unit]	[s]	[€]	
SheetPanelCut	permFactory	2	4	100	[25,50,100]	20	5	sheetPanelSaw
LinearCut	permFactory	2	1	10	[10,10,10]	10	1	joinerySaw
Milling	permFactory	2	5	100	[100,200,300]	30	10	joinerySaw
ManLift	permFactory	0	2	30	[1]	0	0	permFactory
Crane	permFactory	2	2	60	[0.1]	30	0	overheadCrane
ElementInverter	permFactory	1	1	180	[60]	60	0	elementInverter
ManGlueLine	permFactory	2	4	300	[45]	180	0	permFactory
PlaceSheet	permFactory	0	4	0	[30]	0	0	permFactory
ManScrew	permFactory	0	1	0	[60,120,240,480]	0	0	permFactory
AutScrew	permFactory	1	1	90	[5,15,30,60]	30	0	robotArm
AutNails	permFactory	1	1	90	[2]	30	0	robotArm
Mate	permFactory	1	6	0	[1]	0	0	permFactory
GluePress	permFactory	1	6	180	[1]	120	0	gluePress
MarkAndPack	permFactory	0	4	0	[45]	0	0	permFactory
Overhead	permFactory	3	4	0	[36]	0	0	overhead

¹⁾ SI units of processing quantity: 1: Piece [ea.], 2: Weight [kg], 3: Length [m], 4: Area [m²], 5: Volume [m³], 6: Time [s]

2.6 The manufactured product

A timber floor element is used as a case study to assist in describing the method. The dimensions of the element investigated are 9 meters in length by 2.4 meters wide. Manufacture takes up 21.6 m² of the production floor. Details of the floor element specifications are given in Table 5 in Annex A.

2.6.1 Sections

A section is the two-dimensional description of a body in the assembly (see shaded area of Figure 4). It has the following attributes:

- 1) *Cross section*: dimensions along orthogonal axes termed “local 2” and “global 3”. The latter coincides with the predefined assembly vertical axis e₃ to give the section orientation.
- 2) *Purpose*: describes how the section is employed in the product. One of six predefined purposes: structural, adhesive, fastener, non-structural, insulation and technical.
- 3) *Material*: associated material
- 4) *Number*: the number of times the section will be used to extrude bodies
- 5) *Material main axis*: axis that coincides with the normal vector of the section.

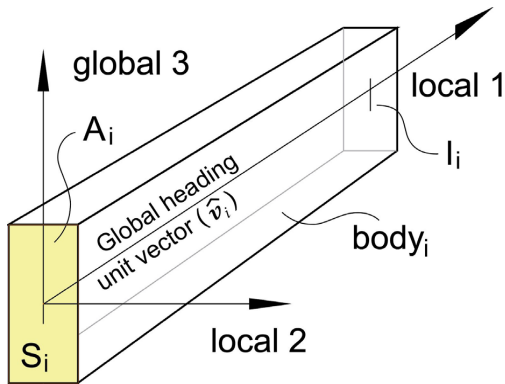


Figure 4. Definition of section and body dimensions and orientations

2.6.2 Bodies

Sections are extruded to form bodies, which are the representation of the physical members of the assembly. A body has the following attributes:

- 1) *Section*: specific section associated with the body
- 2) *Level*: the level of the body within the assembly
- 3) *Heading*: a normal unit vector of the associated section with respect to its global axes (\hat{v})
- 4) *Length (l)*: the extruded length of the body
- 5) *pointOfProcess*: a statement of whether body related consumptions shall be accounted at the factory or on-site
- 6) *indexOfEffort*: a measure of the effort invested in performing an activity, typically associated with density, machineability (feed rate), or the volume of fasteners.
- 7) *fasten.Spec*: a specification of fasteners associated with the body.

For the floor element considered in present study (Figure 5), bodies are grouped into levels, where the structural composite is defined as levels 1 to 3, and adhesive as level 0. Other levels built onto level 1 are numbered successively as follows: 10, 11, 12, etc. The same applies to levels 2 and 3. Figure 5 illustrates the various bodies annotated with their respective levels: a top flange ^①, a core frame ^② consisting of edge joists (hatched), an edge beam (not visible) and field joists, a bottom flange ^③, adhesive ^④, and an internal mass ^⑤. In the same way, additional bodies are used to describe overlays and ceiling systems. Figure 5 is viewed in the direction of the production line (e1) and with e2 and e3 also indicated.

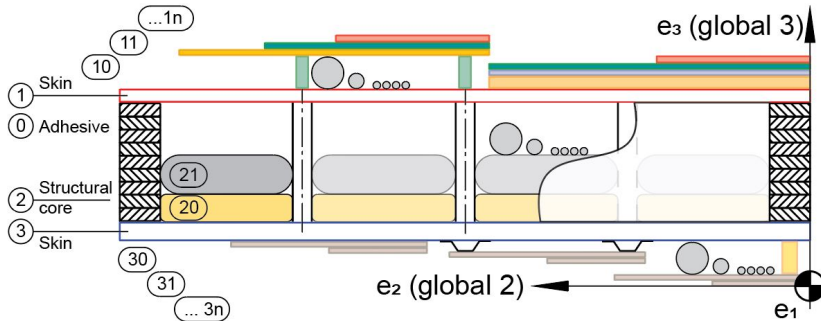


Figure 5. Cross-section of product showing the definition of levels (viewed in the direction of the production line)

Each body is associated with a *pointOfProcess*, and the activity object effectively looks up the value to decide whether activities are performed in the factory or externally. In this paper, only activities carried out in the factory are considered.

2.6.3 Fastener

Fasteners are handled as an optional added feature of a body, thus activating specific activities based on the specification of the fastener. Activities related to fasteners are automatic nailing and screwing, and manual screwing. The specification of fasteners are stored in a separate vector that is appended to bodies (see Table 6 in Annex A). The fastening vector consists of the following components:

- 1) Fastener type: nail or screw
- 2) *Diameter* of the fastener
- 3) Direction of row of fasteners
- 4) *Multiplier* for the number of rows
- 5) *DistanceOrAmount*: whether to calculate the number of fasteners as the distance between fasteners, or as the total number of fasteners along the row defined in (4)
- 6) *Value* of the above argument
- 7) *Unit cost* of a fastener
- 8) *Unit kgCO₂eq* of a fastener
- 9) *Length* of a fastener

2.7 Body Level activities

The resource consumption involved in the manufacture of a body is separated in two: the amount of accrued material, and the resources invested in the activities carried out to produce the body. Consumption of material is a function of its volume and density, while input from the materials database is expressed in terms of unit costs

and unit mass of CO₂ equivalents. Consumption linked to body manufacture is grouped into the Body Level activities illustrated in Figure 3.

2.7.1 Handling and cutting

The initial activities in body manufacture are handling and saw cut operations. Handling is performed both before and after saw cut activity. The handling activity depends on the weight of the body. Bodies weighing less than 25 kg are handled manually, while heavier bodies are handled using an overhead crane. Pre-saw cut handling involves lifting direct material to the saw station for the required number of times either in standard lengths [10m, 12m, 13.5m or 15m], or in the lengths delivered by the supplier. Post-saw cut handling involves the lifting of bodies that have already been subject to cutting.

Structural bodies are cut using either a sheet panel saw or a joinery saw. The type of saw used is determined by (1) the dimensions of the supplied material and the extent to which it conforms to body specifications, (2) the level (1 through 3) in which the body is contained, and (3) the width to height ratio of the body. A joinery saw is used unless the aspect ratio is greater than 20, in which a sheet panel saw is used.

2.7.2 Milling

Milling is performed depending on two conditions. If the thickness of the field joists is less than 36 mm, milling will be carried out on flanges in order for a slice to be created that facilitates gluing. If a fastener must be predrilled, milling will be employed to perform this operation. Predrilling will be carried out either (a) if the IoE of the body is larger than 1, or (b) if the diameter of the fastener is greater than 8 mm.

2.7.3 Place sheet

For bodies with levels at between 10 and 20, or above 30, a place sheet activity is carried out to calculate consumption related to the distribution of sheets. The activity involves both placing and cutting as a function of area.

2.7.4 Screwing and nailing

The preconditions for screwing activity are factory *pointOfProcess* and the use of screws as fasteners are specified for a given body. If the body is at level 3 or above, or at level 1 or below, automatic screwing is used. Bodies at level 2 are fastened using manual screwing. In the case of automatic nailing, the activity is applied if the fastener is a nail and the body is at either level 10 or above, or at level 30 or below.

2.7.5 Gluing

If a body is associated with level 0, either a manual or automatic gluing activity is performed for that body. In this study manual gluing is carried out as opposed to use of the automatic glue line. The activity is carried out for the area of the glue line. As

it is calculated in this study, the length of the adhesive body is essentially the thickness of the glue line.

2.8 Assembly Level activities

Assembly consists of putting bodies together and incurs no material consumption other than that associated with the film used to cover the final product. Activities related to assembly include the mating of bodies, element inversion, the application of glue pressure, mark-up, packing and final handling.

2.8.1 Directionality of structural bodies

In the method developed in present study, unidirectional production can be defined as an assembly process in which the heading of all bodies is oriented in the direction of the production line. Although this is not feasible for most assemblies, a high degree of directionality in production is preferred because it reduces operational requirements and production line complexity, and reduces the time taken to position bodies. For this reason, directional production is quantified. The additional time associated with positioning bodies is not calculated in the general form (Eq. 5), but is expressed in terms of the cumulative time taken to complete Body Level activities, scaled with a directionality factor. Only the volumes of structural bodies (structural volumes) are included in this measure because these are the main contributors to activities that relate to body mating and orientation. Associated additional time is used as input to an activity called *mate* that adds an expenditure vector to the Assembly Level.

The quantification of directionality begins with a calculation of the number of structural volumes that coincide with each of the production line orientations (\mathbf{e}). In this study, only three orientations are used, but further orientations may be used to represent rotations or inverted elements to better reflect deviations from unidirectional production. The volumes are collected in a vector called Structural Volume Heading (**SVH**). This is obtained by multiplying all structural volumes $A_n \cdot l_n$ with their heading unit vector $\hat{\mathbf{v}}_n$ (see Figure 4) and summing the volumes together (Equation 3-9). Consequently, **SVH**[1] contains volumes heading in the direction of the production line (primary volumes), **SVH**[2] volumes perpendicular to the main direction and in-plane to the production floor (secondary volumes), and **SVH**[3] volumes normal to the production floor (tertiary volumes).

$$\mathbf{SVH} = \sum_{n=1}^{structBody} \{A_n \cdot l_n\} \cdot \hat{\mathbf{v}}_n \quad \text{Eq. 9}$$

Since small structural bodies, such as transverse stiffeners, can influence assembly friendliness even at low volumes, the **SVH** parameter is modified to reflect the

number of structural bodies in the various production line orientations. This is performed by populating a vector \mathbf{m} , containing the number of structural bodies in the various orientations, and a scalar \mathbf{M} , which is the sum of the elements in \mathbf{m} . \mathbf{SVH} and \mathbf{m} are then multiplied elementwise (Hadamard product) and divided by \mathbf{M} to give the new, modified \mathbf{nSVH} . This vector is now a representation of the directionality of volumes which also takes the number of bodies into account (Eq. 10).

$$\mathbf{nSVH} = \frac{1}{M} \cdot \{\mathbf{SVH} \circ \mathbf{m}\} \quad \text{Eq. 10}$$

The directionality factor (DF) can now be calculated. Firstly, the ratio of primary orientation volumes represented by $\mathbf{nSVH}[1]$ is divided by the sum of \mathbf{nSVH} . If the next component of \mathbf{nSVH} is greater than zero (i.e. if volumes in the secondary orientation exist), the previous term is multiplied with the ratio of secondary orientation volumes $\mathbf{nSVH}[2]$ by the residual sum of \mathbf{nSVH} . In this paper, only three orientations are considered, so only two steps are required to calculate the DF of the assembly. However, the principle can be extended by repeating the terms of Eq. 11 (below) provided there exist residual volumes in a new orientation. If all volumes of bodies are pointing in the same direction DF equals one.

$$DF = \prod_{\varepsilon=1}^{|\varepsilon|} \begin{cases} \frac{\mathbf{nSVH}[\varepsilon]}{\sum_{\psi=\varepsilon}^{|\varepsilon|} \mathbf{nSVH}[\psi]} & \mathbf{nSVH}[\varepsilon] > 0 \\ 1 & \mathbf{nSVH}[\varepsilon] = 0 \end{cases} \quad \text{Eq. 11}$$

Finally, the time of the mate activity is calculated using Eq. 12:

$$\mathbf{V}_{mate}[1] = \frac{\sum_{i=0}^{numBody} \mathbf{V}_i[0]}{DFM} - \sum_{i=0}^{numBody} \mathbf{V}_i[0] \quad [s] \quad \text{Eq. 12}$$

2.8.2 Invert

Invert is the second activity at Assembly Level. This operation is carried out in preparation for cavity filling and top flange mounting. It involves inverting a subassembly consisting of a bottom flange and the complete structural core after gluing and screwing have been completed. This activity is a combined operation involving both operators and machinery, and the processing unit is piece as duration is only affected by number of inversions.

2.8.3 Glue pressure

Gluing and glue pressure may be carried out at a hardening station, involving both operators and glue press machinery. Hardening time is a predetermined quantity. Normally, glue pressure and hardening are not considered to be cost-effective for production volumes of less than 250,000 m² per year. In the worked example involving timber floors, this activity is replaced using screws to generate glue line pressure.

2.8.4 Mark-up and packing

Mark-up and packing constitute a combined activity that employs both operators and material resources. It employs area as its processing unit, and the parsed amount is the exterior surface of the finished product. Materials consumption involves the film used to package the product.

2.8.5 Final handling

Final handling of the product is carried out by operators in combination with an overhead crane and uses mass as its processing unit. The parsed amount is the transportation weight of the final product ready at the factory gates.

2.8.6 Overhead

The aforementioned activities are grouped in Assembly Level, where associated expenditure vectors are summarized as given in the second term of **Error! Reference source not found.** Production time at the factory is the sum of body time and assembly time.

The final activity is called *overhead* and is treated differently from other activities in that time is not associated with actual production time. Duration for this activity is a fictitious time based on the area that the assembly process occupies on the factory floor ($A_{resProdFlr}$), divided by factory production capacity in area per unit time as shown in Eq. 13.

$$V_{overhead}[1] = \left(\frac{A_{resProdFlr}}{capacity_{areaPerSec}} \right) \quad [s] \quad \text{Eq. 13}$$

The activity overhead is derived from factory resources such as lighting, HVAC, hand tools, and the employment of three service operators. The expenditure vector uses this fictitious duration as input to calculate costs and carbon emissions.

3 Results

3.1 Expenditures due to an activity

Expenditures resulting from a cutting activity of the top flange is used as an example. The aspect ratio command the activity “sheet panel cutting”. This activity combines two underlying resources, and the calculation employs Eq. 3 and Eq. 4, combined with data for operators and the sheet panel saw given in Table 2. The rate of consumption of the two required resources yields the following:

$$C_{operators} = \left(\frac{60000}{\left(46 \frac{2}{3} \cdot 37.5 - 16\right) \cdot 0.85} \right) \cdot \frac{1}{3600} = 11.31 \frac{c\text{€}}{s}$$

$$C_{sheetPanelSaw} = \left(\frac{75000}{(45 \cdot 40 - 10) \cdot 0.5} \right) \cdot \frac{1}{3600} = 23.28 \frac{c\text{€}}{s}$$

$$CO2_{operators} = \left(\frac{\frac{1000}{3}}{\left(46 \frac{2}{3} \cdot 37.5 - 16\right) \cdot 0.85} + \frac{24}{1000} \cdot 0 \right) \cdot \frac{1}{3600} = 63 \frac{mgCO2eq}{s}$$

$$CO2_{sheetPanelSaw} = \left(\frac{\frac{10000}{10}}{(45 \cdot 40 - 10) \cdot 0.5} + \frac{24}{1000} \cdot 12 \right) \cdot \frac{1}{3600} = 0.39 \frac{gCO2eq}{s}$$

The rate of resource consumption calculated in the equations above enable expenditures linked to sheet panel cutting to be calculated based on unit quantity and a duration of one hour. The processing SI unit (T_{uQTY}) for the sheet panel cutting is area [m^2], and for this specific machine 25, 50, or 100 seconds per unit. In this example an intermediate step is taken where one unit of the processed quantity and one hour is inserted into Eq. 5 through to Eq. 8 to reveal the expenditure rates of the activity:

$$V[1] = T(1, IoE) = 100 + [25, 50, 100] \cdot 1 + 20 = [145, 170, 220] \frac{s}{m^2}$$

$$V[2] = C(3600) = 5 + (0.02328 + 2 \cdot 0.01131) \cdot 3600 = 170.22 \frac{€}{hrs}$$

$$V[3] = CL(3600) = 2 \cdot 0.01131 \cdot 3600 = 81.42 \frac{€}{hrs}$$

$$V[4] = CO2(3600, 24) = (3.9 \cdot 10^{-4} + 2 \cdot 6.3 \cdot 10^{-5}) \cdot 3600 = 1.858 \frac{kgCO2eq}{hrs}$$

The dimensions of the top flange body are parsed to the activity object in order to check its dimensions. The thickness of the body must conform to the top flange thickness specification (global 3). The activity object will check if the panel requires cut to the correct width. If cutting is required, the parsed processing unit will be defined by the thickness multiplied by the length of the top flange body. A check is then made to see if the panel requires cutting to the correct length, and the operation of cutting along a second axis is then added to the first to calculate a total cutting area.

Preparation and closure times are added only once for consecutive operations by the same activity on the same body. For this example, the cutting area is 2.4 by 0.043 m. This area is parsed to the activity object together with the density of the material. In the case of the sheet panel saw, the Index of Effort (IoE) is controlled by density (ρ). The activity object chooses the first value in $T_{iQTY}(IoE)$ if the density (ρ) ≤ 500 , the second if $500 < \rho \leq 650$, and the third value if the density is greater than 650 kg/m^3 . The panel used in this example has a density of 510 kg/m^3 and the middle IoE value is used. Inserting parsed values into Eq. 5 through to Eq. 8 produce expenditure quantities rather than rates, and inserting these in Equation 14 produce the activity expenditure vector for top flange cutting:

$$V_{sheetPanelSaw} = [125.16 \quad 10.74 \quad 2.83 \quad 0.0646] [s \quad \text{€} \quad \text{€} \quad kgCO_2eq]$$

3.2 Case study expenditures

The complete resource consumption figures for the finalized product are presented in Table 4. The first column is the name of the cost center followed by columns of expenditures per manufactured area of the finalized timber element. The cost columns are split in total cost, and labor cost. The sums of costs related to activities (sheetPanelSaw to placeSheet), and materials (structural to packing materials) are presented in italics. The bottom row of the table shows the overall costs of the product (in bold font). Note that no materials are associated with insulation nor technical installations (e.g. piping and cables).

Table 4. Resource consumption per area of finalized product

Cost center	Time (V[1])	Cost [€]		CO ₂ (V[4])
	[s]	Total (V[2])	Labour (V[3])	[kgCO ₂ eq]
sheetPanelSaw	11.7	1.00	0.26	6.0e-3
linearSaw	6.6	0.59	0.15	2.5e-3
CNCmachine	0.0	0.00	0.00	0.0
manLift	5.8	0.07	0.07	0.4e-3
crane	96.8	2.29	2.19	23.5e-3
elementInverter	13.9	0.26	0.16	2.6e-3
manScrew	166.7	1.88	1.88	10.5e-3
autScrew	80.6	1.08	0.91	18.2e-3
autNails	0.0	0.00	0.00	0.0
manGlueLine	109.9	3.73	3.73	20.7e-3
mate	7.9	0.18	0.18	1.0e-3
gluePress	0.0	0.00	0.00	0.0
markAndPack	114.2	1.29	1.29	7.2e-3
overhead	36.0	1.64	1.22	29.9e-3
placeSheet	0.0	0.00	0.00	0.0
structural	0.0	107.75	0.00	14.331
adhesive	0.0	0.69	0.00	0.233
fasteners	0.0	1.56	0.00	1.363
nonStructural	0.0	10.94	0.00	0.300
insulation	0.0	0.00	0.00	0.0
technical	0.0	0.00	0.00	0.0
packing	0.0	0.25	0.00	0.025
Production	649.9	14.01	12.04	0.122
Material	0.0	121.19	0.00	16.252
Sum	649.9	135.20	12.04	16.375

The production time is only associated with activities and not with accrued materials. Crane operations are time consuming in addition to manual work as gluing and final marking and packing, all contributing with typically 15 % of the production time. The screwing operations contribute with 40 % of the production time, and in particular the manual screwing operations (25 %). The resulting production time for the timber element is close to 11 minutes per square meter.

The carbon emissions associated with manufacturing activities are very low (less than 1 %), and carbon emissions are mainly stored in materials entering the factory. To increase the readability of the cost figures in the table, the numbers are translated into two charts.

Figure 6 shows the cost distribution for the machinery and labor involved in production line activities. Figure 7 shows the overall costs of the product, distributed according to production activities (equal to the sum of activities costs in Figure 6) and costs arranged in material purpose.

As can be seen in Figure 6, the cost driver of the manufacturing is the labor-intensive activities, contributing with 86% of the manufacturing cost. The directionality factor associated with the mating activity of bodies of the assembly, contribute with 1.5 % of the overall manufacture cost. In perspective, the manufacture cost only contributes

with 10 % of the overall product cost as seen in Figure 7, and that the structural material volumes are the main cost driver overall.

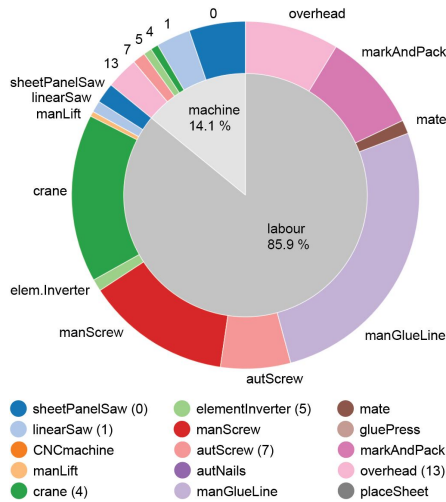


Figure 6. Distribution of production line costs (machinery and labor)

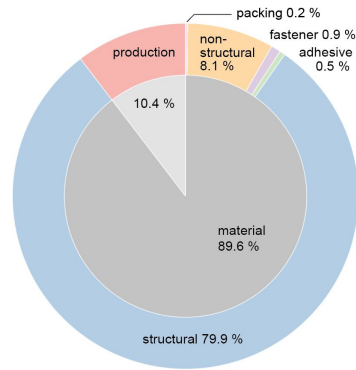


Figure 7. Overall product costs based on production activities and materials costs

4 Discussion

4.1 Principal findings

Manufacturers of timber floor elements are endeavoring to gain a market share in terms of their use in commercial buildings. Currently, a concrete hollow-core element is close to half the cost of a comparable timber floor elements (Norconsult Informasjonssystemer AS and Bygganalyse AS 2019). For timber floor elements this requires cost reduction to be pursued throughout the product details and in the stages of manufacturing. An optimization approach to this necessitates a parametric link between the specification of a product and the manufacturing expenditures. An accurate accounting of the cost of manufacturing is required to formulate methods of optimization of timber elements (Hu et al. 2006), and the environmental challenges the construction sector face, emphasize the importance of the topic. A solution to this has not been brought forward, and the present work has addressed this. The present work has developed an approach that comply with the objectives of the study. The method has certain strengths and weaknesses:

The parametric feature and the architecture of the method enable it to be implemented as a module in optimization workflows where it can be treated as an objective function for competitiveness. The method is organized to benefit from repetition of resources and activities, sections, bodies and assembly.

Accounting of manufacturing resources require initial steps to feed information into the model. The objective of the present work has been seeking to reduce these initial steps by exploiting the possibilities of utilizing information stored in the items being processed, resulting in the item-driven principle. The minimum information for defining a resource is the rate of cost as taken from the accounting figures and the power consumption, whilst the optional input is the embedded carbon emissions and the estimated service lifetime of the resource. The mandatory information for defining an activity is the SI units of the processing quantity, and the time for processing one unit of the quantity. The optional input which will enhance the precision of the accounting, is the number and type of operators, differentiation of processing time due to an index of effort, preparation and closure times, in addition to fixed costs of the activity. Due to this principle, a minimum of initial information will make the accounting run. The effort of the initial steps depends on the complexity of the production line.

Representation of minor tasks and judging which resources and activities that should be incorporated directly and which should not, can influence both the effort of implementation and the accuracy of the method. The optional input of an activity object may contribute to the representation of minor tasks that are otherwise cumbersome to deal with.

The principle of letting an item inherit an expenditure vector is comparable to have a repository added to the item where information can be added and stored. This principle has been suitable for accumulating consumed resources, and elegantly supported by object-oriented programming. The programming principle represent a potential for further development, e.g. price and wage developments.

A factory specific material database must be built where information about suppliers, delivery formats, densities, cost and embodied carbon emissions is organized. In the present work the materials database has been constructed in the form of dictionaries, which enable a product's materials provision to be associated with a choice of suppliers. The effect of selecting between different suppliers can in this way be observed directly in product resource consumption, and this feature may serve as an aid to competitiveness by revealing purchase motivation during negotiations with suppliers.

A consistent method to quantify directionality of production volumes may suffice in expressing added production time due to positioning and alignment of items. The present work has suggested an approach where a complex arrangement of volumes

is substitutes by a single directionality factor using a comprehensible term. To the authors' knowledge, no other method currently exists that reflects directionality along production lines.

4.2 Implications

An accurate parametric link between specification of a timber element and the manufacturing expenditures open several possibilities. It formalizes and document the accounting of resource consumption along the production line, and may facilitate:

- 1) systematic calibration of the manufacture expenditures,
- 2) investigations of excessive production-related resource consumption,
- 3) support in relation to Lean Manufacturing or other resource optimizing strategies
- 4) increased precision in estimated product expenditure even if the product differs from previously manufactured products.

The bottom line is the opportunity to reduce the required margins between actual expenditures and estimates offered in tenders.

4.3 Future research

The flexibility and the parametrization incorporated in the method enables a range of future studies to be performed, and a few proposals is mentioned:

- The method can be implemented in an optimization workflow, where a set of design variables (e.g. dimensions or material type) is altered by a solver to minimize an objective (e.g. cost or carbon emissions), whilst constraining serviceability performances and boundary conditions.
- Sensitivity analyses of how product competitiveness is responding to price developments of materials and salaries.
- The principle of separating activities in levels of completion is a useful feature and increase control of the accounting. In the present work a separation in “Body Level” and “Assembly Level” is performed, but this may be extended. Furthermore, the pointOfProcess associated with a body also enables the method to separate between location of activities. This feature can be used to extend the accounting from the factory gate to as built. It may include transportation, installation, and completion, where resources and activities and pointOfProcess is defined accordingly.
- An interface to Computer Aided Manufacturing (CAM) where geometry and material definitions can be retrieved will ease implementation.

5 Conclusion

A method called Item-Driven Activity-Based Consumption (IDABC) is developed in the present work. In compliance with the objective the method enables a parametric link to be generated between the specification of a timber element and the quantification of manufacturing expenditures. Also, in compliance with the objective, the output of the method serves to quantify competitiveness in terms of production time, total cost, labor cost and carbon emissions.

The parametric architecture of the method enables the implementation in an optimization workflow for timber elements. This has been the main motivation and the paramount objective of the present work, and is a response to missing efforts in the research and the ongoing endeavor of improving timber elements.

Attention to means of reducing implementation effort, as addressed in the objective, led to the item-driven approach that utilizes information stored in the items being processed.

As a worked example the present study is using a timber floor element. However, irrespective of materials and production line operations, the method can be applied to generic products that involve the systematic repetition of body manufacture leading to a final assembly process. As such the IDABC method offers indeterminacy and flexibility in production line accounting.

Definition of resources and activities in the present work was performed following interviews with a Production Line Manager who has a thorough understanding of the operations that take place on the production line. The method has been applied to a specific timber component and assembly line operated by a major manufacturer in Norway and demonstrates good agreement with empirical data.

Acknowledgements

This work is part of a four-year project called “WoodSol” (Wood frame solutions for free space design in urban buildings), funded by a grant (254699/E50) from the Research Council of Norway, whose support is gratefully acknowledged. The authors would also like to express their thanks for the contributions made by fellow doctoral students Aivars Vilguts and Simone Conta during the preparation and execution of this work. We also extend our acknowledgement and gratitude to Åge Holmestad at the company Moelven Limtre AS for valuable discussions during calibration of the method.

Literature cited

- Akintoye, A. 2000. Analysis of factors influencing project cost estimating practice. *Constr. Manag. Econ.* 18(1): 77-89.
- Andersch, A., U. Buehlmann, J. Palmer, J. Wiedenbeck and S. Lawser. 2013. Product Costing Program for Wood Component Manufacturers. *Forest Prod. J.* 63(7/8): 247-256.
- Andersch, A., U. Buehlmann, J. Palmer, J. K. Wiedenbeck and S. Lawser. 2014. Product Costing Guide For Wood Dimension And Component Manufacturers. U. S. D. o. Agriculture, U.S. Forest Service.
- Cai, W., F. Liu, O. Dinolov, J. Xie, P. Liu and J. Tuo. 2018. Energy benchmarking rules in machining systems. *Energy* 142: 258-263.
- de Souza Zanuto, R., A. Hassui, F. Lima and D. A. Dornfeld. 2019. Environmental impacts-based milling process planning using a life cycle assessment tool. *J. Clean. Prod.* 206: 349-355.
- Del Borghi, A. 2013. LCA and communication: environmental product declaration. *Int. J. Life Cycle Assess.*
- Dixon, T., J. Connaughton and S. Green. 2018. Sustainable Futures in the Built Environment to 2050: A Foresight Approach to Construction and Development, John Wiley & Sons.
- Drury, C. 1992. Activity-based costing. *Management and Cost Accounting*, Springer: 273-288.
- Du, Y., Q. Yi, C. Li and L. Liao. 2015. Life cycle oriented low-carbon operation models of machinery manufacturing industry. *J. Clean. Prod.* 91: 145-157.
- Durga Prasad, K. G., K. Venkata Subbaiah and K. Narayana Rao. 2014. Multi-objective optimization approach for cost management during product design at the conceptual phase. *J. Ind. Eng. Int.* 10(1).
- Hertwich, E. G., S. Ali, L. Ciacci, T. Fishman, N. Heeren, E. Masanet, F. N. Asghari, E. Olivetti, S. Pauliuk and Q. Tu. 2019. Material efficiency strategies to reducing greenhouse gas emissions associated with buildings, vehicles, and electronics—a review. *Environmental Research Letters* 14(4): 043004.
- Hill, C. A. S. and J. Dibdiakova. 2016. The environmental impact of wood compared to other building materials. *Int. Wood Prod. J.* 7(4): 215-219.
- Hoozée, S. and S. C. Hansen. 2014. A comparison of activity-based costing and time-driven activity-based costing. *J. Manag. Account. Res.* 30(1): 143-167.
- Howard, A. F. 1988. Modeling sawmill production, costs, and profitability as a guide to preparing bids for timber. *Forest Prod. J.* 38(3): 29-34.
- Hu, L., R. Tang, Y. Liu, Y. Cao and A. Tiwari. 2018. Optimising the machining time, deviation and energy consumption through a multi-objective feature sequencing approach. *Energy Convers. Manag.* 160: 126-140.

- Hu, L. J., R. Desjardins and E. Jones. 2006. Systems approach for optimizing wood-based floor construction. 9th World Conference on Timber Engineering 2006, Portland, OR, United states, Oregon State University Conference Services.
- Kalaiarasi, K. and E. Rajarathnam. 2015. Optimization of multi objective fuzzy integrated inventory model with demand dependent unit cost and lead time constraints. *Int. J. Appl. Eng. Res.* 10(2): 4707-4721.
- Kaplan, R. S. and S. R. Anderson. 2003. Time-driven activity-based costing. Available at SSRN 485443.
- Kaplan, R. S. and S. R. Anderson. 2004. Time-Driven Activity-Based Costing. *Harv. Bus. Rev.* 82(11): 131-138.
- Klanšek, U. and S. Kravanja. 2006. Cost estimation, optimization and competitiveness of different composite floor systems—Part 1: self-manufacturing cost estimation of composite and steel structures. *J. Constr. Steel Res.* 62(5): 434-448.
- Liu, Z., Y. Guo, H. Cao, G. Zhao and Z. Liu. 2017. Embodied energy in dry cutting under consumption of tool and materials. *Procedia CIRP* 61: 535-540.
- Mela, K. and M. Heinisuo. 2014. Weight and cost optimization of welded high strength steel beams. *Eng. Struct.* 79: 354-364.
- Moore, L. and R. Creese. 1990. Manufacturing Cost Estimation. *Cost Eng.* 32(5): 17.
- Namazi, M. 2016. Time Driven Activity Based Costing: Theory, Applications and Limitations. *Iran. J. Manag. Stud.* 9(3): 457-482.
- Norconsult Informasjonssystemer AS and Bygganalyse AS. 2019. Norsk prisbok: et oppslagsverk for byggebransjen. Sandvika, Norconsult informasjonssystemer AS i samarbeid med AS Bygganalyse.
- Pomponi, F. and A. Moncaster. 2016. Embodied carbon mitigation and reduction in the built environment – What does the evidence say? *Journal of Environmental Management* 181: 687-700.
- Ratnasingam, J., T. Ma and M. Perkins. 1999. Productivity in wood machining processes—a question of simple economics? *Eur. J. Wood Wood Prod.* 57(1): 51-56.
- Röck, M., M. R. M. Saade, M. Balouktsi, F. N. Rasmussen, H. Birgisdottir, R. Frischknecht, G. Habert, T. Lützkendorf and A. Passer. 2020. Embodied GHG emissions of buildings – The hidden challenge for effective climate change mitigation. *Applied Energy* 258: 114107.
- Schlömer, S., T. Bruckner, L. Fulton, E. Hertwich, A. McKinnon, D. Perczyk, J. Roy, R. Schaeffer, R. Sims and P. Smith. 2014. Annex III: Technology-specific cost and performance parameters. *Climate change*: 1329-1356.
- Schudeleit, T., S. Züst, L. Weiss and K. Wegener. 2016. The Total Energy Efficiency Index for machine tools. *Energy* 102: 682-693.

Shin, S.-J., J. Woo and S. Rachuri. 2017. Energy efficiency of milling machining: Component modeling and online optimization of cutting parameters. *J. Clean. Prod.* 161: 12-29.

Thies, C., K. Kieckhäfer, T. S. Spengler and M. S. Sodhi. 2019. Operations research for sustainability assessment of products: A review. *Eur. J. Oper. Res.* 274(1): 1-21.

UN Environment and International Energy Agency (IEA). 2017. Towards a zero-emission, efficient, and resilient buildings and construction sector. Global Status Report 2017.

Velarde, G., A. Pirraglia, H. Van Dyk and D. Saloni. 2011. Lean manufacturing in the US South Atlantic Region: An overview of the current state of implementation in the secondary wood industry. *Int. Wood Prod. J.* 2(1): 30-37.

Yongqian, Z., C. Meng, Y. Xuebo and Z. Jin. 2010. A manufacturing cost estimation method based on activity-based costing. 2010 International Conference on Mechanic Automation and Control Engineering, IEEE.

Annex A. Floor element specifications

Table 5. Specification of the bodies making up the assembly

	h	w	l	material	appliance	mass	vol.	cost	CO ₂
	[m]					[kg]	[m ³]	[€]	[kgCO ₂ e q]
topFlg	0.043	2.400	9.000	Kerto_Q	structural	473.7	0.929	743.04	90.00
edgJst0	0.405	0.140	9.000	GL30c	structural	219.4	0.510	306.18	23.92
edgJst1	0.405	0.140	9.000	GL30c	structural	219.4	0.510	306.18	23.92
edgBeam0	0.405	0.140	2.120	GL30c	structural	51.7	0.120	72.12	5.63
edgBeam1	0.405	0.140	2.120	GL30c	structural	51.7	0.120	72.12	5.63
fldJst0	0.405	0.066	8.720	GL28c	structural	100.2	0.233	139.85	10.93
fldJst1	0.405	0.066	8.720	GL28c	structural	100.2	0.233	139.85	10.93
fldJst2	0.405	0.066	8.720	GL28c	structural	100.2	0.233	139.85	10.93
btmFlg0	0.061	2.400	9.000	Kerto_Q	structural	672.0	1.318	1054.08	127.68
adhesive	1	10.068	0.001	Phenol-resorc.	adhesive	5.034	5.033e-3	17.62	5.03
internalMass0	0.094	0.480	8.720	Gravel 8/16	nonStructural	539.4	0.394	59.06	1.62
internalMass1	0.094	0.480	8.720	Gravel 8/16	nonStructural	539.4	0.394	59.06	1.62
internalMass2	0.094	0.480	8.720	Gravel 8/16	nonStructural	539.4	0.394	59.06	1.62
internalMass3	0.094	0.480	8.720	Gravel 8/16	nonStructural	539.4	0.394	59.06	1.62

Table 6. The fastening vector appended to selected bodies

	Ø	l	number	mass	vol.	cost	CO ₂	Type of fastener
	[m]			[kg]	[m ³]	[€]	[kgCO ₂ e q]	
topFlg	0.005	0.1	150	2.30	295e-6	15.00	8.61	Partial thread flange head
edgBeam0	0.008	0.28	12	1.32	169e-6	1.20	4.94	Double-threaded
edgBeam1	0.008	0.28	12	1.32	169e-6	1.20	4.94	
fldJst0	0.008	0.132	4	0.21	27e-6	0.40	0.78	
fldJst1	0.008	0.132	4	0.21	27e-6	0.40	0.78	
fldJst2	0.008	0.132	4	0.21	27e-6	0.40	0.78	
btmFlg0	0.005	0.1	150	2.30	295e-6	15.00	8.61	Partial thread flange head

1.4 Paper IV

Optimisation of costs and carbon emission of timber floor elements

Sveinung Nesheim, Kristo Mela, Kjell Arne Malo, Nathalie Labonnote

For publication in: Engineering Structures

Submitted: 18th February 2021

Accepted: Buoyantly awaiting

Credit author statements

For the Original article presented herein, all authors have contributed to its preparation as described in the below statement:

Sveinung Nesheim: Conceptualization, Methodology, Software, Validation, Formal analysis, Investigation, Resources, Writing - Original Draft, Writing - Review & Editing, Visualization.

Kristo Mela: Methodology, Software, Validation, Investigation, Writing - Original Draft, Writing - Review & Editing.

Kjell Arne Malo: Writing - Review & Editing, Supervision, Project administration, Funding acquisition.

Nathalie Labonnote: Writing - Review & Editing, Supervision.

Optimisation of costs and carbon emission of timber floor elements

Abstract

Long-span timber floor elements increase the adaptability of a building and they exhibit a significant market potential. High cost of the floor elements is a challenge, and the timber sector is under substantial pressure to find more economical solutions without weakening otherwise favourable environmental performance. The range of technical timber-based materials and components, structural typologies, overlays and ceiling systems represent an immense solution space when searching for a competitive design for a specific building application. Finding the optimum solution requires a computational procedure. In this study a recent development for the accounting of manufacturing resources for timber elements is utilized to build an optimisation framework for cost and ECO₂ minimisation of timber floor elements finalized at the factory gate. The design of the element is formulated as a discrete optimisation problem which is solved by a mixed-integer sequential linearization procedure. Various material combinations and constraint combinations are treated. The optimisation framework provides a tool for rapid design exploration that can be used in general design situations. The results of the calculations carried out in this study provide insight on the general trends of optimum floor elements. The optimisation model is used to analyse the characteristics of the optimum designs, and a comparison between the current and the second generation of Eurocode 5 is shown to demonstrate achievable implications.

Keywords

Cost optimization, carbon emission optimisation, long-span, timber floor, mixed-integer sequential linearization procedure (MISLP), Item-Driven Activity-Based Consumption (IDABC), second generation Eurocode 5, competitiveness.

1 Introduction

The built environment is significantly contributing to the climate change today and represents therefore a substantial opportunity for mitigating it tomorrow. The role of the construction sector must increasingly be addressed as a measure to decelerate global warming [1]. Currently this sector is strongly identified with negative climatic

impact, accounting for 36 % of the global energy use and an associated 39 % of the carbon dioxide emissions [2]. Even as 85% of the buildings we will inhabit in 2050 are already built [3], the construction sector is expected to erect some 230 billion square metres of new construction over the next 40 years [2]. The challenge is substantial, and the greenhouse gas (GHG) emissions related to the construction sector are likely to be doubled by 2050 [4]. The last three decades the GHG emissions from the construction sector have increased with 55% and are currently one of the three fastest growing sources [5].

It is a general understanding that the widely agreed emission reduction targets [6] cannot be met without appropriate actions in the construction sector. A recent study on material efficiency for reducing GHG in the construction sector [6] has examined various strategies such as more intensive use of materials, lifetime extension of buildings, light-weight design, and reuse of building components.

Another possibility is to develop new products that meet the imposed technical requirements while simultaneously being economically competitive with reduced GHG emissions. Such elements exhibit a substantial market potential, and the timber sector is endeavouring to gain market shares for commercial building applications. However, there exist no competitive timber flooring systems for this segment, and the potential advantages in carbon emissions must be accompanied with suitable costs. It has been shown that the cost of timber floor elements can be nearly twice the cost of a comparable concrete hollow-core element [7], and the additional challenges of acoustics and serviceability performance are causing the construction sector to be reluctant to accept timber floor elements widely [8]. For timber to become an attractive building material in this market, innovative, competitive and industrialized concepts with high technical qualities and minimal economic risks and investments need to be developed, documented and made readily available.

Timber flooring systems for long-span applications are normally glued thin flange elements with stiffeners and joists constituting the core. The number of joists and stiffeners, the internal added weight and insulation, and the dimensions of all members result in numerous potential combinations to be examined. This number increases drastically when the range of wood products and types of bonding are considered. When outfitting such as overlays and ceiling system is addressed, the number of combinations increases further. And finally, when support and load conditions and serviceability performance levels are regarded, the solution space is immense. With these many parameters, finding a competitive design may not be manageable by manual exploration, and the solution space can in practice only confidently be investigated when assessed computationally.

Timber structures have been optimised for greater material efficiency in [9, 10], with the conclusion that the required amount of material in a construction can be

substantially reduced, but the study does not reflect the resources of manufacturing nor the environmental impact from reduced potential reuse. Incorporating the total manufacturing cost and the environmental impact of the floor element in optimisation are identified as main issues for the present work. For steel structures, cost optimisation has been widely employed in the literature. In [11] a cost centre approach is used which resembles the cost accounting method used in the present work. The minimum cost designs of steel floors are obtained in [12], taking into account the cost of material, labour, equipment, overhead and including profit as well. In [13] the cost objective of composite floors is based on simple summation of costs of accrued material and manufacturing processes. The minimum cost is investigated in terms of how a change in steel price would affect the different structural principles that the composite floor is based on.

In a study by Mahn et al [14] optimisation of wooden floors is conducted in terms of acoustic performance, and in the context of increasing market impact of timber floors. The conclusions of the study are in line with the general concern of a low market share of timber floors. However, no further findings in the study offer support to the present work. Acoustic performance of timber floors is studied in [15], where a comparable hollow-core timber floor is parametrically described and optimised for sound insulation. It is reported that the various parameters could not simultaneously be minimised, leading to the definition of a compromise. A probabilistic robustness analysis based on the Pareto front of two significant parameters was performed to find the optimum compromise.

Optimisation is useful also when there are conflicting criteria, and when different objectives cause disagreeing designs. This is also the case for timber floor elements. Then, the methods of multiobjective optimisation can be employed, for example, to consider cost management such as in [16], where three conflicting criteria (target costing, value engineering and quality function deployment) are integrated in a single-objective optimization to balance cost, functionality and customer satisfaction of a product.

One of the challenges of long-span timber floors has been uncertainties in vibration performance. Unless idealised support conditions and simple floor element construction, the assessment may require numerical analyses. However, the method as proposed for the second generation of Eurocode 5 [17, 18] is based on research efforts over the last 30 years, resulting in a new and rigorous analytical calculation procedure. In the present work the optimisation is based on this method, and the performance is compared to a common analytical method of serviceability [35, 36].

In this study, the cost and ECO2 minimisation of a novel timber floor element is presented, and the design approach is formulated as an optimisation problem that is solved by an appropriate method. The manufacturing cost and ECO2 of the element

are taken as objective functions, and they are evaluated by the parametric accounting method of resources in the manufacturing of timber elements, developed in [19]. This workflow is in accordance with the conclusions of Forintek and the Canadian Wood Council [20] stating that a precise manufacturing cost accounting in combination with an optimisation workflow can offer an efficient solution for the development of competitive timber floor elements.

A mixed-integer sequential linearization procedure is employed to solve the formulated discrete optimisation problem. Various material combinations and constraint combinations are treated. The optimisation model is used to perform a parametric study for alternating span of the element. The results of optimisation are used to analyse the characteristics of the optimum floor element designs.

The objective of the present work is to assist in commercialisation of timber floor elements suitable for adaptable building applications. The optimisation framework provides a tool for rapid design exploration that can be used in general design situations. Moreover, the results of the calculations carried out in this study provide insight on the general trends of optimum floor elements.

The paper is organised as follows. In Section 2, the timber floor element is described in detail, including the cost and ECO2 evaluation. The treated optimisation problem is presented in Section 3, followed by a computational study in Section 4. The implications of the results are discussed in Section 5. Finally, conclusions of the research are drawn in Section 6.

2 Timber floor element

2.1 Structural configuration

A simply supported timber floor element constituting a closed hollow section as shown in Figure 1 is studied. By varying material combinations and the number of joists fourteen base floors are defined. The base floor designs are created from an edging frame of joists ① and interconnecting transverse beams ②. Three or seven field members ③ are fitted between the transverse beams positioned with equal centre to centre distances between all members. In the cavities 100 kg/m² of gravel type 8/16 ④ is deposited to achieve acceptable acoustic performances. A continuous flange is structurally glued on top ⑤ and bottom ⑥ of the frame.

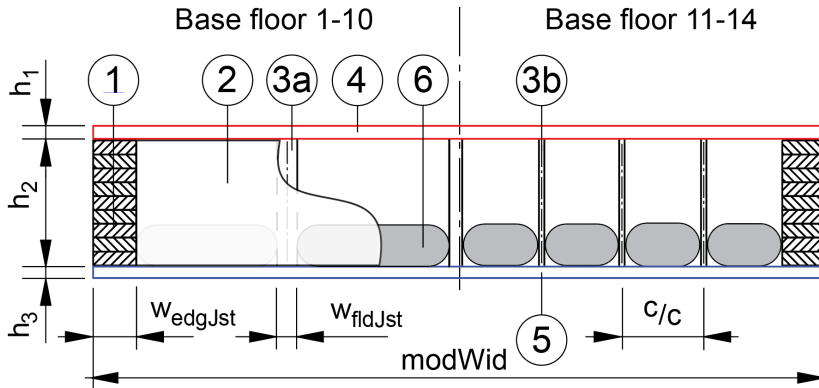


Figure 1: Cross-section of base floors including design variables of the optimisation problem

The base floors are fitted with a combination of non-structural overlay and ceiling system to acceptably estimate as built conditions. The ceiling system is designed to withstand fire exposure either as exposed bottom flange or covered by two layers of gypsum type F. The overlay is either type 1 or type 2 as indicated in Figure 2. This results in four combinations of outfitting of the base floor designs 1 to 14, generating cases 1 to 56:

- Case 1 – 14: Base floor designs with overlay type 1 and exposed ceiling
- Case 15 – 28: Base floor designs with overlay type 1 and ceiling type 1
- Case 29 – 42: Base floor designs with overlay type 2 and exposed ceiling
- Case 43 – 56: Base floor designs with overlay type 2 and ceiling type 1

In Figure 2 the associated cases of base floor 1 are shown.

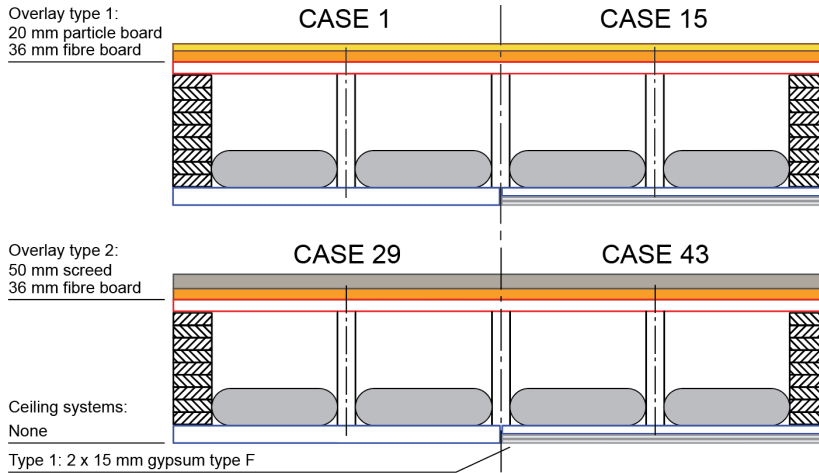


Figure 2: Outfitting of base floor

For the optimisation a constant module width (w_{mod}) of 2.4 m is used, and the design limit state is serviceability. Modifying support conditions, material specification, cavity mass, or thickness of edge beams will alter the optimization problem.

2.2 Material composition

The goal of the optimisation is to explore the potential of changing material of edge frame members ^① ^②, flanges ^④ ^⑤ and field members ^③. The materials are altered according to Table 1 to define the base floor designs. Base floor 1 is referred to as the reference floor. GL30c and GL28c is according to [21]. Laminated Veneer Lumber (LVL) in spruce (S-LVL) and beech (B-LVL) is according to [22]. Two variants of LVL are used: LVLS has unidirectional fibre orientation, while LVLQ has a 20 % of the fibres in crosswise direction. Construction plates in quality HB HLA1 (HB) and OSB3 (OSB) are used for field members [23]. In these cases, the number of field members is seven.

Table 1: Material composition and due combinations

Base floor	Edge joist and beam	Num fldJst	Field joist	Flanges	Possible combinations			
					Case 1-14	Case 15-28	Case 29-42	Case 43-56
1	GL30c	3	GL28c	S-LVLQ	44496	129024	48384	129024
2	GL30c	3	S-LVLS	S-LVLQ	32256	86016	32256	86016
3	GL30c	3	B-LVLS	S-LVLQ	40320	107520	40320	107520
4	GL30c	3	GL28c	B-LVLQ	42336	98784	42336	98784
5	GL30c	3	S-LVLS	B-LVLQ	28224	65856	28224	65856
6	GL30c	3	B-LVLS	B-LVLQ	35280	82320	35280	82320
7	S-LVLS	3	S-LVLS	S-LVLQ	9216	24576	9216	24576
8	B-LVLS	3	B-LVLS	S-LVLQ	31200	83200	31200	83200
9	S-LVLS	3	S-LVLS	B-LVLQ	8064	18816	8064	18816
10	B-LVLS	3	B-LVLS	B-LVLQ	27300	63700	27300	63700
11	GL30c	7	HB HLA1	S-LVLQ	24192	64512	24192	64512
12	GL30c	7	HB HLA1	B-LVLQ	21168	49392	21168	49392
13	GL30c	7	OSB 3	S-LVLQ	16128	43008	16128	43008
14	GL30c	7	OSB 3	B-LVLQ	14112	32928	14112	32928
Number of combinations					374292	949652	378180	949652

The various components of the floor element are available only in given dimensions. The standard delivery formats constitute the discrete values given in Table 2.

Table 2 Allowable dimension values.

Allowable dimensions		Material	Allowable values [mm]
Abbreviation	Description		
HtopFlg	Height of top flange	S-LVLQ	33,39,45,51,57,63,69,75
		B-LVLQ	20,30,40,50,60,70,80
Hjst	Height of joists	GL	90,115,135,180,225,270,315,360,405,450,495,540,585,630
		S-LVLS	200,220,240,300,360,400
		B-LVLS	120,160,200,240,280,320,360,400,440,480,520,560,600
HbtmFlg	Height of bottom flange	S-LVLS	(33,39,45,51,57,) 63,69,75
		B-LVLS	(20,30,40,50,) 60,70,80
Wedge	Width of edge joists	GL	36,48,66,73,90,115,140,165,190,215,140,260
		S-LVLS	27,33,39,45,51,57,63,75
		B-LVLS	40,50,60,80,100,120,160,200,240,280
Wfield	Width of field joists	GL	36,48,66,73,90,115,140,165,190,215,140,260
		S-LVLS	27,33,39,45,51,57,63,75
		B-LVLS	40,50,60,80,100,120,160,200,240,280
		HB	7,8,9,10,11,12
		OSB	12,15,18,22

The bottom flange is intended either to be exposed to fire or covered by two layers of 15 mm gypsum type F. Rules for structural fire design [24] with guidance from [25], [26] and chapter 11 in the Norwegian technical requirements for construction works [27] are used to calculate the required thickness. Hazard class 4 and fire class 3 are used, presupposing a complete fire scenario of 90 minutes. The design philosophy is that the floor element shall have the capacity to withstand actions of accidental limit state without the bottom flange present. The minimum thickness of

the bottom flange material is then calculated from the charring rate of the material for the fire scenario. Both spruce LVLQ and beech LVLQ have charring rate of 0.65 mm/min leading to a minimum thickness of 59 mm for exposed bottom flange (leaving the dimensions in brackets out of Table 2, or 19.5 mm when two layers of gypsum type F is used as ceiling system. Restraining internal mass from fire exposure is not considered.

2.2.1 Design variables

The optimisation problem described below in Section 3 consists of an objective function that is to be minimised with respect to chosen design variables subject to given constraints. The structural responses used as constraint or objective functions are written as functions of the design variables. Therefore, the relevant responses used in design are written here in the form $f(\mathbf{x})$, where \mathbf{x} is the vector of design variables. This vector consists of five dimensions of the cross-section (see Figure 1 for the definition of symbols):

$$\mathbf{x} = \{h_1 \quad h_2 \quad h_3 \quad w_{edgJst} \quad w_{fldJst}\} \quad [mm] \quad \text{Eq. 1}$$

The design variables are discrete such that $h_1 \in H_{topFlg}$, $h_2 \in H_{jst}$, $h_3 \in H_{btmFlg}$, $w_{edgJst} \in W_{edge}$, and $w_{fldJst} \in W_{field}$. The corresponding allowable values are given in Table 2.

2.3 Essential structural properties

For the formulation of the optimisation problem, the objective functions of the floor element are retrieved at factory exit, whereas the constraints are derived from the governing design requirements. Floor element design is generally stiffness-driven, and the constraints are defined to reflect serviceability, and not ultimate limit resistance. For comparison two methods are used to define the serviceability constraints. Additionally, building height is included as a constraint because of the financial importance the parameter has for tall timber building projects. In the following, the equations for calculating the relevant structural responses are presented.

Longitudinal and transversal bending stiffness (EI) is calculated with simple linear elasticity as stated in Eurocode 5 Rules for buildings [28] section 7.3.3, with effective width of flanges b_i and position of neutral axes (a_i) calculated accordingly. Note that the properties and method of execution for the structural connection between flange and field joist differs depending on the thickness of the joist. If the thickness is 36 mm and above, the structural connection is glued and screwed. If the member is less than 36 mm, a tapered slice is machined in the flanges and the field members (webs) are glued in this slice. These are definitions entered into the

IDABC-method for the floor element application [19]. Due to the diverse methods the factor for composite effect (γ) is herein defined at a constant 1.0.

$$EI(\mathbf{x}) = \sum_{i=1}^3 (E_i I_i + \gamma_i E_i A_i a_i^2) \quad , \text{ where } A_i = h_i b_i \quad \text{Eq. 2}$$

2.3.1 Element depth

The depth of a floor element is an essential cost parameter for building projects. In this study, the element depth is taken as a constraint, and it is used in Pareto analyses to see the effect on cost and ECO2 as the element depth is constrained. The element depth is simply the sum of the layer thicknesses:

$$h_{CHS}(\mathbf{x}) = h_1 + h_2 + h_3 \quad \text{Eq. 3}$$

2.3.2 Fundamental frequency

Controlling the vibrations of the floor element in serviceability limit state is a key design requirement, and it is expressed in terms of the fundamental frequency, f_1 , which is calculated according to [18] section 9.3.4 as follows:

$$f_1(\mathbf{x}) = k_{e,2}(\mathbf{x}) \frac{18}{\sqrt{w_{sys}(\mathbf{x})}} \quad \text{Eq. 4}$$

System deformations due to self-load, $w_{sys}(\mathbf{x})$, are calculated as

$$w_{sys}(\mathbf{x}) = \frac{5 \cdot g(\mathbf{x}) \cdot L^4}{384 \cdot EI_L(\mathbf{x})} + \frac{g(\mathbf{x}) \cdot L^2}{8 \cdot GA_L(\mathbf{x})} \quad \text{Eq. 5}$$

The frequency multiplier $k_{e,2}$ is calculated to reflect the effect of the transverse floor stiffness as reproduced in Eq. 6. For the present work the system width of the flooring system (B) is defined at a constant $1.5L$, where L is the span.

$$k_{e,2}(\mathbf{x}) = \sqrt{1 + \left(\frac{L}{B}\right)^4 \frac{D_T(\mathbf{x})}{D_L(\mathbf{x})}} \quad \text{Eq. 6}$$

The apparent stiffness (D) of flooring system is the bending stiffness of a section divided by the extent of the section [Nm^2/m]. The apparent bending stiffness longitudinal (D_L) and transversally (D_T) in given in Eq. 7 and Eq. 8.

$$D_L(\mathbf{x}) = \frac{EI_L(\mathbf{x})}{w_{mod}} \quad \text{Eq. 7}$$

$$D_T(\mathbf{x}) = \frac{EI_{T,midSection}(\mathbf{x})}{L_{midSection}} \quad \text{Eq. 8}$$

$L_{midSection}$ is the length of the mid-section in direction of span (L). In the present work where the floor element has only one compartment in the longitudinal direction, and where transverse beams only are located at the end of the floor element, the length of the mid-section is defined at half the span length of the floor element.

2.3.3 Unit load deflection

Mid span deflection due to a unit point load is used to assess serviceability in the methods of serviceability applied herein. The calculated deflection is strongly influenced by the support conditions and the analytical representation of the deflection. The present work applied the Winkler theorem for describing beams on elastic foundation [29, 30] in order to improve the representation of two-way deflection from unit point load at midspan (Eq. 9).

$$p = \frac{d^4 w(\mathbf{x})}{dx^4} + k \cdot w(\mathbf{x}) \quad \text{Eq. 9}$$

This is done by equating a fictitious Winkler foundation [29, 30] to the uniform deformation $w(\mathbf{x})$ caused by the floor element acting as an equivalent beam (Eq. 10).

$$w(\mathbf{x}) = \frac{p \cdot L^3}{48 \cdot EI_L(\mathbf{x})} + K_{sfd} \frac{p \cdot L}{4 \cdot GA_L(\mathbf{x})} \quad \text{Eq. 10}$$

- p : unit point load 1 kN
- K_{sfd} : constant in prediction of shear force deformations. For rectangular section, $K_{sfd} = 1.2$ [31]
- GA_L : Shear stiffness in longitudinal direction. Only longitudinal members will in practice contribute to the shear capacity from bending, i.e. edge-^① and field joists^③ in Figure 1.

By using the effective length of the transverse midsection of the floor element as the length of the foundation (L_{wink}), the Winkler foundation stiffness (k) can be expressed as:

$$k(\mathbf{x}) = \frac{p}{\frac{L_{wink}(\mathbf{x})}{w(\mathbf{x})}} \quad \text{Eq. 11}$$

Finally, the deflection constraint due to unit point load is calculated by determining the maximum deflection of the transversal cross section of the floor resting on the elastic foundation as:

$$w_{wink}(\mathbf{x}) = \frac{\beta(\mathbf{x}) \cdot p}{2 \cdot k(\mathbf{x})} \cdot \frac{2 + \cosh \beta(\mathbf{x})x + \cos \beta(\mathbf{x})x}{\sinh \beta(\mathbf{x})x + \sin \beta(\mathbf{x})x} \quad \text{Eq. 12}$$

Where

$$\beta(\mathbf{x}) = \sqrt[4]{\frac{k(\mathbf{x})}{4 \cdot EI_{T,midSection}(\mathbf{x})}} \quad \text{Eq. 13}$$

2.3.4 Dynamic response

The dynamic response of the floor element is represented by three constraints. This is the criterion by Hu and Chui [32] representing a current common practice, and the acceleration and velocity expressions as described in the proposal for the second generation of Eurocode 5 [18].

The Hu and Chui (HC) parameter is a convenient and simple expression for the fundamental frequency and unit point load deflection (Eq. 14).

$$HC(\mathbf{x}) = \frac{\left(\frac{f_1(\mathbf{x})}{18.7}\right)^{2.27}}{w_{wink}(\mathbf{x})} \quad \text{Eq. 14}$$

An approach for calculating floor response is proposed in the second generation of Eurocode 5 [17, 18]. The approach relates responses to human perception levels in terms of root mean square acceleration levels of the ISO baseline curve [33]. Acceleration levels dominate the human perception between 4 and 8 Hz. Consequently, the acceleration is used to assess floor performance levels in this frequency range and is a selected constraint (Eq. 15). The ISO baseline curve level is constant in this frequency at $a_{RMS}=0.005 \text{ m/s}^2$. For human induced vibration, this frequency range is associated with a resonant floor design because the step frequency and the associated four first harmonics may coincide with the first natural frequency of the floor element.

$$a_{rms}(\mathbf{x}) = \frac{\alpha(\mathbf{x}) \cdot F}{7 \cdot \zeta \cdot M^*(\mathbf{x})} \quad \text{Eq. 15}$$

- α Fourier coefficient $\alpha = e^{-0.4 \cdot f_1}$
- F Vertical force imposed by walking person (700 N)
- ζ Modal damping ratio of 3 %
- M^* Modal mass $M^* = \frac{mLB}{4}$
- m Mass (kg) of floor per unit area (m^2)

Due to the ratio of stiffness and mass, long-span timber floor elements typically have a first natural frequency above 8 Hz. Above 8 Hz the ISO baseline curve is not

constant (see Figure 3). As can be seen however, by integrating the baseline curve from 8 Hz, the corresponding velocity is constant at $v_{RMS}=0.0001$ m/s [17]. This new constant is used as reference for floor performance levels above 8 Hz, and is a selected constraint (Eq. 16). For floor elements with first natural frequency above 8 Hz the floor response will be transient when subject to human induced vibration.

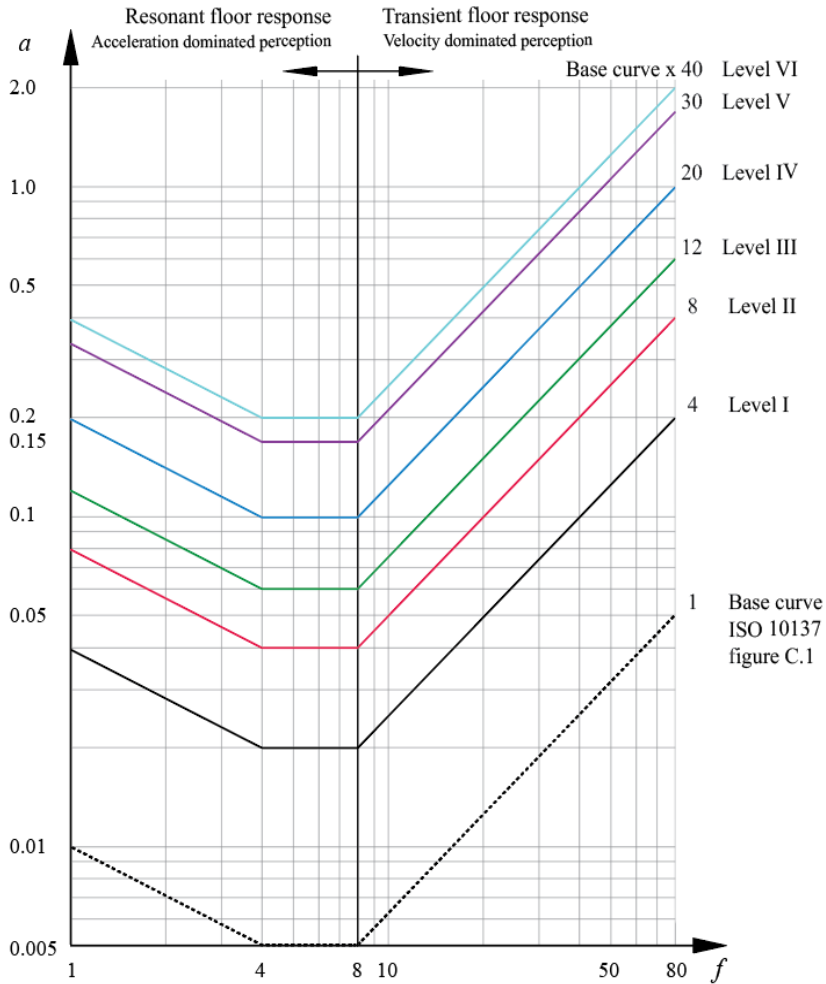


Figure 3: Floor performance levels with respect to the ISO baseline curve

$$v_{rms}(\mathbf{x}) = K_{imp}(\mathbf{x}) \cdot \frac{0.7 \cdot I_m(\mathbf{x})}{M^*(\mathbf{x}) + 70} (0.65 - 0.01 \cdot f_1(\mathbf{x})) (1.22 - 11 \cdot \zeta) \cdot \eta(\mathbf{x}) \quad \text{Eq. 16}$$

$$K_{imp} \text{ Higher modes multiplier for transient floor response } K_{imp} = \max \left\{ 0.48 \left(\frac{B}{L} \right) \left(\frac{DL}{DT} \right)^{0.25}, 1 \right\}$$

$$I_m \text{ Mean modal impulse } I_m = \frac{42 \cdot f_w^{1.43}}{f_1^{1.3}}$$

f_w Walking frequency (2 Hz)

$$\eta = \begin{cases} 1.52 - 0.55 \cdot K_{imp} & 1.0 \leq K_{imp} \leq 1.5 \\ 0.69 & \text{otherwise} \end{cases}$$

2.3.5 Final deformation

Deformation from permanent and imposed loads is a selected constraint:

$$w_{fin}(\mathbf{x}) \leq w_{maxFin} \quad \text{Eq. 17}$$

For imposed loading category of use D2 (Areas in department stores) as defined in Eurocode 1 Actions on structure [34] is used. This is used for indeterminacy as the level is covering all categories. D2 states distributed load: $q = 5000 \text{ N/m}^2$ and point load: $Q = 7000 \text{ N}$. The deformation is calculated as equivalent beam.

2.4 Economical and ecological performance

Cost and embodied carbon emissions are taken as objective functions in this study, and they are evaluated using a manufacturing expenditure accounting procedure developed in [19]. This method is called Item-Driven Activity-Based Consumption (IDABC). The method generates a parametric link between product specification and the expenditures in the manufacturing of a timber element. Expenditures cover manufacturing activities and accrued materials and it is presented as four indicators of competitiveness.

IDABC resembles the much used Time-driven Activity-Based Costing (TDABC) [35] in how the manufacturing line is modelled as resources combined to perform required activities. However, where the TDABC uses predetermined duration of activities to calculate costing, the IDABC method utilize information stored in the items subject to manufacture to calculate durations. For any item the activity requests a specific quantity based on predetermined SI unit associated with the activity, which in turn is used to calculate activity duration. Based on the duration of the activity and the definition of the activity and the underlying resources, manufacturing resources are determined.

Manufacturing of a floor element is typically divided into two parts: i) the making of components; and ii) the process of assembly. This separation is also seen in

IDABC where components are made from direct material and then assembled to a final product. As can be seen in [FPJ], an expenditure vector is generated for all items at every activity the item is subject to during the manufacturing.

The expenditure vector V_η (Eq. 18) comprise four quantities. This is the duration T_η [s], cost C_η [€], the part of cost associated with labor LC_η [€], and the ECO2 [kgCO₂eq], where η represent an item subject to an activity.

$$V_\eta = \{T_\eta \quad C_\eta \quad LC_\eta \quad ECO2_\eta\} \quad [s \quad \text{€} \quad \text{€} \quad \text{kgCO}_2\text{eq}] \quad \text{Eq. 18}$$

The total expenditure of the product is the accumulated expenditures for body level and assembly level activities. See Eq. 19.

$$V_{product} = \sum_{i=0}^{numBody} \sum_{j=0}^{numAct} V_{i,j} + \sum_{k=0}^{numAsmby} \sum_{l=0}^{numAct} V_{k,l} \quad \text{Eq. 19}$$

Specification of factory resources and activities are as defined in [19]. The conditions for applying the various activities, specification of fasteners, as well as principles of defining sections and material assignment likewise.

The cost objective is thus the total cost of the product finalized at the factory gates as offered by the wood component manufacturer $C_{product}$. The embodied carbon emissions of the product $ECO2_{product}$ have the same boundary conditions, normally referred to as cradle-to-gate, or A1 to A3 in the Environmental Product Declaration (EPD). The definition of resources and activities associated with the manufacturing of a timber element will change from one manufacturer to another, and the definition used in the present work is given in [19]. Unit cost and embodied carbon emissions of direct material are given in Annex A Table 6.

3 Optimisation

3.1 Framework

The optimisation framework consists of three modules as shown in Figure 4: i) Design premise; ii) Item-Driven Activity-Based Consumption; and iii) Optimisation. The background for the first two modules was described in Section 2. Their output is the cost and ECO2, and the constraint function values. This information is input to the optimisation module (MISLP Optimise in Figure 4). The output of the optimisation module is the optimised product. In this Section, the details of optimisation are provided.

All modules are parametric and they have been implemented using the principles of Object Oriented Programming in Python [36].

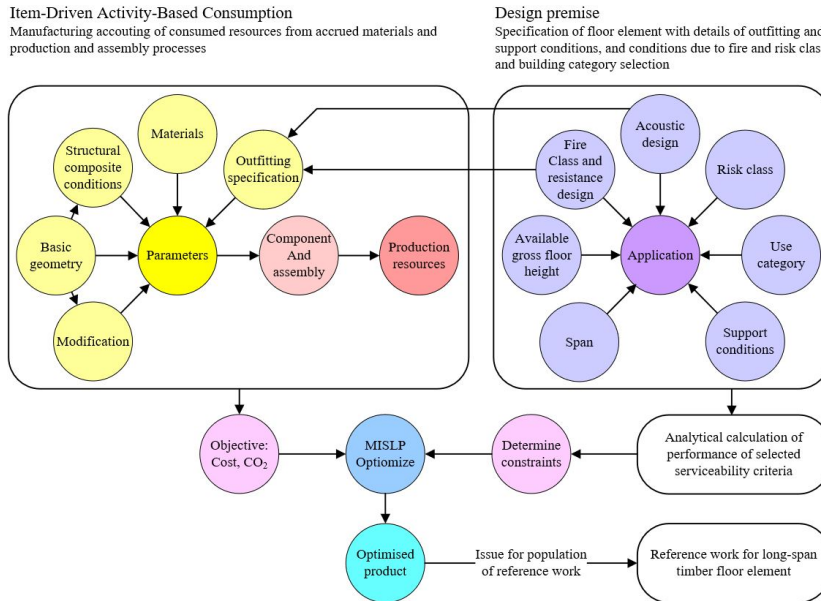


Figure 4: Calculation framework for optimisation

3.2 Problem formulation

3.2.1 Constraint combinations and levels

The constraints are derived from Section 2. The constraints are arranged in three constraint combinations (CC) each with levels as stated in Table 3. Combination 1 is the current common practice for floor element design in Norway. This is based on the Ohlsson method of the current Eurocode [28], but where the Hu & Chui term rather than the unit impulse velocity is used [37, 38]. Combination 2a and 2b is the method proposed for the second generation of Eurocode 5 [18]. Here a separation in floor response is made, where resonant floor response ($4.5 \leq f_1[\text{Hz}] < 8$) is assessed by acceleration, and transient floor response assessed by velocity ($f_1[\text{Hz}] \geq 8$).

Table 3: Constraint combinations and levels

	Current Eurocode 5 ¹⁾	Second generation of Eurocode 5	
		Resonant floor response	Transient floor response
CC	1	2a	2b
$h_{CHS,min}$ [m]	1 or changing from 0.8 to 0.3 in Pareto-analysis		
$f_{1,min}$ [Hz]	10	4.5	8
$f_{1,max}$ [Hz]	–	8	–
w_{1kN} [mm]	1.3	{0.25 0.25 0.5 0.8 1.2 1.6} ¹⁾	
Dynamic	$HC_{min} = 1$ [–]	$a_{rms,max} = 0.005 \cdot R^2$ $\left[\frac{m}{s^2}\right]$	$v_{rms,max} = 0.0001 \cdot R^2$ $\left[\frac{m}{s}\right]$
$w_{fin,max}$ [m]	$\frac{L}{200}$		

¹⁾ According to National Annex for Norway and SINTEF Building Research Design Guides [38]

^{2,3)} Array for Floor Performance Levels (FPL) 1 to 6

³⁾ Response factor levels [18]: $R(FPL) = \{4 \ 8 \ 12 \ 20 \ 30 \ 40\}$

3.2.2 Problem statement

The optimum design problem of the floor element can now be written as:

$$\min f(\mathbf{x})$$

such that:

Eq. 20

$$\begin{aligned}
 f_{1,min} &\leq f_1(\mathbf{x}) \\
 f_{1,max} &> f_1(\mathbf{x}), \text{ for CC2a only} \\
 HC_{min} &\leq HC(\mathbf{x}), \text{ for CC1 only} \\
 a_{rms,max} &\geq a_{rms}(\mathbf{x}), \text{ for CC2a only} \\
 v_{rms,max} &\geq v_{rms}(\mathbf{x}), \text{ for CC2b only} \\
 h_{CHS,min} &< h_{CHS}(\mathbf{x}) \\
 w_{1kN} &\geq w_{wink}(\mathbf{x}) \\
 w_{maxFin} &\geq w_{fin}(\mathbf{x}) \\
 h_1 &\in H_{topFlg} \\
 h_2 &\in H_{jst} \\
 h_3 &\in H_{btmFlg} \\
 w_{edgJst} &\in W_{edge} \\
 w_{fldJst} &\in W_{field}
 \end{aligned}$$

Where $f(\mathbf{x})$ is cost C or embodied carbon emissions ECO_2 of the floor element per area (m^2) as derived from Section 2. Note that some of the constraints will be removed depending on the constraint combination. The constants appearing on the left-hand side in the constraints are taken from Table 3 for each constraint combination.

The problem as stated in Eq. 20 is a discrete nonlinear optimisation problem consisting of five design variables and five or six constraints depending on the constraint combination. The problem is small-scale, and the objective and constraint

functions are evaluated effortlessly through analytical expressions. For a given structural setup (span, materials, etc.), the problem may be solved by a brute force approach, where all combinations of design variable values are enumerated. This is performed for all cases to locate the cost and ECO2 minima as well as the computational effort required, but to rationally expedite the design space exploration, the problem of Eq. 20 is solved by a suitable optimisation method. As the design variables correspond to cross-sectional dimensions, they can be relaxed and treated as continuous variables during optimisation. Moreover, the functions of the optimisation problem are continuously differentiable. This allows the use of gradient-based optimisation methods.

3.3 Mixed-Integer Sequential Linearization Procedure

The optimisation method employed in this study is based on solving a sequence of linear mixed-integer optimisation problems. This method is a discrete extension of the well-known sequential linear programming (SLP) approach [39]. At each iteration point, the nonlinear functions are approximated by their linearization. The design variables are treated as continuous variables when solving the linearization. Discrete values can be enforced by introducing binary variables as follows.

Let x be a discrete variable with the allowable values $X = \{\hat{x}_1, \hat{x}_2, \dots, \hat{x}_d\}$. Then, introduce binary variables, $y_j \in \{0,1\}$, $j = 1,2, \dots, d$. The variable x can be forced to have one of its allowable values by adding the following linear constraints to the optimization problem:

$$x = \sum_{j=1}^d \hat{x}_j y_j \quad \text{Eq. 21}$$

$$\sum_{j=1}^d y_j = 1 \quad \text{Eq. 22}$$

The latter equation ensures that exactly one binary variable takes the value 1, whereas the former equation sets the discrete value corresponding to the non-zero binary variable for x .

Each discrete variable is supplemented with its own binary variables and constraints of Eq. 21 and Eq. 22. During optimisation, the discrete variables can be treated as continuous variables. Note that also the binary variables can be relaxed, so methods employing relaxation of discrete variables can be applied.

Consider the following optimization problem

$$\begin{aligned}
& \min_{\mathbf{x}} f(\mathbf{x}) \\
& \text{such that } g_i(\mathbf{x}) \leq 0, i = 1, 2, \dots, m \\
& \quad \mathbf{Ax} \leq \mathbf{b} \\
& \quad \mathbf{Cx} = \mathbf{d}
\end{aligned} \tag{Eq. 23}$$

where g_i are nonlinear and continuously differentiable functions, and the matrices \mathbf{A} and \mathbf{C} as well as the vectors \mathbf{b} and \mathbf{d} are constants. The vector of design variables, \mathbf{x} , includes both continuous and discrete variables.

In one iteration of the *mixed-integer sequential linearization procedure* (MISLP), the original optimisation problem is linearized at the current iteration point, \mathbf{x}^k :

$$\begin{aligned}
& \min_{\mathbf{x}} f(\mathbf{x}^k) + \nabla f(\mathbf{x}^k)^T (\mathbf{x} - \mathbf{x}^k) \\
& \text{such that } g_i(\mathbf{x}^k) + \nabla g_i(\mathbf{x}^k)^T (\mathbf{x} - \mathbf{x}^k) \leq 0, i = 1, 2, \dots, m \\
& \quad \mathbf{Ax} \leq \mathbf{b} \\
& \quad \mathbf{Cx} = \mathbf{d}
\end{aligned} \tag{Eq. 24}$$

The problem of Eq. 24 is a mixed-integer linear optimisation problem (MILP), which can be solved, for example, by the branch-and-cut method that is implemented in various optimisation software packages. Even with the binary variables, this linearized problem can be considered small-scale for the timber floor optimisation problem of Eq. 20.

It is well-known that the SLP as well as the MISLP method may not converge in its basic form. The method can be stabilised by introducing so-called *move limits* that restrict the feasible set of the linearized problem. The move limits are written as additional bound constraints for the design variables. the move limits can be expressed as a portion of the total range of the variable, or in terms of local allowable change, say 15% of the current value. In any case, the move limits can be written as

$$\underline{\Delta}_i^k \leq x_i - x_i^k \leq \overline{\Delta}_i^k \tag{Eq. 25}$$

where $\underline{\Delta}_i^k$ and $\overline{\Delta}_i^k$ are the prescribed bounds. In this study, the bounds are related to the range of variable values, i.e.

$$\begin{aligned}
\underline{\Delta}_i^k &= C_1(\overline{x}_i - x_i) \\
\overline{\Delta}_i^k &= C_2(\overline{x}_i - \underline{x}_i)
\end{aligned} \tag{Eq. 26}$$

where C_1 and C_2 are constants. In this study, the initial values $C_1 = 0.5$ and $C_2 = 0.5$ were used. Over the iterations, these constants are updated by the following rule

$$C_i \leftarrow (1 - \gamma)C_i \quad \text{Eq. 27}$$

where $\gamma = 0.001$ was used in this study.

For the application of the MISLP method on the timber floor optimisation problem, binary variables are introduced as described in Eq. 21 and Eq. 22 which are the only linear constraints. Note that the binary variables appear only in the linear equality constraints that do not need linearization. For binary variables, no move limits were prescribed, but they were allowed to change from 0 to 1, or vice versa, when solving the linearized problem.

If the linearized problem is feasible, its optimum is a design, where all discrete variables attain an allowable discrete value. This feature is enabled by the binary variables. Without the binary variables, the linearized problem will likely provide a design, where the design variables non-allowable values, which means that solution process is not as efficient.

The design provided by the linearized problem may not necessarily satisfy the original nonlinear constraints. Moreover, the move limits may restrict the feasible set of the linearization such that even if its solution satisfies the original nonlinear constraints, the design may not be optimal for the original problem. Consequently, the linearization is performed sequentially until the obtained design does not change more than by a given tolerance.

For the MISLP method to begin, an initial design is required. In this study, the initial design is based on engineering judgement. The initial design for base floors 1 to 10 (three joists as field members) and 11 to 14 (seven webs as field members) is based on the cross-section of two floor element designs built and tested and used as a reference floor throughout the project that the present work is a part of. Base floor 1 and 11 have the same dimensions as the reference floors, while the initial design for similar base floors are adjusted by shifting the dimension up to the nearest matching dimension of available standard formats of associated materials.

As for the modules of objective and constraint, the modelling of the optimisation problem is performed in Python [36], and the Google AI OR-Tools for Python [40] are used to solve the MILP sub-problem.

4 Results

The performance of the MISLP optimisation technique was evaluated by comparing the design obtained by MISLP to the global minimum found by manual exploration of the solution space in all 56 cases. Both cost minimum and ECO2 minimum were compared. As seen from Table 1 the sum of possible combinations of the base floors

is $9.5 \cdot 10^5$. These combinations were run with four different outfitting giving a total of $2.65 \cdot 10^6$ combinations. The computational effort for performing this exploration is demanding. Currently a contemporary desktop computer (Intel(R) Core(TM) i7-8700 CPU at 3.20GHz with 64 GB RAM) was calculating 2.65 runs per second, requiring 395 hrs to find the optimum solutions for these cases, or on average of 600 minutes per case. In comparison the average duration of the optimisation approach was less than two seconds per case.

For the comparative study 9 m span was used and Floor Performance Level 4 was used when assessing the floor in accordance with the proposal for the second generation of Eurocode 5. The error was calculated as the ratio of the minimum found by the optimisation method to the associated global minimum found by manual exploration. In Table 4 the statistical indicators of accuracy of the optimisation method is presented. It can be concluded that in general, the MISLP approach performs very well, considering its simplicity and low computational time. The results from the manual exploration and due comparison to the MISLP optimum is given in 0.

Table 4: Indicators of accuracy of the optimisation

Deviation from global cost and ECO2 minimum	Current Eurocode 5 (with Hu and Chui)		Second generation of Eurocode 5			
	Cost	ECO2	Resonant response		Transient response	
			Cost	ECO2	Cost	ECO2
Mean error	3.81%	4.65%	1.41%	1.00%	1.83%	2.25%
Standard deviation of error	7.78%	8.73%	1.58%	1.18%	2.40%	3.49%

Optimum designs are also compared to the two reference floor elements (base floor 1 and 11). The reference floor element is an efficient design previously developed in the research programme financing the present work. For the reference floor elements, the width of the edge joists is constrained to a minimum width of 140 mm to allocate space for treaded rods. This constraint is therefore also used in the optimum case in the comparison presented in Table 5. The minimum width constraint of edge joists is not used elsewhere in the present work and is a special case to compare cost and ECO2 with the reference floor elements only. The optimum of cost and ECO2 produce the same solution for the variant of base floor 1 and 11 with minimum edge joist constraint.

Table 5: Comparison to reference floor elements

Floor element property	Base floor I		Base floor 11		
	Reference	Optimum	Reference	Optimum	
h_1 [mm]	45	33	45	39	
h_2 [mm]	405	450	405	450	
h_3 [mm]	63	63	63	63	
w_{edgeJst} [mm]	140 ¹⁾	140 ¹⁾	140 ¹⁾	140 ¹⁾	
w_{fldst} [mm]	66	48	8	7	
Cost [€/m ²]	137.58	130.40	145.74	144.75	
ECO2 [kgCO ₂ eq/m ²]	21.71	20.10	26.48	26.03	
f_1 [Hz]	10 ≤	10.16	10.17	9.67	10.06
w_{1kN} [mm]	1.3 >	0.198	0.20	0.21	0.19
HC [DL]	1 ≤	1.266	1.247	1.073	1.248
w_{maxFin} [mm]	45 ≥	16.79	16.31	18.02	16.82

¹⁾ Edge joist minimum width constrained to 140 mm

For a floor element where the transverse deflection is not a negligible contribution to overall deflection, the Winkler method is enhancing the precision and provide good estimates for the two-way deflection. On average the analytical deflection of the floor element calculated as an equivalent beam produce 60 % of the deformation computed numerically [41], whilst the Winkler theory of elastic foundation is evaluating the deflection 10 % above the deformation computed numerically. For the application in the present paper the Winkler method both provide increased accuracy and estimates to conservative side for the deflection.

Because of the discrete design variables, the optimisation will produce stepwise results. To increase the readability of the results and to better see trends, the results are plotted as a polynomial fit of degree 5 of the data points. In Figure 5 two different cases are plotted to see the difference between the optimum solution and the fitted curve. For all cases a similar fit is seen, only with slight variations due to the steps of which dimensions for the design variables is offered.

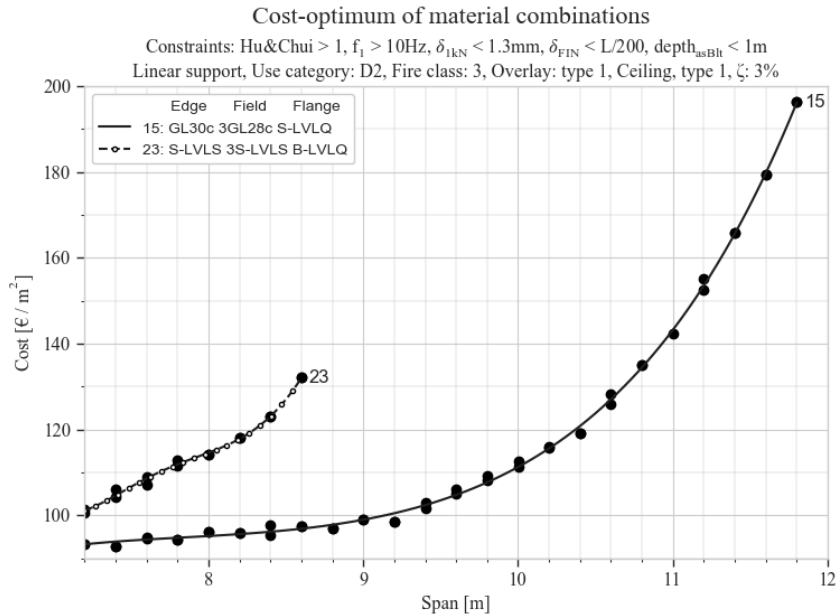


Figure 5: Optimum data points and polynomial fitted curve for cases 15 and 23.

5 Discussion

5.1 Principal findings

Fourteen base floors each with four different systems of ceiling and overlays were optimised and compared to manual exploration of global minimums of cost and ECO2. The optimisation exhibits 1) compatible interaction with modules for calculation of objectives and constraints, 2) handling of changing composition of material and outfitting, 3) handling discrete design variables, 4) high and even level of accuracy, 5) high convergence rate and consequently small calculation time.

To demonstrate the implications the method may offer the industry, the optimisation framework is applied to produce cost-optimum designs for spans associated with adaptable buildings. The span ranges from 7.2 m to 12.6 m in steps of 0.2 m. Both the current common method of serviceability [35, 36] and the method proposed for the second generation of Eurocode 5 [17, 18] are used, and comparison between the methods is also presented.

5.2 Implications

5.2.1 Cost optimum of base floor designs

Current common method based on Hu and Chui [32] is used to generate cost-optimum for base floors with overlay type 1 and ceiling type 1. Ceiling type 1 implies that the minimum thickness of the bottom flange in practice is controlled by serviceability as opposed to fire resistance. The general trend shows a low gradient for cost for spans up to about 10 meters. For greater spans, the cost increases more strongly. See Figure 6. This is associated with available edge joist heights. Flange volumes are cost-drivers, and the cost-optimum solution will increase the height of joists unless constrained. Both case 15 and 18 with glulam frame and spruce and beech LVL respectively, perform well both with respect to span and cost. Floor elements with beech LVL (case 18) are slightly more expensive than spruce LVL (case 15) but offer marginally longer spans. Only limited spans are found for cases 21 and 23 due to the limited height offered for spruce LVLS. Only certain material combinations offer span towards 12 meters.

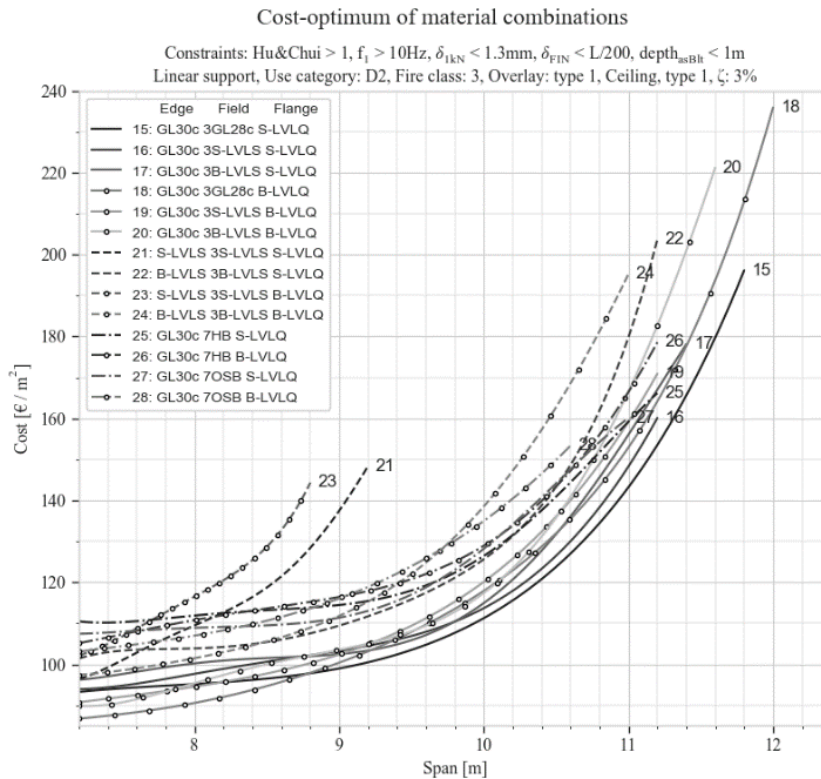


Figure 6: Cost-optimum of material combinations for cases 15 through 28.

5.2.2 Correlation of cost and ECO2

For the same cases as in 5.2.1, the embodied carbon emissions (ECO2) are plotted with respect to span in Figure 7. Both cost and ECO2 are strongly linked to the volume of accrued materials, hence the strong correlation. A regression of case 15 shows that a linear model explains 99.4 % (R^2) of the variance of the dependent variable, and that cost-optimum for most cases produce a well performing ECO2-design. As for section 5.2.1, case 15 demonstrates good performance. On the other hand, a larger variance in designs based on beech LVL can be seen. This is because the available thicknesses of spruce LVL which is offered at 6 mm steps, whilst the step is 10 mm for beech LVL. (See case 18 in Figure 7).

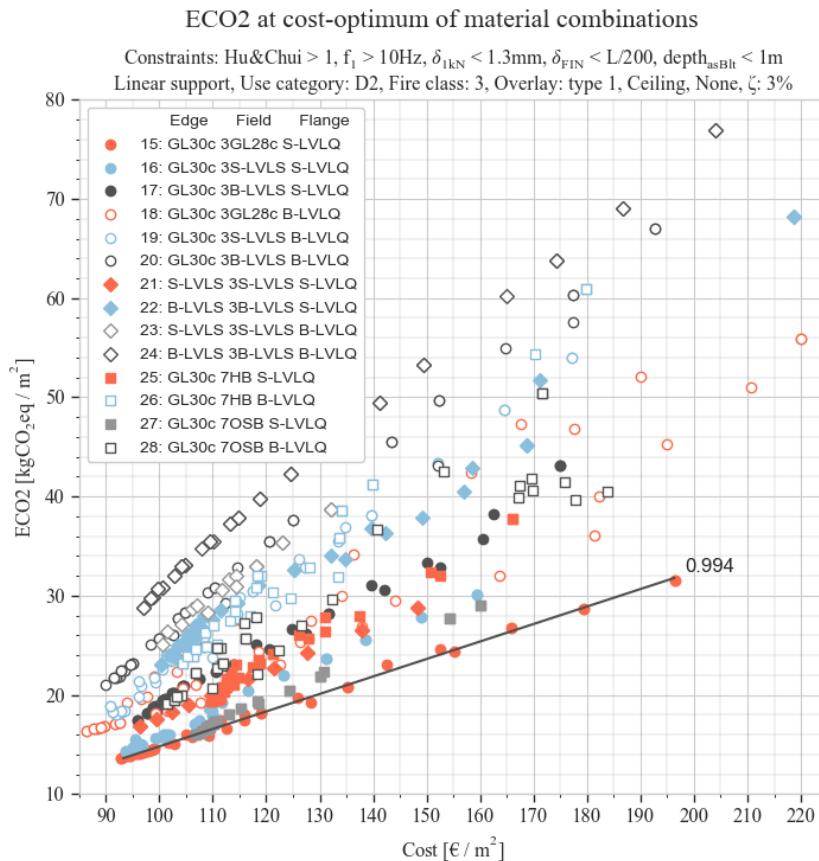


Figure 7: ECO2 at cost-optimum of material combinations for cases 15 through 28. Each marker represents a single material combination for a certain span.

5.2.3 Cost to depth ratio of cost-optimum designs

The ratio of cost to floor depth is presented in Figure 8. Both parameters are indicators of competitiveness. By consulting Figure 6, cost is increasing slowly until the available standard dimensions for the frame no longer offers increasing heights. By consulting Figure 9, the depth of the floor is also seen steadily to increase, contributing the negative gradient of the ratio. As can be shown, as increased flange thickness is dominating the design, the gradient is turning positive.

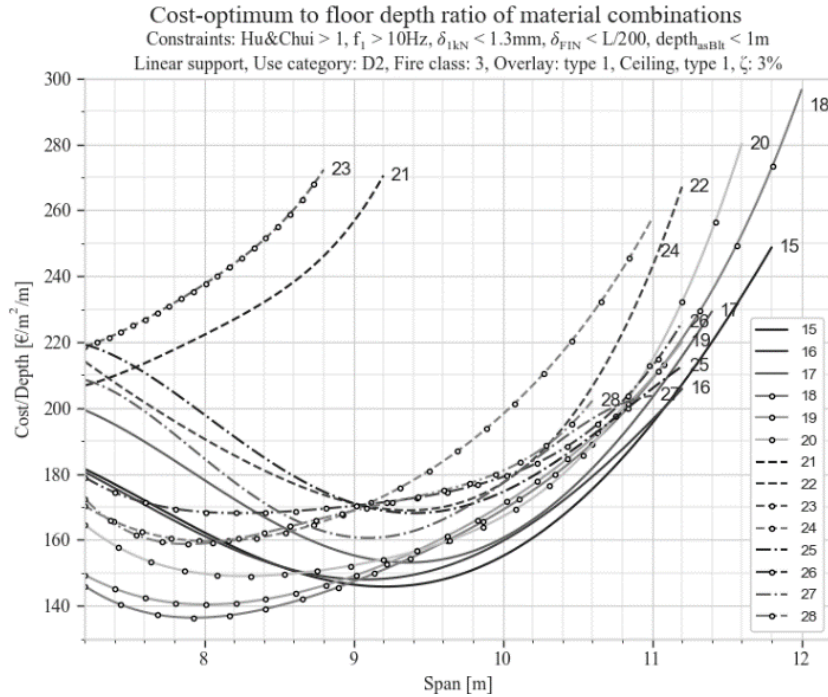


Figure 8: Cost-optimum to floor depth ratio of material combinations for cases 15 through 28.

5.2.4 Comparison of serviceability methods

To further examine effect of floor depth at cost-optimum, the current common method of Hu and Chui is compared to the new method proposed for the second generation of Eurocode for case 15 (See Figure 9). The dashed lines represent resonant floor element design ($4.5 \leq f_1[\text{Hz}] < 8$), continuous lines represent transient floor element designs ($f_1[\text{Hz}] \geq 8$), and the dash-dot line representing the current common method. Concerning the new method for the Eurocode, resonant and transient floor designs both produce the same design for performance level 4 to 6. For resonant floor design, the best performance level found is three at a minimum

span of 9 m satisfying the maximum fundamental frequency (f_1). The results suggest that lower building depths may be found for resonant floor designs with respect to both the current common method and transient floor design. The findings suggest that floor element designs with a resource-efficient solution to lowering fundamental frequency (as increased internal mass), may offer a potential for LSTFE with low building heights.

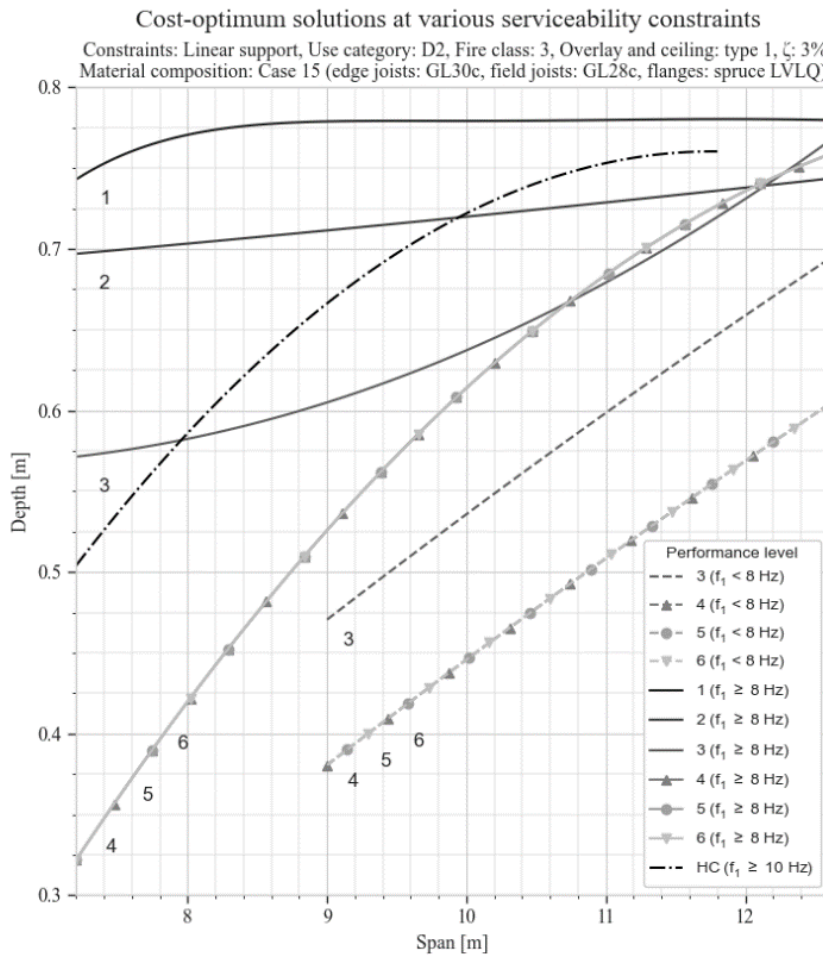


Figure 9: Cost-optimum solutions at various serviceability constraints

5.2.5 Cost to depth trade-off

The proposal for method of calculating serviceability in the second generation of Eurocode 5 [17, 18] provides flexibility in floor design by employing the ISO baseline curve [33]. The method offers flexibility in calculations by either satisfying acceleration or velocity criterion and addressing required human perception levels for a specific building project through performance levels. The performance levels also serve as a convenient parameter to consider diverse socio-cultural attitude and expectations in the national annex. In the present work the performance levels proposed for Norway are used [18]. When applying a given performance level for a floor design, the cost-optimum will produce a floor depth. However, because floor depth also is a cost indicator for a building project, the interaction between floor depth and floor element cost is interesting. Consequently, the present work has applied the optimisation framework for a trade-off analysis in the sense of multi-criteria optimisation between depth and cost. In Figure 10 the cost-optimum designs are presented for performance levels 1 to 6 for transient floor design, as floor depth is constrained from 0.8 m to 0.3 m in steps of 2 mm. As can be seen, depending on the performance level, the floor element cost increase as the floor depth is constrained. Generally, the ratio of cost to depth is increasing with increasing span. For performance level 1 at 8.4 m, reducing depth from 0.75 m to 0.5 m is associated with a 10 % cost, whilst at 11.4 m reducing depth by 0.1 m is associated by an additional cost of 25 %.

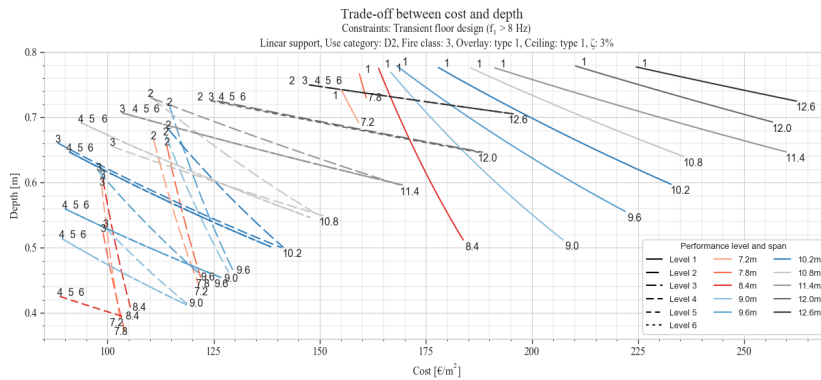


Figure 10: Trade-off between cost and depth

5.2.6 Cost and ECO2 as built

The cost and ECO2 used as objective function in the optimisation framework cover manufacturing activities and accrued materials until the floor element is ready for transport at the factory gates. Associated as-built levels of cost and ECO2 requires further calculations of cost and ECO2 of activities including transport, installation and completion on-site. This is not covered in the present work, but projected levels of materials specified for as-built are presented in this section. In Figure 11 cost and ECO2 for the floor element at factory gate are presented as bottom bars and bottom horizontal line. Cost and ECO2 of material added to the floor on site is presented as the top bar for the cost, and as the black line with top horizontal line for ECO2.

In this chart base floor 1 is used with four different outfitting. See Figure 2 for a reminder of cases 1, 15, 29 and 43. As expected, the 50 mm screed contributes considerably to the ECO2 (cases 29 and 43), as well as the 2 x 15 mm gypsum type F (see case 1 compared to case 15). The latter may argue the case of using timber rather than gypsum in the fire resistance design when this is an option due to the ECO2 benefits of avoiding gypsum. The observed cost-optimum benefits from a heavy non-structural plate is caused by the effect the increased mass has on the serviceability criteria. However, the excessive cost is gained when adding the cost of the screed. The additional cost of installation will further increase this cost. For 7.2 m case 1 and 43 is explained by specific numbers:

The cost of the floor element at factory gate is 104 and 96 €/m² for cases respectively. When including required material for completion on site the costs are risen to 130 and 126 €/m². The weight of the screed of case 43 causes the serviceability constraint to be accepted with less structural timber than for the lighter floor element of case 1.

For the ECO2 the competitive figures are different. The increased structural timber of case 1 results in ECO2 of 17 kgCO₂eq/m² whilst case 43 contains 14 kgCO₂eq/m² as delivered from factory. The ECO2 figures as installed are respectively 23.5 and 48.5 kgCO₂eq/m².

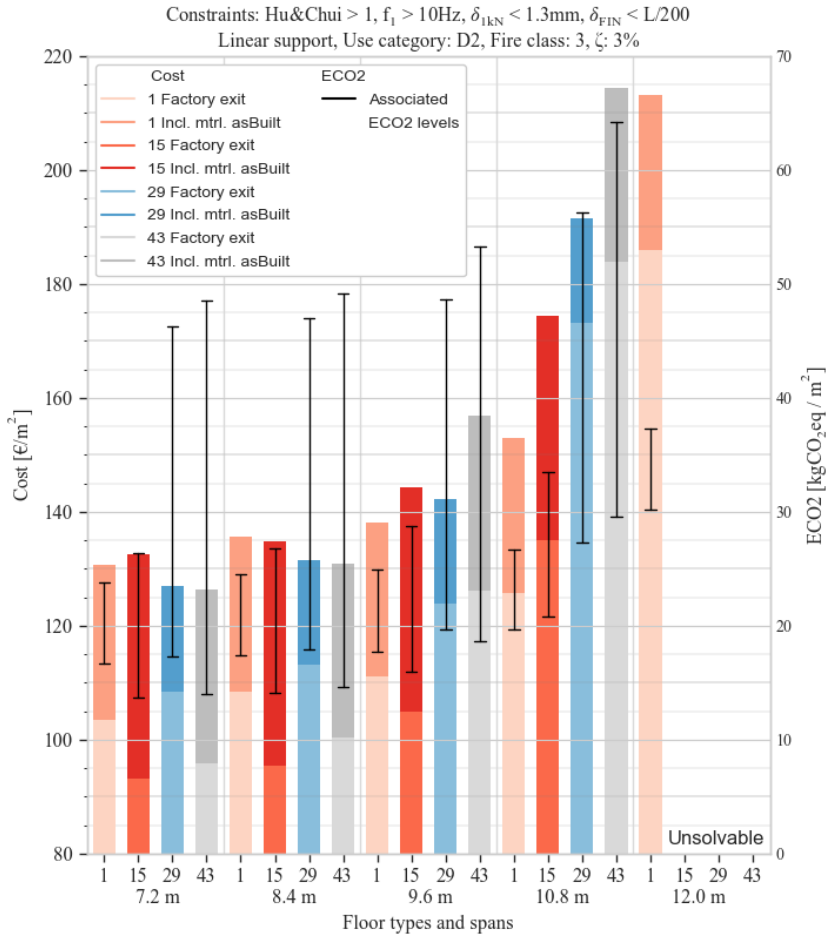


Figure 11: Projected levels of cost and ECO2 due to additional materials (base floor 1 with four different outfitting)

5.3 Future research

Effect of transverse stiffeners are not included in the study, nor is the effect of changes of the edge beams. The effect of changes in these members will not be properly be reflected in an analytical assessment of the floor element performance. The optimisation algorithm must therefore be implemented in a workflow where a numerical representation of the floor element is calculating serviceability performance, preferably using probabilistic methods of load modelling to lower the computational time to a level feasible of producing data for a reference work [42].

6 Conclusions

The optimisation workflow implemented in this study provides a seamless dataflow between the designer and manufacturer (cost data). MISLP proved to be efficient and reliable and detect solutions close to the global optimum. The MISLP optimisation method demonstrates adequate properties and performances required to be run directly from a server to generate immediate designs based on parameters collected from the user interface. The ability to reliably and efficiently explore the solution space in a rapidly growing market of novel engineered wood products opens a range of implications briefly demonstrated in section 5.2.

- Mean error and standard deviation between the global optimum and the solution obtained by MISLP are significantly larger for constraint combinations based on Hu and Chui than with acceleration and velocity. This is associated with the fact that the Hu and Chui constraint are composed of two other constraints.
- With respect to the 600 minutes analysis time per case for manual exploration of the solution space, the optimisation approach took less than two seconds per case. The analysis duration may be sufficiently fast for an online reference work.
- Predetermination of floor element designs in conventional charts is challenging due to the six Floor Performance Levels (FPL). This is an argument for an online reference work.
- Glulam as joists is outperforming alternatives. Glulam has a competitive combination of cost, ECO2, stiffness and standard format range. The combination of glulam and spruce-LVL-Q in flanges performs generally best. Glulam in combination with beech LVL-Q slightly increase span, but at a high cost (2 % increase in span at 20 % increase in cost).
- Flange-driven performance increase is expensive, and it is increasingly dominating after 9.4 m for most base floor designs.
- Minimum cost and ECO2 correlate well as both are related to accrued material volume.
- The distribution of optimum design is generally responding well for FPL 1 to FPL 3, whilst similar designs is typically found for FPL 4 to FPL 6. This is linked to the activation of final deflection constraint.
- Pareto-analysis of the trade-off between cost and depth yields the cost increase as floor depth is constrained. Generally, the ratio of cost to depth is increasing with increasing span.
- The cost and ECO2 of the floor element as built deviate significantly from quantities as manufactured, depending on the design strategy for fire resistance and overlay.

The timber sector is under substantial pressure to find competitive solutions for an increasing demand for long-span floor elements suitable to adaptable and sustainable buildings. Due to the findings of the present work, a huge potential for the manufacturers in the successful adaptation to algorithm aided design may be realistic, given that the infrastructure of the suppliers and production line can cope with the indeterminacy.

The combined investments in the modules of the presented workflow may offer the required computational foundation for a ready reference, thus assist in commercialisation of long-span timber floor elements suitable for adaptable building applications. All codes in the optimisation workflow are based on open source which may simplify in producing public available results.

The present work is a contribution in the endeavour of industrialising timber manufacturing and in the establishment of parametric framework covering the value chain from design to manufacturing [43-45].

Note that changing cost and properties of materials, in addition to the manufacturing cost will influence the optimum design. The optimum design may therefore change between manufacturers.

Acknowledgements

This work is part of the four-year project “Woodsol – Wood frame solutions for free space design in urban buildings” realized through the research grant from The Research Council of Norway (254699/E50). The support is gratefully acknowledged. The authors would also like to acknowledge the contribution by Jaakko Huusko (formerly Tampere University) for the support on implementation of the computer code.

References

- [1] Iyer-Raniga, U., *Zero Energy in the Built Environment: A Holistic Understanding*. Applied Sciences, 2019. **9**: p. 3375.
- [2] UN Environment and International Energy Agency (IEA), *Towards a zero-emission, efficient, and resilient buildings and construction sector. Global Status Report 2017*. 2017.
- [3] Dixon, T., J. Connaughton, and S. Green, *Sustainable Futures in the Built Environment to 2050: A Foresight Approach to Construction and Development*. 2018: John Wiley & Sons.
- [4] Pomponi, F. and A. Moncaster, *Embodied carbon mitigation and reduction in the built environment – What does the evidence say?* Journal of Environmental Management, 2016. **181**: p. 687-700.

- [5] Ge, M. and J. Friedrich. *4 Charts Explain Greenhouse Gas Emissions by Countries and Sectors*. 2020 February 06, 2020; Available from: <https://www.wri.org/blog/2020/02/greenhouse-gas-emissions-by-country-sector>.
- [6] Hertwich, E.G., et al., *Material efficiency strategies to reducing greenhouse gas emissions associated with buildings, vehicles, and electronics—a review*. Environmental Research Letters, 2019. **14**(4): p. 043004.
- [7] Norconsult Informasjonssystemer AS and Bygganalyse AS, *Norsk prisbok: et oppslagsverk for byggebransjen*. 2019-02 ed. Norsk prisbok: et oppslagsverk for byggebransjen. 2019, Sandvika: Norconsult informasjonssystemer AS i samarbeid med AS Bygganalyse.
- [8] Hurmekoski, E., R. Jonsson, and T. Nord, *Context, drivers, and future potential for wood-frame multi-story construction in Europe*. Technological Forecasting and Social Change, 2015. **99**: p. 181-196.
- [9] Mayencourt, P. and C. Mueller, *Hybrid analytical and computational optimization methodology for structural shaping: Material-efficient mass timber beams*. Engineering Structures, 2020. **215**: p. 110532.
- [10] Stanić, A., B. Hudobivnik, and B. Brank, *Economic-design optimization of cross laminated timber plates with ribs*. Composite Structures, 2016. **154**: p. 527-537.
- [11] Mela, K. and M. Heinisuo, *Weight and cost optimization of welded high strength steel beams*. Engineering Structures, 2014. **79**: p. 354-364.
- [12] Platt, B.S. and P.V. Mtenga. *Parametric optimization of steel floor system cost using Evolver*. 2007.
- [13] Klanšek, U. and S. Kravanja, *Cost estimation, optimization and competitiveness of different composite floor systems—Part 2: Optimization based competitiveness between the composite I beams, channel-section and hollow-section trusses*. Journal of Constructional Steel Research, 2006. **62**(5): p. 449-462.
- [14] Mahn, J., et al. *Competitive wooden floor systems - Multi-objective optimization based on acoustics improvement*. in *42nd International Congress and Exposition on Noise Control Engineering 2013, INTER-NOISE 2013: Noise Control for Quality of Life*. 2013.
- [15] Coguenanff, C., et al. *Acoustic performance optimization under parameter and model uncertainties of a wood based floor*. in *42nd International Congress and Exposition on Noise Control Engineering 2013, INTER-NOISE 2013: Noise Control for Quality of Life*. 2013.
- [16] Durga Prasad, K.G., K. Venkata Subbaiah, and K. Narayana Rao, *Multi-objective optimization approach for cost management during product design at the conceptual phase*. Journal of Industrial Engineering International, 2014. **10**(1).

- [17] Abeysekera, I., et al., *Development of a floor vibration design method for Eurocode 5*. New Zealand timber design, 2019. **27**(1).
- [18] CEN, *EN 1995-1-1 SC5.T3 Final draft prEN*. 2020, European committee for standardization: Brussels.
- [19] Nesheim, S., K.A. Malo, and N. Labonnote, *Competitiveness of timber floor elements: An assessment of structural properties, production, costs and carbon emissions*. Forest Products Journal, 2021.
- [20] Hu, L.J., R. Desjardins, and E. Jones. *Systems approach for optimizing wood-based floor construction*. in *9th World Conference on Timber Engineering 2006*. 2006. Portland, OR, United states: Oregon State University Conference Services.
- [21] CEN, *EN 14080-2013 Timber structures- Glued laminated timber and glued solid timber - Requirements*. 2013, European Committee for Standardization: Brussels, Belgium.
- [22] CEN, *NS-EN 14279:2004+A1:2009 Laminated Veneer Lumber (LVL) - Definitions, classification and specifications*. 2009, European Committee for Standardization: Brussels, Belgium.
- [23] CEN, *NS-EN 13986:2004+A1:2015 Wood-based panels for use in construction - Characteristics, evaluation of conformity and marking*. 2015, European Committee for Standardization: Brussels, Belgium.
- [24] CEN, *NS-EN 1995-1-2:2004+NA:2010*, in *Design of timber structures - Part 1-2: General - Structural fire design*. 2010, European Committee for Standardization: Brussels, Belgium.
- [25] Östman, B. and S.P.S.t. forskningsinstitut, *Brandsäkra trähus 3 : nordisk-baltisk kunskapsöversikt och vägledning*. Version 3. ed. SP rapport (Sveriges provnings- och forskningsinstitut). Vol. 2012:18. 2012, Stockholm: SP Sveriges Tekniska Forskningsinstitut.
- [26] Friquin, K.L., et al., *Brannsikkerhet i trebygg over 4 etasjer - Bruk av trekonstruksjoner i brannklasse 3*. 2016, SINTEF Building and Infrastructure: Trondheim. p. 122.
- [27] DIBK, *Regulations on technical requirements for construction works TEK17*, in *Norwegian Building Authority*. 2017.
- [28] CEN, *NS-EN 1995-1-1:2004+A1:2008+NA:2010*, in *Design of timber structures - Part 1-1: General - Common rules and rules for buildings*. 2010, European committee for standardization: Brussels.
- [29] Clastornik, J., et al., *Beams on Variable Winkler Elastic Foundation*. Journal of Applied Mechanics, 1986. **53**(4): p. 925-928.
- [30] Froio, D. and E. Rizzi, *Analytical solution for the elastic bending of beams lying on a variable Winkler support*. Acta Mechanica, 2016. **227**(4): p. 1157-1179.

- [31] Aune, P., *Trekonstruksjoner : 1 : Materialer, dimensjonering, forbindelser*. Vol. 1. 1992, Trondheim: Tapir.
- [32] Hu, L.J. and Y.H. Chui, *Development of a design method to control vibrations induced by normal walking action in wood-based floors*, in *Proceedings of the 8th World Conference on Timber Engineering*. 2004: Lahti, Finland. p. 217-222.
- [33] ISO, *ISO 10137:2007 Bases for design of structures - Serviceability of buildings and walkways against vibrations*. 2007, International Organization for Standardization.
- [34] CEN, *NS-EN 1991-1-1:2002+NA:2019*, in *Actions on structures - Part 1-1: General actions - Densities, self-weight, imposed loads for buildings*, European Committee for Standardization: Brussels, Belgium.
- [35] Kaplan, R.S. and S.R. Anderson, *Time-Driven Activity-Based Costing*. Harvard Business Review, 2004. **82**(11): p. 131-138.
- [36] Guido van Rossum, *The Python Language*. 2003, Network Theory Ltd.
- [37] SINTEF Community, *522.351 Trebjelkelag. Dimensjonering og utførelse*, in *ISSN 2387-6328*. 2011, SINTEF Building and Infrastructure: Oslo.
- [38] Homb, A., *Kriterier for opplevde vibrasjoner i etasjeskillere. Delrapport fra prosjektet «Comfort properties of timber floor constructions»*. 2007.
- [39] Arora, J.S., *Introduction to Optimum Design*. 2004: Elsevier Academic Press.
- [40] Perron, L. and V. Furnon, *OR-Tools*. 2019, Google.
- [41] Dassault Systèmes, *Abaqus CAE*. 2017, Dassault Systèmes Simulia corp.
- [42] Nesheim, S., K.A. Malo, and N. Labonnote, *Conditions and features of a design tool for long-span timber floor elements (Manuscript submitted for publication)*, in *World Conference in Timber Engineering 2021*. 2021: Santiago.
- [43] Willmann, J., et al., *Robotic timber construction — Expanding additive fabrication to new dimensions*. Automation in Construction, 2016. **61**: p. 16-23.
- [44] Weinand, Y., *Advanced Timber Structures: Architectural Designs and Digital Dimensioning*. 2017: Birkhäuser.
- [45] Mork, J.H., et al., *Generating timber truss bridges—examining the potential of an interdisciplinary parametric framework for architectural engineering*. 2016.
- [46] Manufacturers of timber elements in Norway, *Direct material supply costs*, S. Nesheim, Editor. 2020.
- [47] Moelven Törebody AB, *EPD Glulam beams and pillars*. 2016.

- [48] Skaar, C., B. Solem, and P. R  ther, *Composite floors in urban buildings: Options for a low carbon building design*, in *Forum Wood Building Nordic*. 2017, Forum Wood Building Nordic Trondheim 17: Trondheim Norway.
- [49] Norgips, *EPD Norgips Fireboard*. 2020.
- [50] Metsa Wood, *Emissions and environmental impacts*. 2017.

Annex A. Material supply cost and carbon emissions

Table 6: Direct material supply cost and ECO2

Material	Cost [€ per m ³]	ECO2 [g CO ₂ per kg]
Adhesive	2965 [46]	1000 [46]
Beech LVL	635 [46]	364.9 [46]
Fasteners	See Table 7	
Fibre board 36 mm	275 [7]	243 [7]
Glulam	510 [46]	144.2 [47]
Gravel 8/16	150 [46]	3 [48]
Gypsum type F	400 [7]	200.8 [49]
HB HLA 1'	1000 approx. from [7]	661 [7]
OSB 3	520 [7]	208 [7]
Particle board P6/22	785 [7]	409 [7]
Screed	170 [7]	1355.9 [48]
Spruce LVL	595 [46]	254.9 [50]

Table 7: Fastener specification used to calculate fastener vector of body or assembly

Fastened member	1) Type	dia	Row-Dir ²⁾	multiplier ³⁾	4) $\frac{D}{A}$	Value	unit-Cost	unit-CO ₂ ⁵⁾	Len ⁶⁾	Type
		[mm]					[€]	[kgCO ₂ eq]	[m]	
Top flange	S	5	1	fldJstNum+2	D	0.3	0.05	None	0.1	Partial tread flange head
Edge beam	S	8	3	2	D	0.05	0.1	None	None	Double threaded fastener
Field joist	S	8	3	2	D	0.05	0.1	None	None	Double threaded fastener
Trns. stiffener	S	6.3	3	2	D	0.05	0.1	None	None	NA
Bottom flange	S	5	1	fldJstNum+2	D	0.3	0.1	None	0.1	Partial tread flange head
Overlay	N	4	1	fldJstNum+2	D	0.1	0.01	None	None	NA
Ceiling	S	3	1	fldJstNum+2	D	0.2	0.01	None	None	NA
Floor element	S	8	2	2	D	0.1	0.1	None	0.2	Partial tread flange head

1) N: nail, or S: screw. If screw and: $\varnothing > 8$ mm or machinability > 1 or density of material > 650 kg/m³; predrilling is performed

2) Global direction of row of fasteners in body in question

3) Multiplier of the row as defined in rowing direction

4) Calculate the preceding Value as distance between fasteners (D) or total amount of fasteners (A) along one row

5) None or a number. If None a value is calculated based on the volume using unitMassCO₂eq of steel.

6) Length of fastener or None. If None length is calculated as twice the plate thickness or beam width (aspect ratio parsed as condition)

Annex B. Dataset for quantifying accuracy of the optimisation

Table 8: Global cost optimum compared to MISLP for current common method (Hu and Chui)

Material		Constraints							Manual cost optimum														MISLP		
edge	frida	fig	overlay	Ceiling system	f1	Deflection			Type	ID	Dimensions				Constraint level					Objective		error			
						min	max	w _{max} [mm]			w _{min} [mm]	logfig_tck	confict	bramfig_tck	epfig_w	figda_w	f1	w	wfin	fa	Rv		HC	cost	CO2
GL30c	GL28c	S-LVLQ	Type1	None	10	NA	1.3	45	HC	0_0_1	0.033	0.495	0.063	0.036	0.036	10.37	0.23	15.85	1.78	9.88	1.13	109.6	17.5	109.6	0.0%
GL30c	S-LVLS	S-LVLQ	Type1	None	10	NA	1.3	45	HC	0_1_2	0.033	0.495	0.063	0.036	0.036	10.35	0.23	15.70	1.77	9.81	1.13	111.5	19.2	111.4	-0.1%
GL30c	B-LVLS	S-LVLQ	Type1	None	10	NA	1.3	45	HC	0_2_3	0.033	0.495	0.063	0.036	0.04	10.69	0.22	14.35	1.50	9.15	1.29	115.0	22.6	114.5	-0.5%
GL30c	GL28c	B-LVLQ	Type1	None	10	NA	1.3	45	HC	0_3_4	0.02	0.585	0.06	0.036	0.036	10.61	0.22	14.48	1.52	9.77	1.24	110.0	26.9	107.3	-2.4%
GL30c	S-LVLS	B-LVLQ	Type1	None	10	NA	1.3	45	HC	0_4_5	0.02	0.54	0.06	0.036	0.045	10.27	0.24	15.19	1.71	9.84	1.09	111.9	29.0	112.0	0.1%
GL30c	B-LVLS	B-LVLQ	Type1	None	10	NA	1.3	45	HC	0_5_6	0.02	0.54	0.06	0.036	0.04	10.37	0.23	14.64	1.61	9.55	1.14	113.3	32.2	110.4	-2.6%
S-LVLS	S-LVLS	S-LVLQ	Type1	None	10	NA	1.3	45	HC	0_6_7	0.045	0.4	0.069	0.027	0.075	10.06	0.22	15.68	1.86	8.38	1.12	127.6	24.3	123.6	-3.1%
B-LVLS	B-LVLS	S-LVLQ	Type1	None	10	NA	1.3	45	HC	0_7_8	0.033	0.48	0.063	0.04	0.04	10.33	0.22	15.19	1.67	9.14	1.19	119.0	28.6	113.7	-0.2%
S-LVLS	S-LVLS	B-LVLQ	Type1	None	10	NA	1.3	45	HC	0_8_9	0.04	0.4	0.07	0.027	0.075	10.01	0.21	14.82	1.72	7.93	1.17	131.7	38.8	137.6	4.5%
B-LVLS	B-LVLS	B-LVLQ	Type1	None	10	NA	1.3	45	HC	0_9_10	0.02	0.56	0.06	0.04	0.04	10.59	0.21	13.78	1.40	9.01	1.32	120.0	39.9	116.9	-2.5%
GL30c	HB	S-LVLQ	Type1	None	10	NA	1.3	45	HC	0_10_11	0.033	0.495	0.063	0.036	0.007	10.35	0.23	16.03	1.80	9.71	1.15	124.4	23.6	124.2	-0.1%
GL30c	HB	B-LVLQ	Type1	None	10	NA	1.3	45	HC	0_11_12	0.02	0.54	0.06	0.036	0.007	10.11	0.23	16.14	1.87	10.15	1.05	122.3	33.2	122.1	-0.2%
GL30c	OSB	S-LVLQ	Type1	None	10	NA	1.3	45	HC	0_12_13	0.033	0.495	0.063	0.036	0.012	10.14	0.23	16.60	1.94	9.95	1.07	121.6	39.9	121.4	-0.2%
GL30c	OSB	B-LVLQ	Type1	None	10	NA	1.3	45	HC	0_13_14	0.02	0.585	0.06	0.036	0.012	10.55	0.22	14.66	1.54	9.74	1.26	121.7	29.6	119.1	-2.1%
GL30c	GL28c	S-LVLQ	Type1	1	10	NA	1.3	45	HC	0_15	0.033	0.63	0.033	0.036	0.036	10.96	0.27	13.39	1.29	12.34	1.10	99.1	14.5	98.9	-0.2%
GL30c	S-LVLS	S-LVLQ	Type1	1	10	NA	1.3	45	HC	0_1_16	0.033	0.63	0.033	0.036	0.033	10.64	0.28	14.13	1.46	12.04	1.00	101.1	16.0	100.7	-0.4%
GL30c	B-LVLS	S-LVLQ	Type1	1	10	NA	1.3	45	HC	0_2_17	0.033	0.585	0.033	0.036	0.04	10.64	0.28	13.69	1.41	12.13	1.00	102.7	20.2	102.4	-0.3%
GL30c	GL28c	B-LVLQ	Type1	1	10	NA	1.3	45	HC	0_3_18	0.03	0.63	0.03	0.036	0.036	10.99	0.28	12.89	1.22	12.84	1.09	99.7	21.9	97.6	-2.1%
GL30c	S-LVLS	B-LVLQ	Type1	1	10	NA	1.3	45	HC	0_4_19	0.03	0.63	0.03	0.036	0.039	10.98	0.27	12.72	1.20	12.72	1.10	102.2	24.1	101.3	-0.8%
GL30c	B-LVLS	B-LVLQ	Type1	1	10	NA	1.3	45	HC	0_5_20	0.02	0.63	0.04	0.036	0.04	10.78	0.26	12.85	1.26	11.51	1.11	106.1	28.3	102.5	-3.4%
S-LVLS	S-LVLS	S-LVLQ	Type1	1	10	NA	1.3	45	HC	0_6_21	0.063	0.4	0.075	0.027	0.075	10.09	0.17	13.93	1.55	6.63	1.43	141.9	27.4	137.9	-2.8%
B-LVLS	B-LVLS	S-LVLQ	Type1	1	10	NA	1.3	45	HC	0_7_22	0.033	0.6	0.033	0.04	0.04	10.74	0.26	13.17	1.28	11.55	1.11	109.3	28.3	108.9	-0.4%
S-LVLS	S-LVLS	B-LVLQ	Type1	1	10	NA	1.3	45	HC	0_8_23	0.06	0.4	0.07	0.027	0.075	10.02	0.17	13.33	1.45	6.57	1.42	144.5	44.1		
B-LVLS	B-LVLS	B-LVLQ	Type1	1	10	NA	1.3	45	HC	0_9_24	0.03	0.6	0.03	0.04	0.04	10.79	0.26	12.68	1.20	12.00	1.09	109.9	35.7	109.5	-0.4%
GL30c	HB	S-LVLQ	Type1	1	10	NA	1.3	45	HC	0_10_25	0.033	0.63	0.033	0.036	0.007	10.74	0.27	14.03	1.41	12.99	1.06	113.7	22.1	113.3	-0.3%
GL30c	HB	B-LVLQ	Type1	1	10	NA	1.3	45	HC	0_11_26	0.03	0.63	0.03	0.036	0.007	10.86	0.27	13.30	1.28	12.77	1.07	114.3	29.5	113.9	-0.3%
GL30c	OSB	S-LVLQ	Type1	1	10	NA	1.3	45	HC	0_12_27	0.033	0.63	0.033	0.036	0.015	10.74	0.26	13.79	1.38	12.14	1.08	113.4	30.0	110.1	-2.9%
GL30c	OSB	B-LVLQ	Type1	1	10	NA	1.3	45	HC	0_13_28	0.03	0.63	0.03	0.036	0.012	10.63	0.28	13.79	1.39	13.08	1.00	111.2	24.7	110.7	-0.4%
GL30c	GL28c	S-LVLQ	Type2	None	10	NA	1.3	45	HC	0_0_29	0.033	0.63	0.063	0.036	0.036	10.27	0.17	12.33	1.23	7.51	1.48	116.9	18.4	116.7	-0.1%
GL30c	S-LVLS	S-LVLQ	Type2	None	10	NA	1.3	45	HC	0_1_30	0.033	0.63	0.063	0.036	0.039	10.27	0.17	12.20	1.21	7.45	1.49	119.3	20.5	118.5	-0.7%
GL30c	B-LVLS	S-LVLQ	Type2	None	10	NA	1.3	45	HC	0_2_31	0.033	0.585	0.063	0.036	0.04	10.11	0.18	12.42	1.27	7.29	1.40	120.5	24.1	120.2	-0.3%
GL30c	GL28c	B-LVLQ	Type2	None	10	NA	1.3	45	HC	0_3_32	0.03	0.63	0.06	0.036	0.036	10.28	0.17	11.88	1.15	7.56	1.49	118.8	29.9	138.8	16.8%
GL30c	S-LVLS	B-LVLQ	Type2	None	10	NA	1.3	45	HC	0_4_33	0.02	0.63	0.06	0.036	0.051	10.02	0.18	12.42	1.28	7.59	1.32	120.3	30.6	114.4	-4.9%
GL30c	B-LVLS	B-LVLQ	Type2	None	10	NA	1.3	45	HC	0_5_34	0.03	0.585	0.06	0.036	0.04	10.16	0.18	11.92	1.18	7.32	1.42	122.5	35.6	118.4	-3.3%
S-LVLS	S-LVLS	S-LVLQ	Type2	None	10	NA	1.3	45	HC	0_6_35	0.033	0.6	0.063	0.04	0.04	10.23	0.16	11.98	1.16	7.00	1.55	127.1	32.2	126.7	-0.4%
B-LVLS	B-LVLS	S-LVLQ	Type2	None	10	NA	1.3	45	HC	0_7_36	0.033	0.6	0.063	0.04	0.04	10.23	0.16	11.98	1.16	7.00	1.55	127.1	32.2	126.7	-0.4%
S-LVLS	S-LVLS	B-LVLQ	Type2	None	10	NA	1.3	45	HC	0_8_37	0.033	0.63	0.063	0.036	0.039	10.27	0.17	12.20	1.21	7.45	1.49	119.3	20.5	118.5	-0.7%
B-LVLS	B-LVLS	B-LVLQ	Type2	None	10	NA	1.3	45	HC	0_9_38	0.03	0.6	0.06	0.04	0.04	10.28	0.16	11.50	1.08	7.03	1.58	129.1	43.7	126.5	-2.0%
GL30c	HB	S-LVLQ	Type2	None	10	NA	1.3	45	HC	0_10_39	0.033	0.63	0.063	0.036	0.007	10.23	0.17	12.49	1.25	7.37	1.50	131.4	26.0	131.0	-0.3%
GL30c	HB	B-LVLQ	Type2	None	10	NA	1.3	45	HC	0_11_40	0.03	0.63	0.06	0.036	0.007	10.14	0.17	12.40	1.25	7.58	1.43	130.3	32.7	129.8	-0.4%
GL30c	OSB	S-LVLQ	Type2	None	10	NA	1.3	45	HC	0_12_41	0.033	0.63	0.063	0.036	0.015	10.29	0.17	12.20	1.20	7.20	1.56	131.2	21.9	127.9	-2.5%
GL30c	OSB	B-LVLQ	Type2	None	10	NA	1.3	45	HC	0_13_42	0.03	0.63	0.06	0.036	0.012	10.07	0.17	12.40	1.25	7.58	1.43	130.3	32.7	129.8	-0.4%
GL30c	GL28c	S-LVLQ	Type2	1	10	NA	1.3	45	HC	0_0_43	0.039	0.63	0.039	0.036	0.048	10.00	0.21	12.41	1.27	8.80	1.15	110.9	16.6	110.7	-0.2%
GL30c	S-LVLS	S-LVLQ	Type2	1	10	NA	1.3	45	HC	0_1_44	0.033	0.63	0.039	0.036	0.063	10.15	0.21	11.85	1.17	8.91	1.17	115.6	19.9	115.8	33.0%
GL30c	B-LVLS	S-LVLQ	Type2	1	10	NA	1.3	45	HC	0_2_45	0.033	0.63	0.039	0.036	0.05	10.07	0.21	11.96	1.20	8.92	1.15	113.6	23.8	109.6	-3.5%
GL30c	GL28c	B-LVLQ	Type2	1	10	NA	1.3	45	HC	0_3_46	0.03	0.63	0.04	0.036	0.048	10.01	0.22	12.13	1.22	9.18	1.12	110.8	25.1	110.3	-0.4%
GL30c	S-LVLS	B-LVLQ	Type2	1	10	NA	1.3	45	HC	0_4_47	0.03	0.63	0.03	0.036	0.063	10.04	0.24	11.96	1.20	10.21	1.02	111.6	26.5	123.2	9.4%
GL30c	B-LVLS	B-LVLQ	Type2	1	10	NA	1.3	45	HC	0_5_48	0.03	0.63	0.03	0.036	0.06	10.25	0.23	11.25	1.07	9.72	1.12	115.5	32.5	110.2	-4.6%
S-LVLS	S-LVLS	S-LVLQ	Type2	1	10	NA	1.3	45	HC	0_6_49	0.033	0.63	0.063	0.04	0.04	10.23	0.16	11.98	1.16	7.00	1.55	127.1	32.2	126.7	-0.4%
B-LVLS	B-LVLS	S-LVLQ	Type2	1	10	NA	1.3	45	HC	0_7_50	0.033	0.6	0.045	0.04	0.06	10.03	0.19	11.77	1.15	7.92	1.27	125.4	33.8	121.3	-3.3%
S-LVLS	S-LVLS	B-LVLQ	Type2	1	10	NA	1.3	45	HC	0_8_51	0.033	0.63	0.063	0.036	0.039	10.27	0.17	12.20	1.21	7.45	1.49	119.3	20.5	118.5	-0.7%
B-LVLS	B-LVLS	B-LVLQ	Type2	1	10	NA	1.3	45	HC	0_9_52	0.03	0.6	0.04	0.04	0.06	10.09	0.20	11.42	1.09	8.39	1.24	125.3	42.4	167.9	34.0%
GL30c	HB	S-LVLQ	Type2	1																					

Table 9: Global cost optimum compared to MISLP for second generation of Eurocode 5 (Resonant response)

edge	Material		Constraints						Manual cost optimum													MISLP			
			orientation	Ceiling system	f1		Deflection		Type	ID	Dimensions						Constraint level					Objective		[0.5, 1.5]	
					min	max	wmax [mm]	wmin [mm]			topfig_tsk	coyfig	lamefig_tsk	ebbfig_w	fidfig_w	f1	w	wfin	Ra	Rv	HC	cost	CO2		
GL30c	GL28c	S-LVLQ	Type1	None	4.5	8	0.8	45	Arms	0_0_1	0.033	0.27	0.063	0.036	0.036	6.48	0.49	41.99	8.92	15.47	0.19	97.4	16.0	-100.0%	
GL30c	S-LVL5	S-LVLQ	Type1	None	4.5	8	0.8	45	Arms	0_1_2	0.033	0.27	0.063	0.036	0.039	6.47	0.48	41.71	8.86	15.40	0.19	98.5	17.0	-100.0%	
GL30c	B-LVL5	S-LVLQ	Type1	None	4.5	8	0.8	45	Arms	0_2_3	0.033	0.27	0.063	0.036	0.04	6.62	0.46	39.24	8.21	14.72	0.20	101.3	18.8	-100.0%	
GL30c	GL28c	B-LVLQ	Type1	None	4.5	8	0.8	45	Arms	0_3_4	0.02	0.315	0.06	0.036	0.036	6.27	0.51	42.94	9.11	16.13	0.17	95.4	25.2	-100.0%	
GL30c	S-LVL5	B-LVLQ	Type1	None	4.5	8	0.8	45	Arms	0_4_5	0.02	0.315	0.06	0.036	0.039	6.52	0.50	41.91	8.85	15.91	0.17	96.6	26.3	-100.0%	
GL30c	B-LVL5	B-LVLQ	Type1	None	4.5	8	0.8	45	Arms	0_5_6	0.02	0.315	0.06	0.036	0.04	6.51	0.48	38.85	8.06	15.32	0.19	97.7	28.4	-100.0%	
S-LVL5	S-LVL5	S-LVLQ	Type1	None	4.5	8	0.8	45	Arms	0_6_7	0.033	0.3	0.063	0.027	0.027	6.66	0.47	39.60	8.26	15.46	0.20	100.8	17.6	100.9	0.1%
B-LVL5	B-LVL5	S-LVLQ	Type1	None	4.5	8	0.8	45	Arms	0_7_8	0.033	0.28	0.063	0.04	0.04	6.77	0.43	37.11	7.49	14.09	0.23	105.4	22.7	-100.0%	
S-LVL5	S-LVL5	B-LVLQ	Type1	None	4.5	8	0.8	45	Arms	0_8_9	0.02	0.3	0.06	0.027	0.045	6.17	0.53	43.73	9.36	16.03	0.15	98.0	27.4	96.7	-1.3%
B-LVL5	B-LVL5	B-LVLQ	Type1	None	4.5	8	0.8	45	Arms	0_9_10	0.02	0.28	0.06	0.04	0.05	6.04	0.52	44.67	9.47	15.68	0.15	103.0	32.4	-100.0%	
GL30c	HB	S-LVLQ	Type1	None	4.5	8	0.8	45	Arms	0_10_11	0.033	0.27	0.063	0.036	0.007	6.48	0.48	42.06	8.90	15.28	0.19	112.1	19.7	-100.0%	
GL30c	HB	B-LVLQ	Type1	None	4.5	8	0.8	45	Arms	0_11_12	0.02	0.315	0.06	0.036	0.007	6.55	0.47	39.54	8.16	15.43	0.20	110.0	29.3	-100.0%	
GL30c	OSB	S-LVLQ	Type1	None	4.5	8	0.8	45	Arms	0_12_13	0.033	0.27	0.063	0.036	0.018	6.57	0.49	41.75	8.57	15.27	0.15	102.1	17.4	109.9	4.6%
GL30c	OSB	B-LVLQ	Type1	None	4.5	8	0.8	45	Arms	0_13_14	0.02	0.315	0.06	0.036	0.018	6.64	0.45	37.90	7.73	14.89	0.21	105.0	27.0	-100.0%	
GL30c	GL28c	S-LVLQ	Type1	1	4.5	8	0.8	45	Arms	0_15	0.033	0.315	0.033	0.036	0.036	6.13	0.69	44.53	9.52	21.53	0.11	82.0	12.4	82.3	0.4%
S-LVL5	S-LVL5	B-LVLQ	Type1	1	4.5	8	0.8	45	Arms	0_16	0.033	0.315	0.033	0.036	0.039	6.14	0.69	44.10	9.42	21.39	0.12	83.3	13.5	84.2	1.1%
GL30c	B-LVL5	S-LVLQ	Type1	1	4.5	8	0.8	45	Arms	0_17	0.033	0.315	0.033	0.036	0.04	6.26	0.66	41.69	8.81	20.53	0.13	86.3	15.7	86.4	0.1%
GL30c	GL28c	B-LVLQ	Type1	1	4.5	8	0.8	45	Arms	0_18	0.02	0.36	0.03	0.036	0.036	6.08	0.80	44.52	9.47	25.44	0.10	78.7	17.5	-100.0%	
S-LVL5	S-LVL5	B-LVLQ	Type1	1	4.5	8	0.8	45	Arms	0_19	0.02	0.45	0.02	0.036	0.039	6.77	0.79	35.99	7.22	28.18	0.13	79.0	16.9	77.2	-2.3%
GL30c	B-LVL5	B-LVLQ	Type1	1	4.5	8	0.8	45	Arms	0_20	0.02	0.45	0.02	0.036	0.018	6.75	0.79	36.26	6.56	27.02	0.14	82.4	20.0	-100.0%	
S-LVL5	S-LVL5	S-LVLQ	Type1	1	4.5	8	0.8	45	Arms	0_21	0.033	0.36	0.033	0.027	0.027	6.54	0.63	38.89	8.04	20.72	0.15	85.9	14.4	-100.0%	
B-LVL5	B-LVL5	S-LVLQ	Type1	1	4.5	8	0.8	45	Arms	0_22	0.033	0.32	0.033	0.04	0.04	6.90	0.63	40.68	8.38	19.92	0.13	80.3	20.0	90.3	0.0%
S-LVL5	S-LVL5	B-LVLQ	Type1	1	4.5	8	0.8	45	Arms	0_23	0.02	0.36	0.03	0.039	0.039	6.12	0.78	43.50	9.16	24.96	0.10	81.5	20.3	81.6	0.1%
B-LVL5	B-LVL5	B-LVLQ	Type1	1	4.5	8	0.8	45	Arms	0_24	0.02	0.44	0.02	0.04	0.04	6.76	0.75	39.14	6.80	26.75	0.13	86.3	25.6	-100.0%	
GL30c	HB	S-LVLQ	Type1	1	4.5	8	0.8	45	Arms	0_25	0.033	0.315	0.033	0.036	0.008	6.12	0.68	44.77	9.54	21.25	0.12	97.6	17.1	96.8	-0.9%
GL30c	HB	B-LVLQ	Type1	1	4.5	8	0.8	45	Arms	0_26	0.02	0.45	0.02	0.036	0.007	7.12	0.72	33.11	6.36	27.20	0.16	91.8	21.0	91.0	-0.8%
GL30c	OSB	S-LVLQ	Type1	1	4.5	8	0.8	45	Arms	0_27	0.033	0.315	0.033	0.036	0.018	6.13	0.67	44.10	9.36	20.92	0.12	91.6	14.3	95.8	4.5%
GL30c	OSB	B-LVLQ	Type1	1	4.5	8	0.8	45	Arms	0_28	0.02	0.405	0.02	0.036	0.023	6.57	0.80	37.95	7.72	28.24	0.12	87.1	17.9	88.9	2.0%
GL30c	GL28c	S-LVLQ	Type2	None	4.5	8	0.8	45	Arms	0_29	0.033	0.315	0.063	0.036	0.036	5.94	0.40	37.83	7.28	12.38	0.18	99.8	16.3	99.7	-0.1%
GL30c	S-LVL5	S-LVLQ	Type2	None	4.5	8	0.8	45	Arms	0_30	0.033	0.315	0.063	0.036	0.027	5.63	0.42	42.14	8.25	13.33	0.15	100.6	16.8	100.7	0.1%
GL30c	B-LVL5	S-LVLQ	Type2	None	4.5	8	0.8	45	Arms	0_31	0.033	0.27	0.063	0.036	0.05	5.53	0.45	42.87	8.41	12.66	0.14	103.4	19.7	101.5	-1.8%
GL30c	GL28c	B-LVLQ	Type2	None	4.5	8	0.8	45	Arms	0_32	0.02	0.315	0.06	0.036	0.048	5.99	0.48	44.76	8.71	13.60	0.12	97.8	25.5	95.5	-2.4%
GL30c	S-LVL5	B-LVLQ	Type2	None	4.5	8	0.8	45	Arms	0_33	0.02	0.36	0.06	0.036	0.027	5.46	0.45	43.84	8.50	14.04	0.14	98.4	26.0	97.5	-0.9%
GL30c	B-LVL5	B-LVLQ	Type2	None	4.5	8	0.8	45	Arms	0_34	0.02	0.315	0.06	0.036	0.04	5.98	0.48	44.55	8.66	13.53	0.12	99.7	28.4	99.7	0.1%
S-LVL5	S-LVL5	B-LVLQ	Type2	None	4.5	8	0.8	45	Arms	0_35	0.033	0.3	0.063	0.027	0.039	5.71	0.44	40.71	7.94	12.74	0.15	101.1	18.2	-100.0%	
B-LVL5	B-LVL5	S-LVLQ	Type2	None	4.5	8	0.8	45	Arms	0_36	0.033	0.28	0.063	0.04	0.04	5.55	0.43	42.64	8.25	12.63	0.15	105.4	22.7	105.5	0.1%
S-LVL5	S-LVL5	B-LVLQ	Type2	None	4.5	8	0.8	45	Arms	0_37	0.02	0.36	0.06	0.027	0.027	5.43	0.47	44.16	8.57	14.03	0.13	99.3	27.1	99.3	0.0%
B-LVL5	B-LVL5	B-LVLQ	Type2	None	4.5	8	0.8	45	Arms	0_38	0.02	0.32	0.06	0.04	0.04	5.43	0.45	43.18	8.28	13.24	0.13	103.7	32.7	103.7	0.0%
GL30c	HB	S-LVLQ	Type2	None	4.5	8	0.8	45	Arms	0_39	0.033	0.315	0.063	0.036	0.007	5.93	0.40	37.99	7.29	12.23	0.19	114.5	20.5	114.5	0.1%
GL30c	HB	B-LVLQ	Type2	None	4.5	8	0.8	45	Arms	0_40	0.02	0.315	0.06	0.036	0.008	5.43	0.46	44.43	8.62	13.61	0.13	111.0	29.8	110.1	-0.8%
GL30c	OSB	S-LVLQ	Type2	None	4.5	8	0.8	45	Arms	0_41	0.039	0.27	0.063	0.036	0.015	5.53	0.43	43.35	8.47	12.59	0.15	108.6	28.2	112.1	3.2%
GL30c	OSB	B-LVLQ	Type2	None	4.5	8	0.8	45	Arms	0_42	0.02	0.315	0.06	0.036	0.018	5.46	0.45	43.50	8.40	13.86	0.14	105.0	27.0	109.1	3.9%
GL30c	GL28c	S-LVLQ	Type2	1	4.5	8	1.2	45	Arms	0_43	0.033	0.36	0.033	0.036	0.036	5.65	0.58	40.56	7.78	17.43	0.11	84.5	12.7	84.7	0.3%
GL30c	S-LVL5	S-LVLQ	Type2	1	4.5	8	0.8	45	Arms	0_44	0.033	0.36	0.033	0.036	0.027	5.40	0.61	44.59	8.64	18.58	0.10	85.1	13.3	85.1	0.0%
GL30c	B-LVL5	B-LVLQ	Type2	1	4.5	8	0.8	45	Arms	0_45	0.033	0.36	0.033	0.036	0.04	5.82	0.55	37.62	7.12	16.54	0.13	89.0	16.4	88.6	-0.4%
GL30c	GL28c	B-LVLQ	Type2	1	4.5	8	0.8	45	Arms	0_46	0.02	0.45	0.02	0.048	0.036	5.54	0.77	42.28	8.09	25.73	0.08	79.5	15.7	74.7	-6.0%
GL30c	S-LVL5	B-LVLQ	Type2	1	4.5	8	0.8	45	Arms	0_47	0.02	0.45	0.02	0.036	0.039	5.59	0.79	41.29	7.92	25.31	0.08	79.0	16.9	76.8	-2.8%
GL30c	B-LVL5	B-LVLQ	Type2	1	4.5	8	0.8	45	Arms	0_48	0.02	0.45	0.02	0.036	0.04	5.78	0.75	38.10	7.22	24.01	0.09	82.0	20.0	79.6	-3.4%
S-LVL5	S-LVL5	S-LVLQ	Type2	1	4.5	8	0.8	45	Arms	0_49	0.033	0.36	0.033	0.027	0.027	5.38	0.63	44.75	8.68	18.58	0.09	85.9	14.4	-100.0%	
B-LVL5	B-LVL5	B-LVLQ	Type2	1	4.5	8	0.8	45	Arms	0_50	0.033	0.32	0.033	0.04	0.05	5.34	0.61	44.27	8.43	17.35	0.10	92.7	21.0	92.6	-0.1%
S-LVL5	S-LVL5	B-LVLQ	Type2	1	4.5	8	0.8	45	Arms	0_51	0.02	0.4	0.03	0.027	0.039	5.56	0.70	41.23	7.88	20.66	0.09	83.3	20.4	-100.0%	
B-LVL5	B-LVL5	B-LVLQ	Type2	1	4.5	8	0.8	45	Arms	0_52	0.02	0.44	0.02	0.04	0.04	5.62	0.73	39.96	7.47	24.23	0.09	86.3	25.6	83.5	-3.3%
GL30c	HB	S-LVLQ	Type2	1	4.5	8	0.8	45	Arms	0_53	0.033	0.36	0.033	0.036	0.007	5.58	0.58	41.70	8.00	17.47	0.11	99.1	17.3	99.1	0.0%
GL30c	HB	B-LVLQ	Type2	1																					

Table 10: Global cost optimum compared to MISLP for second generation of Eurocode 5 (Transient response)

edge		Material		Constraints		Deflection		Manual cost optimum																		MISLP	
								Dimensions										Constraint level				Objective		[0.5, 1.5]			
fidist	flc	overlay	Ceiling system	min	max	w _{max} [mm]	w _{lim} [mm]	Type	ID	topflg_tsk	ceylflg_tsk	bazflg_tsk	edg_us_w	fidg_us_w	f1	w	wfln	Rv	HC	cost	CO2	cost	error				
GL30c	GL28c	S-LVLQ	Type1	None	8	NA	0.8	45	Vrms	0_0_1	0.033	0.36	0.063	0.036	0.036	8.09	0.34	26.52	4.57	12.57	0.44	102.3	16.6	102.5	0.2%		
GL30c	S-LVL5	S-LVLQ	Type1	None	8	NA	0.8	45	Vrms	0_1_2	0.033	0.36	0.063	0.036	0.039	8.09	0.34	26.31	4.54	12.49	0.44	103.7	17.9	104.3	0.6%		
GL30c	B-LVL5	S-LVLQ	Type1	None	8	NA	0.8	45	Vrms	0_2_3	0.033	0.36	0.063	0.036	0.04	8.31	0.33	24.44	4.07	11.83	0.49	106.8	20.3	106.8	0.0%		
GL30c	GL28c	B-LVLQ	Type1	None	8	NA	0.8	45	Vrms	0_3_4	0.02	0.45	0.06	0.036	0.036	8.50	0.32	22.97	3.63	12.24	0.53	102.7	26.0	102.2	-2.4%		
GL30c	S-LVL5	B-LVLQ	Type1	None	8	NA	0.8	45	Vrms	0_4_5	0.02	0.405	0.06	0.036	0.045	8.03	0.35	25.45	4.54	12.56	0.42	103.5	27.6	102.3	-1.2%		
GL30c	B-LVL5	B-LVLQ	Type1	None	8	NA	0.8	45	Vrms	0_5_6	0.02	0.405	0.06	0.036	0.04	8.09	0.34	24.68	4.17	12.26	0.44	105.1	29.9	105.0	-0.1%		
S-LVL5	S-LVL5	S-LVLQ	Type1	None	8	NA	0.8	45	Vrms	0_6_7	0.033	0.36	0.063	0.027	0.039	8.06	0.35	26.41	4.58	12.50	0.42	104.6	19.0	105.6	1.0%		
B-LVL5	B-LVL5	S-LVLQ	Type1	None	8	NA	0.8	45	Vrms	0_7_8	0.033	0.36	0.063	0.04	0.04	8.24	0.32	24.55	4.02	11.58	0.49	110.8	25.1	110.8	-0.1%		
S-LVL5	B-LVL5	B-LVLQ	Type1	None	8	NA	0.8	45	Vrms	0_8_9	0.02	0.4	0.06	0.027	0.051	8.07	0.35	24.94	4.23	12.30	0.42	105.9	29.2	103.8	-2.0%		
B-LVL5	B-LVL5	B-LVLQ	Type1	None	8	NA	0.8	45	Vrms	0_9_10	0.02	0.44	0.06	0.04	0.04	8.62	0.29	21.31	3.20	11.18	0.59	111.8	36.3	109.0	-2.5%		
GL30c	HB	S-LVLQ	Type1	None	8	NA	0.8	45	Vrms	0_10_11	0.033	0.36	0.063	0.036	0.007	8.09	0.34	26.69	4.58	12.59	0.44	116.8	21.2	116.8	0.0%		
GL30c	HB	B-LVLQ	Type1	None	8	NA	0.8	45	Vrms	0_11_12	0.02	0.405	0.06	0.036	0.007	8.02	0.32	26.08	4.44	12.63	0.43	114.6	31.4	114.7	-0.2%		
GL30c	OSB	S-LVLQ	Type1	None	8	NA	0.8	45	Vrms	0_12_13	0.033	0.36	0.063	0.036	0.018	8.21	0.33	25.42	4.27	11.88	0.48	112.1	18.6	114.3	2.0%		
GL30c	OSB	B-LVLQ	Type1	None	8	NA	0.8	45	Vrms	0_13_14	0.02	0.405	0.06	0.036	0.022	8.22	0.32	24.03	3.94	11.89	0.49	112.7	28.5	114.4	1.5%		
GL30c	GL28c	S-LVLQ	Type1	1	8	NA	0.8	45	Vrms	0_0_15	0.033	0.45	0.033	0.036	0.036	8.28	0.43	23.98	3.91	16.26	0.37	89.3	13.3	89.4	0.1%		
S-LVL5	S-LVL5	S-LVLQ	Type1	1	8	NA	0.8	45	Vrms	0_1_16	0.033	0.45	0.033	0.036	0.039	8.29	0.42	23.67	3.85	16.12	0.37	91.1	14.9	91.3	0.2%		
GL30c	B-LVL5	S-LVLQ	Type1	1	8	NA	0.8	45	Vrms	0_2_17	0.033	0.45	0.033	0.036	0.04	8.51	0.40	21.97	3.45	15.25	0.42	94.5	17.9	94.4	-0.1%		
GL30c	GL28c	B-LVLQ	Type1	1	8	NA	0.8	45	Vrms	0_3_18	0.02	0.495	0.03	0.036	0.036	8.10	0.50	24.65	4.10	19.45	0.30	88.3	18.3	88.5	-0.2%		
S-LVL5	S-LVL5	S-LVLQ	Type1	1	8	NA	0.8	45	Vrms	0_4_19	0.02	0.495	0.03	0.036	0.039	8.16	0.49	24.03	3.96	19.15	0.31	88.0	20.1	85.9	-2.3%		
GL30c	B-LVL5	B-LVLQ	Type1	1	8	NA	0.8	45	Vrms	0_5_20	0.033	0.45	0.033	0.036	0.04	8.49	0.42	22.08	3.49	14.04	0.43	91.5	23.4	88.5	-2.3%		
S-LVL5	S-LVL5	S-LVLQ	Type1	1	8	NA	0.8	45	Vrms	0_6_21	0.033	0.4	0.039	0.027	0.057	8.03	0.43	24.62	4.17	14.85	0.34	97.7	17.6	95.8	-2.0%		
B-LVL5	B-LVL5	S-LVLQ	Type1	1	8	NA	0.8	45	Vrms	0_7_22	0.033	0.44	0.033	0.04	0.04	8.27	0.40	23.00	3.64	15.20	0.39	98.5	23.5	98.3	-0.2%		
S-LVL5	B-LVL5	B-LVLQ	Type1	1	8	NA	0.8	45	Vrms	0_8_23	0.03	0.4	0.04	0.027	0.051	8.09	0.41	23.34	3.83	14.44	0.36	99.5	26.5	103.8	4.3%		
B-LVL5	B-LVL5	B-LVLQ	Type1	1	8	NA	0.8	45	Vrms	0_9_24	0.02	0.48	0.03	0.04	0.04	8.11	0.47	23.33	3.78	18.15	0.32	95.4	29.5	94.1	-1.4%		
GL30c	HB	S-LVLQ	Type1	1	8	NA	0.8	45	Vrms	0_10_25	0.033	0.45	0.033	0.036	0.007	8.16	0.43	24.84	4.11	16.31	0.36	103.8	18.9	103.6	-0.1%		
GL30c	HB	B-LVLQ	Type1	1	8	NA	0.8	45	Vrms	0_11_26	0.02	0.495	0.03	0.036	0.007	8.26	0.47	23.86	3.85	19.00	0.33	100.9	24.3	100.7	-0.2%		
GL30c	OSB	S-LVLQ	Type1	1	8	NA	0.8	45	Vrms	0_12_27	0.033	0.45	0.033	0.036	0.012	8.03	0.43	25.52	4.30	16.58	0.34	101.6	15.3	101.4	-0.2%		
GL30c	OSB	B-LVLQ	Type1	1	8	NA	0.8	45	Vrms	0_13_28	0.02	0.495	0.03	0.036	0.012	8.13	0.48	24.49	4.03	19.30	0.32	98.2	20.7	97.9	-0.3%		
GL30c	GL28c	S-LVLQ	Type2	None	8	NA	0.8	45	Vrms	0_0_29	0.033	0.495	0.063	0.036	0.036	8.50	0.23	18.21	2.54	8.97	0.72	109.6	17.5	109.6	0.0%		
GL30c	S-LVL5	S-LVLQ	Type2	None	8	NA	0.8	45	Vrms	0_1_30	0.033	0.45	0.063	0.036	0.045	8.08	0.25	19.99	2.99	9.21	0.59	110.7	19.2	109.4	-1.2%		
GL30c	B-LVL5	S-LVLQ	Type2	None	8	NA	0.8	45	Vrms	0_2_31	0.033	0.45	0.063	0.036	0.04	8.18	0.25	19.31	2.83	8.86	0.62	112.3	21.8	112.2	-0.1%		
GL30c	GL28c	B-LVLQ	Type2	None	8	NA	0.8	45	Vrms	0_3_32	0.02	0.54	0.06	0.036	0.036	8.20	0.25	19.10	2.76	9.51	0.62	107.6	26.6	105.0	-2.4%		
S-LVL5	S-LVL5	B-LVLQ	Type2	None	8	NA	0.8	45	Vrms	0_4_33	0.02	0.54	0.06	0.036	0.039	8.28	0.24	18.39	2.64	9.37	0.64	109.7	28.5	107.2	-2.3%		
GL30c	B-LVL5	B-LVLQ	Type2	None	8	NA	0.8	45	Vrms	0_5_34	0.02	0.495	0.06	0.036	0.04	8.02	0.28	19.61	2.90	9.37	0.57	110.6	31.4	110.4	-0.2%		
S-LVL5	S-LVL5	S-LVLQ	Type2	None	8	NA	0.8	45	Vrms	0_6_35	0.039	0.4	0.063	0.027	0.075	8.06	0.25	19.62	2.92	8.59	0.59	120.5	22.7	116.8	-3.0%		
B-LVL5	B-LVL5	S-LVLQ	Type2	None	8	NA	0.8	45	Vrms	0_7_36	0.033	0.48	0.063	0.04	0.04	8.56	0.22	17.40	2.34	8.37	0.77	119.0	28.6	116.1	-2.4%		
S-LVL5	B-LVL5	B-LVLQ	Type2	None	8	NA	0.8	45	Vrms	0_8_37	0.04	0.4	0.06	0.027	0.063	8.10	0.25	18.81	2.71	8.55	0.61	122.0	35.3	126.4	3.6%		
B-LVL5	B-LVL5	B-LVLQ	Type2	None	8	NA	0.8	45	Vrms	0_9_38	0.02	0.52	0.06	0.04	0.04	8.32	0.23	18.00	2.47	8.85	0.69	117.3	38.7	116.9	-0.9%		
GL30c	HB	S-LVLQ	Type2	None	8	NA	0.8	45	Vrms	0_10_39	0.033	0.495	0.063	0.036	0.007	8.47	0.23	18.40	2.57	8.85	0.73	124.4	23.6	123.2	-0.3%		
GL30c	HB	B-LVLQ	Type2	None	8	NA	0.8	45	Vrms	0_11_40	0.02	0.54	0.06	0.036	0.007	8.34	0.23	18.52	2.60	9.27	0.68	122.3	33.2	122.1	-0.2%		
GL30c	OSB	S-LVLQ	Type2	None	8	NA	0.8	45	Vrms	0_12_41	0.033	0.495	0.063	0.036	0.012	8.30	0.23	18.08	2.74	9.04	0.68	121.6	19.9	121.4	-0.2%		
GL30c	OSB	B-LVLQ	Type2	None	8	NA	0.8	45	Vrms	0_13_42	0.02	0.54	0.06	0.036	0.012	8.19	0.24	19.16	2.75	9.47	0.64	119.5	29.2	119.1	-0.3%		
GL30c	GL28c	S-LVLQ	Type2	1	8	NA	0.8	45	Vrms	0_0_43	0.033	0.585	0.033	0.036	0.036	8.55	0.30	17.43	2.36	11.99	0.57	96.7	14.2	94.2	-2.6%		
GL30c	B-LVL5	S-LVLQ	Type2	1	8	NA	0.8	45	Vrms	0_1_44	0.033	0.54	0.033	0.036	0.039	8.02	0.33	19.72	2.91	12.64	0.44	96.3	15.8	98.7	2.5%		
GL30c	B-LVL5	B-LVLQ	Type2	1	8	NA	0.8	45	Vrms	0_2_45	0.033	0.54	0.033	0.036	0.04	8.31	0.31	18.08	2.54	11.87	0.51	100.0	19.4	99.7	-0.3%		
GL30c	GL28c	B-LVLQ	Type2	1	8	NA	0.8	45	Vrms	0_3_46	0.02	0.63	0.02	0.036	0.048	8.08	0.45	19.42	2.84	17.76	0.33	91.7	17.1	86.6	-5.6%		
GL30c	B-LVL5	B-LVLQ	Type2	1	8	NA	0.8	45	Vrms	0_4_47	0.02	0.63	0.02	0.036	0.051	8.19	0.44	18.70	2.68	17.38	0.35	94.8	20.0	88.6	-6.5%		
GL30c	S-LVL5	S-LVLQ	Type2	1	8	NA	0.8	45	Vrms	0_5_48	0.02	0.63	0.02	0.036	0.04	8.05	0.44	19.23	2.81	17.57	0.35	93.3	23.0	90.3	-3.3%		
S-LVL5	S-LVL5	S-LVLQ	Type2	1	8	NA	0.8	45	Vrms	0_6_49	0.045	0.4	0.069	0.027	0.075	8.03	0.22	18.60	2.66	7.44	0.67	127.6	24.3	123.6	-3.1%		
B-LVL5	B-LVL5	S-LVLQ	Type2	1	8	NA	0.8	45	Vrms	0_7_50	0.033	0.56	0.033	0.04	0.04	8.51	0.28	17.02	2.25	11.31	0.59	106.6	27.1	103.6	-2.9%		
S-LVL5	B-LVL5	B-LVLQ	Type2	1	8	NA	0.8	45	Vrms	0_8_51	0.05	0.4	0.05	0.027	0.075	8.01	0.24	18.23	2.36	13.57	0.61	125.3	36.1	131.2	4.8%		
B-LVL5	B-LVL5	B-LVLQ	Type2	1	8	NA	0.8	45	Vrms	0_9_52	0.02	0.6	0.03	0.04	0.04	8.35	0.33	17.52	2.36	13.57	0.48	103.6	33.1	96.7	-6.3%		
GL30c	HB	S-LVLQ	Type2	1	8	NA	0.8	45	Vrms	0_10_53	0.033	0.585	0.033	0.036	0.007	8.38	0.30	18.									

Table 11: Global ECO2 optimum compared to MISLP for current common method (Hu and Chui)

		Constraints								Manual CO2 optimum														MISLP	
edge	Material	flistz	flc	ontology	Ceiling system			Deflection		Type	ID	Dimensions						Constraint level				Objective		[0.5, 1.5]	
					min	max	min	max	toplg_tot			ceflght	benflc_tot	edg_b_w	flidg_w	f1	w	wfin	Ra	Rc	Hc	cost	CO2	CO2	error
GL30c	GL28c	S-LVLQ	Type1	None	10	NA	1.3	45	HC	0 0 1	0.033	0.495	0.063	0.036	0.036	10.37	0.23	15.85	1.78	9.88	1.13	109.6	17.5	17.5	0.3%
GL30c	S-LVLS	S-LVLQ	Type1	None	10	NA	1.3	45	HC	0 1 2	0.033	0.54	0.063	0.036	0.027	10.32	0.22	15.98	1.81	10.29	1.15	111.9	18.6	18.6	0.0%
GL30c	B-LVLS	S-LVLQ	Type1	None	10	NA	1.3	45	HC	0 2 3	0.033	0.495	0.063	0.036	0.04	10.69	0.22	14.35	1.50	9.15	1.29	115.0	22.6	22.1	-2.0%
GL30c	GL28c	B-LVLQ	Type1	None	10	NA	1.3	45	HC	0 3 4	0.02	0.585	0.06	0.036	0.036	10.61	0.22	14.48	1.52	9.77	1.24	110.0	26.9	26.6	-1.3%
GL30c	S-LVLS	B-LVLQ	Type1	None	10	NA	1.3	45	HC	0 4 5	0.02	0.585	0.06	0.036	0.033	10.30	0.23	15.79	1.71	10.16	1.13	112.1	28.4	28.3	-0.4%
GL30c	B-LVLS	B-LVLQ	Type1	None	10	NA	1.3	45	HC	0 5 6	0.02	0.54	0.06	0.036	0.04	10.37	0.23	14.64	1.61	9.55	1.14	113.3	32.2	31.4	-2.3%
S-LVLS	S-LVLS	S-LVLQ	Type1	None	10	NA	1.3	45	HC	0 6 7	0.051	0.4	0.069	0.027	0.063	10.05	0.21	15.74	1.86	8.30	1.14	127.9	24.3	23.4	-3.6%
B-LVLS	B-LVLS	S-LVLQ	Type1	None	10	NA	1.3	45	HC	0 7 8	0.033	0.48	0.063	0.04	0.04	10.33	0.22	15.19	1.67	9.14	1.19	119.0	28.6	28.0	-2.2%
S-LVLS	S-LVLS	B-LVLQ	Type1	None	10	NA	1.3	45	HC	0 8 9	0.04	0.4	0.07	0.027	0.075	10.01	0.21	14.82	1.72	7.93	1.17	131.7	38.8	41.3	6.6%
B-LVLS	B-LVLS	B-LVLQ	Type1	None	10	NA	1.3	45	HC	0 9 10	0.02	0.56	0.06	0.04	0.04	10.59	0.21	13.78	1.40	9.01	1.32	120.0	39.9	38.4	-3.7%
GL30c	HB	S-LVLQ	Type1	None	10	NA	1.3	45	HC	0 10 11	0.033	0.495	0.063	0.036	0.007	10.35	0.23	16.01	1.80	9.71	1.15	124.4	23.6	23.6	0.0%
GL30c	HB	B-LVLQ	Type1	None	10	NA	1.3	45	HC	0 11 12	0.02	0.54	0.06	0.036	0.007	10.11	0.23	15.30	1.87	11.35	1.05	123.3	32.4	32.3	-0.3%
GL30c	OSB	S-LVLQ	Type1	None	10	NA	1.3	45	HC	0 12 13	0.033	0.495	0.063	0.036	0.012	10.14	0.23	16.60	1.94	9.95	1.07	121.6	19.9	19.9	0.0%
GL30c	OSB	B-LVLQ	Type1	None	10	NA	1.3	45	HC	0 13 14	0.02	0.585	0.06	0.036	0.012	10.55	0.22	14.66	1.54	9.74	1.26	121.7	29.6	29.1	-1.6%
GL30c	GL28c	S-LVLQ	Type1	1	10	NA	1.3	45	HC	0 15	0.033	0.63	0.033	0.036	0.036	10.96	0.27	13.39	1.29	12.34	1.10	99.1	14.5	14.5	0.1%
GL30c	S-LVLS	S-LVLQ	Type1	1	10	NA	1.3	45	HC	0 1 16	0.033	0.63	0.033	0.036	0.033	10.64	0.28	14.13	1.46	12.84	1.00	101.1	16.0	16.0	-0.2%
GL30c	B-LVLS	S-LVLQ	Type1	1	10	NA	1.3	45	HC	0 2 17	0.033	0.585	0.033	0.036	0.04	10.64	0.28	13.69	1.41	12.13	1.00	102.7	20.2	20.2	0.0%
GL30c	GL28c	B-LVLQ	Type1	1	10	NA	1.3	45	HC	0 3 18	0.02	0.63	0.02	0.036	0.115	11.65	0.33	10.85	0.89	14.67	1.04	118.6	20.7	19.2	-7.0%
GL30c	S-LVLS	B-LVLQ	Type1	1	10	NA	1.3	45	HC	0 4 19	0.03	0.63	0.03	0.048	0.033	10.68	0.27	13.50	1.35	13.18	1.04	104.9	23.8	23.3	-2.1%
GL30c	B-LVLS	B-LVLQ	Type1	1	10	NA	1.3	45	HC	0 5 20	0.02	0.63	0.03	0.09	0.04	10.62	0.27	13.48	1.33	13.94	1.02	113.8	27.4	26.0	-5.0%
S-LVLS	S-LVLS	S-LVLQ	Type1	1	10	NA	1.3	45	HC	0 6 21	0.069	0.4	0.075	0.027	0.063	10.00	0.17	14.21	1.60	6.60	1.41	142.2	27.4	26.5	-3.2%
B-LVLS	B-LVLS	S-LVLQ	Type1	1	10	NA	1.3	45	HC	0 7 22	0.033	0.56	0.039	0.04	0.04	10.36	0.26	14.16	1.49	11.14	1.02	110.2	27.9	27.6	-1.1%
S-LVLS	S-LVLS	B-LVLQ	Type1	1	10	NA	1.3	45	HC	0 8 23	0.06	0.4	0.07	0.027	0.075	10.02	0.17	13.33	1.45	6.57	1.42	144.5	44.1		
B-LVLS	B-LVLS	B-LVLQ	Type1	1	10	NA	1.3	45	HC	0 9 24	0.03	0.6	0.03	0.04	0.04	10.79	0.26	12.68	1.20	12.00	1.09	109.9	35.7	35.4	-0.9%
GL30c	HB	S-LVLQ	Type1	1	10	NA	1.3	45	HC	0 10 25	0.033	0.63	0.033	0.036	0.007	10.74	0.27	14.03	1.41	12.39	1.06	113.7	22.1	22.0	-0.1%
GL30c	HB	B-LVLQ	Type1	1	10	NA	1.3	45	HC	0 11 26	0.03	0.63	0.03	0.036	0.007	10.86	0.27	13.30	1.28	12.17	1.07	114.3	29.5	29.3	0.0%
GL30c	OSB	S-LVLQ	Type1	1	10	NA	1.3	45	HC	0 12 27	0.033	0.63	0.033	0.048	0.012	10.54	0.26	14.48	1.49	12.58	1.04	113.7	17.7	17.3	-2.4%
GL30c	OSB	B-LVLQ	Type1	1	10	NA	1.3	45	HC	0 13 28	0.03	0.63	0.03	0.036	0.012	10.63	0.28	13.79	1.39	13.08	1.00	111.2	24.7	24.7	-0.1%
GL30c	GL28c	S-LVLQ	Type2	None	10	NA	1.3	45	HC	0 0 29	0.033	0.63	0.063	0.036	0.036	10.27	0.17	12.33	1.23	7.51	1.48	116.9	18.4	18.4	0.1%
GL30c	S-LVLS	S-LVLQ	Type2	None	10	NA	1.3	45	HC	0 1 30	0.033	0.63	0.063	0.036	0.039	10.27	0.17	12.20	1.21	7.45	1.49	119.3	20.5	19.9	-3.0%
GL30c	B-LVLS	S-LVLQ	Type2	None	10	NA	1.3	45	HC	0 2 31	0.033	0.585	0.063	0.036	0.04	10.11	0.18	12.42	1.27	7.29	1.40	120.5	24.1	24.1	0.0%
GL30c	GL28c	B-LVLQ	Type2	None	10	NA	1.3	45	HC	0 3 32	0.02	0.63	0.06	0.048	0.048	10.00	0.18	12.61	1.29	7.65	1.36	120.3	28.2	32.4	15.0%
GL30c	S-LVLS	B-LVLQ	Type2	None	10	NA	1.3	45	HC	0 4 33	0.02	0.63	0.06	0.036	0.051	10.02	0.18	12.43	1.28	7.59	1.32	120.3	30.6	29.3	-4.2%
GL30c	B-LVLS	B-LVLQ	Type2	None	10	NA	1.3	45	HC	0 5 34	0.02	0.63	0.06	0.073	0.04	10.00	0.16	12.38	1.24	7.52	1.48	128.5	34.9	33.6	-3.5%
S-LVLS	S-LVLS	S-LVLQ	Type2	None	10	NA	1.3	45	HC																
B-LVLS	B-LVLS	S-LVLQ	Type2	None	10	NA	1.3	45	HC																
S-LVLS	S-LVLS	B-LVLQ	Type2	None	10	NA	1.3	45	HC																
B-LVLS	B-LVLS	B-LVLQ	Type2	None	10	NA	1.3	45	HC																
GL30c	HB	S-LVLQ	Type2	None	10	NA	1.3	45	HC																
GL30c	HB	B-LVLQ	Type2	None	10	NA	1.3	45	HC																
GL30c	OSB	S-LVLQ	Type2	None	10	NA	1.3	45	HC																
GL30c	OSB	B-LVLQ	Type2	None	10	NA	1.3	45	HC																
GL30c	GL28c	S-LVLQ	Type2	1	10	NA	1.3	45	HC																
GL30c	S-LVLS	S-LVLQ	Type2	1	10	NA	1.3	45	HC																
GL30c	B-LVLS	S-LVLQ	Type2	1	10	NA	1.3	45	HC																
GL30c	GL28c	B-LVLQ	Type2	1	10	NA	1.3	45	HC																
GL30c	S-LVLS	B-LVLQ	Type2	1	10	NA	1.3	45	HC																
GL30c	B-LVLS	B-LVLQ	Type2	1	10	NA	1.3	45	HC																
S-LVLS	S-LVLS	S-LVLQ	Type2	1	10	NA	1.3	45	HC																
B-LVLS	B-LVLS	S-LVLQ	Type2	1	10	NA	1.3	45	HC																
S-LVLS	S-LVLS	B-LVLQ	Type2	1	10	NA	1.3	45	HC																
B-LVLS	B-LVLS	B-LVLQ	Type2	1	10	NA	1.3	45	HC																
GL30c	HB	S-LVLQ	Type2	1	10	NA	1.3	45	HC																
GL30c	HB	B-LVLQ	Type2	1	10																				

Table 12: Global ECO2 optimum compared to MISLP for second generation of Eurocode 5 (Resonant response)

edge	Material	flidist	flg	Constraints				Manual CO2 optimum															MISLP [0.5, 1.5]		
				overlay	Cutting system	f1		Deflection		Type	ID	Dimensions			Constraint level					Objective					
						min	max	wmax [mm]	wfin [mm]			topflg_tot	coeffflg	banflg_tot	edflg_w	flidflg_w	f1	w	wfin	Ra	Rb	HC		cost	CO2
GL30c	GL28c	S-LVLQ	Type1	None	4.5	8	0.8	45	Arms	0_0_1	0.033	0.27	0.063	0.036	0.036	6.48	0.49	41.99	8.92	15.47	0.19	97.4	16.0		
GL30c	S-LVLS	S-LVLQ	Type1	None	4.5	8	0.8	45	Arms	0_1_2	0.033	0.27	0.063	0.036	0.033	6.35	0.50	43.65	9.38	15.89	0.17	99.5	16.7		
GL30c	B-LVLS	S-LVLQ	Type1	None	4.5	8	0.8	45	Arms	0_2_3	0.033	0.27	0.063	0.036	0.04	6.62	0.46	39.24	8.21	14.72	0.20	101.3	18.8		
GL30c	GL28c	B-LVLQ	Type1	None	4.5	8	0.8	45	Arms	0_3_4	0.021	0.315	0.06	0.036	0.036	6.27	0.51	42.94	9.11	16.13	0.17	95.4	25.2		
GL30c	S-LVLS	B-LVLQ	Type1	None	4.5	8	0.8	45	Arms	0_4_5	0.021	0.315	0.06	0.036	0.033	6.16	0.52	44.45	9.52	16.51	0.16	97.5	26.0		
GL30c	B-LVLS	B-LVLQ	Type1	None	4.5	8	0.8	45	Arms	0_5_6	0.021	0.315	0.06	0.036	0.04	6.51	0.48	38.85	8.06	15.12	0.19	99.7	28.4		
S-LVLS	S-LVLS	S-LVLQ	Type1	None	4.5	8	0.8	45	Arms	0_6_7	0.033	0.3	0.063	0.027	0.027	6.66	0.47	39.60	8.26	15.46	0.20	100.8	17.6	17.6	-0.1%
B-LVLS	B-LVLS	S-LVLQ	Type1	None	4.5	8	0.8	45	Arms	0_7_8	0.039	0.24	0.063	0.04	0.04	6.23	0.48	43.81	9.31	14.89	0.17	106.2	22.3		
S-LVLS	S-LVLS	B-LVLQ	Type1	None	4.5	8	0.8	45	Arms	0_8_9	0.02	0.36	0.06	0.027	0.027	6.61	0.47	38.46	7.90	15.66	0.20	98.4	27.1	27.0	-0.4%
B-LVLS	B-LVLS	B-LVLQ	Type1	None	4.5	8	0.8	45	Arms	0_9_10	0.02	0.28	0.06	0.04	0.05	6.04	0.52	44.67	9.47	15.68	0.15	103.0	32.4		
GL30c	HB	S-LVLQ	Type1	None	4.5	8	0.8	45	Arms	0_10_11	0.033	0.27	0.063	0.036	0.007	6.48	0.48	42.06	8.90	15.28	0.19	112.1	19.7		
GL30c	HB	B-LVLQ	Type1	None	4.5	8	0.8	45	Arms	0_11_12	0.021	0.315	0.06	0.036	0.007	6.55	0.47	39.54	8.16	14.43	0.20	110.0	29.3		
GL30c	OSB	S-LVLQ	Type1	None	4.5	8	0.8	45	Arms	0_12_13	0.033	0.27	0.063	0.036	0.04	6.97	0.47	41.48	8.75	15.07	0.18	105.1	17.4	17.7	1.5%
GL30c	OSB	B-LVLQ	Type1	None	4.5	8	0.8	45	Arms	0_13_14	0.021	0.315	0.06	0.036	0.012	6.46	0.47	40.49	8.42	15.65	0.19	107.7	26.9		
GL30c	GL28c	S-LVLQ	Type1	1	4.5	8	0.8	45	Arms	0_15	0.033	0.315	0.033	0.036	0.036	6.13	0.69	44.53	9.52	21.53	0.11	82.0	12.4	12.5	0.6%
GL30c	S-LVLS	S-LVLQ	Type1	1	4.5	8	0.8	45	Arms	0_1_16	0.033	0.36	0.033	0.036	0.027	6.56	0.61	38.85	7.98	20.72	0.15	85.1	13.3	13.3	-0.2%
GL30c	B-LVLS	S-LVLQ	Type1	1	4.5	8	0.8	45	Arms	0_2_17	0.033	0.315	0.033	0.036	0.04	6.26	0.66	41.69	8.81	20.53	0.13	86.3	15.7	15.7	0.2%
GL30c	GL28c	B-LVLQ	Type1	1	4.5	8	0.8	45	Arms	0_3_18	0.021	0.45	0.02	0.048	0.036	6.73	0.77	36.83	7.36	28.58	0.13	79.5	15.7		
GL30c	S-LVLS	B-LVLQ	Type1	1	4.5	8	0.8	45	Arms	0_4_19	0.021	0.495	0.02	0.036	0.027	6.95	0.74	39.50	6.77	28.30	0.14	79.8	16.4	16.0	-2.7%
GL30c	B-LVLS	B-LVLQ	Type1	1	4.5	8	0.8	45	Arms	0_5_20	0.021	0.315	0.06	0.036	0.04	6.87	0.74	42.14	8.24	26.72	0.14	82.4	26.6	26.6	0.1%
S-LVLS	S-LVLS	S-LVLQ	Type1	1	4.5	8	0.8	45	Arms	0_6_21	0.033	0.36	0.033	0.027	0.027	6.54	0.63	38.99	8.04	20.72	0.15	85.9	14.4		
B-LVLS	B-LVLS	S-LVLQ	Type1	1	4.5	8	0.8	45	Arms	0_7_22	0.033	0.32	0.033	0.04	0.04	6.30	0.63	40.68	8.38	19.92	0.13	90.3	20.0	19.8	-0.7%
S-LVLS	S-LVLS	B-LVLQ	Type1	1	4.5	8	0.8	45	Arms	0_8_23	0.02	0.4	0.03	0.027	0.027	6.34	0.75	40.77	8.48	24.87	0.11	82.1	19.6	19.5	-0.7%
B-LVLS	B-LVLS	B-LVLQ	Type1	1	4.5	8	0.8	45	Arms	0_9_24	0.02	0.44	0.02	0.04	0.04	6.76	0.75	34.91	6.80	26.75	0.13	86.3	25.6		
GL30c	HB	S-LVLQ	Type1	1	4.5	8	0.8	45	Arms	0_10_25	0.033	0.315	0.033	0.036	0.008	6.12	0.68	44.77	9.54	21.25	0.12	97.6	17.1	16.6	-2.9%
GL30c	HB	B-LVLQ	Type1	1	4.5	8	0.8	45	Arms	0_11_26	0.021	0.405	0.02	0.066	0.007	6.51	0.78	39.97	8.04	29.48	0.12	94.4	20.8	20.5	-1.7%
GL30c	OSB	S-LVLQ	Type1	1	4.5	8	0.8	45	Arms	0_12_27	0.033	0.315	0.033	0.036	0.018	6.13	0.67	40.10	9.36	20.92	0.12	91.6	14.3	14.5	1.9%
GL30c	OSB	B-LVLQ	Type1	1	4.5	8	0.8	45	Arms	0_13_28	0.021	0.45	0.02	0.036	0.012	7.03	0.73	33.82	6.56	27.54	0.15	89.6	17.6	17.4	-1.1%
GL30c	GL28c	S-LVLQ	Type2	None	4.5	8	0.8	45	Arms	0_29	0.033	0.315	0.063	0.036	0.036	5.94	0.40	37.83	7.28	12.38	0.18	99.8	16.3	16.4	0.3%
GL30c	S-LVLS	S-LVLQ	Type2	None	4.5	8	0.8	45	Arms	0_1_30	0.033	0.315	0.063	0.036	0.027	5.63	0.42	42.14	8.25	13.33	0.14	104.8	19.2	18.9	-2.0%
GL30c	B-LVLS	S-LVLQ	Type2	None	4.5	8	0.8	45	Arms	0_2_31	0.033	0.27	0.063	0.066	0.04	5.43	0.44	44.84	8.76	13.01	0.14	104.8	19.2	18.9	-2.0%
GL30c	GL28c	B-LVLQ	Type2	None	4.5	8	0.8	45	Arms	0_3_32	0.021	0.36	0.06	0.036	0.036	5.78	0.42	39.05	7.46	13.03	0.16	97.8	25.5	25.2	-1.0%
GL30c	S-LVLS	B-LVLQ	Type2	None	4.5	8	0.8	45	Arms	0_4_33	0.021	0.36	0.06	0.036	0.027	5.46	0.45	43.84	8.50	14.04	0.14	98.4	26.0	26.0	-0.1%
GL30c	B-LVLS	B-LVLQ	Type2	None	4.5	8	0.8	45	Arms	0_5_34	0.021	0.315	0.06	0.036	0.04	5.38	0.48	44.53	8.66	13.53	0.12	99.7	28.4	28.4	0.1%
S-LVLS	S-LVLS	S-LVLQ	Type2	None	4.5	8	0.8	45	Arms	0_6_35	0.033	0.3	0.063	0.027	0.033	5.58	0.45	42.76	8.39	13.17	0.14	102.1	17.9		
B-LVLS	B-LVLS	S-LVLQ	Type2	None	4.5	8	0.8	45	Arms	0_7_36	0.033	0.28	0.063	0.04	0.04	5.55	0.43	42.64	8.25	12.63	0.15	105.4	22.7	22.6	-0.5%
S-LVLS	S-LVLS	B-LVLQ	Type2	None	4.5	8	0.8	45	Arms	0_8_37	0.02	0.36	0.06	0.027	0.027	5.43	0.47	44.16	8.57	14.03	0.13	99.3	27.1	27.1	-0.1%
B-LVLS	B-LVLS	B-LVLQ	Type2	None	4.5	8	0.8	45	Arms	0_9_38	0.02	0.32	0.06	0.04	0.04	5.43	0.45	43.38	8.28	13.24	0.13	103.7	32.7	32.6	-0.4%
GL30c	HB	S-LVLQ	Type2	None	4.5	8	0.8	45	Arms	0_10_39	0.039	0.27	0.063	0.036	0.007	5.50	0.44	44.02	8.63	12.77	0.14	115.7	20.5	20.5	0.2%
GL30c	HB	B-LVLQ	Type2	None	4.5	8	0.8	45	Arms	0_11_40	0.021	0.315	0.06	0.036	0.008	5.43	0.46	44.43	8.62	13.61	0.13	111.0	29.8	29.3	-1.7%
GL30c	OSB	S-LVLQ	Type2	None	4.5	8	0.8	45	Arms	0_12_41	0.033	0.315	0.063	0.036	0.012	5.85	0.49	39.00	7.53	12.44	0.18	112.1	18.1	18.1	0.1%
GL30c	OSB	B-LVLQ	Type2	None	4.5	8	0.8	45	Arms	0_13_42	0.021	0.315	0.06	0.036	0.018	5.46	0.45	35.50	6.40	13.36	0.14	105.0	27.0	27.3	1.0%
GL30c	GL28c	S-LVLQ	Type2	1	4.5	8	1.2	45	Arms	0_43	0.033	0.36	0.033	0.036	0.036	5.65	0.58	40.56	7.78	14.33	0.11	84.5	12.7	12.8	0.5%
GL30c	S-LVLS	S-LVLQ	Type2	1	4.5	8	0.8	45	Arms	0_1_44	0.033	0.36	0.033	0.036	0.027	5.40	0.61	44.59	8.64	18.58	0.10	85.1	13.3	13.3	0.2%
GL30c	B-LVLS	S-LVLQ	Type2	1	4.5	8	0.8	45	Arms	0_2_45	0.033	0.36	0.033	0.036	0.04	5.82	0.55	37.62	7.12	16.54	0.13	89.0	16.4	16.4	0.2%
GL30c	GL28c	B-LVLQ	Type2	1	4.5	8	0.8	45	Arms	0_3_46	0.021	0.45	0.02	0.048	0.036	5.54	0.77	42.28	8.09	25.73	0.08	79.5	15.7	15.4	-1.9%
GL30c	S-LVLS	B-LVLQ	Type2	1	4.5	8	0.8	45	Arms	0_4_47	0.021	0.495	0.02	0.036	0.027	5.72	0.74	39.59	7.54	25.46	0.09	79.9	16.4	16.0	-2.7%
GL30c	B-LVLS	B-LVLQ	Type2	1	4.5	8	0.8	45	Arms	0_5_48	0.021	0.45	0.02	0.036	0.04	5.78	0.75	38.10	7.22	24.01	0.09	82.0	20.0	19.3	-3.6%
S-LVLS	S-LVLS	S-LVLQ	Type2	1	4.5	8	0.8	45	Arms	0_6_49	0.033	0.36	0.033	0.027	0.027	5.38	0.63	44.75	8.68	18.58	0.09	85.9	14.4		
B-LVLS	B-LVLS	S-LVLQ	Type2	1	4.5	8	0.8	45	Arms	0_7_50	0.033	0.32	0.039	0.04	0.04	5.40	0.56	43.45	8.24	16.19	0.11	93.9	20.7	20.6	-0.6%
S-LVLS	S-LVLS	B-LVLQ	Type2	1	4.5	8	0.8	45	Arms	0_8_51	0.02	0.4	0.03	0.027	0.033	5.41	0.72	39.65	8.39	21.99	0.08	83.8	20.0		
B-LVLS	B-LVLS	B-LVLQ	Type2	1	4.5	8	0.8	45	Arms	0_9_52	0.02	0.44	0.02	0.04	0.04	5.62	0.75	39.96	7.47	24.23	0.09	86.3	25.6	24.2	-5.4%
GL30c	HB	S-LVLQ	Type2	1	4.5	8	0.8	45	Arms	0_10_53	0.033	0.36	0.033	0.036	0.007	5.58	0.58	43.70	8.00	17.47					

Table 13: Global ECO2 optimum compared to MISLP for second generation of Eurocode 5 (Transient response)

edge	Material		Constraints						Manual CO2 optimum													MISLP			
			coverly	Ceiling system	f1		Deflection		Type	ID	Dimensions					Constraint level			Objective		[0.5, 1.5]	error			
					min	max	wmax [mm]	wfin [mm]			toprig_cot	ceiling_cot	benrig_cot	edgeL_w	ribL_w	t1	w	wfin	Ra	Rv			HC	cost	CO2
GL30c	GL28c	S-LVLQ	Type1	None	8	NA	0.8	45	Vrms	0_0_1	0.033	0.36	0.063	0.036	0.036	8.09	0.34	26.52	4.57	12.57	0.44	102.3	36.6	16.7	0.4%
GL30c	S-LVL5	S-LVLQ	Type1	None	8	NA	0.8	45	Vrms	0_1_2	0.033	0.405	0.063	0.036	0.027	8.35	0.32	24.86	4.10	12.58	0.51	105.1	17.5	17.6	0.1%
GL30c	B-LVL5	S-LVLQ	Type1	None	8	NA	0.8	45	Vrms	0_2_3	0.033	0.36	0.063	0.036	0.04	8.31	0.33	24.44	4.07	11.83	0.49	106.8	20.3	20.3	0.2%
GL30c	GL28c	B-LVLQ	Type1	None	8	NA	0.8	45	Vrms	0_3_4	0.02	0.45	0.06	0.036	0.036	8.50	0.32	22.97	3.63	12.14	0.53	102.7	36.0	25.8	-1.0%
GL30c	S-LVL5	B-LVLQ	Type1	None	8	NA	0.8	45	Vrms	0_4_5	0.02	0.45	0.06	0.048	0.027	8.00	0.32	26.00	4.40	13.18	0.46	105.3	27.0	26.8	-0.9%
GL30c	B-LVL5	B-LVLQ	Type1	None	8	NA	0.8	45	Vrms	0_5_6	0.02	0.405	0.06	0.036	0.04	8.09	0.34	24.68	4.17	12.26	0.44	105.1	29.9	29.9	0.1%
S-LVL5	S-LVL5	S-LVLQ	Type1	None	8	NA	0.8	45	Vrms	0_6_7	0.033	0.4	0.063	0.027	0.027	8.24	0.34	25.45	4.28	12.71	0.46	105.7	18.8	18.7	-0.3%
B-LVL5	B-LVL5	S-LVLQ	Type1	None	8	NA	0.8	45	Vrms	0_7_8	0.033	0.36	0.063	0.04	0.04	8.24	0.32	24.55	4.02	11.58	0.49	110.8	25.1	24.9	-0.6%
S-LVL5	S-LVL5	B-LVLQ	Type1	None	8	NA	0.8	45	Vrms	0_8_9	0.02	0.4	0.06	0.027	0.051	8.07	0.35	24.94	4.23	12.30	0.42	105.9	29.2	28.7	-1.8%
B-LVL5	B-LVL5	B-LVLQ	Type1	None	8	NA	0.8	45	Vrms	0_9_10	0.02	0.44	0.06	0.04	0.04	8.62	0.29	21.31	3.20	11.18	0.59	111.8	36.3	34.9	-3.8%
GL30c	HB	S-LVLQ	Type1	None	8	NA	0.8	45	Vrms	0_10_11	0.033	0.36	0.063	0.036	0.007	8.09	0.34	26.69	4.58	12.39	0.44	116.8	26.0	21.3	0.2%
GL30c	HB	B-LVLQ	Type1	None	8	NA	0.8	45	Vrms	0_11_12	0.02	0.45	0.06	0.036	0.04	8.46	0.34	24.68	4.42	12.75	0.43	116.8	29.0	33.4	0.0%
GL30c	OSB	S-LVLQ	Type1	None	8	NA	0.8	45	Vrms	0_12_13	0.033	0.36	0.063	0.036	0.018	8.21	0.32	25.42	4.27	11.88	0.48	112.1	38.6	38.6	-0.4%
GL30c	OSB	B-LVLQ	Type1	None	8	NA	0.8	45	Vrms	0_13_14	0.02	0.405	0.06	0.036	0.015	8.04	0.34	25.64	4.34	12.53	0.44	114.6	28.3	28.3	0.0%
GL30c	GL28c	S-LVLQ	Type1	1	8	NA	0.8	45	Vrms	0_0_15	0.033	0.45	0.033	0.036	0.036	8.28	0.43	23.98	3.91	16.26	0.37	89.3	33.3	33.4	0.4%
GL30c	S-LVL5	S-LVLQ	Type1	1	8	NA	0.8	45	Vrms	0_1_16	0.033	0.495	0.033	0.036	0.027	8.47	0.40	22.89	3.61	16.37	0.42	91.8	34.4	34.4	0.0%
GL30c	B-LVL5	S-LVLQ	Type1	1	8	NA	0.8	45	Vrms	0_2_17	0.033	0.45	0.033	0.036	0.04	8.51	0.40	21.97	3.45	15.25	0.42	94.5	31.9	31.9	0.1%
GL30c	GL28c	B-LVLQ	Type1	1	8	NA	0.8	45	Vrms	0_3_18	0.02	0.63	0.02	0.036	0.048	9.72	0.45	16.96	2.12	19.49	0.42	91.7	37.1	36.3	-5.2%
GL30c	S-LVL5	B-LVLQ	Type1	1	8	NA	0.8	45	Vrms	0_4_19	0.02	0.63	0.02	0.036	0.045	9.57	0.45	17.37	2.24	19.82	0.48	92.0	37.9	39.1	-1.2%
GL30c	B-LVL5	B-LVLQ	Type1	1	8	NA	0.8	45	Vrms	0_5_20	0.033	0.45	0.033	0.036	0.04	8.62	0.41	21.34	3.19	15.99	0.44	93.3	35.2	32.7	-1.4%
S-LVL5	S-LVL5	S-LVLQ	Type1	1	8	NA	0.8	45	Vrms	0_6_21	0.039	0.4	0.039	0.027	0.045	8.02	0.41	24.76	4.18	14.29	0.36	97.8	37.6	37.1	-2.5%
B-LVL5	B-LVL5	S-LVLQ	Type1	1	8	NA	0.8	45	Vrms	0_7_22	0.033	0.44	0.033	0.04	0.04	8.27	0.40	23.00	3.64	15.20	0.39	98.5	35.3	33.3	-0.9%
S-LVL5	S-LVL5	B-LVLQ	Type1	1	8	NA	0.8	45	Vrms	0_8_23	0.03	0.4	0.03	0.027	0.075	8.11	0.45	23.20	3.82	16.13	0.33	99.7	35.4	28.7	12.7%
B-LVL5	B-LVL5	B-LVLQ	Type1	1	8	NA	0.8	45	Vrms	0_9_24	0.02	0.48	0.03	0.04	0.04	8.11	0.47	23.53	3.78	18.15	0.32	95.4	29.5	29.2	-0.8%
GL30c	HB	S-LVLQ	Type1	1	8	NA	0.8	45	Vrms	0_10_25	0.033	0.45	0.033	0.036	0.007	8.16	0.43	24.84	4.11	16.31	0.36	103.8	38.9	38.9	0.1%
GL30c	HB	B-LVLQ	Type1	1	8	NA	0.8	45	Vrms	0_11_26	0.02	0.495	0.03	0.036	0.007	8.26	0.47	23.86	3.85	19.00	0.33	100.9	34.5	24.5	0.0%
GL30c	OSB	S-LVLQ	Type1	1	8	NA	0.8	45	Vrms	0_12_27	0.033	0.45	0.033	0.036	0.012	8.03	0.43	25.52	4.30	16.58	0.34	101.6	35.3	35.3	0.0%
GL30c	OSB	B-LVLQ	Type1	1	8	NA	0.8	45	Vrms	0_13_28	0.02	0.495	0.03	0.036	0.012	8.13	0.48	24.49	4.03	19.30	0.32	98.2	30.7	20.7	0.0%
GL30c	GL28c	S-LVLQ	Type2	None	8	NA	0.8	45	Vrms	0_0_29	0.033	0.495	0.063	0.036	0.036	8.50	0.23	18.21	2.54	8.97	0.72	109.6	37.5	37.5	0.3%
GL30c	S-LVL5	S-LVLQ	Type2	None	8	NA	0.8	45	Vrms	0_1_30	0.033	0.54	0.063	0.036	0.027	8.46	0.22	18.36	2.57	9.35	0.73	111.9	38.6	38.3	-1.9%
GL30c	B-LVL5	S-LVLQ	Type2	None	8	NA	0.8	45	Vrms	0_2_31	0.033	0.45	0.063	0.036	0.04	8.18	0.25	19.31	2.83	8.96	0.62	112.3	21.8	21.8	0.1%
GL30c	GL28c	B-LVLQ	Type2	None	8	NA	0.8	45	Vrms	0_3_32	0.02	0.54	0.06	0.036	0.036	8.20	0.25	19.10	2.76	9.51	0.62	107.6	26.6	26.3	-1.1%
GL30c	S-LVL5	B-LVLQ	Type2	None	8	NA	0.8	45	Vrms	0_4_33	0.02	0.585	0.06	0.036	0.027	8.14	0.24	19.37	2.81	9.91	0.63	112.4	28.3	27.5	-2.9%
GL30c	B-LVL5	B-LVLQ	Type2	None	8	NA	0.8	45	Vrms	0_5_34	0.02	0.495	0.06	0.036	0.04	8.02	0.26	19.61	2.90	9.37	0.57	110.6	31.4	31.4	0.0%
S-LVL5	S-LVL5	S-LVLQ	Type2	None	8	NA	0.8	45	Vrms	0_6_35	0.051	0.4	0.063	0.027	0.051	8.02	0.24	19.90	2.97	8.43	0.60	120.0	22.7	21.8	-3.8%
B-LVL5	B-LVL5	S-LVLQ	Type2	None	8	NA	0.8	45	Vrms	0_7_36	0.033	0.44	0.069	0.04	0.04	8.08	0.22	19.51	2.83	8.90	0.66	119.8	28.2	27.2	-3.5%
S-LVL5	S-LVL5	B-LVLQ	Type2	None	8	NA	0.8	45	Vrms	0_8_37	0.04	0.4	0.06	0.027	0.063	8.10	0.25	18.81	2.71	8.55	0.61	122.0	35.3	37.5	6.2%
B-LVL5	B-LVL5	B-LVLQ	Type2	None	8	NA	0.8	45	Vrms	0_9_38	0.02	0.52	0.06	0.04	0.04	8.32	0.23	18.00	2.47	8.85	0.69	117.3	38.7	38.4	-0.7%
GL30c	HB	S-LVLQ	Type2	None	8	NA	0.8	45	Vrms	0_10_39	0.039	0.45	0.063	0.036	0.007	8.15	0.24	19.78	2.91	8.94	0.64	125.3	23.6	23.6	0.0%
GL30c	HB	B-LVLQ	Type2	None	8	NA	0.8	45	Vrms	0_11_40	0.02	0.54	0.06	0.036	0.007	8.34	0.23	18.52	2.60	9.27	0.68	122.3	33.2	33.2	0.0%
GL30c	OSB	S-LVLQ	Type2	None	8	NA	0.8	45	Vrms	0_12_41	0.033	0.495	0.063	0.036	0.012	8.30	0.23	19.08	2.74	9.04	0.68	121.6	39.9	39.9	0.0%
GL30c	OSB	B-LVLQ	Type2	None	8	NA	0.8	45	Vrms	0_13_42	0.02	0.54	0.06	0.036	0.012	8.19	0.24	19.16	2.75	19.47	0.64	119.6	35.2	29.9	0.0%
GL30c	GL28c	S-LVLQ	Type2	1	8	NA	0.8	45	Vrms	0_0_43	0.033	0.585	0.033	0.036	0.036	8.55	0.30	17.43	2.36	11.99	0.57	96.7	34.2	33.9	-1.8%
GL30c	S-LVL5	S-LVLQ	Type2	1	8	NA	0.8	45	Vrms	0_1_44	0.033	0.585	0.033	0.036	0.027	8.00	0.32	19.93	2.95	13.17	0.46	99.0	35.5	35.5	-0.1%
GL30c	B-LVL5	S-LVLQ	Type2	1	8	NA	0.8	45	Vrms	0_2_45	0.033	0.54	0.033	0.036	0.04	8.31	0.31	18.08	2.54	11.87	0.51	100.0	39.4	39.4	0.0%
GL30c	GL28c	B-LVLQ	Type2	1	8	NA	0.8	45	Vrms	0_3_46	0.02	0.63	0.02	0.036	0.048	8.08	0.45	19.42	2.84	17.76	0.33	91.7	37.1	36.5	-3.6%
GL30c	S-LVL5	B-LVLQ	Type2	1	8	NA	0.8	45	Vrms	0_4_47	0.02	0.63	0.02	0.048	0.045	8.00	0.43	19.69	2.88	17.99	0.34	95.1	39.7	38.1	-8.2%
GL																									

2 Conference proceedings papers

2.1 Paper V

Assessing adequacy of numerical representation for optimisation performances in long span timber floors

Sveinung Nesheim, Kjell Arne Malo

For publication in: conference proceedings of World Conference in Timber Engineering 2018, Seoul

Credit author statements

For the Original article presented herein, all authors have contributed to its preparation as described in the below statement:

Sveinung Nesheim: Conceptualization, Methodology, Software, Validation, Formal analysis, Investigation, Resources, Writing - Original Draft, Writing - Review & Editing, Visualization.

Kjell Arne Malo: Writing - Review & Editing, Supervision, Project administration, Funding acquisition.

Assessing adequacy of numerical representation for optimisation performances in long span timber floors

Abstract

Proving confidence and adequacy in numerical representation is of vital importance when optimising a construction through finite element analyses. The numerical representation must be robust to tackle a variation in geometric parameters, and the computational demand minimised as the process of optimisation generally requires a large number of iterations. Assessing goodness of fit of a numerical representation also depends on the component and its complexity and the available data for validation. Herein such assessment is applied to a long span timber floor, which is part of a modular building system in the research project Woodsol. The assessment aims at suggesting criteria for building a flexible and consistent numerical representation with sound approximations of first fundamental modes of deflection, at least computational effort. Prior to presenting the method of qualification the numerical representation, early stages of prototyping and testing of the floor is briefly explained and linked to the above mentioned method.

Keywords

Floor element, Finite element, Numerical representation, Eigen frequency, Modal shape, Optimization'

1 Introduction

Flooring systems capable of spanning ten meters permits an attractive and flexible floor plan offering new possibilities to commercial premises and office buildings. Woodsol is one of a handful of research initiatives currently addressing this topic in the Nordic countries. The initiatives are all investigating timber-based building system incorporating prefabricated floor elements with an increased structural role. Consequently, the stability of the buildings are in various manners dependent of the capacity of the flooring system and vice versa to a certain degree. The structural collaboration is dependent on a range of properties all connected to stiffness and damping and the modes of deflection, and in Woodsol different work packages investigates the various properties of joints and columns and flooring system in a

joint effort of developing the building system. This paper brings attention to development steps subsequent to concept development and initial testing, to where the basis for confidently working through the solution space of the floor element is required. In this process validating the numerical representation and its adequacy is essential. This paper presents results from laboratory tests of a basic floor element which is compared to a range of simulations using finite element analysis (FEA). As will be shown, proper combination and selection of finite elements impose significant influences to the predicted eigen frequencies (hereafter EF) and computational demand, and the accuracy and applicability of the numerical representation has huge variations and pitfalls.

2 Attention to floor element

2.1 Role

The Woodsol building system receives stability from moment resisting frames composed of columns rigidly connected to beams, and where the beams are embedded in the floor elements, making the floor element an inherent structural component of the building system. Advantages is that it allows both façades and internal walls parallel to the plane of the moment resisting frames to be non-constructive, which in turn offers flexible wall solutions and building programme. Initially this principle is treated in its simplest form where the columns is connected to each corner of a basic floor element to provide moment resisting frames. The typical scenario for moment resisting frames is that actions from the global building response may influence the performance of the floor, while the global stability of the building depends directly on the stiffness of the floor element and the moment resisting connections. Each connection between the column and an edge beam in the floor resist currently moment loads in the range of 100 kNm with a corresponding rotational stiffness reaching 10 MNm/rad.

2.2 Particulars

The basic floor elements is a cassette-type composite structure currently with continuous top and bottom flanges with interlaying joists and edge beams of glulam. The element width is 2.4 m as governed by transport limitations when transported horizontally. A full-scale model with span of 9 m has recently been built and tested and compared to numerical analysis. A cross-section of the tested basic floor elements is shown in figure 1. This floor element is subject to further studies pursuing optimisation of performance and production.

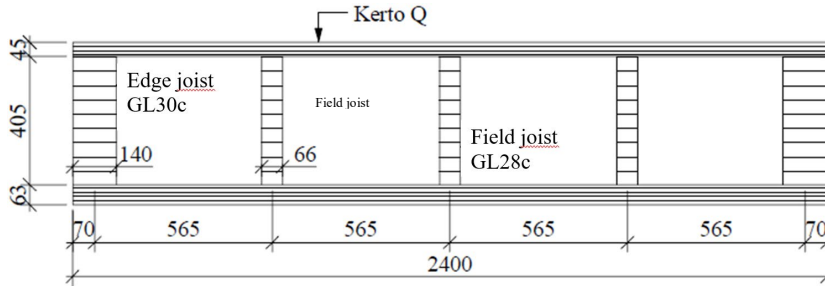


Fig. 1: Cross section of tested floor

2.3 Simply supported response

2.3.1 General

A few key performances is briefly quoted below: Longitudinal and transversal flexural rigidity (EI) is respectively 135 MNm^2 and 80 MNm^2 , corresponding to a first natural frequency of 14.7 Hz when the floor is simply supported. However, in actual use, a number of additional layers increases the weight, and using a pre-accepted composition with integral cast, an increase in weight of 105% is reducing the fundamental frequency to 9.8 Hz. The 1 kN deflection measured to 0.2 mm corresponds to a 85% utilisation of the serviceability criteria by Hu and Chui [1]. The RMS-acceleration from footfall has been calculated to 0.39 m/s^2 and falls within the limit according to the TRADA-method [2], and the element complies with the regulations as given by Eurocode 5 [3]. In general, the performance of the floor element is promising particularly when assessing the distributing effects and damping from adjacent and coupled elements in the modular flooring system.

2.3.2 Measurement of eigen frequencies

While deflection is predicted with good accuracy using finite element analysis (FEA), modal shapes and corresponding eigen frequencies has proved more demanding to simulate with confidence. The lateral acceleration has been difficult to simulate reliably, and even if the first modes of deflection typically agree with measurements, the numerical simulations tend to produce lower EF for higher modes. For the simply supported condition modal response was measured using the rowing hammer technique, and EF for the four first modal shapes are given in the below table:

Table 1: Measured and predicted EF simply supported element

Mode shape	Measured EF [Hz]	Predicted EF [Hz]
1	14.69	14.65
2	21.19	21.54
3	36.72	32.03
4	42.59	36.52

The deviations between the measured and predicted EF are increasing with increasing modal shape. Now, it is highly relevant that the measured EF only represent one sample of an actually built floor and that another floor element would perform differently. However, the deviations are still increasing with increasing modal shape, either arguing the case of an inadequate numerical representation, or vibrations in the frequency range of interest dissipated from the supporting structures influencing the measurements.

2.4 Floating support response

In order to decrease the source of inaccuracy, an experimental modal analysis (EMA) was designed particularly to assess the modal response and to produce data for validation of the numerical representation of the floor element. Validating overall stiffness through eigen frequencies and modal shapes is a vigorous indicator of serviceability performances for floor elements, and is a cost- and time-efficient method. As explained in a separate report [4] the test was designed with free-free boundary conditions to address the challenge with energy dissipation from the support structure and to minimize the uncertainty in the dynamic behaviour of the supporting structure. In order to achieve this the floor element was mounted on air cushions at each corner of the floor element where the structure is at its stiffest, and inflating the air cushions to an appropriate level. This setup provides the rigid body a resonance frequency of some 3.5 Hz, providing a fair approximation of a free-free boundary condition. In short the EMA was carried using the roving hammer technique with three impulses recorded for each excitation point. Two figures explaining the setup is presented below:



Fig. 2: Experimental modal analysis setup

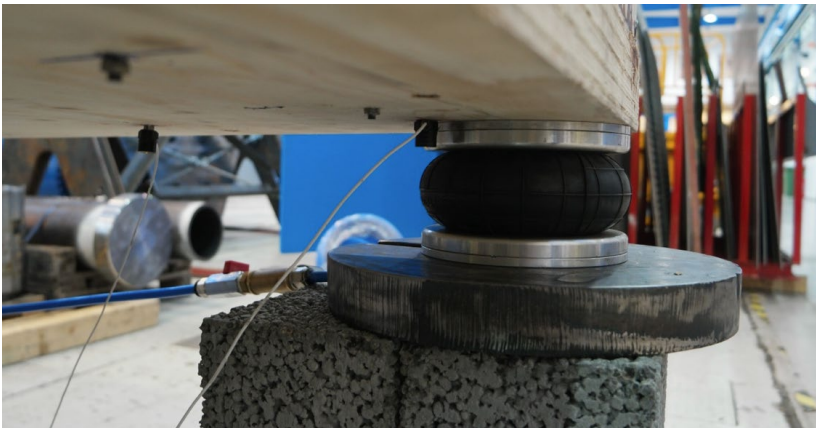


Fig. 3: Parker 6'' 9109-series air cushions in position

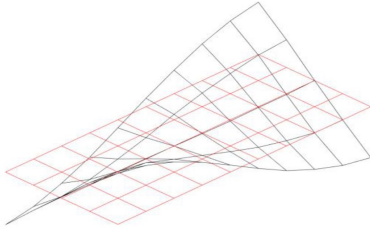
Through the Abnavibe toolbox the eleven first eigen frequencies was extracted from the EMA, and the eigen vectors at a 5 by 10 matrix represent the actual mode shape for the tested floor element. In Table 1 the modal shapes and the corresponding resonance frequencies for the measured and predicted eigen frequencies are compared. However, only the first eight modes is investigated herein as the related study assess low frequency response for the flooring system (i.e. up to 80 Hz as defined in Woodsol), and an adjacent study is assessing vibrations in excess of typically 50 – 80 Hz.

Table 2: Measured and predicted EF for free-free conditions

EMS measured EF

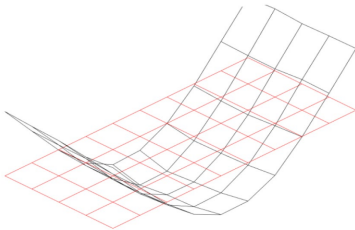
1st torsional: 17.4% difference

Mode 1: 26.03 Hz



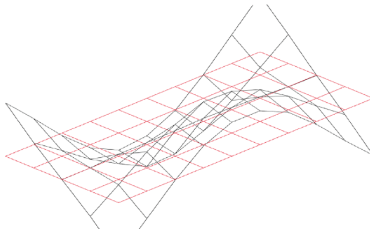
1st longitudinal: 1.8% difference

Mode 2: 31.93 Hz



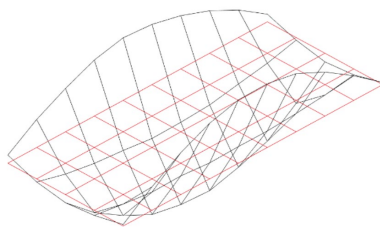
2nd torsional: 6.6% difference

Mode 3: 42.07 Hz



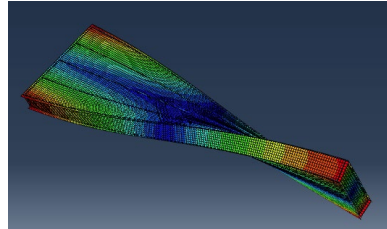
1st transverse: 14.5 difference

Mode 4: 42.68 Hz

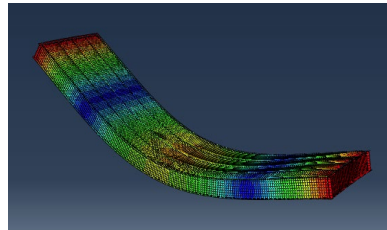


FEA predicted EF

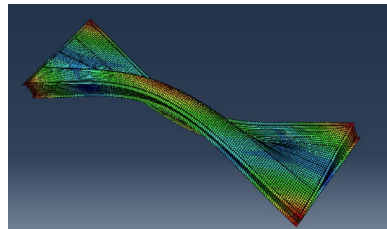
Mode 1: 23.86 Hz



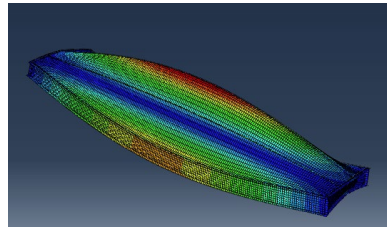
Mode 2: 31.64 Hz



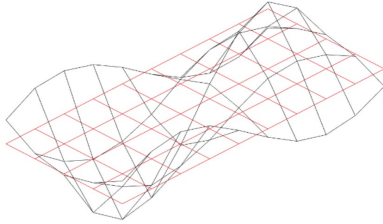
Mode 4: 40.12 Hz



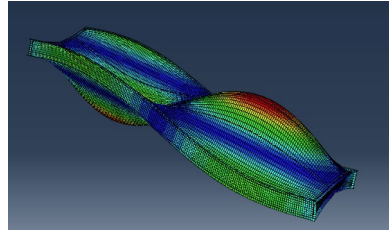
Mode 3: 37.86 Hz



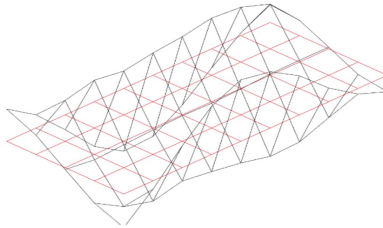
Higher order: 9.6% difference
Mode 5: 65.68 Hz



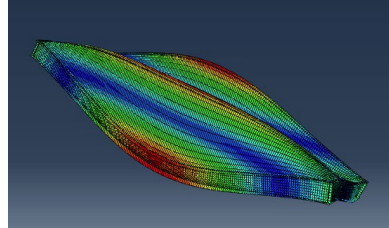
Mode 6: 60.53 Hz



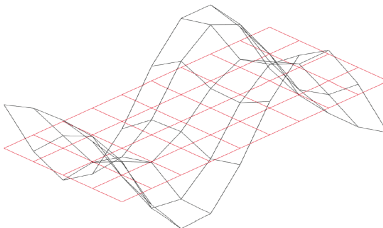
2nd transverse: 19.5% difference
Mode 6: 71.89 Hz



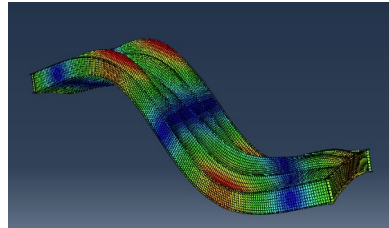
Mode 5: 60.50 Hz



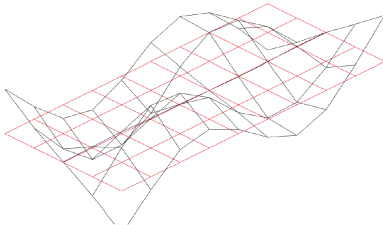
2nd longitudinal: 6.4% difference
Mode 7: 72.33 Hz



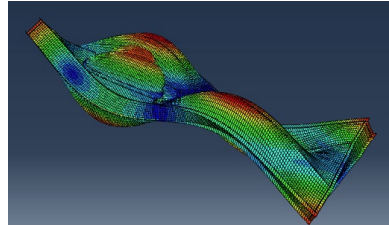
Mode 7: 68.48 Hz



Higher order: 8.0% difference
Mode 8: 74.96 Hz



Mode 8: 70.42 Hz



As the figure and numbers show, the torsional and transverse predictions disagree in particular to measured eigen frequencies, encouraging further studies.

2.5 Typical stresses and behaviour

For a closed hollow box section without transverse stiffeners, the below stresses and responses are important for the numerical model to be able to reproduce:

- Compression stresses, shear lag and local buckling of the top flange
- In-plane bending of the joists
- In-plane shear of joists as well as local buckling
- Tension in bottom flange as well as shear lag
- Flange curling and representation of transverse bending of the floor element. The response will impose bending with respect to longitudinal axis and out-of-plane shear for the joists.
- Twisting is likely to occur and rotational stiffness is essential. The model must be able to represent St. Venant behaviour for the complete element.

3 Numerical representation

3.1 Approach to the problem

Carefully addressing the above-mentioned responses in connection with the structural dimensions of each member will give indications to which type of finite element (hereafter element) that will produce reliable results. However, as the model is composed of a number of different members of varying size and role, this assessment is not straightforward. The number of available elements is vast, and e.g. Abaqus/Standard that is used in this analysis offers some 550 elements [5], and even if only about 20 of these are applicable for the problem, it is still a large number of possible elements. Moreover, due to requirements of building a numerical representation capable of optimisation, it is of essential importance to keep the computational effort at a minimum, whilst maintaining the precision.

3.2 Material properties

The material model for the analysis is given in Table 3 respectively for density (ρ), Young's-modulus (E), Poisson's-ratio (ν), and shear modulus (G). The material model for glulam is taken from tests by Dahl [6] and for Kerto-Q from sources at Metsä Wood directly [7].

Table 3: Material model in engineering constants format

Property	GL28c	GL30c	Kerto-Q
ρ [kg/m ³]	430	430	510
E_1 [N/m ²]	12500E6	13000E6	10500E6
E_2 [N/m ²]	300E6	300E6	2000E6
E_3 [N/m ²]	300E6	300E6	130E6
ν_{12} [1]	0.39	0.39	0.11
ν_{13} [1]	0.49	0.49	0.81
ν_{23} [1]	0.64	0.64	0.07
G_{12} [N/m ²]	650E6	650E6	600E6
G_{13} [N/m ²]	650E6	650E6	120E6
G_{23} [N/m ²]	65E6	65E6	22E6

3.3 Boundary conditions

For eigen frequency analyses, boundary conditions are suppressed, and system mass not associated with gravitational accelerations, hence the simulation is only solving the eigenvalue problem. For the deflection analyses, the model is simply supported along the bottom edge or vertices of the edge joists, and the ends reinforced by an ingrained skin or stringer, respectively for solid and shell, for comparable performance to the actual treaded rods that the floor is supported to. The reinforcement covering the entire end face of the edge joists is modelled in steel with a thickness of 35 mm in order to have the same amount of mass as the rods.

3.4 Element selection

3.4.1 General evaluation

The floor element consists of members that are all tied together, and no slip is assumed. The analysis must in particular produce accurate eigen frequencies and bending modes dominated by both lateral and transversal deformations, as well as energy dissipation through the elements. Only the serviceability is of major interest, and the deformations will not cause severe distortion of the mesh. Looking at the various members, the typical structural dimensions indicate which element theory that is applicable for the specific member, and the following assessment is referring to [8], [9] and [10].

3.4.2 Conventional shell elements

Three Mindlin-Reissner elements is found to have appropriate properties for the model. Reduced integration is normally preferred as the main structural response is dominated by bending, and as full integration normally produce stiffer behaviour due to shear locking. The formulation is used to avoid spurious shear modes, but is not able to detect strains at the integration points, and can possibly cause hourglassing.

This mechanism can be reduced by introducing more elements through the section experiencing the bending. S4R is a robust linear shell element frequently used in applications where the thickness is small with respect to the length of the member, and it is an obvious candidate for the analysis. The full-integration version of the same element might produce too stiff behaviour, but the general purpose S4-element is specifically used for in-plane bending problems and does not suffer from parasitic locking, thus also an obvious candidate. Apart from linear shell element, the quadratic S8R is promising since the meshing in the model is designed to be regular. The S8R is capable of representing beams in particular since it converges to shear flexible theory for moderate to thick members and could be ideal for field joists with changing thicknesses. Discrete Kirchoff elements (S4R5) is not assessed, but is generally a cost-effective element for large models much like a floor element.

3.4.3 Continuum shell elements

Continuum shells are much appreciated in the top flange as it is particularly suitable for composite description when modelled as a solid. In this analysis the continuum shell will only be composed of a single layer through the thickness, but it is important to map its performance for later use. The continuum shell normally offers an accurate description of through-thickness response for composite laminate structures, and the only applicable element for the mesh is SC8R.

3.4.4 Solid elements

For members where the typical shell thickness is more than 1/10 of the structural dimensions, solid elements might be a good option. These are more computationally demanding than shells, and the analysis will compare the performance between solids and shell with the penalty of computational demand. The work of Labonotte et al, [11] have used the reduced integration formulation C3D8R for vibration studies of floor elements, and the same element is recommended in [12]. However, the formulation might, as mentioned, require a larger number of nodes to properly converge, thus increasing the computational effort. The analysis will also use the linear C3D8 as well as the 20-node quadratic brick with reduced integration (C3D20R). Finally C3D8 with incompatible modes is very interesting. C3D8I have an additional degree of freedom (DoF) for bending purposes, enabling capture bending more accurately even with a single element through the thickness, hence having a potential of being computationally efficient.

3.5 Element combination and size

3.5.1 Building the combinations

To compare the performance of the various elements, a framework of base feature combinations is first made. The base feature is the fundamental description deciding if the member is a shell or a solid. The framework presuppose that both edge joists

and both edge beams are equally modelled, resulting in four different members to assemble into unique combinations. Two base features and four different members combines into $2^4 = 16$ combinations as presented in Table 4. The exception from this composition is for the scenarios investigating continuum shell as top flange element where its base feature consequently is kept constant, only varying the bottom flange according to Table 4.

Table 4: Base feature combination chart

Edge members		Field joists	Flanges
Joists	Beams		
solid	solid	Solid	solid
			shell
		Shell	solid
			shell
	shell	Solid	solid
			shell
shell	solid	solid	solid
			shell
		shell	solid
			shell
	shell	solid	solid
			shell
		shell	solid
			shell

Each combination above is referred to as scenarios, and the combinations as a whole as groups. Each group keep the seed size and associated mesh constant, and mesh size variation, which is of vital importance of the overall adequacy, is controlled by the seed size one group one at a time. Normally, a series consist of four groups with changing seed size. The seed sizes are calculated for an overall fit to the dimensions of the members for fitting a regular (quadrilateral or hexahedral) mesh, rather than a more complex three-node mesh as used in [13]. The seed sizes used in the entire analysis is 70, 50, 35, and 25 mm.

3.5.2 Compatible element combinations

For the solids base feature the following elements will be assigned: C3D8, C3D8R, C3D20R, C3D8I and SC8R. The continuum shell is modelled as a solid and listed here. The shell elements assessed is S4, S4R, and S8R. There are however limitations on how to combine these elements. For the regular mesh generated in this analysis linear elements are obviously not combined with quadratic elements. The elements

is arranged in six different combinations corresponding to the six series. Table 5 presents the compatible element combinations used in the analysis, and place them in the six series each with four (three) groups with varying seed size. Note that for quadratic elements, the smallest seed size was either aborted (series BCFF1: 52 of 64 scenarios completed), or not included in the analysed (series BCFF5). The six series as a whole is referred to as the dataset.

Table 5: Compatible combinations of elements

Series	Shell	Solid	Seed size range			
			Group 1	Group 1	Group 1	Group 4
BCFF0	S4	C3D8	0.07	0.05	0.035	0.025
BCFF1	S4R	C3D8R	0.07	0.05	0.035	(0.025)
BCFF2	S8R	C3D20R	0.07	0.05	0.035	0.025
BCFF3	S4	C3D8I	0.07	0.05	0.035	0.025
BCFF4	S4R	C3D8I	0.07	0.05	0.035	0.025
BCFF5	S8R	C3D20R SC8R	0.07	0.05	0.035	

3.6 Analysis and results format

The analysis is performed in Abaqus/Standard. The dataset is read by a Python script which also is building the model, defining the type of job to be performed, and finally writing results to a text file. In addition to pairing identification for controlling that a specific scenario is belongs to a specific output, the text file contain information of number of nodes in the model as well as eigen frequencies for the ten first fundamental frequencies. The number of nodes is used to quantify the computational demand for each scenario. The dataset was imported into Matlab for post-processing and interpretation of the results.

4 Interpretation

4.1 Outline and strategy

Each of the six series in the dataset is treated separately and equally. The overall strategy is to assess how the predicted eigen frequencies (PEF) from the numerical analyses is performing with respect to the two objectives mutually, meaning that the overall condition is met if and only if both objectives are met: The first objective is based on the distribution of results within each series. The larger the distribution, the less agreement within the series, hence a less robust combination of elements, whilst a small distribution and consequently a high consensus between the PEF in the series, is arguing the case of a robust combination of elements, least influenced by seed size,

hence the sought propensity of an adequate element combination. The second objective, which is more tangible, is assessing the performance of PEF with respect to the measured eigen frequencies (hereafter EFAS) as explained in section 2.4. The reason for keeping attention to the first objective in addition to the obvious comparison to measured values, is that the measured values are based on one sample only, thus associated with an inherent uncertainty. Another built floor would naturally perform differently, though within limits. The measured eigen frequencies are still of superior importance, but can hardly be argued to be kept as the sole reference for validation. Finally, scenarios from the entire dataset having an overall high goodness of fit to both objectives, is assessed with respect to its computational demand. A scenario with high goodness of fit for both objectives, which in addition have a low computational demand, is a suitable candidate for bringing further in the assessment and project.

4.2 Processing and visualization

4.2.1 Filtering with Root Mean Square Error

As can be seen from the below Figure 4, the mean values for PEF (Predicted Eigen Frequency) differs from EFAS (Eigen Frequency As Measured) and is consistently lower than the measured values. The figure is showing the minimum and maximum PEF for each series as error bars with respect to the mean predicted EF value. The measured eigen frequencies are plotted for reference. Root Mean Square Error (RMSE) is calculated for each scenario with respect to the two objectives described introductorily. For the first RMSE-calculation, the overall regression is calculated for the six series, and the RMSE is calculated with respect to the regression of the series for which the specific scenario belongs to. Secondly, the other RMSE is calculated with respect to EFAS, see equation (1).

$$rmsE_i = \sqrt{\frac{\sum_{j=1}^n (EFAS_{1,j} - PEF_{i,j})^2}{n}} \quad (1)$$

The RMSE is then applied to filter each scenario for goodness of fit both with respect to the simulation consensus, and the measured eigen frequency. A visualization of the latter is presented in Figure 5. This figure show which single scenario for each series that have PEF closest to EFAS, which scenarios is within the 95% and 80% best fit, and finally rest of the scenarios with least fit to EFAS plotted as dots. As can be seen the filtering is reducing the number of valuable results, but the selection is too large to draw any conclusion.

PART II: Dissemination – Paper V

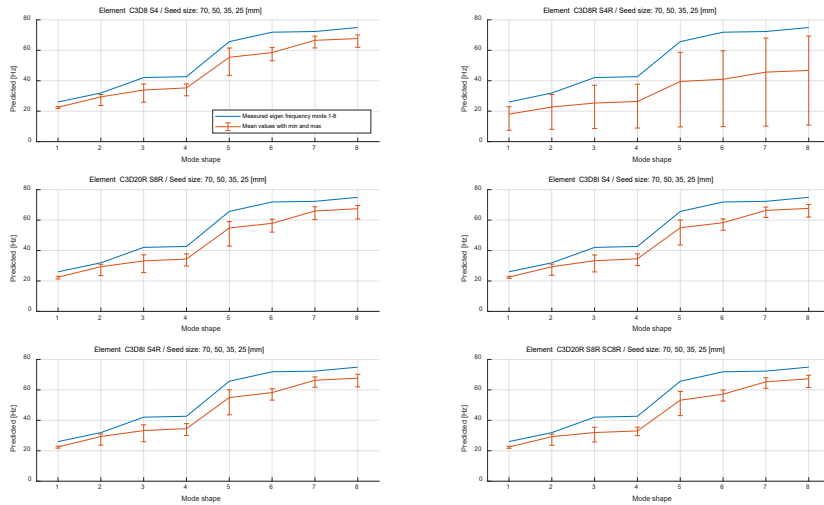


Fig. 4: Simulation minima and maxima as errorbars from mean values at fundamental eigen frequencies

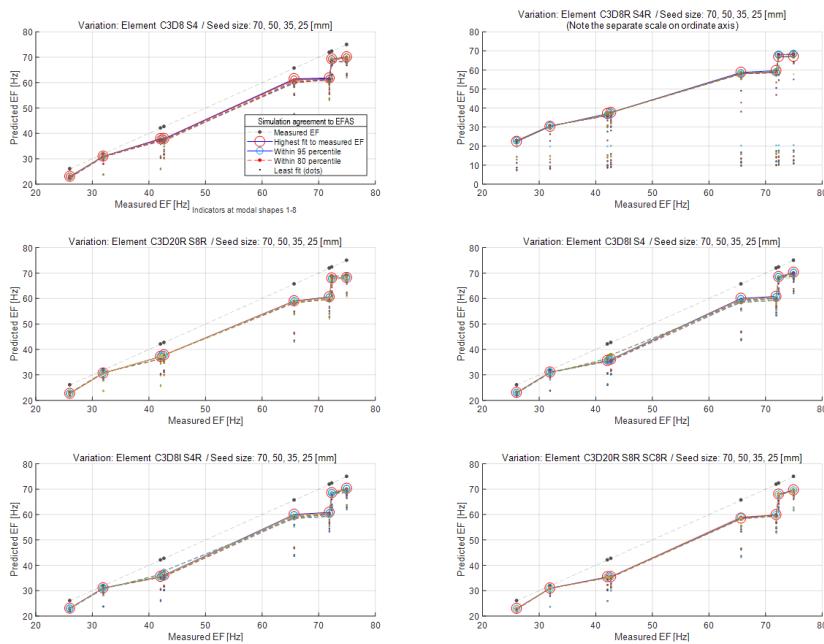


Fig. 5: Simulation agreement to measured eigenfrequencies (EF)

The figures show a unifying performance for all series except the series involving linear elements with reduced integration. As expected, and as described in section 3.4.2 and 3.4.4 particularly the cubic linear element with reduced integration is more dependent on a larger number of elements through the section to converge. As seen in the below figure, the seed size must be decreased from 70 mm til 25 mm before the formulation is converging. In an optimisation procedure this formulation will be computationally demanding.

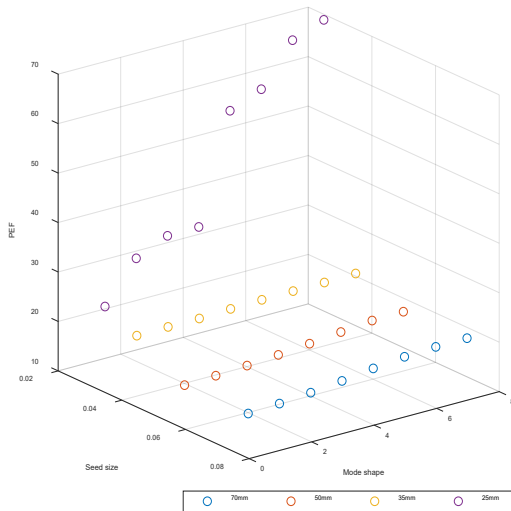


Fig. 6: Converging EF predictions as seed size decrease for the C3D8R (all solids)

Looking at Figure 1 and Figure 5 again, the deviation from mean predicted values to the measured values can as described in section 4.1 be related to the specific performance of the built floor with respect to the mean values used in the material model. An increasing deviation is most certainly also associated with the dry conditions in the test facility. From the material storage where the relative air humidity is kept constant at 65 %, the test facility is much dryer, and the moisture content of the members are reduced from 12 % to as low as 5 %. This obviously affect the stiffness, and current studies are investigating and quantifying the effect this have on the floor performance. The deviation jump as seen from mode shape six to seven is related to lack of censoring in the test floor where only vertical accelerations were recorded.

4.2.2 Mutual fulfilment of objectives

As a preparation for the comparison of goodness of fit to number of nodes in the model, and hence the overall adequacy for the scenarios, a simple rule is applied to the two RMSE-arrays containing values for errors to consent and EFAS for the

dataset. The RMSE is once more filtered to detect how many, and which of the scenarios, that have an RMSE lower than a certain threshold. The threshold is now designed to be comparable across the series, hence calculated for the entire dataset. The threshold both for consent and for EFAS is calculated the same way and is simply the mean value for each of the two RMSE for the entire dataset, minus the mean of the standard deviation for the dataset. This filter removes any scenario with a RMSE larger than the common threshold value with respect to the mean and standard deviation for 1) the numerical consensus for the dataset, and 2) the measured eigen frequencies. As previously, the rule also demand that both conditions shall be fulfilled mutually, producing a list of resulting scenarios that both is positioned one standard deviation above the numerical consensus, and at the same time is predicting eigen frequencies with an accuracy one standard deviation above the mean performance.

4.2.3 Number of nodes as indicators for computational demand

The number of nodes can efficiently be used as an indicator for the required computational effort to solve the associated DoF for the numerical representation. As is demonstrated in paragraph four in section 4.2.1 and illustrated in Figure 6, most finite element formulations will converge towards the strong form solution as the mesh is refined. This is however not associable with time- and cost-efficient FEA, and particularly not when the FEA is used in an optimisation routine. It is of crucial importance to have a model that reliably perform precise simulations with the least amount of computational effort in order to enable an iterative simulation scheme normally used in optimisation.

As prepared in the previous section, the filtered scenarios is now slightly adapted to allow weighted comparison: The resulting scenarios all having a mutual RMSE below the threshold value is normalized between 0 and 1. The associated number of nodes is equally normalized. The minimum and maximum limits used in the normalization is the extremes for the entire dataset, because the scenarios is taken from various series. The vector sum of the normalized mutual RMSE and number of nodes is then calculated for each scenario, indicating the resulting performance of each of the scenarios. Finally, the scenarios is sorted in ascending order. The scenario with the lowest vector sum has both the least root mean square error to both measured eigen frequency and overall numerical consensus of the entire dataset, and at the same time has a low number of nodes and will perform well in an optimisation routine. In the below Figure 7, the mutual RMSE is plotted against node numbers for all scenarios below the objective threshold value. Consequently, the scenarios that has a combined lowest root mean square error with respect to the threshold values, and at the same time has a number of nodes as low as practicably feasible for the particular performance, will have the least radial distance (i.e. vector sum) from origo. Table 6 is showing the same numbers but limited to only cover the scenarios

listed in the legend of Figure 7. These are the eleven scenarios with the lowest vector sum of the entire dataset, i.e. out of a total of 356 scenarios as Table 5 explains.

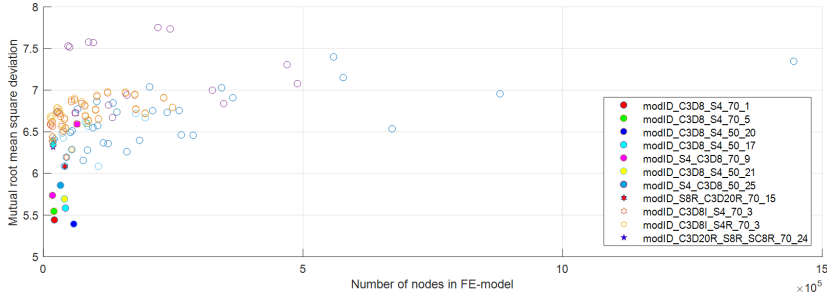


Fig. 7: Mutual Root Mean Square Error as function of computational effort

Table 6: Scenarios with lowest Root Mean Square Error and highest computational effort

Scenario (modID)	RMS error	Num node (1e3)	Seed size [mm]	Outer frame				Internal		Flanges					
				Edge joist		Edge beam		Field joist		Feature type		Element code			
				Type	Elem	Type	Elem	Type	Elem	Top	Bottom	Top	Bottom		
General 4-node shell in combination with 8-node linear solid element															
C3D8 S4 70 1	5.44	21.5	0.07	solid	C3D8	solid	C3D8	solid	C3D8			shell	S4		
C3D8 S4 70 5	5.54	20.6				shell	S4					solid	C3D8	shell	S4
C3D8 S4 50 20	5.39	58.8	0.05	solid	C3D8	solid	C3D8	solid	C3D8			solid	C3D8		
C3D8 S4 50 17	5.58	42.9				shell	S4					solid	C3D8	shell	S4
S4 C3D8 70 9	5.73	17.9	0.07	shell	S4	solid	C3D8	solid	C3D8			shell	S4		
C3D8 S4 50 21	5.69	41.1	0.05	solid	C3D8	shell	S4	solid	C3D8			shell	S4		
S4 C3D8 50 25	5.85	33.4	0.05	shell	S4	solid	C3D8	solid	C3D8			shell	S4		
8-node doubly curved thick shell in combination with 20-node quadratic brick both with reduced integration:															
S8R C3D20R 70 15	6.08	41.1	0.07	shell	S8R	shell	S8R	shell	S8R	shell	S8R	shell	S8R		
S8R C3D20R 70 11	6.19	44.5				solid	C3D20R							shell	S8R
C3D20R S8R 70 7	6.28	55.1				solid	C3D20R							shell	S8R
General 4-node shell in combination with 8-node linear brick element with incompatible modes															
C3D8I S4 70 3	6.32	18.5	0.07	solid	C3D8I	solid	C3D8I	shell	S4	shell	C3D8I	shell	S4		
C3D8I S4 70 7	6.39	17.7				shell	S4							solid	C3D8I
C3D8I S4 70 1	6.40	21.5				solid	C3D8I							solid	C3D8I
General 4-node shell with reduced integration in combination with 8-node linear brick element with incompatible modes															
C3D8I S4R 70 3	6.35	18.5	0.07	solid	C3D8I	solid	C3D8I	shell	S4R	shell	C3D8I	shell	S4R		
C3D8I S4R 70 1	6.41	21.5				shell	S4R	solid	C3D8I						
C3D8I S4R 70 7	6.44	17.7				shell	S4R	shell	S4R						
Quadratic shell and solid both reduced integration in combination with composite compatible continuum shell in top flange															
C3D20R S8R SC8R 70 24	6.59	64.9	0.07	solid	C3D20R	solid	C3D20R	solid	C3D20R	solid	shell	SC8R	S8R		
C3D20R S8R SC8R 70 26	6.72	61.7				shell	S8R							solid	C3D20R
C3D20R S8R SC8R 70 0	6.60	83.4				solid	C3D20R							solid	C3D20R

4.2.4 Final selection with arguments

In the above table combinations of elements and seed sizes having the lowest overall deviation to the objectives is listed in descending order of RMSE. As can be seen, several assumptions from section 3.4 can be identified: Both the edge joists and edge beams have an overall best performance when modelled as a solid. For linear elements C3D8 with or without incompatible modes also perform well. For the field joists these are similarly in most cases found to be performing best with solid elements. However, in an optimisation procedure where the thickness of the field

joists differs, the criteria for choosing solids might quickly rather suggest a Mindlin-Reissner formulation. A reliable choice might therefore be to hold the element constant to S4 (the S4R has relatively high RMSE with respect to S4) for the field joist in combination with C3D8I for edge joists and beams, unless changed as a function of thickness of the field joist during model generation. An alternative is keeping the field joist element constant as a S8R, and changing affected elements to quadratic formulation. The flanges are in the majority of scenarios modelled as a shell with linear elements. The general modelling of joists and flanges (sheathing) thus resembles the configuration suggested in [14]. When composite flanges are not analysed as shells, this work is modelling the composite with continuum elements. In this case the bottom flange is modelled as a quadratic shell element. There is not identified any particular reason for choosing continuum shell formulation instead of conventional shells for model composite flanges.

5 Conclusion

The majority of analyses reviewed during this work use reduced integration, either as linear shells or solids, for the entire floor element. As this study provides information about, this approach might not be associable with an efficient optimisation routine. For flooring system where the mesh in practice is undistorted, computational demand can be reduced while keeping the precision high if the numerical representation is done more selectively. Full integration can successfully be applied to linear shell elements, whilst reduced integration rather can be reserved to quadratic shell formulations when needed in combinations with e.g. S8R formulation for field joists. For the scenarios in Table 6 and likewise, the numerical representation is less influenced by mesh size, and is converging with high precision with a reasonable amount of elements. The table is listing the scenarios in descending order of overall adequacy. Dependent on the structural dimensions of the members, these can all be applied for closed hollow box timber-based floor element. The scenarios have a combined lowest root mean square error with respect to the threshold values for 1) analysis consent, and 2) measured eigen frequencies, and has at the same time a low number of nodes, thus performing well in an optimisation routine. There are no evidence of suggesting a constant combination of elements, but generally the following combinations are all promising and favourable given a comparable relative seed size:

- For moderately thick to thick joists and beams a solid C3D8 formulation, whilst flanges in conventional S4 shells,

- For a robust field joist formulation accepting varying thicknesses the S8R shell formulation in combination with C3D20R for thick edge joists and beams. S8R in flanges.
- For a linear version of the above, field joists modelled with S4 in combination with C3D8I for edge joists and beams, and S4 for flanges.
- For a solid flange formulation, the continuum shell performs well in combination with C3D20R in thick joists and flanges.

The above combinations all perform well within the scope studied herein. However, the recommendations and findings should be accompanied with experiments when possible, but more importantly with experience, sceptics and general understanding of the mathematics, possibilities and limitations of the finite element method.

Acknowledgments

This work is part of the four year project “WoodSol – Wood frame solutions for free space design in urban buildings” realized through the research grant from The Research Council of Norway (254699/E50). The support is gratefully acknowledged. The authors would also like to acknowledge the contribution by students Henning Bjørge, Terje Kristoffersen and Sissel Solibakke Moe in the preparation and execution of the work.

References

- [1] Hu, L.J. and Y.H. Chui, *Development of a design method to control vibrations induced by normal walking action in wood-based floors*, in *Proceedings of the 8th World Conference on Timber Engineering*. 2004: Lahti, Finland. p. 217-222.
- [2] Weckendorf, J., et al., *Vibration serviceability performance of timber floors*. European Journal of Wood and Wood Products, 2016. **74**(3): p. 353-367.
- [3] CEN, *NS-EN 1995-1-1:2004+A1:2008+NA:2010*, in *Design of timber structures - Part 1-1: General - Common rules and rules for buildings*. 2010, European committee for standardization: Brussels.
- [4] Conta, S., *Experimental modal analysis on Woodsol prototype floor element*. 2017: NTNU, Trondheim, Norway. p. 16.
- [5] Dassault Systèmes, *Abaqus/Standard Element Index*. 2014, Dassault Systèmes Simulia corp.
- [6] Dahl, K.B. and K.A. Malo, *Linear shear properties of spruce softwood*. Wood Science and Technology, 2009. **43**(5): p. 499-525.
- [7] Hakkarainen, J., *Properties of Kerto LVL for FEM calculations*. 2016, Metsä Wood.

- [8] Bell, K., *An engineering approach to Finite Element Analysis of linear structural problems*. 2014, Bergen, Norway: Fagbokforlaget. 656.
- [9] Dassault Systèmes, *Element selection in Abaqus*. 2007, Dassault Systèmes Simulia corp.
- [10] Mirianon, F., T. Toratti, and S. Fortino, *A Method to model wood by using ABAQUS finite element software : Part 1. Constitutive model and computational details*, in *VTT Publication 687*. 2008, [Espoo, Finland] : VTT Technical Research Centre of Finland.
- [11] Labonnote, N., A. Ronnquist, and K.A. Malo, *Prediction of material damping in timber floors, and subsequent evaluation of structural damping*. *Materials and Structures*, 2015. **48**(6): p. 1965-75.
- [12] Haiman, M. and N. Turcic, *Timber-Lightweight Aggregate Composite Floor Structure*. *Materials Science Forum*, 2013. **730-732**: p. 486-91.
- [13] Ebadi, M.M., G. Doudak, and I. Smith. *Dynamic characteristics of glulam beam and deck-element floors*. in *2016 World Conference on Timber Engineering*. 2016. Vienna University of Technology.
- [14] Glisovic, I. and B. Stevanovic. *Vibrational behaviour of timber floors*. in *11th World Conference on Timber Engineering 2010, WCTE 2010, June 20, 2010 - June 24, 2010*. 2010. Trentino, Italy: Trees and Timber Institute.

2.2 Paper VI

Conditions and features of a design tool for long-span timber floor elements

Sveinung Nesheim, Kjell Arne Malo, Nathalie Labonnote

For publication in: conference proceedings of World Conference in Timber Engineering 2021, Santiago

Credit author statements

For the Original article presented herein, all authors have contributed to its preparation as described in the below statement:

Sveinung Nesheim: Conceptualization, Methodology, Software, Validation, Formal analysis, Investigation, Resources, Writing - Original Draft, Writing - Review & Editing, Visualization.

Kjell Arne Malo: Writing - Review & Editing, Supervision, Project administration, Funding acquisition.

Nathalie Labonnote: Writing - Review & Editing, Supervision.

Conditions and features of a design tool for long-span timber floor elements

Abstract

A handbook for long-span timber floor elements would be of significant assistance to increase the market shares of timber floors for commercial building applications. Based on collected information from architects, engineers and manufacturers, the study elaborates on the contents of a handbook. The presented study also reviews factors influencing the competitiveness of timber floor elements for commercial buildings, and combines the findings to scope the features and requirements of a design tool that could supply information to a handbook. Gaps and required research to realize a reliable design tool that would efficiently generate data for a handbook is exposed and described.

Keywords

Cassette, Commercialisation, Competitiveness, Design methodology, Guideline, Handbook, Hollow core, Long-span, Market impact, Optimisation, Ready reference, Systems analysis, SWOT, Timber floor element.

1 Introduction

The cost of long-span timber floor elements is high compared to a concrete hollow core element [1], and the incentive for choosing a flooring system with a lower global warming potential is currently not a sufficiently weighty argument for the building industry. In addition, timber floor elements are experiencing challenges in vibration performance, and the timber industry is struggling to gain market shares. As new engineered wood products, fasteners and adhesives are continuously introduced to the market, a prosperous backdrop for a new generation of competitive long-span timber floor elements may be seen, but assistance must be provided.

In Norway an electronic handbook is freely available for concrete floor elements [2]. The handbook readily guides architects and engineers in the use of concrete floor elements. A comparable asset for long-span timber floor elements (LSTFE) would be of significant assistance to increase the market shares of timber floors for commercial building applications. This reference work could have the format of a

handbook or a guideline that could be available through a website, possibly with an additional option of a printed version if the market claims this.

The data that this reference should be built upon must comprise competitive designs, and the presented work consequently addresses factors influencing competitiveness of LSTFE. The study elaborates on the required and expected content of the reference to genuinely assist in introducing LSTFE to the market.

The objective of the present work is to suggest a design approach for a calculation tool that could be used to generate useful and reliable data, and to uncover gaps and further developments required to realize this tool.

2 Methods

2.1 Scope of floor element types

Timber floor elements suitable for commercial building applications are typically cassette type elements. As shown in Figure 1, the elements principally comprise a continuous top flange ④ feasibly with longitudinal slits for access and acoustic influence. Either separate bottom flanges at each joist, or a continuous bottom flange ⑤ as in Figure 1 constitutes the structurally stressed skins of the element. The elements could have different edge joists ① and field joists ③ depending on the support conditions, typically positioned either at constant centre distance, or at constant cavity spacing. Transversally, the elements could comprise edge beams ② in addition to a number of optional transverse stiffeners fitted between the joists.

Optionally, as part of the prefabrication, cavities can be filled with insulation, mass or technical installations ⑥. Mass can also be added as a non-structural overlay in addition to other outfitting assisting to meet design requirements ⑦. This is also features that could be added during manufacturing.

Depending on the requirements of the floor, a ceiling system ⑧ is optionally installed on-site. The flanges are typically glued structurally to the core, with an optional use of additional fasteners. The scope of the presented study is limited to this type of element.

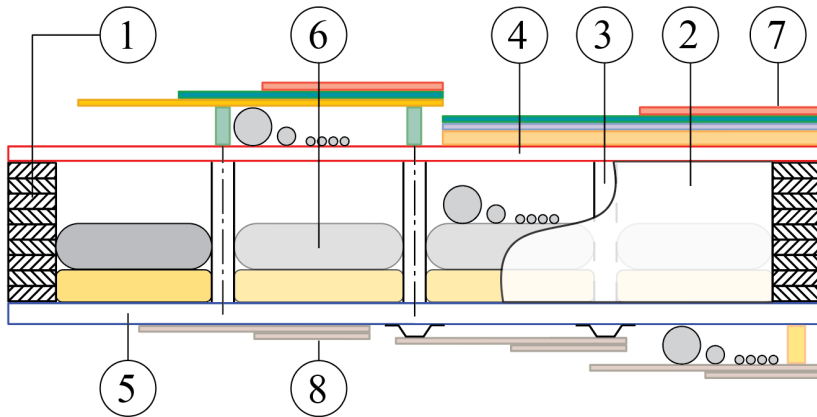


Fig. 1: Cross section of typical LSTFE

2.2 SWOT-analysis

An analysis of interior Strengths and Weaknesses, and exterior Opportunities and Threats (SWOT-analysis) [3] was performed to organise information about the recent developments in the sector of commercial timber buildings, with a focus on long-span timber floors (LSTFE). The objective of the SWOT-analysis was to prioritize principles and parameters that would aid the increased competitiveness for LSTFE, and consequently implemented in the design approach. Information retrieval was based on review of recent research and market potential of the associated sector, and informal interviews of a selection of the main contractors and manufacturers of timber elements in Norway.

2.3 Systems analysis

Systems analysis is used to identify targets and purpose of a system to see how the various processes of the system perform. A simplified systems analysis was established to categorize topics influencing the market impact of timber floor elements for commercial building applications. The analysis was used to elaborate the purpose and scope of a ready reference work, and to gain overview of the possible features and requirements of a design tool that this reference could be based upon. The analysis was also used to elaborate on effects that the various processes and decisions incorporated in a design approach would have on each other.

3 Results and discussion

3.1 SWOT of timber floor elements

3.1.1 Strengths and weaknesses (interior)

Concerning material properties, strengths of utilizing timber in commercial building systems are particularly found in the relative stiffness and carbon emissions (embodied energy) [4]. In Ashby [5], materials are presented and illustrated in terms of their suitability in various mechanical applications. In the following three figures from this source is referenced, but not reproduced due to copy rights. Applied as columns and beams, the ratio of stiffness to cost per unit volume is among the highest for wood, as can be found in figure 3.26 in [5]. In this figure the dotted line in the middle is the guideline for a stiff beam of minimum cost ($E^{0.5}/C_{v,R}$).

The environmental performance of wood also shows excellent properties. As can be found in figure 14.7 in [5], the ratio of stiffness to embodied energy per unit volume is among the highest for wood. Note that the performance of non-technical ceramics requires tensile armour, strongly increasing cost and carbon emissions.

Weaknesses of wood applied to floor elements is associated with vibration performances. Vibration response in terms of human perception can be reduced by increasing stiffness, damping and mass. The most efficient approach depends on the fundamental frequency of the floor. For a floor element with fundamental frequency above 4.5 Hz, vibration performance responds well to increased mass, but the material properties of wood are not the best candidate to assist. As can be found in the modulus to density plot of figure 3.3 in [5], the density of wood is considerably lower than metals and ceramics for the same stiffness. Note that for a stiff beam with a maximum density, a guideline perpendicular to ($E^{0.5}/\rho$) must be used.

Moving to design rules, the market potential of long-span timber floor is weakened due to the unsettled agreement of international guidelines for evaluation of human induced vibrations. The literature on the topic is extensive, and in the presented findings emphasis on recent studies is kept. Strengths and weaknesses of the various approaches for evaluation of serviceability have been reviewed by several studies [6-11]. Recent research tends to agree to utilize the research on human perception [12, 13] by employing ISO baseline levels of accelerations and velocities [14-16].

Research related to development of design rules for Eurocode is taking advantage of this, and is likely to introduce serviceability criteria with performance classes based on analytical expressions for dynamic response [17]. The analytical solutions are deterministic methods based on Fourier series assuming the load model from one step to be reproduced by the next in a periodic process [18, 19]. The analytical

solutions utilize estimates of damping to improve the description of vibration response, but the precision is consequently sensitive to the level of damping ratio used. Many parameters influence the damping ratio of timber floor elements. The type of floor element, the support conditions and interconnection between the floor elements, the properties of outfitting, and the use of the building are all influencing parameters. The continuous assessment of long-span timber floors, either numerically, in-situ or as full-scale laboratory tests, are crucial to build information that will enable a reliable level of damping ratio to be selected for the various floor types and applications.

Several studies are arguing that deterministic methods will produce conservative responses for loads that by nature are stochastic [20, 21], which is the case for footfall [22]. The deterministic models tend to overestimate resonant response particularly when induced by higher order of footfall load harmonics. While improved deterministic models for human induced loading is developed for high-frequency floors [23], this is only marginally helpful for long-span timber floors typically characterised by a resonant floor response. Moreover, since the much-debated cut-off frequency between resonant and transient floor response tend to shift upwards from eight hertz a few years ago to current proposals of 14 Hz [24], long-span timber floors are likely not to utilize these improved models.

Retaining analytical solutions are still sought to be required for commonly available guidelines, but the drawbacks of analytical methods increase as the availability and application of Finite Element Analysis (FEA) increase. Keeping in mind the above-mentioned overestimates of dynamic responses, FEA based on deterministic load models nevertheless produce useful results as reported by many studies [25-27].

Currently, this analysis approach is conveniently available in several commercial software for serviceability assessment of floor elements. However, as the above mentioned FEA approaches of computing human induced vibration actually are ignoring Human-Structure Interaction (HSI) [28], alternatives are aspired. In [29] an equivalent moving force based on spring-mass theory is developed to reflect HSI. However, time-step analyses will always be computationally demanding, and when adding HSI the analyses will require even more computational effort. Consequently, time-history FEA is not very suitable, or even incompatible, with optimisation of design where numerous iterations of altering geometry and material composition is required.

An alternative to deterministic methods is to rather model human loading as a stochastic process. In probabilistic methods the interaction of human and the variability in the human step is encountered for, and the demanding time-step analyses is replaced by a single domain transformation of the degrees of freedom of the model in question. In probabilistic methods a spectral density model is used to

represent human induced loads [30]. Such analyses can be performed analytically by employing stochastic vibration theory [31, 32], but the analyses require an accurate mode shape (Eigenvector) to predict the responses. For CLT or stressed skin panel where the flexural rigidity is well defined in both directions, a floor element with simple support conditions can be solved analytically with modal analyses, but in most building applications FEA is required to obtain reliable results.

Recent studies are promising and appear to have met the level of walking load samples required to generate a spectral density model for stochastic dynamic response of floor elements. In the work of Chen et al [21] Power Spectral Density (PSD) models are generated for single human walking load, and in [33] a similar work is performed to obtain PSD models for jumping load. In a study by Wang et al [34], the development is extended to a PSD model for crowd walking load.

For optimisation of long-span timber floor designs, the proposed analytical method for the new Eurocode [17, 18] may offer a good compromise between simplified methods of assessing serviceability [35, 36] and more sophisticated numerical analyses. However, if FEA can be used, the stochastic load models are assessed to be a promising way forward. The method is a computationally efficient approach where the precise probabilistic dynamic vibration response directly can be used to assess the performance of the floor with respect to the human perception levels given by the ISO baseline.

3.1.2 Opportunities and threats (exterior)

City fires from The Great Fire of London to more recent incidents at the beginning of the 20th century, caused national building regulations to have substantial restrictions for use of timber in tall buildings in most European countries. In Norway, the restrictions were relieved as late as 1997 when material-neutral regulations were introduced. In practice this has caused building construction systems of steel and concrete to achieve a substantial lead in developments. The Norwegian Directorate of Public Construction and Property (Statsbygg) have investigated the consequences and concluded that timber-based building systems are associated with higher risk for building contractors in comparison to other materials [37].

Currently, the trend is more positive. In the Nordic countries several recent commercial timber-based building projects have forced technical developments ahead [38-41], and the demonstration projects are increasing market trust, as studied in [4]. Throughout the European countries, governmental programmes are established to promote timber-based building systems for commercial and high-rise buildings. The building sector is expected to erect quarter of a trillion square metres of new construction over the next 40 years [42], and it is a general understanding that countries cannot meet emission reduction targets without reducing energy

consumption in the building sector. Consequently, one of the main drivers of increased use of timber is its environmental performance.

In North America and Western Europe, the forest is managed and certified. This is however not the case for most forest areas of the world, and timber-based building systems must ensure the use of certified timber. Mapping of certified forests are a helpful means to ensure that the outtake of timber is sustainable [43]. In Norway, like in most forests worldwide, the portion of small-diameter trees tend to overstock, and opportunities of utilising this resource is currently studied [44].

The Principles of circular economy and bio-economy strengthens the sustainability of timber construction further, as can be read in the Finnish study of Hynynen [45]. This study also emphasis the timber industry as particularly suitable to stimulate regional economic developments. The environmental performances of timber-based building systems are reported to vary. In [46] the differences from conventional beam and columns to CLT systems with low global warming potential show nearly a 10 % reduction in carbon emission in a 50-year service time. A similar consequence is revealed in [47] where carbon emissions in floor elements are studied. Here timber floor elements are found to have lower carbon emissions than comparable floor elements in other material, but it is also shown that a 50-80% higher carbon emissions can be expected for the same timber product if suppliers and components are not selected with care.

In [48] two different analysis methods have been used to throw light on future potential for timber-frame for multi-storey buildings in Europe. The analysis performed in 2014 show high correlation between future potential and the regulatory framework and the construction industry structure. Risk aversion in the value chain of the timber construction industry is assessed to be a significantly larger obstacle than competition from alternative construction principles and materials. The study also argues that competition between manufacturers of timber elements in combination with better cooperation between suppliers of wood products and construction industry is required to increase the competitiveness.

The study supports findings from the timber sector in Norway. A survey presented by the Nordic Network for Tall Wood Buildings and the Norwegian Institute of Wood Technology report that cooperation between parties are essential to increase market impact [49].

In [4] opportunities are reported to be the high level of prefabrication, potential of systematic feedback of expertise, and in the improved responsibility in planning and construction. Huge potential is also found in modular commercial building applications, and in a recent review of Ferdous et al. [50], advancement are discussed in terms of challenges and opportunities. A review of new connections for timber structures elaborate on the potential of joining timber components [51]. For both

product types a common threat is the lack of standardisation. With respect to the sector of prefabricated concrete elements, the timber sector has very little agreement of standardised solutions for prefabricated modules and timber connections.

Findings from informal interviews of parties of the Norwegian timber industry emphasise the importance of improved knowledge and precisions of costing. This concerns both capital expenditures of manufacturing and construction, and operational expenses throughout the service lifetime. The much-debated challenge in fire resistance is expressed to be manageable, whilst challenges of acoustics and vibration requires attention. These experiences are reflected by the study of Kuzman et al. [4]. Interviews of members of the Norwegian building and construction sector emphasised that the cost of long-span timber floor elements is substantially higher than comparable concrete hollow core elements, and the incentive for choosing a flooring system that improves carbon emission accounting is currently not a sufficiently weighty argument to choose timber-based flooring systems for commercial buildings.

Opportunities for timber-based building systems are associated with timber-concrete composites. The guidelines issued by the COST Action FP1402 [52] are supporting this development, and a positive influence on the market potential is certain, as observed in Germany [53]. In general, the awareness and attention to hybrid timber building systems, is likely to increase market shares of timber, and to improve the environmental performance of the building sector. Joint ventures for buildings in timber in combination with steel, concrete or brick all have the potential of improving the built environment, and the shared knowledge and strengths certainly have the potential to offer common benefits.

Interviews with manufacturers and reviews [4, 54] mention the suitability for industrial applications as one of the main strengths and opportunities for wood. Timber-based building components are accurately and efficiently CNC machined. The opportunity can be viewed in terms of increased scale and machine-aided operations, where components can be assembled into finalized products. Complete parametric frameworks for design and manufacturing as in the work of Mork et al. [55] and robotic timber manufacturing [56, 57] are some of a range of studies of this topic. Survey of novel timber architecture worldwide has concluded that the opportunities are particularly high for wood [58, 59].

3.2 Systems analysis

The basis of the systems analysis was information collected during project group workshops. The project group associated with the research project comprised manufacturers of wood components, architects, building and construction companies, and research institutes. The collected material consisted of more than

one hundred drivers, conditions and factors that a successful commercialisation of long-span timber floor elements would have to regard. In the systems analysis this information was sorted and arranged, and the organisation of information was performed in order to elaborate on the content of a ready reference for LSTFE. The systems analysis resulted in a simplified definition of the content that the reference should address, and the resulting content was used for scoping the computational foundation of which the reference work could be based. The systems analysis was used strategically for development and conceptualisation of this tool.

Floor element design offered in a ready reference work should be competitive, causing the underlying design principle to be envisioned as an optimisation tool. An optimisation tool requires an objective, and findings from the SWOT-analysis indicated cost to be one of the key indicators. Competitiveness was in addition based on assessment of the value chain, the processes of realization, and the disciplines involved during realisation. Combined findings guided towards defining competitiveness as a joint performance of resource-efficiency and the adaptability and applicability of the floor element. The resource-efficiency was in turn defined as capital expenditures and carbon emissions in terms of economy. Due to this definition, the systems analysis reflecting the content of the reference work, took the form of a framework between realisation processes and economic impacts, with the LSTFE design tool in the centre. See Figure 2.

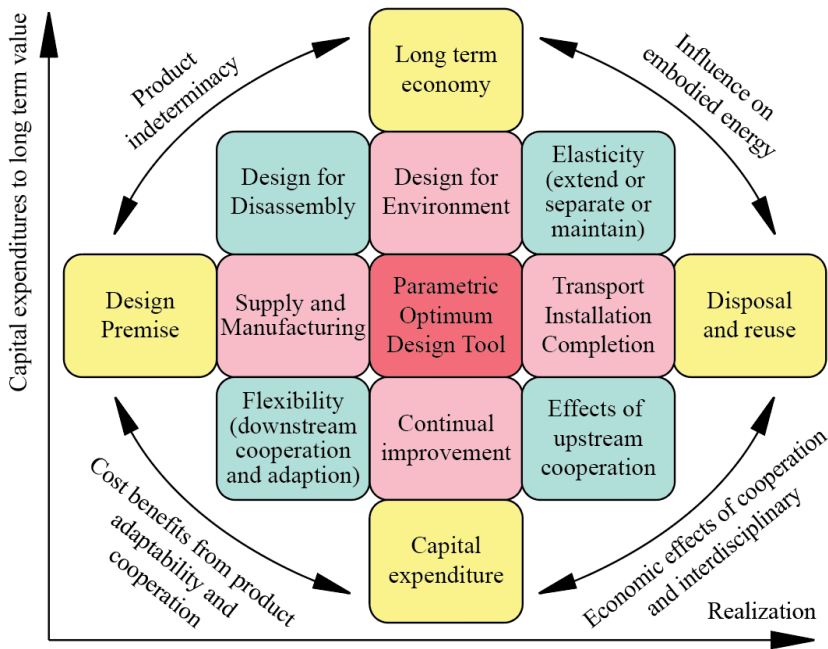


Fig. 2: Framework of realization processes and economic impacts. Yellow: Measurable quantities; Pink: Direct interface to the design tool; Green: Interactions and secondary effects

Topics related to realization processes were grouped in entities along the abscissa axis, whilst topics related to resource consumption, in economic terms, grouped in entities along the ordinate axis. In principle, topics comprising design parameters was linked to the optimisation design tool and is therefore pointing inwards, whilst topics comprising indicators of competitiveness are directed outwards to the measurable quantities of the outer quadrants. Interactions and information transfer occur between any two entities in the diagram. Realisation processes incorporate the following four main phases from left to right:

- Design premise, where the product requirements are specified
- Suppliers and manufacturer
- Transport from manufacturer to building site, installation and completion; and
- Disposal and reuse.

Resource consumption and potential is described in economic terms from cost of design and manufacturing (capital expenditure) and economic consequences of continual improvement, to economic effects related to carbon emissions as sales arguments (Design for Environment) and perspectives of second-hand value.

Placing the optimisation tool at the centre of the entities might cause confusion when interpreting the figure. However, during conceptualisation of the design approach, the principle offered perspectives for scoping and market attention for the ready reference work of which the design tool should generate data.

During development of the strategy of the parametric design tool, the diagram helped in identifying how the various parameters and indicators would influence each other, and how they could influence the outer quadrants.

Starting with upstream processes of realisation, the reference work should include topics addressing the possibilities to influence Design for Disassembly (DFD), and methods to adapt the basic floor element design (flexibility). Flexibility could cover floor element shapes deviating from rectangular shape, as well as methods of retaining capacity, or rules of reduced capacity, for apertures cut in webs or flanges. Possible locations and details of apertures should also be included.

For downstream realisation processes, information to assist late-phase alterations such as extension or division of floor elements should be described, possibly in addition to typical actions of maintenance. Depending on the attention to DFD, information concerning disposal and reuse should be stated. A particular focus should be given principles of redocumentation and CE marking to assist reuse.

3.3 Conceptualization of design tool

Based on the framework developed in the system analysis, the principle and parameters of the design tool were established. The tool should be able to control parameters from the entire realisation process. Included parameters would range from specification of the floor element comprising outfitting and internal installations, to parameters describing any significant contributions influencing competitiveness until the floor element was manufactured and ready for transport. Calculation of serviceability performance would have to regard the support conditions, category of use, fire- and hazard class of the building of which the floor element would be applied. To address the solution space offered by possible material combinations, the tool must incorporate a material database where typical material types and associated dimensions can be collected and stored. To achieve a competitive design, the design tool must be able to adjust members and retrieve capacities where possible. It must therefore comprise an optimisation algorithm, consequently requiring that several parameters are parametrically linked. The architecture of the design tool is presented in Figure 3.

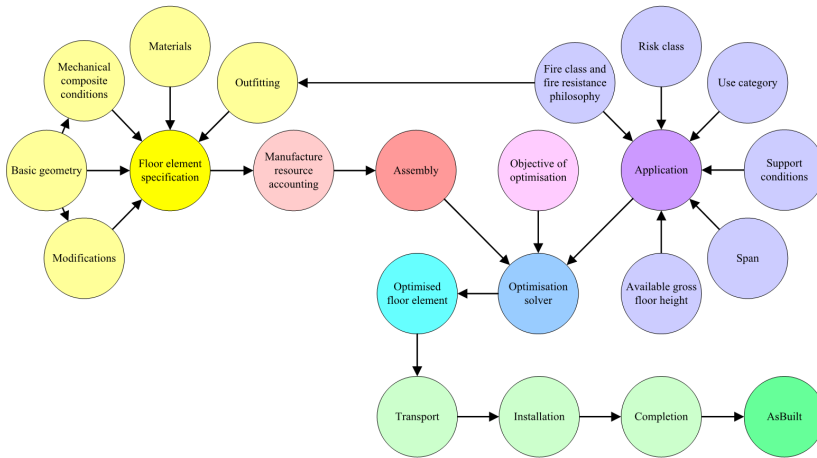


Fig. 3: Design principle of an optimisation tool for long-span timber floor elements

The design tool is currently built and tested using analytical calculation for serviceability performance. In this phase the multi-objective evolutionary Galapagos solver in Grasshopper [54] is used. This is a powerful genetic algorithm, but the challenge is to control the development and avoid local and multiple minima. For both a more precise calculation of the floor element and increased control of optimisation, iSight [55] in combination with Abaqus [60] is also used where a Design of Experiment is generated to explore a defined solution space.

Both methods require a large number of iterations, and the development of the principle continuous as obstacles and limitations are uncovered.

4 Conclusion

As experience and possibilities mature, the enthusiasm and expertise in using wood in commercial buildings are growing rapidly, but the way forward is still challenging. In this study, a contribution to the content of a ready reference work to assist in commercialisation of long-span timber floor elements is presented. From this a design tool that this reference work can be based on is elaborated, and the architecture of a holistic optimisation tool is presented.

The constraints of the floor element, ranging from support and load conditions to limits of serviceability, can be solved either analytically or by FEA. The resulting numbers of combination of support and load conditions, span and the various influences of both outfitting and building application, would require a web-based

reference work, with the possibility of retrieving the required design through filtering of conditions.

Two possible strategies to the continuous development of a tool that could generate data for a ready reference work for long-span timber floor elements are proposed:

- a) An analytical solution can be run directly at a server and present design for floor elements based on settings in the user interface. This would reduce design premise limitations as any combination of settings are attempted to be solved. This would on the other side reduce precision of serviceability calculations and consequently increase the required tolerances. Open source codes for optimisation, objective and constraints would make publication of results uncomplicated.
- b) A comprehensive Design of Experiment (DoE) can be built from which FEA is performed based on probabilistic load models. This would require a substantial computational effort upfront, where optimised designs would be mapped to a searchable database. The scope of the DoE would define the design premise limitations. Since copy right and software licence are related to the use of the software, and not to the results of the use, publication of results should principally still be uncomplicated.

4.1 Future developments

The initial tests of the design tool have uncovered valuable information that will be used in the continuous improvement and development of the principle. Further effort is required on the following topics in order to successfully develop and implement a design tool that could serve as a basis for a ready reference work of long-span timber floor elements:

- 1) Supported by the findings in this study, and by Forintek and the Canadian Wood Council [61], the development of a method that increase the precision and options in the accounting of cost and carbon emission related to manufacture of timber floor elements is required. The method must be compatible with the optimisation tool addressed herein.
- 2) A suitable optimisation solver that can work on a small number of iterations would increase the possibility of exploring the solution space of designs, particularly when employing FEA. Whilst numerous iterations are performed per second for an analytical solution, a single iteration using FEA would require several minutes for a probabilistic method, and several hours for a deterministic method with HIS.
- 3) Timber floor elements is completion friendly. For timber floor elements with a continuous bottom flange completion is particularly convenient. Time to completion, and consequently cost, is therefore associated with

competitiveness with respect to comparable alternatives in concrete. The cost of transportation and installation must also be addressed as means of increased competitiveness. Due to the lower mass of LSTFE, the number of elements per transporting vehicle will be higher for timber than for concrete floor elements. This affect cost and carbon emissions. The required capacity of building crane will due to weight also be lower for timber than for concrete floor elements. The topic must be addressed, and comparisons made to provide numbers of competitiveness.

- 4) Cost-efficient solutions that can aid in adjusting serviceability performance of a timber flooring system without changing the design of the floor elements may serve to increase the competitiveness. Such solutions may also contribute to standardisation of timber floor elements.

The current work is a response to the conclusions in [61] and to a request by the Norwegian Research Council for results that can aid in commercialise long-span timber floor elements.

Acknowledgments

This work is part of the four-year project “Woodsol – Wood frame solutions for free space design in urban buildings” realized through the research grant from The Research Council of Norway (254699/E50). The support is gratefully acknowledged.

References

- [1] Norconsult Informasjonssystemer AS and Bygghanalyse AS, *Norsk prisbok: et oppslagsverk for byggebransjen*. 2019-02 ed. Norsk prisbok: et oppslagsverk for byggebransjen. 2019, Sandvika: Norconsult informasjonssystemer AS i samarbeid med AS Bygghanalyse.
- [2] Betongelementforeningen. *Betongelementboka*. 2018; Available from: <https://betongelementboka.betongelement.no/betongapp/default.html>.
- [3] Gürel, E. and M. Tat, *SWOT analysis: a theoretical review*. Journal of International Social Research, 2017. **10**(51).
- [4] Kuzman, M.K. and D. Sandberg, *A new era for multi-storey timber buildings in Europe*, in *Forest Products Society International Convention : 26/06/2016 - 29/06/2016*. 2016, Forest Products Society: Madison.
- [5] Ashby, M.F., *Materials selection in mechanical design*. Fifth edition ed. 2017: Butterworth-Heinemann.

- [6] Jaafari, C. and J. Mohammadi, *Floor Vibration Control as a Serviceability Requirement in Design Standards and Practices*. Practice Periodical on Structural Design and Construction, 2018. **23**(2): p. 04018003.
- [7] Zhang, B., et al., *Comparison of vibrational comfort assessment criteria for design of timber floors among the European countries*. Engineering Structures, 2013. **52**: p. 592-607.
- [8] Negreira, J., et al., *Psycho-vibratory evaluation of timber floors - Towards the determination of design indicators of vibration acceptability and vibration annoyance*. Journal of Sound and Vibration, 2015. **340**: p. 383-408.
- [9] Glisovic, I. and B. Stevanovic. *Vibrational behaviour of timber floors*. in *11th World Conference on Timber Engineering 2010, WCTE 2010, June 20, 2010 - June 24, 2010*. 2010. Trentino, Italy: Trees and Timber Institute.
- [10] Ebrahimpour, A. and R.L. Sack, *A review of vibration serviceability criteria for floor structures*. Computers & Structures, 2005. **83**(28): p. 2488-2494.
- [11] Toratti, T. and A. Talja, *Classification of human induced floor vibrations*. Building Acoustics, 2006. **13**(3): p. 211-221.
- [12] Murray, T.M. and B. Davis. *Evaluation of problem floors because of human induced vibrations*. in *Proceedings of the 8th International Conference on Structural Dynamics, EURO-DYN 2011*. 2011.
- [13] Murray, T.M. *Floor vibrations: The human tolerance side of the equation*. in *Proceedings of the International Modal Analysis Conference - IMAC*. 1999.
- [14] Hu, L., et al. *Development of ISO baseline vibration design method for timber floors*. in *WCTE 2018 - World Conference on Timber Engineering*. 2018.
- [15] Sedlacek, G., et al., *Design of floor structures for human induced vibrations*. 2009, Luxembourg : OPOCE: Luxembourg.
- [16] ISO, *ISO 10137:2007 Bases for design of structures - Serviceability of buildings and walkways against vibrations*. 2007, International Organization for Standardization.
- [17] CEN, *EN 1995-1-1 SC5.T3 Final draft prEN*. 2020, European committee for standardization: Brussels.
- [18] Abeysekera, I., et al., *Development of a floor vibration design method for Eurocode 5*. New Zealand timber design, 2019. **27**(1).
- [19] Willford, M.R., P. Young, and M. CEng, *A design guide for footfall induced vibration of structures*. 2006: Concrete Society for The Concrete Centre.
- [20] Paskalov, A. and S. Reese, *Deterministic and probabilistic floor response spectra*. Soil Dynamics and Earthquake Engineering, 2003. **23**(7): p. 605-618.
- [21] Chen, J., J. Wang, and J.M. Brownjohn, *Power spectral-density model for pedestrian walking load*. Journal of Structural Engineering, 2019. **145**(2): p. 04018239.

- [22] Racic, V., A. Pavic, and J.M.W. Brownjohn, *Experimental identification and analytical modelling of human walking forces: Literature review*. Journal of Sound and Vibration, 2009. **326**(1): p. 1-49.
- [23] Middleton, C.J. and J.M.W. Brownjohn, *Response of high frequency floors: A literature review*. Engineering Structures, 2010. **32**(2): p. 337-352.
- [24] Mohammed, A.S., A. Pavic, and V. Racic, *Improved model for human induced vibrations of high-frequency floors*. Engineering Structures, 2018. **168**: p. 950-966.
- [25] Xiong, H., J. Kang, and X. Lu. *Finite element analysis on dynamic behavior of timber floor subjected to pedestrian-induced force*. in *World Conference on Timber Engineering 2012, WCTE 2012*. 2012.
- [26] Caprani, C.C. and E. Ahmadi, *Formulation of human–structure interaction system models for vertical vibration*. Journal of Sound and Vibration, 2016. **377**(Supplement C): p. 346-367.
- [27] Ebadi, M.M., G. Doudak, and I. Smith, *Finite-Element Modeling and Parametric Study of Glulam Beam-and-Deck Floors*. Journal of Structural Engineering (United States), 2017. **143**(9).
- [28] Shahabpoor, E., A. Pavic, and V. Racic, *Interaction between Walking Humans and Structures in Vertical Direction: A Literature Review*. Shock and Vibration, 2016. **2016**: p. 22.
- [29] Ahmadi, E., C.C. Caprani, and A. Heidarpour, *An equivalent moving force model for consideration of human-structure interaction*. Applied Mathematical Modelling, 2017. **51**(Supplement C): p. 526-545.
- [30] Brownjohn, J.M., A. Pavic, and P. Omenzetter, *A spectral density approach for modelling continuous vertical forces on pedestrian structures due to walking*. Canadian Journal of Civil Engineering, 2004. **31**(1): p. 65-77.
- [31] Chopra, A.K., *Dynamics of structures : theory and applications to earthquake engineering*. 4th ed. ed. Prentice-Hall international series in civil engineering and engineering mechanics. 2012, Boston, Mass: Prentice Hall.
- [32] Strømmen, E.N., *Structural dynamics*. 2014: Springer.
- [33] Xiong, J. and J. Chen, *Power spectral density function for individual jumping load*. International Journal of Structural Stability and Dynamics, 2018. **18**(02): p. 1850023.
- [34] Wang, J., et al., *Spectral Model for Crowd Walking Load*. Journal of Structural Engineering, 2020. **146**(3): p. 04019220.
- [35] Hu, L.J. and Y.H. Chui, *Development of a design method to control vibrations induced by normal walking action in wood-based floors*, in *Proceedings of the 8th World Conference on Timber Engineering*. 2004: Lahti, Finland. p. 217-222.

- [36] CEN, *NS-EN 1995-1-1:2004+A1:2008+NA:2010*, in *Design of timber structures - Part 1-1: General - Common rules and rules for buildings*. 2010, European committee for standardization: Brussels.
- [37] Statsbygg, *Tre for bygg og bygg for tre. Kunnskapsgrunnlag for økt bruk av tre i offentlige bygg*. 2013: Det Kongelige landbruks- og matdepartement, Oslo, Norway.
- [38] Abrahamsen, R.B. and K.A. Malo. *Structural design and assembly of "Treet" – A 14-storey timber residential building in Norway*. in *World conference on timber engineering*. 2014.
- [39] Abrahamsen, R. and M.L. AS. *Mjøstårnet-Construction of an 81 m tall timber building*. in *International House Forum*. 2017.
- [40] Keskisalo, M. *Use of tension rods in wood construction – 14 storeys with laminated veneer lumber as shear walls: Lighthouse Joensuu*. in *Internationales Holzbau-Forum IHF 2018*. 2018.
- [41] Jensen, A.V. and N. Craig, *Wood in Construction-25 cases of Nordic Good Practice*. 2019: Nordic Council of Ministers.
- [42] UN Environment and International Energy Agency (IEA), *Towards a zero-emission, efficient, and resilient buildings and construction sector. Global Status Report 2017*. 2017.
- [43] Kraxner, F., et al., *Mapping certified forests for sustainable management - A global tool for information improvement through participatory and collaborative mapping*. *Forest Policy and Economics*, 2017. **83**: p. 10-18.
- [44] Bukauskas, A., et al., *Whole timber construction: A state of the art review*. *Construction and Building Materials*, 2019. **213**: p. 748-769.
- [45] Hynynen, A., *Future in Wood? Timber Construction in Boosting Local Development*. *European Spatial Research and Policy*, 2016. **23**(1): p. 127.
- [46] Dodoo, A., L. Gustavsson, and R. Sathre, *Lifecycle carbon implications of conventional and low-energy multi-storey timber building systems*. *Energy and Buildings*, 2014. **82**: p. 194-210.
- [47] Skaar, C., B. Solem, and P. Rüter, *Composite floors in urban buildings: Options for a low carbon building design*, in *Forum Wood Building Nordic*. 2017, Forum Wood Building Nordic Trondheim 17: Trondheim Norway.
- [48] Hurmekoski, E., R. Jonsson, and T. Nord, *Context, drivers, and future potential for wood-frame multi-story construction in Europe*. *Technological Forecasting and Social Change*, 2015. **99**: p. 181-196.
- [49] *Taking wood to the top*, Nordic Network for Tall Wood Buildings and Norwegian Institute of Wood Technology (NTI), Editors. 2018: Survey at Green Building Conference Copenhagen.

- [50] Ferdous, W., et al., *New advancements, challenges and opportunities of multi-storey modular buildings – A state-of-the-art review*. Engineering Structures, 2019. **183**: p. 883-893.
- [51] Schober, K.-U. and T. Tannert, *Hybrid connections for timber structures*. European Journal of Wood and Wood Products, 2016. **74**(3): p. 369-377.
- [52] Dias, A., *Design of Timber-concrete Composite Structures: A State-of-the-art Report by COST Action FP1402/WG 4*. 2018: Shaker Verlag.
- [53] Knauf, M., *Market potentials for timber-concrete composites in Germany's building construction sector*. European Journal of Wood and Wood Products, 2017. **75**(4): p. 639-649.
- [54] Eliasson, L., S. Berg, and D. Sandberg, *Some aspects on the more efficient use of wood in the industrial manufacture of single-family timber houses*. Pro Ligno, 2015. **11**(4): p. 418-425.
- [55] Mork, J.H., et al., *Generating timber truss bridges—examining the potential of an interdisciplinary parametric framework for architectural engineering*. 2016.
- [56] Willmann, J., et al., *Robotic timber construction — Expanding additive fabrication to new dimensions*. Automation in Construction, 2016. **61**: p. 16-23.
- [57] Weinand, Y., *Advanced Timber Structures: Architectural Designs and Digital Dimensioning*. 2017: Birkhäuser.
- [58] Aage, N., et al., *Advanced topology optimization methods for conceptual architectural design*, in *Advances in Architectural Geometry 2014*. 2015, Springer. p. 159-179.
- [59] Mayo, J., *Solid wood: case studies in mass timber architecture, technology and design*. 2015: Routledge.
- [60] Dassault Systèmes, *Abaqus CAE*. 2017, Dassault Systèmes Simulia corp.
- [61] Hu, L.J., R. Desjardins, and E. Jones. *Systems approach for optimizing wood-based floor construction*. in *9th World Conference on Timber Engineering 2006*. 2006. Portland, OR, United states: Oregon State University Conference Services.

3 Presentations and appearances

3.1 Presentations

- I. Nesheim, S. 2017. Experience from timber-based flooring systems at NTNU. Asplan Viak Oslo, Forum for trekonstruksjoner. Timber Concrete Composite floor systems. [188]

Oral presentation of the findings from testing and analysis of timber-based floor element at NTNU the recent years. The presentation addressed particularly Timber-Concrete Composite (TCC) solutions made current by new guideline on TCC.

- II. Nesheim, S. 2018. Closed hollow wood sections in long-span flooring systems. NTNU Wood Workshop 2018. [189]

Oral presentation of the conceptualisation of multi-parameter approach for optimisation of the Woodsol flooring system. The presentation included the idea of why measures to reduce cost may be a paramount concern in the research on timber floor elements.

- III. Nesheim, S. 2019. Optimisation strategies for timber floor element. Tampere University Finland. [190]

Oral presentation of the Woodsol building system and the strategies for optimisation of the floor element. The presentation was an introductory part in the establishment of the cooperation between the Norwegian University of Science and Technology and the Tampere University on pursuing competitiveness on timber floor elements through optimisation.

- IV. Nesheim, S. 2019. Brief on Woodsol floor developments. NTNU Wood Workshop 2019. [191]

Oral presentation of the Woodsol floor element developments and strategies. Time line for achievements and planned work presented in addition to causes of strategies presupposing numerical models.

3.2 Appearances

- I. Nesheim, S. 2019. Norge nå. Mjøstårnet - verdens høyeste trehus. NRK, Norwegian Broadcasting Corporation. [192]

Talk on national television about the recent history of timber building in Norway and why governing rules and regulations now facilitate for building taller in timber. Additional talk on carbon emission of tall timber buildings

Etter strævet kan du steikja flek
og lesa kinesiske vers.

– Olav H. Hauge, “Kvardag”, 1966

Annex A. Codes and drafts

Annex A.I Material database code

author: Sveinung Nesheim

Versioning and change control

1.2 (20191112) Moved application from EWPmtrlBase to CHSperfCalc.section (Current version)

1.1 (20191103) Changed from list to dictionary for libMtrl in order to find material directly from input file. libForm remains unchanged.

1.0 (20191031) Last working version

Common preparations of Python script

```
import numpy as np
import pandas as pd
import os
```

```
#singleLine=None
singleLine=0
```

```
with open("%s\\CHS_input.tsv" % os.getcwd()) as input_file: # Hardcoded input filename
    if singleLine==None:
        for line in input_file:
            extracted_line=line
            extracted_list=extracted_line.split('\t')
            span=float(extracted_list[8])
            modWid=float(extracted_list[9])
    else:
        extracted_line=input_file.readlines()[singleLine]
        extracted_list=extracted_line.split('\t')
        span=float(extracted_list[8])
        modWid=float(extracted_list[9])
```

Precalculations ECO2

Resulting value in CO2 equivalents in g per kg

```
def calcECO2(kgPerUnit, weightUnits, kgECO2perUnit, units, URLref):
    rho=kgPerUnit/weightUnits
    eco2=kgECO2perUnit*1000/units/rho
    return {'rho':rho, 'eco2':eco2, 'ref':URLref}
```

```
eco2GlulamMoelven=calcECO2(430,1,62,1,'https://www.epd-norge.no/getfile.php/139412-1538388506/EPDer/Byggevarer/Heltreprodukter/NEPD-456-318-EN_Glulam-Beams-and-Pillars_1.pdf')
eco2gypsum=calcECO2(12.5, 0.015, 2.51, 0.015, 'https://www.epd-norge.no/bygningsplater/norgips-fireboard-brann-type-df-brn-article2561-318.html')
eco2kertoQ=calcECO2(510, 1, 130, 1, 'https://www.metsawood.com/global/Tools/MaterialArchive/MaterialArchive/Kerto-manual-lvl-emissions.pdf')
eco2baubuche=eco2kertoQ.copy()
eco2baubuche['rho']=eco2baubuche['rho']/510*730
eco2baubuche['eco2']=eco2baubuche['eco2']/510*730
eco2screed=calcECO2(1652,1,10.56,0.025,'Skaar, C., B. Solem and P. R  ther. 2017. Composite floors in urban buildings: Options for a low carbon building design. Forum Wood Building Nordic. Trondheim Norway, Forum Wood Building Nordic Trondheim 17.')
```

Definition of standard specifications for applicable building components

```
stdSheetLen_feet=[4,5,8,9,10,12]
stdSheetLen=list(np.around(np.multiply(stdSheetLen_feet,12*0.0254),1))

stdSheetWid_feet=[5/3,2,3,4,5]
stdSheetWid=list(np.around(np.multiply(stdSheetWid_feet,12*0.0254),1))
```

Material format library

```
class MaterialFormat:
```

```
    """ Adds retail/available material formats as lists to a list object (libForm). Each object in the list is structured with mandatory name and primary dimensions first, followed by secondary dimension and production length if available. All dimensions must be given as list even with none or one item. All dimensions in meters of course. The content of the library can be viewed in the dictionary named libFormCat"""
```

```

cat={}
items=0

def __init__(self, name, primary, secondary, length, reference=None):
    self.name=name
    self.pri=primary # Most significant dimension: Thickness for panels or height for beams
    self.sec=secondary
    self.l=length
    self.reference=reference

    MaterialFormat.cat[self.name]=MaterialFormat.items
    MaterialFormat.items+=1

libForm=[]
"""for i in range(libFormImport.shape[0]):

libForm.append(MaterialFormat(libFormImport['group'][i],[libFormImport['primary'][i],[libFormImport['seconda
ry'][i],[libFormImport['length'][i],libFormImport['reference'][i]]))

libForm.append(MaterialFormat('Glulam',[0.09, 0.115, 0.135, 0.18, 0.225, 0.27, 0.315, 0.36, 0.405, 0.45, 0.495,
0.54, 0.585, 0.63],[0.036, 0.048, 0.066, 0.073, 0.09, 0.115, 0.14, 0.165, 0.19, 0.215, 0.24, 0.26],[,]))
libForm.append(MaterialFormat('StructuralTimber',[0.073,0.098,0.123,0.148,0.173,0.198,0.223],[0.036,0.048,0.07
3],[,]))
libForm.append(MaterialFormat('KBP',[0.2, 0.25, 0.3],[0.036, 0.048, 0.07],[,]))
libForm.append(MaterialFormat('BN',[0.225,0.25,0.27,0.3,0.315,0.35,0.36,0.4,0.405],[0.048],[12,]))
libForm.append(MaterialFormat('CLT',[0.06,0.08,0.09,0.1,0.12,0.14,0.16,0.18,0.2,0.22,0.24,0.26,0.28,0.3],[1.2,2.4
.295,3.5],[16.5,]))
libForm.append(MaterialFormat('KQ',[0.033, 0.039, 0.045, 0.051, 0.057, 0.063, 0.069, 0.075],[modWid,2.5],[,])) #
The following ticks are only for slim panels (up to 225 mm width): 0.021, 0.021, 0.024, 0.027, 0.03,
libForm.append(MaterialFormat('KQ sand',[0.031, 0.037, 0.043, 0.049, 0.055, 0.061, 0.067,
0.073],[modWid,2.5],[,])) # 0.019, 0.022, 0.025, 0.028,
libForm.append(MaterialFormat('KS',[0.2, 0.22, 0.24, 0.3, 0.36, 0.4],[0.027, 0.033, 0.039, 0.045, 0.051, 0.057,
0.063, 0.075],[,]))
libForm.append(MaterialFormat('KS sand',[0.2, 0.22, 0.24, 0.3, 0.36, 0.4],[0.025, 0.031, 0.037, 0.043, 0.049, 0.055,
0.061, 0.073],[,]))
libForm.append(MaterialFormat('BBQ',[0.02, 0.03, 0.04, 0.05, 0.06, 0.07, 0.08],[modWid/2,1.82],[18,]))
libForm.append(MaterialFormat('BBS',[0.12, 0.16, 0.2, 0.24, 0.28, 0.32, 0.36, 0.4, 0.44, 0.48, 0.52, 0.56,
0.6],[0.04,0.05, 0.06, 0.08, 0.1, 0.12, 0.16, 0.2, 0.24, 0.28],[18,])) # Similar to formatBB GL75
libForm.append(MaterialFormat('OSB',[0.012, 0.015, 0.018, 0.022],[stdSheetWid,stdSheetLen,))
libForm.append(MaterialFormat('PrtBrd',[0.018, 0.022, 0.038],[stdSheetWid,stdSheetLen,))
libForm.append(MaterialFormat('Plywood',[0.012, 0.015, 0.018, 0.021, 0.024, 0.027,
0.03],[stdSheetWid,stdSheetLen,))
libForm.append(MaterialFormat('MDF',[0.008, 0.009, 0.01, 0.012, 0.016, 0.018, 0.019, 0.022, 0.025, 0.028, 0.03,
0.038],[stdSheetWid,stdSheetLen,))
libForm.append(MaterialFormat('HDF',[0.007, 0.008, 0.009, 0.01, 0.011, 0.012],[stdSheetWid,stdSheetLen,))
libForm.append(MaterialFormat('woodFibreBoard',[0.02, 0.036],[stdSheetWid,stdSheetLen,))
libForm.append(MaterialFormat('PlasterBoard',[0.006, 0.009, 0.011, 0.013, 0.015],[stdSheetWid,stdSheetLen,))
libForm.append(MaterialFormat('Fermacell',[0.01, 0.0125, 0.015, 0.018, 0.020, 0.025,
0.03],[stdSheetWid,stdSheetLen,))
libForm.append(MaterialFormat('Rockwool',[0.02,0.025,0.03,0.04,0.05,0.06,0.07,0.08,0.09,0.1],[1.2,],[1.8,],[ETA
09/0275]))
libForm.append(MaterialFormat('Bulk',[,],[,],[,]))
libForm.append(MaterialFormat('steicoFlex',[0.04,0.05,0.06,0.08,0.1,0.12,0.14,0.16,0.18,0.2,0.22,0.24],[0.575],[1.
22],[TG20440g]))
libForm.append(MaterialFormat('Custom0',[,],[,],[,]))
libForm.append(MaterialFormat('Custom1',[,],[,],[,]))
libForm.append(MaterialFormat('Custom2',[,],[,],[,]))
libForm.append(MaterialFormat('Custom3',[,],[,],[,]))
libForm.append(MaterialFormat('Custom4',[,],[,],[,]))

Material model library
# For GWP: co2 equivalents in g per kg reference: https://www.vtt.fi/inf/pdf/technology/2013/T115.pdf
# Some assessments to find values for GWP for LVL are based on numbers used in previous versions:
# Kilogram CO2-equivalents per m3
# kgCO2eq_m3_KQ_MtsW=136

```

PART III: Appendix – Codes and drafts

```
# kgCO2eq_m3_Timb_Mlvn=53

#from PARAPECHS import altCurrencyDict # Does not work of some obscure reason

altCurrencyDict={'NOK':11.81,} # date: medio April 2020. NOK:10.16(Des2019)
# All entries in SI-units

class MaterialProperty:
    """ All required material properties as lists and dictionaries. Dictionaries are used when the value is likely to differ
    between e.g. suppliers or manufacturers, so that a specific key can be used in the analysis. The full declaration is
    available at: http://www.rts.fi/ymparistoseloste/ys028EN.pdf. It is based on the national methodology following the
    basic principles stated in the ISO standard series 14040 and 14020. The declaration covers the product stage A1–A3
    (Cradle to Gate). In addition, due to the expected market, transport CO2 emissions is calculated for the typical
    market scenario"""

    cat={}
    items=0

    def __init__(self, name, elasticType, elastic, density, unitVolCost, unitMassCO2eq, unitMassCO2uptake, form,
chrRate=None):
        self.name=name
        self.elasticType=elasticType
        self.elastic=elastic
        self.density=density
        self.unitVolCost=unitVolCost # Dictionary of supplier specific material cost in euro per cubic meter
        self.unitMassCO2eq=unitMassCO2eq # Dictionary of supplier specific CO2 equivalents in g per kg
        self.unitMassCO2uptake=unitMassCO2uptake # Dictionary of supplier specific CO2 uptake in g per kg
        self.form=form
        self.chrRate=chrRate # mm per min# Is the material restricted to a format

        MaterialProperty.cat[self.name]=MaterialProperty.items
        MaterialProperty.items+=1

libMtrl={}

# For e.g. timber complete engineering constants are used, whilst for most Engineered Wood Products, transverse
isotropy is used
# Engineering constants Abaqus [E and G: N/m^2]: E1, E2, E3, Nu12, Nu13, Nu23, G12, G13, G23
# Density [kg/m^3]
# Supplier A: Not reproduced in the officially available version

libMtrl['S355']=MaterialProperty('S355','ISOTROPIC',(209.E9,
0.3),7800,{'A':3600,},{'A':3750,},{'A':0,},libForm[20,])
libMtrl['Adhesive']=MaterialProperty('Adhesive','ISOTROPIC',(209.E9,
0.3),1000,{'A':35000/altCurrencyDict['NOK'],},{'A':1000,},{'A':0,},libForm[20,]) # Elastic properties not set.

libMtrl['GL28c']=MaterialProperty('GL28c','ENGINEERING_CONSTANTS',(12500.E6,300.E6,300.E6,0.39,0.49
,0.64,650.E6,650.E6,65.E6),430,{'A':6000/altCurrencyDict['NOK'],},{'A':eco2GlulamMoelven['eco2'],},{'A':1730
,},libForm[0],0.7) # Corresponds to Moelven S-beam
libMtrl['GL30c']=MaterialProperty('GL30c','ENGINEERING_CONSTANTS',(13000.E6,300.E6,300.E6,0.39,0.49
,0.64,650.E6,650.E6,65.E6),430,{'A':6000/altCurrencyDict['NOK'],},{'A':eco2GlulamMoelven['eco2'],},{'A':1730
,},libForm[0],0.7)
libMtrl['GL32c']=MaterialProperty('GL32c','ENGINEERING_CONSTANTS',(13700.E6,460.E6,460.E6,0.39,0.49
,0.64,850.E6,850.E6,30.E6),450,{'A':np.NaN,},{'A':eco2GlulamMoelven['eco2'],},{'A':1730,},libForm[0],0.7)
libMtrl['CLT']=MaterialProperty('CLT','ENGINEERING_CONSTANTS',(13700.E6,460.E6,460.E6,0.39,0.49,0.6
4,850.E6,850.E6,30.E6),470,{'A':6000/altCurrencyDict['NOK'],},{'A':115,},{'A':1730,},libForm[4],0.8)
libMtrl['BN']=MaterialProperty('BN','ENGINEERING_CONSTANTS',(12000.E6,230.E6,230.E6,0.39,0.49,0.64,4
40.E6,440.E6,30.E6),500,{'A':5500/altCurrencyDict['NOK'],},{'A':109,},{'A':1730,},libForm[3],0.7)
libMtrl['KbeamPlus']=MaterialProperty('KbeamPlus','ENGINEERING_CONSTANTS',(14000.E6,370.E6,370.E6,0.39,0.49,0.64,690.E6,690.E6,69.E6),450,{'A':5500/altCurrencyDict['NOK'],},{'A':109,},{'A':1730,},libForm[2],0
.7)

# libForm[5] for standard, else libForm[6] for sanded
```

```

libMtrl['Kerto_Q']=MaterialProperty('Kerto_Q','ENGINEERING_CONSTANTS',(10500.E6,2000.E6,130.E6,0.11
,0.81,0.7,600.E6,120.E6,22.E6),510,{'A':7000/altCurrencyDict['NOK'],},{'A':eco2kertoQ['eco2'],},{'A':1730,},lib
Form[5],0.65) # HAKKARAINEN, J. 2016. Properties of Kerto LVL for FEM calculations. Metsä Wood.
# For BauCuChe
# NB: Numbers not obtained for: E3, nu12, nu13, nu23, G23. Respective numbers for Kerto used
# Assume plate thickness is always above 20 mm, hence properties for 30<tck<80 is used. BauBuche Q (approx. 15
% cross-plyies)
libMtrl['BauBuche_Q']=MaterialProperty('BauBuche_Q','ENGINEERING_CONSTANTS',(12800.E6,2000.E6,13
0.E6,0.11,0.81,0.7,820.E6,430.E6,22.E6),730,{'A':7500/altCurrencyDict['NOK'],},{'A':eco2baubuche['eco2'],},{'
A':1730,},libForm[9],0.65) # BAUTECHNIK, D. I. F. 2016. Board BauBuche S/Q German technical approval. In:
GMBH, P. F. (ed.) Z-9.1-838. Berlin: Deutsches Institut für Bautechnik.
libMtrl['Kerto_S']=MaterialProperty('Kerto_S','ENGINEERING_CONSTANTS',(13800.E6,450.E6,130.E6,0.61,0.
74,0.6,600.E6,600.E6,11.E6),510,{'A':6500/altCurrencyDict['NOK'],},{'A':eco2kertoQ['eco2'],},libFor
m[7],0.65) # HAKKARAINEN, J. 2016. Properties of Kerto LVL for FEM calculations. Metsä Wood.
# NB: Baucuche S: Numbers not obtained for: E3, nu12, nu13, nu23, G23. Numbers for Kerto S used
libMtrl['BauBuche_S']=MaterialProperty('BauBuche_S','ENGINEERING_CONSTANTS',(16800.E6,470.E6,130.
E6,0.61,0.74,0.6,760.E6,850.E6,11.E6),730,{'A':7000/altCurrencyDict['NOK'],},{'A':eco2baubuche['eco2'],},{'A':
1730,},libForm[10],0.65) # BAUTECHNIK, D. I. F. 2016. Board BauBuche S/Q German technical approval. In:
GMBH, P. F. (ed.) Z-9.1-838. Berlin: Deutsches Institut für Bautechnik.

libMtrl['GypsumTypeA']=MaterialProperty('GypsumTypeA','ISOTROPIC',(1800.E6,0.2),900,{'A':350,},{'A':eco2
gypsum['eco2'],},{'A':0,},libForm[17],) # Cost from NP. Check charring rate and density for both A and F type
gypsum
libMtrl['GypsumTypeF']=MaterialProperty('GypsumTypeF','ISOTROPIC',(1800.E6,0.2),900,{'A':400,},{'A':eco2g
ypsum['eco2'],},{'A':0,},libForm[17],) # Approx cost from NP
# https://www.hunton.no/wp-content/uploads/2018/09/fermacell_gypsum-fibreboards_eta-03-0050.pdf
libMtrl['Fermacell']=MaterialProperty('Fermacell','ENGINEERING_CONSTANTS',(3800.E6,3800.E6,3800.E6,0.
2,0.2,0.2,1600.E6,1600.E6,1600.E6),1150,{'A':450,},{'A':1967,},{'A':0,},libForm[18],) # Approx cost

libMtrl['Plywood']=MaterialProperty('Plywood','ISOTROPIC',(1700.E6,0.3),600,{'A':1450,},{'A':229,},{'A':1731,
},libForm[13],1.1) # NorskPrisbok cost (02.4.6.3.0206 Platekledning på innervegg, kryssfiner furu, kvalitet II/BB,
t = 12 mm, ubehandlet, skrudd )
libMtrl['OSB_3']=MaterialProperty('OSB_3','ENGINEERING_CONSTANTS',(3000.E6,1400.E6,300.E6,0.02,0.0
2,0.68,1080.E6,1080.E6,50.E6),600,{'A':520,},{'A':208,},{'A':1692,},libForm[11],1.0) # NorskPrisbok
(02.3.5.5.0400 Platekledning, OSB, 18 mm, underlag), Fictive charRate
# P6 type particle board: Floor boards that can withstand severe stress, for interior use
libMtrl['P6_6_13']=MaterialProperty('P6_6_13','ENGINEERING_CONSTANTS',(2500.E6,2500.E6,2500.E6,0.2,
0.2,0.2,1200.E6,1200.E6,1200.E6),650,{'A':785,},{'A':409,},{'A':1564,},libForm[12],1.0) # NorskPrisbok cost
(02.5.5.3.0130 Undergulv av plater. Sponplater t = 22), Fictive charRate
libMtrl['P6_13_20']=MaterialProperty('P6_13_20','ENGINEERING_CONSTANTS',(2400.E6,2400.E6,2400.E6,0.
2,0.2,0.2,1150.E6,1150.E6,1150.E6),600,{'A':785,},{'A':409,},{'A':1564,},libForm[12],1.0) # NorskPrisbok cost
(02.5.5.3.0130 Undergulv av plater. Sponplater t = 22), Fictive charRate
libMtrl['P6_20_25']=MaterialProperty('P6_20_25','ENGINEERING_CONSTANTS',(2100.E6,2100.E6,2100.E6,0.
2,0.2,0.2,1050.E6,1050.E6,1050.E6),550,{'A':785,},{'A':409,},{'A':1564,},libForm[12],1.0) # NorskPrisbok cost
(02.5.5.3.0130 Undergulv av plater. Sponplater t = 22), Fictive charRate
libMtrl['HB_HLA_1']=MaterialProperty('HB_HLA_1','ENGINEERING_CONSTANTS',(5300.E6,1000.E6,300.E
6,0.02,0.02,0.68,2100.E6,2100.E6,50.E6),900,{'A':1000,},{'A':661,},{'A':1437,},libForm[15],1.5) # Fictive
charRate and approx cost, HardBoard acc. to EN 622-2(2004'ENGINEERING_CONSTANTS') type HB.HLA 1
# Hunston Silencio: Density + dyn stiff from TG 2330ge: The dynamic stiffness for Hunton Silencio 36 is 8 MN/m3
measured according to NS-ISO 9052-1 (EN 29052-1).
libMtrl['Silencio']=MaterialProperty('Silencio','ISOTROPIC',(162.E6,
0.3),250,{'A':275,},{'A':243,},{'A':1240,},libForm[16],) # New form required. Cost from Norsk Prisbok
(02.5.5.3.0180 Isolasjon for trinnyd) # Poissons estimated. E-modulus from: e-mail 23.05.2017 07.33 from
Torgersen Klætte, Torger <Torger.Klaette@moelven.no>; SV: Spørsmål etter prøving av Moelven Trä8

# Kristian, B. D. and F. F. I. O. T. I. F. K. Norges Teknisk-Naturvitenskapelige Universitet. 2009. Mechanical
properties of clear wood from Norway spruce, Norges teknisk-naturvitenskapelige universitet, Fakultet for
ingeniørvitenskap og teknologi, Institutt for konstruksjonsteknikk.
libMtrl['C14']=MaterialProperty('C14','ENGINEERING_CONSTANTS',(7000.E6,230.E6,230.E6,0.39,0.49,0.64,4
40.E6,440.E6,30.E6),350,{'A':4500/altCurrencyDict['NOK'],},{'A':50,},{'A':1500,},libForm[1],0.8)
libMtrl['C16']=MaterialProperty('C16','ENGINEERING_CONSTANTS',(8000.E6,270.E6,270.E6,0.48,0.42,0.5,30
5.E6,500.E6,50.E6),370,{'A':4500/altCurrencyDict['NOK'],},{'A':50,},{'A':1500,},libForm[1],0.8)
libMtrl['C18']=MaterialProperty('C18','ENGINEERING_CONSTANTS',(9000.E6,300.E6,300.E6,0.39,0.49,0.64,5
60.E6,560.E6,30.E6),380,{'A':4500/altCurrencyDict['NOK'],},{'A':50,},{'A':1500,},libForm[1],0.8)

```

PART III: Appendix – Codes and drafts

```
libMtrl['C24']=MaterialProperty('C24','ENGINEERING_CONSTANTS',(11000.E6,370.E6,370.E6,0.39,0.49,0.64,690.E6,690.E6,30.E6),420,{'A':4500/altCurrencyDict['NOK'],},{'A':50,},{'A':1500,}, libForm[1], 0.8)
libMtrl['C30']=MaterialProperty('C30','ENGINEERING_CONSTANTS',(12000.E6,400.E6,400.E6,0.39,0.49,0.64,750.E6,750.E6,30.E6),380,{'A':5500/altCurrencyDict['NOK'],},{'A':50,},{'A':1500,}, libForm[1], 0.8)
```

```
libMtrl['Gravel_8_16']=MaterialProperty('Gravel_8_16','ISOTROPIC',(0,0),1370,{'A':150,},{'A':3,},{'A':0,},libForm[20],)
```

```
libMtrl['Concrete']=MaterialProperty('Screed','ISOTROPIC',(20.E9,0.2),2100,{'A':170,},{'A':eco2screed['eco2'],},{'A':0,},libForm[20],) # Norsk Prisbok (02.5.3.0180 Betong, påstøp normal). Inkl arbeid: 260 euro/m3
```

```
libMtrl['Glysol']=MaterialProperty('Glysol','ISOTROPIC',(15.E9,0.2),2000,{'A':100,},{'A':30,},{'A':0,},libForm[20],)
```

```
libMtrl['Rockwool']=MaterialProperty('Rockwool','ISOTROPIC',(15.E9,0.25),180,{'A':100,},{'A':320,},{'A':0,},libForm[19],) # Fictive cost. Jones, D. and C. Brischke (2017). Performance of bio-based building materials, Woodhead Publishing.
```

```
libMtrl['steicoFlex']=MaterialProperty('steicoFlex','ISOTROPIC',(50.E6,0.3),50,{'A':250,},{'A':150,},{'A':1000,},libForm[21], 0.8) # Guestimates mostly
```

```
libMtrl['Custom0']=MaterialProperty('Custom0','ENGINEERING_CONSTANTS',(12000.E6,400.E6,400.E6,0.39,0.49,0.64,750.E6,750.E6,30.E6),380,{'A':600,},{'A':60,},{'A':1500,}, libForm[22], 0.8) # Copied from C30 for now
```

```
libMtrl['Custom1']=MaterialProperty('Custom1','ENGINEERING_CONSTANTS',(12000.E6,400.E6,400.E6,0.39,0.49,0.64,750.E6,750.E6,30.E6),380,{'A':600,},{'A':60,},{'A':1500,}, libForm[23], 0.8)
```

```
libMtrl['Custom2']=MaterialProperty('Custom2','ENGINEERING_CONSTANTS',(12000.E6,400.E6,400.E6,0.39,0.49,0.64,750.E6,750.E6,30.E6),380,{'A':600,},{'A':60,},{'A':1500,}, libForm[24], 0.8)
```

```
libMtrl['Custom3']=MaterialProperty('Custom3','ENGINEERING_CONSTANTS',(12000.E6,400.E6,400.E6,0.39,0.49,0.64,750.E6,750.E6,30.E6),380,{'A':600,},{'A':60,},{'A':1500,}, libForm[25], 0.8)
```

```
libMtrl['Custom4']=MaterialProperty('Custom4','ENGINEERING_CONSTANTS',(12000.E6,400.E6,400.E6,0.39,0.49,0.64,750.E6,750.E6,30.E6),380,{'A':600,},{'A':60,},{'A':1500,}, libForm[26], 0.8)
```

Ply direction of MetsaWood Kerto

The following product specifications are suppressed, but may be used in PSACHS

```
# kertoPnlPlyNumActual=[7,7,8,9,10,11,13,15,17,19,21,23,25]
# kertoPnlPlyNumActual_dict = dict(zip(list(range(len(kertoPnlPlyNumActual))),kertoPnlPlyNumActual))
#
kertoPnlLayupActual=[(0,90,0,0,0,90,0),(0,0,90,0,90,0,0),(0,0,90,0,0,90,0,0),(0,0,90,0,0,0,90,0,0),(0,0,90,0,0,0,0,90,0,0),
#(0,0,90,0,0,0,90,0,0,0,90,0,0),(0,0,90,0,0,0,0,90,0,0,0),(0,0,90,0,0,0,0,90,0,0,0),(0,0,90,0,0,0,0,90,0,0,0),
#(0,0,90,0,0,0,90,0,0,0,90,0,0,0,90,0,0),(0,0,90,0,0,0,0,90,0,0,0,90,0,0,0),(0,0,90,0,0,0,0,90,0,0,0,0,90,0,0),
# kertoPnlPlyNum=[5,5,5,5,5,5,7,7,7,9,11,11,11]
#
kertoPnlPlyDir=[(0,90,0,90,0),(0,90,0,0,90,0),(0,90,0,90,0),(0,90,0,90,0),(0,90,0,90,0),(0,90,0,90,0),(0,90,0,90,0,90,0),
#(0,90,0,90,0,90,0),(0,90,0,90,0,0),
# (0,90,0,90,0,90,0,90,0),(0,90,0,90,0,90,0,90,0),(0,90,0,90,0,90,0,90,0),(0,90,0,90,0,90,0,90,0)]
# kertoPnlPlyDir_dict = dict(zip(list(range(len(kertoPnlPlyDir))),kertoPnlPlyDir))
#
kertoPnlPlyTck=[(0.003,0.003,0.009,0.003,0.003),(0.006,0.003,0.003,0.003,0.006),(0.006,0.003,0.006,0.003,0.006),
#(0.006,0.003,0.009,0.003,0.006),(0.006,0.003,0.012,0.003,0.006),(0.006,0.003,0.015,0.003,0.006),(0.006,0.003,0.009,0.003,0.009,0.003,0.006),
#(0.006,0.003,0.012,0.003,0.012,0.003,0.006),(0.006,0.003,0.015,0.003,0.015,0.003,0.006),(0.006,0.003,0.009,0.003,0.015,0.003,0.006),
#(0.006,0.003,0.009,0.003,0.015,0.003,0.009,0.003,0.006),(0.006,0.003,0.012,0.003,0.009,0.003,0.009,0.003,0.012,0.003,0.006),
#(0.006,0.003,0.015,0.003,0.009,0.003,0.009,0.003,0.015,0.003,0.006)]
# kertoPnlPlyTck_dict = dict(zip(list(range(len(kertoPnlPlyTck))),kertoPnlPlyTck))
#
kertoPnlPlyTckSand=[(0.001,0.003,0.009,0.003,0.003),(0.004,0.003,0.003,0.003,0.006),(0.004,0.003,0.006,0.003,0.006),
#(0.004,0.003,0.009,0.003,0.006),(0.004,0.003,0.012,0.003,0.006),(0.004,0.003,0.015,0.003,0.006),(0.004,0.003,0.009,0.003,0.009,0.003,0.006),
#(0.004,0.003,0.012,0.003,0.012,0.003,0.006),(0.004,0.003,0.015,0.003,0.015,0.003,0.006),(0.004,0.003,0.009,0.003,0.015,0.003,0.006),
#(0.004,0.003,0.009,0.003,0.015,0.003,0.009,0.003,0.006),(0.004,0.003,0.012,0.003,0.009,0.003,0.009,0.003,0.012,0.003,0.006),
#(0.004,0.003,0.015,0.003,0.009,0.003,0.009,0.003,0.015,0.003,0.006)]
# kertoPnlPlyTckSand_dict = dict(zip(list(range(len(kertoPnlPlyTck))),kertoPnlPlyTck))
```

Annex A.II PSACHS development information

Title: Python Script for Abaqus for Closed Hollow Sections (PSACHS)
 Author: Sveinung Nesheim
 Organisation: NTNU, Norway
 E-mail: sne@ntnu.no
 Current version: See version history below
 Version date: 2020.03.06

About

Description:

Theoretical presumptions:

Code written for Abaqus 2017

Language: Python 2.7.3

Versioning and change control

VERSION HISTORY including: LAST WORKING VERSION (LWV) + WORK IN PROGRESS (WIP)

Change control (MAKE SURE TO UPDATE THE PARAMETER PSACHSver):

7.4.1 (20200306) Replace screedMassDensity and screed_tck with overlayDstrMass

7.4.0 (20191025) Added concrete as Concrete Damage Plasticity + optional interaction to flanges (tie or cohesive) in five new parameters: topFlgIntAct,btmFlgIntAct,Knn,Kss,Ktt; Functions objectFunction() and cvtyMass() removed. Parameters sandBagType and sandBagFormat kept but obsolete.

7.3.n The Tampere editions:

7.3.0 (20191010) (Splitting material properties to separate file)

7.3.1 (20191010) Introducing option of different center joist section

7.3.2 (20191022) Added line support for suspension of floor along transverse edge of top flange

7.2.5 Dynamic odb reference: Get current viewport session

7.2.4 Include PSACHS VERSION CODE for reference to which script is run to generate the given results (also used for static text file endpoint used by the General Data Swipe in iSight)

7.2.3 Make running routines and sequences more robust: moved userInput() to final query; hardcoding SID and referencing from that single point; defaultParameters now conditionally; query on GUI mode

7.2.2 In performJob() look for .lck-file and remove if found + explicitly open .odb in read-only mode. jobId not implemented.

7.2.1 Revert to let pair be collected from textfile rather than being generated in setup()

7.2.0 Cleanup and fixing bugs in finding nodes, as well as general cleanup of generation of names and numbers and filenames

7.1.1 Change from static to dynamic file reference (including path to current working directory) for in and out data + two separate out-files (current and appended results)

7.1.0 Change from axial springs to 3D-linear uncoupled cartesian springs and removal of BC when spring-conditions

7.0.0 Object function as new script function

6.4.0 Change wire section assignment in ln2753, 2756

6.3.0 Based on 6.2.3: Functionality for copying parts with new names to a pattern in assembly using LAP#-identifier

6.2.3 Changes to applicator and receiver: ln727, 728

6.2.2 20180924 ln3186 to 3196 BC free clamped

6.1.1 20180530 Separate A0F0_receiver tied to bottom flange to probe deflections

5.n Separate applicator for load definition

4.n Flexible end restraints

3.n Text file read and write

2.n Shell and solid

1.n Solid base feature only

References

Dassault Systèmes (2007). Element selection in Abaqus, Dassault Systèmes Simulia corp.

Dassault Systèmes (2014). Abaqus analysis user's guide, Dassault Systèmes Simulia corp.

Dassault Systèmes (2014). Abaqus/Standard Element Index, Dassault Systèmes Simulia corp.

Mirianon, F., et al. (2008). A Method to model wood by using ABAQUS finite element software : Part I. Constitutive model and computational details. VTT Publication 687, [Espoo, Finland] : VTT Technical Research Centre of Finland.

Annex A.III PSACHS input file format

Line	Parameter	Format	Description
0	pair	int	Running number (per series) from the input file forwarded to the output file as a quality control measure
1	SN	int	Analysis serial number. Used in combination with Pair for a unique identification of an analysis.
2	seriesDscr	str	Description of the purpose or intention with a series of analyses.
3	bcType	str	Boundary condition types: bcType='BCFF': Free-Free: No restraining BC: Free-free oscillations bcType='BCLN': Floor element is suspended in a continuous hinge along transverse edge of top flange bcType='BCPR': Floor element is suspended in a continuous hinge peripherally around top flange Pinned connections: All translations constrained at bottommost fibres either along horizontal edge (solid edge joists) or on central vertex (shell edge joists) bcType='BCFP': Free-Pinned: Realistically pinned with no residual horizontal forces from deflection bcType='BCXP': Fixed-Pinned: Standard pinned with residual horizontal forces from deflection Hybrid connections (pinned and clamped): BC assigned to the edge joists end face (solid edge joists) or vertical edge (shell edge joists) bcType='BCFH': Free-Hybrid: One side clamped and the other side pinned with free translations in the horizontal plane bcType='BCXH': Fixed-Hybrid: One side clamped and the other side pinned with fixed translation Clamped connections bcType='BCFC': Free-Clamped: Both sides clamped but with free translation in X-direction at X0-level

			<p>bcType=='BCXC': Fixed-clamped: Both sides standard clamped as defined in Abaqus Boundary conditions with connector behaviour (normally cartesian springs): Insert any number representing rotational stiffness in Nm per radians after 'S*' bcType.startswith('SP', 0, 2):# X0 side spring (S) and X1 side pinned (P) bcType.startswith('SC', 0, 2): X0 side spring (S) and X1 side clamped (C) bcType.startswith('SS', 0, 2): Both sides with spings (SS) bcType.startswith('SFE', 0, 3): # X0 side spring and X1 as Free End (FE) Following the two first letters: Choose whether the BC at X0 is free to translate along X-direction or not (F or X) Valid keys: SPF; SPX; SCF; SCX; SSF; SSX SFE: Cantilever with specified rotational stiffness Note: If the connection is pinned the edge joists only rest on the lowermost fibre: edge for solid, and point (vertex) for shell. If the connection is fixed (encastre), the edge joist is fixed along the entire height of the beam: surface for solid, and along edge for shell. For an intermediate realistic rotational stiffness, the rotational spring is attached to the entire height of the beam as for fixed connection</p>
4	D22	float	Axial stiffness in N/m. Note that D11 is not used since the value is related to rotational stiffness and not axial stiffness
5	D33	float	Axial stiffness in N/m
6	ptLoad	float	Point load in N
7	dstrLoad	float	Distributed load N/m^2

PART III: Appendix – Codes and drafts

8	span	float	Span
M	modWid	float	Module width
10	cvtyHgt	float	Cavity height (height of joists)
11	edgJst0_wid	float	Width of edge joist 0
12	edgJst0_off_y	float	Inward offset of edge joist 0
13	edgJst1_wid	float	Width of edge joist 1
14	edgJst1_off_y	float	Inward offset of edge joist 1
15	edgBeam0_wid	float	Width of edge beam 0
16	edgBeam1_wid	float	Width of edge beam 1
17	diffCntJst	str	Y or N. If Y (Yes) then the centre joist differs from the field joist dimensions.
18	evenJstCvty	str	Y or N. If Y (Yes) the distribution of joists is done at even cavity spacings, else at even centre distances.
19	cntJst_wid	float	Width of centre joist
20	fldJst_num	int	Number of field joists
21	fldJst_wid	float	Width of field joists
22	fldTrns_num	int	Number of transverse stiffeners
23	fldTrns_wid	float	Width of transverse stiffeners
24	topFlg_tck	float	Top flange thickness
25	btmFlg_tck	float	Bottom flange thickness
26	edgJst0_mtrl	str	Edge joist 0 material
27	edgJst1_mtrl	str	Edge joist 1 material
28	SC_mtrl	str	Specification of material for stiffening stringers
29	edgBeam0_mtrl	str	Edge beam 0 material
30	edgBeam1_mtrl	str	Edge beam 1 material
31	cntJst_mtrl	str	Centre joist material
32	fldJst_mtrl	str	Field joist material
33	fldTrns_mtrl	str	Field transverse stiffener material
34	cvtyMassDensity	float	Density of cavity mass
35	sandBagType	str	Not applicable
36	sandBagFormat	str	Not applicable
37	cvtyDstrMass	float	Density of distributed mass on bottom flange
38	topFlg_mtrl	str	Top flange material
39	topFlgIntAct	str	If “Cohesive” the spring/shear stiffness of the interaction between flange and web is applied. Else tied.
40	topFlgKnn	float	Specification of stiffness between flange and web in direction of NN.

41	topFlgKss	float	Specification of stiffness between flange and web in direction of SS.
42	topFlgKtt	float	Specification of stiffness between flange and web in direction of TT.
43	topFlg_plyNum	int	Number of plies formulated for the top flange. 1 for normal base feature.
44	topFlg_plyOrient	float	Orientation of fibres of plies with respect to longitudinal axis. The orientation of stacked plies have alternating signs.
45	btmFlg_mtrl	str	Same definitions as for top flange
46	btmFlgIntAct	str	
47	btmFlgKnn	float	
48	btmFlgKss	float	
49	btmFlgKtt	float	
50	btmFlg_plyNum	int	
51	btmFlg_plyOrient	float	
52	overlayDstrMass	float	Distributed mass on top flange (weight of overlay)
53	edgJst_membType	str	Shell or solid
54	edgBeam_membType	str	Shell or solid
55	cntJst_membType	str	Shell or solid
56	fldJst_membType	str	Shell or solid
57	fldTrns_membType	str	Shell or solid
58	topFlg_membType	str	Shell or solid
59	btmFlg_membType	str	Shell or solid
60	seedSizeGlobal	float	Element size
61	edgJst_elemCode	key	Element code
62	edgBeam_elemCode	key	Element code
63	cntJst_elemCode	key	Element code
64	fldJst_elemCode	key	Element code
65	fldTrns_elemCode	key	Element code
66	topFlg_elemCode	key	Element code
67	btmFlg_elemCode	key	Element code
68	applicator_elemCode	key	Element code

Annex A.IV Script for PSD of individual walking load

Title: PSD for individual walking load
 Author: Sveinung Nesheim
 Organisation: NTNU, Norway
 E-mail: sne@ntnu.no
 Language/version: Python

This function is to obtain the PSD of individual walking load (with body weight)

input:
 fp: walking frequency
 f_int: frequency internal
 W: body weight: unit in N

output: psd_all - PSD of individual walking load (unit in N^2*s); f_all - frequency axis

example input:
 [f_all,psd_all]=individualwalking_autoPSD(1.5,0.001,700)

References

[1] Chen, J., et al. (2019). "Power spectral-density model for pedestrian walking load." Journal of Structural Engineering 145(2): 04018239.

```
import numpy as np
import pandas as pd
import matplotlib.pyplot as plt
import seaborn as sns; sns.set()
plt.rcParams["font.family"] = "Times New Roman"
```

```
case=0

# Pedestrian walking weight
W=700 #[N]

f_ps=[1.5, 1.65, 1.75, 1.8, 1.95, 2.0, 2.1, 2.25]
f_p=f_ps[0]

# Frequency internal
f_int=0.001

# List of harmonic and subharmonic indexes:
intHarmon=np.linspace(0.5,4,8)

# List of harmonic and subharmonic indexes including 0:
intAll=np.linspace(0,4,9)

para=[]
para.append(pd.DataFrame(index=['harmonic','subharmonic'],columns=['A1','b1','sigma1','A2','b2','sigma2']))
para[0].iloc[0,:]=[40.094,1,0.01,5.063,1,0.034]
para[0].iloc[1,:]=[15.771,1,0.017,6.515,1,0.06]

para.append(pd.DataFrame(index=['harmonic','subharmonic'],columns=['A1','b1','sigma1','A2','b2','sigma2']))
para[1].iloc[0,:]=[40.08,1,0.00999,5.061,1,0.03345]
```

```
para[1].iloc[1,:]=[15.7710391853351,1,0.0168,6.51457304910572,1,0.06029]
```

```
sAll=[]
sAll.append(pd.DataFrame(index=['a','b','c','d'],columns=intAll))
sAll[0].loc['a,:']=[-0.0821,0.00110,-0.1383,-0.0017,-0.0082,0.00090,0.00290,0.00150,-0.0016]
sAll[0].loc['b,:']=[0.49520,-0.0052,0.79370,0.00890,0.05570,-0.0047,-0.0144,-0.0080,0.00890]
sAll[0].loc['c,:']=[-0.8875,0.00860,-1.4124,-0.0153,-0.1193,0.00810,0.02290,0.01440,-0.0158]
sAll[0].loc['d,:']=[0.51690,-0.0039,0.81220,0.00880,0.08380,-0.0044,-0.0107,-0.0083,0.00990]
```

```
sAll.append(pd.DataFrame(index=['a','b','c','d'],columns=intAll))
sAll[1].loc['a,:']=[-0.020844075,-0.004349856,-0.054719840654203,-0.001917956,-0.01713799,-0.000210823,0.002557938,4.06E-04,9.03E-06]
sAll[1].loc['b,:']=[0.174649793,0.023344148,0.353720472237947,0.010314941,0.10437207,0.001328438,-0.012829301,-0.002142927,0.000163404]
sAll[1].loc['c,:']=[-0.330947116,-0.040649458,-0.646414042479735,-0.017665496,-0.207157649,-0.002702621,0.020823946,3.69E-03,8.34E-05]
sAll[1].loc['d,:']=[0.195922879,0.023988841,0.370795636752807,0.010111411,0.136285824,0.001985073,-0.010003183,-0.001929422,0.000324677]
```

```
def S(case,n): # for n=0,0.5,1,...,4
    return
sAll[case].loc['a,n']*np.power(f_p,3)+sAll[case].loc['b,n']*np.power(f_p,2)+sAll[case].loc['c,n']*f_p+sAll[case].loc['d,n]
```

```
s=[]
for i in range(len(intAll)):
    s.append(S(case,intAll[i]))
```

```
s0=s[0]
s=s[1::]

ssum=sum(s)
beta=s0/ssum
ss=s/ssum*s0
f_all=np.arange(0,10,f_int)
psdAll=np.zeros(len(f_all))
```

```
# Subharmonics
for j in range(4):
    ""
    See equation (6) in [1]
    ""
    jj=j+0.5
    f_start=np.argmin(abs(f_all-0.95*f_p*jj))
    f_part=np.arange(0.95,1.05,f_int/f_p/jj)
    a1 = para[case].loc['subharmonic','A1']
    a2 = para[case].loc['subharmonic','A2']
    b1 = para[case].loc['subharmonic','b1']
```

```

b2 = para[case].loc['subharmonic','b2']
c1 = para[case].loc['subharmonic','sigma1']
c2 = para[case].loc['subharmonic','sigma2']
psdPart = (a1*np.exp(-np.power((f_part-b1)/c1,
2))+a2*np.exp(-np.power((f_part-b2)/c2,
2)))/f_p/jj*ss[j*2]*W**2
f_end=f_start+len(psdPart)
psdAll[f_start:f_end]=psdPart

# Harmonics
for j in range(4):
    f_start=np.argmax(abs(f_all-0.95*f_p*(j+1)))
    f_part=np.arange(0.95,1.05,f_int/f_p/(j+1))
    a1 = para[case].loc['harmonic','A1']
    a2 = para[case].loc['harmonic','A2']
    b1 = para[case].loc['harmonic','b1']
    b2 = para[case].loc['harmonic','b2']
    c1 = para[case].loc['harmonic','sigma1']
    c2 = para[case].loc['harmonic','sigma2']
    psdPart = (a1*np.exp(-np.power((f_part-b1)/c1,
2))+a2*np.exp(-np.power((f_part-b2)/c2,
2)))/f_p/(j+1)*ss[j*2+1]*W**2
    f_end=f_start+len(psdPart)
    psdAll[f_start:f_end]=psdPart

fig, ax = plt.subplots()
plt.suptitle('PSD of individual walking load',
fontsize=16)
ax = plt.subplot(111, xlabel='Frequency [Hz]',
                ylabel='PSD [N^2/Hz]',
                title='')

for item in ([ax.title, ax.xaxis.label, ax.yaxis.label] +
ax.get_xticklabels() + ax.get_yticklabels()):
    item.set_fontsize(12)
ax.title.set_fontsize(12)
plt.style.use('seaborn-whitegrid')#seaborn-paper')
plt.plot(f_all,psdAll)
plt.set_yscale('log')

def f(n):
    return
np.linspace(0.95*n*f_p,1.05*n*f_p,resolution)

#Normalized frequency
def f_norm(n):
    return f(n)/(n*f_p)

f_s=f_norm(1)*1*f_p

# Two-term Gaussian PSD for single harmonic (or
subharmonic) n in E(0.5, 1, ..., 4)
def Gn(n): # for n=0.5,1,...,4
    return
(beta*S(n)/(n*f_p))*(PSDfit.loc[n,'A1']*np.exp(-
np.power((f_norm(n)-1)/PSDfit.loc[n,'sigma1'],
2))+PSDfit.loc[n,'A2']*np.exp(-
np.power((f_norm(n)-1)/PSDfit.loc[n,'sigma2'], 2)))

def plot_Gn(n):
    fig, ax = plt.subplots()
    ax.plot(f_norm(n), Gn(n))
    ax.set(xlabel='Normalized frequency f/(n*fp)
[DL]', ylabel='Normalized PSD [DL]',
title='Normalized single harmonic two-term Gaussian
PSD fit')
    ax.grid()
    #ax.set_ylim(0,50)
    #fig.savefig("test.png")
    plt.show()

plot_Gn(0.5)
fig, ax = plt.subplots()
for i in range(len(intHarmon)):
    ax.plot(f_norm(intHarmon[i]), Gn(intHarmon[i]))

ax.set(xlabel='Normalized frequency f/(n*fp) [DL]',
ylabel='Normalized PSD [DL]', title='Normalized
two-term Gaussian PSD fit for all harmonics')
ax.grid()
#ax.set_ylim(0,50)
ax.set_xlim(0.95,1.05)
#fig.savefig("test.png")
plt.show()

G=np.zeros(resolution)
for i in range(len(intHarmon)):
    G+=Gn(intHarmon[i])

fig, ax = plt.subplots()
ax.plot(f_norm(1), G)
ax.set(xlabel='Normalized frequency f/(n*fp) [DL]',
ylabel='Normalized PSD [DL]', title='Normalized
two-term Gaussian PSD fit')
ax.grid()
#ax.set_ylim(0,50)
#fig.savefig("test.png")
plt.show()

Scaling (denormalization)

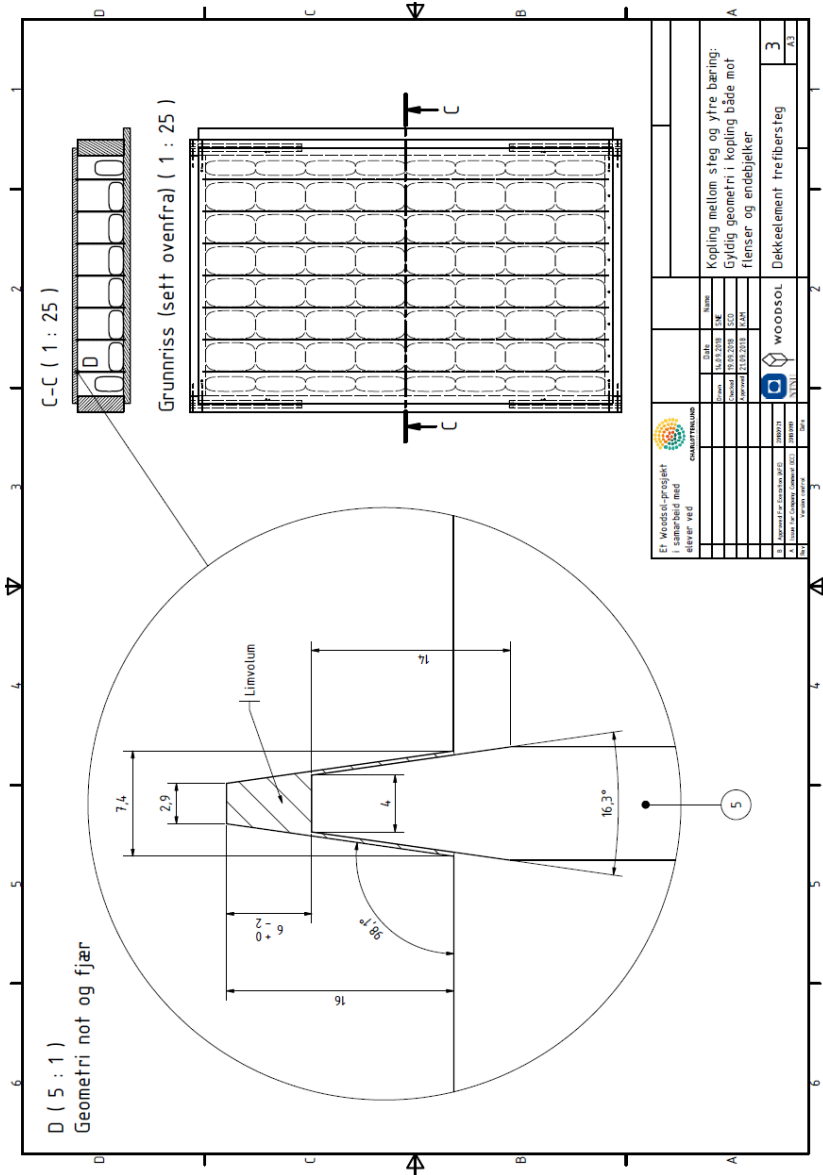
def Gn_denorm(n):
    return W**2/(n*f_p)*Gn(n)

G_denorm=np.zeros(resolution)
for i in range(len(intHarmon)):
    G_denorm+=Gn_denorm(intHarmon[i])

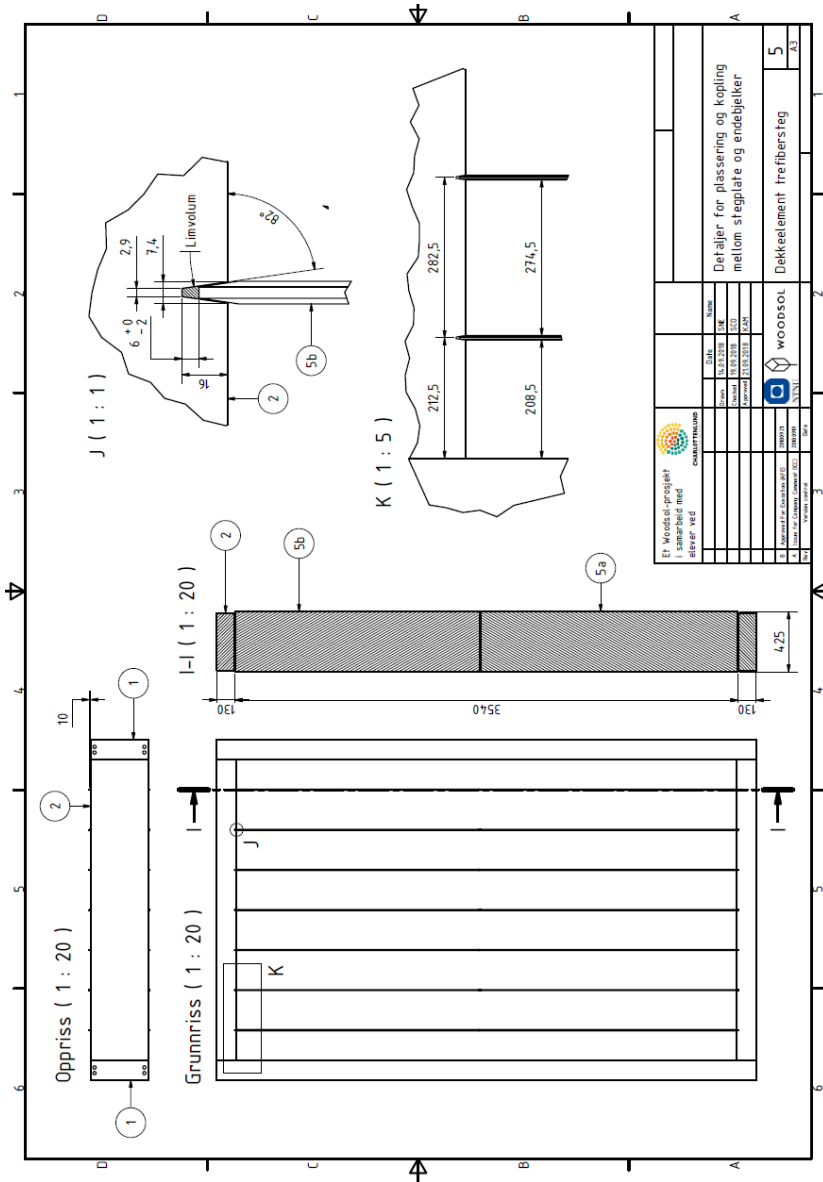
fig, ax = plt.subplots()
plt.style.use('seaborn-whitegrid')#seaborn-paper')
ax.plot(f_norm(1), G_denorm)
ax.set(xlabel='Normalized frequency f/(n*fp) [DL]',
ylabel='Scaled PSD [N^2/s]', title='Scaled two-term
Gaussian PSD fit')
ax.grid()
#ax.set_ylim(0,50)
#fig.savefig("test.png")
plt.show()

```

Annex A.V Technical drawings of thin field web floor element



		Er Woodsol-prosjektet i samarbeid med...	
Prosjektleder:	Utviklet av:	Godkjent av:	Godkjent av:
1. Woodsol Prosjekt (2022)	2. Woodsol Prosjekt (2022)	3. Woodsol Prosjekt (2022)	4. Woodsol Prosjekt (2022)
Woodsol		Dekkelement trefibersteg	
Woodsol		3	



Annex B. Philosophic exercises

Two short texts in Norwegian were written during the doctorate. The texts are personal philosophical exercises concerning the fatigue and the meaningfulness, and on the selection of methods, in relation to the doctoral process.

Annex B.I Skrik I – Slit i ukjent terreng

Ein har ei viss formeining om kvar ein skal, og ei slags vissheit eller von om at målet vil tre klarare fram di nærare ein kjem, men vegen dit er krevjande og lang. Nett no er det tett kratt og skodda er tjukk og klam i bratta. Terrenget er òg uvant no i byrjinga, og tidt vert det så ulent og stygt at ein lyt gå rundt eit gjel eller ein knaus ein uforvarande har gått seg fram på. Og på veg over høgda, når ein skimtar varden og skal byrje å forsvare sine val, vert ein piska av kaldt og stikkande drev i ansiktet medan vinden uanstrengd filleristar deg, og spør med si krasse røyst om kvifor du kom hit. Stormen kastar vêret i tette råk over kammen og i korte augneblink bles den sjølv egga fri for skodde og let ein skimte landskapet der framme. Oftast ser ein berre ei ny seig stigning eller beint fram uframkomelege opprivne fjell som kneisar opp framfor deg, og ein dett mest i hop vonlaus, men utan mykje val. Men stundom let ein sjå eit fagert landskap der framme og vinden stryk deg kjærleg langs andletet og tørkar tårene etter slitet og liksom ønsker deg god tur vidare. Det er når ein kjem seg opp ei forferdelig kneik eller står på ein tinde og kan legge ruta i eit augneblink av godt vêr at det godt å gå og det heile gjev meining for ei tid. Men når kulden og myrkre trugar og ein ikkje ser handa framfor seg og vinden skrålar og kvin om farar og samanhengar ein ikkje klarer å fatte, ja då er det så tungt at ein mest vil gje opp. Men kva skal ein gå attende til? Har ein ikkje forlate alt det trygge for å klare denne reisa? Det er ingen veg attende, og ein lyt stå i vêret og lære vinden sitt språk og terrenget og lese. Ditt våpen er vilja og motet, og om det ser håplaut ut kan du ikkje gje deg, for du har ikkje noko anna val du forpinte akademiske infanterist. Men medan ulvane jagar din såre tanke og bol, kan det hende at det er du som vinn og ulvane vert magiske fortryllande hyl under nattesvart kvelv. Kan hende du stoggar opp og blir var månen som lyser mildt og med sitt bleike lys syner deg eit gamalt trakk. Her har det gått andre før deg. Ein ser ut til å ha freista og gå langsetter ei smal berghylle bortover der, og ein annan latar til å ha klive bortetter eggja der oppe. Fotefara frå andre vitnar om at denne reisa ikkje kan vere heilt meiningslaus. Der inne i hugen brenn det eit ønske om å bidra med noko. Om å snu nokre nye steinar og pirke i noko som kan vere til det beste for alle. Om det er noko aldri så lite så er det verd å kjempe for. Og så må ein berre stundom løfte blikket for å erkjenne nettopp det og slik hente mot. Ein må glede seg over strabasane òg. For dette er også undringa og forundringa si reise, og dei rikaste skildringane finn du der andre ikkje har sett. Ikkje vær redd for å krype i ukjende krokar eller balansere på dei yste steinane. Kun den duglege vil forfølge det dulgte, og morgonsola varmar like godt den yste post som den inste krins. Ein dag vil også du stå ved det som virka som ein utilgjengeleg varde og forstå vinden sitt språk og tale med den om kva du har funne og gjort.

Annex B.II Skrik II – Strinakkjen og jordormen

Eg stend i regnet og bryt stein. Nokre er handterlege fine stablesteinar i gneis og gabbro, andre er store emner i granitt, men oftast med god kløv. Eg har eit godt blikk for slikt, og ei gamal steinsleggje som ligg så godt i nevene. Med godt handelag og nokre gode meislar er det mest ei glede, skjønt stundom må ein snakke litt med steinen. Eit par fine tette blokker har eg funne til overdekning og er omhyggelig plassert med strø mellom. Steinar som er runde og små legg eg i rydningsrøys bortpå her. Eg vil mure meg ei lita stove her. Snorbein og tett, og på utsida ei heling inn. Eg har så mange planar at eg veit mest ikkje kvar eg skal byrje. Eg løfter på hua og ser inn i vêret. Det har regna støtt dei siste dagane, og ryggen verker etter å ha velta og slite på ugripelege steinar. Oppe i sprengningsrøysa braut eg fleire enkelt ut med talje og stubbebrytar, men her nede sit dei djupt i molda og no står eg fast med ein skikkelig strinakkje. Jorda ligg våt og sleip og eg klarer verken å tyde form eller storleik. Når eg støtar spettet mot den lét den ikkje som fjell, og eg tek til å grave vekk jord langs eine sida før eg legg brystet på steinen og med handa let fingrane varsamt følge steinen ned i den blaute jorda til eg så vidt vert var ei formending før den forsvinn i djupe molda. Eg veit ikkje om det er eit søkk eller botnen, men eg tek straks ein anna stein og legg ned i molda og køyrer jarstauren ned mellom steinane og støyter og tvinger enden på plass der kor søkket tykkjest å være. Så prøvar eg forsiktig, men vogamaten er for mjuk i molda. Eg vil grave vekk meir, men dess meir eg grev dess meir regnvatn renn ned i holet og snart er det ikkje råd å sjå kva eg gjer. Eg legg eit par solide stablesteinar i lad i søla før eg på ny set spettet ned mellom steinane. Denne gongen er det godt hold og eg synest eg får lea den, men idet eg legg meg over spettet, brest ein av dei fine stablesteinane og eg forbannar tankeløysa. Eg står og plukker på trebolane då Kjell kjem forbi og spør meg om livet og slikt og eg forklarar han om strinakkjen. Han har arbeidd med litt av kvart og vil låne meg ei gammal fjellboremaskin han har ståande (om eg berre er varsom med boret). Det er eit tungt beist han kjem attende med og eg balar med å få den i gong. Sola bryt såvidt gjennom skylaget idet eg steller med luftfilter og vøler stiften, og vêret er beint fram godt når eg freistar å få start igjen. Eg dreg så jævlig i snora at pulsen hamrar i panna og svetten renn under helsetrøya, og eg trur eg skal få infarkt idet maskina endelig tenner nokre slag. Ikkje lenge etter står eg tilfreds i ei sky av solbaka steinstøv og to-taktseksos. Maskina slår illtert under meg og sjølv om eg slit noko jævlig med å løfte den oppatt når den med eitt forsvinn under meg, så veit eg at dette er ein stein og ikkje berg. Ikkje lenge etter er det to fine borehol i steinen, og med kile og blikk er problemet hånterlig. Den eine delen legg seg tungt over og havnar djupt ned i det vassfylte holet. Men det er greitt. Slik er det når ein bryt og snur steinar, for livet eller murlivet. Det er altets ibuande faenskap og det kan ein ikkje rå med. Det er vel kva professor Colin Macfarlane ved Strathclyde kalla jordormen. Men i morgon vert vêret godt og problemet mindre enn halvparten av kva det var i dag.

